The Pennsylvania State University

The Graduate School

College of Engineering

# INVESTIGATING THE SENSE OF LISTENER ENVELOPMENT IN CONCERT HALLS USING THIRD-ORDER AMBISONIC REPRODUCTION OVER A LOUDSPEAKER ARRAY AND A HYBRID ROOM ACOUSTICS SIMULATION METHOD

A Thesis in

Acoustics

by

Matthew T. Neal



Submitted in Partial Fulfilment
of the Requirements
for the Degree of

Master of Science

August 2015

The thesis of Matthew T. Neal was reviewed and approved* by the following:

**Michelle C. Vigeant**
Assistant Professor of Acoustics and Architectural Engineering
Thesis Adviser

**Daniel A. Russell**
Professor of Acoustics
Director of Distance Education

**Victor W. Sparrow**
Professor of Acoustics
Interim Head of the Graduate Program of Acoustics

*Signatures are on file in the Graduate School.

# Abstract

The AUralization and Reproduction of Acoustic Sound-fields (AURAS) facility, a 32 channel concert hall auralization loudspeaker array, was developed within an anechoic chamber at The Pennsylvania State University. The primary goal for this facility is for use in subjective testing in concert hall acoustics, specifically on the perception of Listener Envelopment (LEV). The array is equipped with 30 two-way loudspeakers constructed to have a flat frequency response from 60 Hz to 20 kHz (after digital equalization) along with two subwoofers. The loudspeaker-based auralizations are performed using third-order, near-field compensated Higher-Order Ambisonics (HOA). To provide flexibility in creating different sound fields with different perceptions of LEV, auralizations were created using simulations. These simulations were then used in a subjective study looking at LEV. Simulated impulse responses were created using a room simulation program, created in MATLAB. This program uses a hybrid simulation technique of the image source method and statistical reverberation, simulating the geometry for a simple rectangular room. With fine control over the room's auralization parameters, a wide variety of auralizations were created, altering the room's size, reverberation time, early-to-late energy scaling, and overall A-weighted sound pressure level. The Ambisonic signals for the auralizations were simulated in MATLAB, and then the signals were decoded into loudspeaker signals using VST plug-ins in the digital audio workstation REAPER. Twenty-one musicians rated their perceived LEV for the auralizations using a graphic interface developed in Max 7 (IRB Protocol #41733). The interface allowed real-time switching between auralizations, providing side-by-side comparison of stimuli. Overall A-weighted level was found to have the strongest correlation with LEV. An increase in RT also showed statistically significant changes in LEV ratings, but this change was only noticeable in tests where all stimuli were presented at the same level. This result indicates that the effect of RT upon LEV ratings can be masked by the effect of level on LEV. The effect of early-to-late energy scaling also produced a significant increase in LEV ratings, where higher amounts of

late energy, relative to the early energy, produced higher perceptions of LEV. A potential cutoff point, where an increase in late energy does not change LEV perception, may be present, but the limited range of early-to-late energy scaling factors prevents any clear conclusion on this possible non-linear relationship. This result was also found when level equalization was performed within the early-to-late energy scaling stimuli set. The effects of receiver location and hall size were not found to produce significant changes in LEV, but this study contained only a limited number of receiver locations, and assumed a rectangular room geometry. Future work is needed to confirm the balance between the effects of level, RT, and early-to-late energy scaling. A more comprehensive study, including a wide range of receiver locations and hall geometries, should be conducted to better understand how LEV perception changes with hall geometry. This project was supported through the National Science Foundation, Award #1302741.

# Table of Contents

# List of Tables

# List of Figures

# List of Acronyms

| Acronym | Description |
|---|---|
| ACN | Ambisonic Channel Numbering |
| ANOVA | Analysis of Variance |
| ASW | Apparent Source Width |
| BEM | Boundary Element Method |
| BRIR | Binaural Room Impulse Response |
| BSH | Boston Symphony Hall |
| C80 | Clarity Index for Music |
| CAV | Center for Acoustics and Vibration (at Penn State) |
| EDT | Early Decay Time |
| FEM | Finite Element Method |
| FIR | Finite Impulse Response |
| GUI | Graphical User Interface |
| HOA | Higher-Order Ambisonics |
| HRIR | Head-Related Impulse Response |
| HRTF | Head-Related Transfer Function |
| IACC | Interaural Cross-Correlation Coefficient |
| IACF | Interaural Cross-Correlation Function |
| ILD | Interaural Level Difference |
| IR | Impulse Response |
| IRB | Internal Review Board |
| ITD | Interaural Time Difference |
| $J_{LF}$ | Early Lateral Energy Fraction |
| LE | Lateral Efficiency |
| LEV | Listener Envelopment |

| | |
|---|---|
| $L_J$ | Late Lateral Energy Level |
| LLF | Late Lateral Fraction |
| MADI | Multichannel Audio Digital Interface |
| MUSHRA | Multiple Stimulus Test with Hidden Reference and Anchor |
| NFC-HOA | Near-Field Compensated Higher-Order Ambisonics |
| R | Room Impression Index (*Raumeindrucksmass*) |
| RIR | Room Impulse Response |
| RMS | Root-Mean-Square |
| RT | Reverberation Time |
| $SBT_s$ | Spatially-Balanced Center Time |
| SDM | Spatial Decomposition Method |
| SI | Spatial Impression |
| SN3D | Semi-Normalized 3-Dimensional (normalization scheme) |
| SPRAL | Sound Perception and Room Acoustics Laboratory (Penn State) |
| T30 | Reverberation Time measured from the first 30 dB of the decay |
| VBAP | Vector-Base Amplitude Panning |
| WFS | Wave Field Synthesis |

# Acknowledgements

Funding for this project was made possible through the National Science Foundation, Award #1302741. Their financial support of this project has allowed me to remain at Penn State to work on concert hall acoustics research in this country.

It is difficult to even begin to thank the many people who have been vital in the learning, research, execution, and completion of this massive project. Thank you to the many individuals who helped along the way in this project, in both official and unofficial roles. Thanks to Dave Dick and Martin Lawless for putting up with me, and always being go to listening subjects, sounding boards for questions of all kinds, and co-conspirators in all of my endless antics that went on in Research West (and Research West-West). A special thanks to Dave Dick again for always taking the time to work together and collaborate, whether willingly or unwillingly, and for the constant times I tested your patience. Thanks to Kritika for saving us from the flood! Thanks to Acadia, Dave, Eric, Kritika, Martin, and Rachel for putting up with me and my spontaneous singing outbursts on a day-to-day basis. Research West would not have been the same without any of you.

Thanks to Colton Snell for his help in the construction of the loudspeakers for a summer undergraduate research project. Also, thanks to Andrew Coward for expert contribution in both time and advice during the loudspeaker and anechoic chamber construction process – you truly might have the best home workshop in all of State College, PA! The loudspeaker array would not have been completed without either of your help. Thanks as well to Dr. Vic Sparrow and Dr. Dan Russell for agreeing to be on my thesis committee, reading this long document, and for being wonderful and inspiring professors throughout my graduate studies. This project could not have been possible without the funding through an Early CAREER Award from the National Science Foundation. I am honored and grateful that I have been able to receive funding to study concert hall acoustics, in a country where funding in such an area is almost impossible to come by!

To the same end, a HUGE thanks is due to my thesis supervisor and mentor, Dr. Michelle Vigeant. Michelle, you have been my most involved, thoughtful, and meaningful academic adviser to date, and I'm very excited to see what we can accomplish through the upcoming Ph.D. work! None of the opportunities I have had so far would have been possible if you had not made the move to Penn State three years ago. It has been a joy and a pleasure to not only observe first-hand, but be an integral part of getting your lab and research at Penn State off the ground. Thanks for your time, patience, diligence, and also your openness with us as students. You have learned what it takes to be a great adviser from Dr. Lily Wang, but you have also used your own strengths to positively impact your students, myself included.

Although not directly involved in my research, there are many others that have truly impacted my life on a personal note. Although I have worked hard to get to this point in my life, I am the person I am today, and the person I am continually being molded into because of so many others. Thanks to all of my friends back home and from Penn State. You guys have made my life anything but boring, and I'm happy to already have more good friends than some people get in a lifetime. Thanks to my parents, Craig Neal and Dottie Neal, for always supporting me in anything I do. I love you guys. Thanks to my siblings, Adam, Jessica, Benjamin, Andrew, and Haley, who not only have always supported me throughout the year, but have also put up with (and participated in) all of my crazy antics. Thanks to Nate Daman, Dave Bowman, and Mike Baldner who are and will be amazing examples of men of God in my life.

Lastly, and most certainly not the least, I'd like to thank my personal Lord and Savior, Jesus Christ. All of the opportunities I have had to date, both personally and professionally, I owe to you. No matter what happens in my future career, professional life, and personal life, I am grateful to have confidence in my eternal life with you. Thank you for the cross and for not requiring me to earn my salvation, a lesson I continue to learn and remind myself of daily. You have done so much through my life (this thesis included), and I can't wait to see what you have in store.

Ephesians 2: 8-9 & Ephesians 3: 20

# Chapter 1: Introduction

Assessing and understanding the subjective impact of concert halls upon a listener proves to be quite complex. When an individual sits down to listen to a concert, they bring many factors into their own perception. Do they know the pieces that will be performed? Are they familiar with the composer? Do they know someone who is performing? Are they inclined to key in on listening to the trumpets? Cellos? Tenors? What are their architectural tastes? What did the concert-goer eat for lunch? Did they get a good night's sleep? With so much information and events impacting a listener's mood and senses, the task becomes quite difficult at an individual level. Despite this difficulty, it is still the job of the architectural acoustician to design a room that will be well liked, pleasing to the majority of concert-goers, even with so many preferences at play.

As an architectural acoustician, the primary concern is to satisfy the client or building owner. Despite the need to satisfy the person who is paying the bills, care must still be taken to satisfy the general public, who will be attending the concert and dictating the public's opinion of the space. This creates the need for subjective testing in concert hall acoustics. Like differing preferences in fine food and fine wine, many concert-goers have their own preferences, but some key, overall aspects exist about which most people agree. For the researchers in concert hall acoustics, these common attributes are sought to be identified, and then quantified, into a usable metric which the architectural acoustician can apply. Such a metric would help to ensure that a hall's acoustic impression is as intended. One specific subjective aspect, which most listeners and researchers alike believe to be favorable, is the sense of listener envelopment (LEV). LEV is defined as feeling surrounded or immersed within a sound field.

The importance of LEV, and the general idea of spaciousness, has been understood for quite some time, but no clear way of quantifying this sense had been fully accepted. Many different objective measures of LEV and spaciousness have been

proposed, but it is unclear as to which specific measures truly correlate to the fundamental sense of being immersed in sound. To date, most research in LEV has used rather simplistic recreations of sound fields, which have no physical basis from either measurements or a physical room model. Sound fields are simulated typically with five to eight loudspeakers, and reflections are played at a level with a particular time delay from the direct sound. Finally, reverberation is applied to specifically selected speakers, depending upon the preference of the researchers. Although these simplistic methods were sophisticated in the 1970's and 80's, physical sound field reconstruction and modeling has come a long way since that time.

The present works aims to create and construct a facility providing spatially accurate auralization for concert hall acoustics subjective testing. Since LEV has been clearly linked to the direction of arrival of reflections, it is important to ensure accurate spatial reproduction at the listener location. The AURAS facility was developed in which spatially accurate auralizations, from either room measurements or simulation, could be implemented and played over a loudspeaker array. The array has been constructed within a controlled environment, an anechoic chamber, and careful signal processing has been used throughout, to ensure as accurate an auralization as is possible. Near-field compensated third-order Ambisonics has been used as a reproduction method, in an attempt to physically reconstruct the sound field at the listener's location in a controlled manner.

The goal for the facility was to create a user-friendly, controllable environment, in which auralization could be reproduced from both spherical microphone array measurements and simulations. To provide the flexibility and control desired, a hybrid simulated method was developed in MATLAB, which utilized the image source method and statistical reverberation to simulate a spatial room impulse response for a simple rectangular geometry. A wide variety of auralizations can be created with this program, through fine control of the room size, material properties, source location, and receiver location. Additionally, the auralization is made with a physical basis, allowing for a realistic simulation, reminiscent of a constructible hall. This

simulation method was implemented first in a subjective study, testing the subjective perception of listener envelopment (LEV) in concert halls. To date, many simulations for LEV testing have not provided the dual combination of flexible control and a physical-basis.

This thesis will encompass the entirety of creating the AURAS facility, developing a physically-based simulation method for higher-order Ambisonic reproduction, and using the facility for subjective testing in concert hall acoustics. Initially, Chapter 2 presents previous work in the topic of LEV, and background in concert hall auralization is given. Then, a comprehensive look at the construction of the AURAS facility is provided in Chapter 3, ranging from loudspeaker construction to software and hardware control. Chapter 4 provides details on the room acoustics simulation that was used to finely control the auralizations reproduced in an anechoic chamber. Chapter 5 describes the subjective testing methods used in the current LEV study, and Chapter 6 presents the results of this initial study of LEV using a physically-based sound field. Finally conclusions are drawn and suggestions for future work are given in Chapter 7.

The construction of such a facility for concert hall acoustics auralization is quite complex, and this research tool opens the door to many opportunities in the future. Even outside of concert hall acoustics, the research potential for a facility that can accurately recreate sound fields is favorable. With the provided simulation techniques, robust setup, organization, and operation of the loudspeaker array, the AURAS facility can assist in vastly expanding our knowledge of subjective perception in concert hall acoustics.

# Chapter 2: Background Information

This chapter covers previous research that has been performed on the perception of LEV in concert hall acoustics (Section 2.1) and methods of reproducing spatially accurate sound fields (Section 2.2). To begin, the origins of the idea of spaciousness and LEV are provided, and the original research that helped to define LEV is given. Since many different components or aspects of a sound field have been proposed to impact LEV, the following sections each address a different aspect of LEV perception. Included in these different aspects are lateral reflections, reflections from non-lateral directions, temporal characteristics of reflections, frequency dependent reverberation, and binaural hearing. In addition, background information for the simulation method implemented within the present study is provided.

## 2.1: Listener Envelopment in Concert Hall Acoustics

LEV has been defined by many researchers, all agreeing upon its importance to acoustic perception. The ISO standard for room acoustics measurement defines it as "a sense of being immersed or enveloped in the sound,"[1] and Beranek defines it as "the degree to which the reverberant sound seems to surround the listener–to come from all directions rather than from limited directions."[2] Originally, the idea of LEV in concert hall acoustics was known as a general phenomenon, and was coined "spaciousness" or "spatial impression". The term has had many different names since then, and the concept has continually evolved since its origins. The importance of the spatial characteristics of a sound field has been known for quite some time, but no attempt to physically quantify this perception was made until the late 1970's.

### 2.1.1: Overall Room Impression and LEV

Of first importance, it must be noted that LEV has been found to correlate with the overall impression of a room. In this thesis, overall room impression (ORI) is used to describe the overall sense in which a listener either likes or dislikes the acoustics of a hall, including all subjective attributes which play into each individual's tastes and preferences. These attributes can often be quite hard to quantify, but multiple studies

have attempted to find the individual subjective perceptions in concert hall acoustic impression that most highly correlate with ORI. In 1988, Barron did an extensive survey of British concert halls, where listeners rated various qualities of the acoustic environment, including intimacy, warmth, brilliance, clarity, reverberance, LEV, balance, loudness, background noise, and overall acoustic impression of the hall.[3] Listeners rated the halls during a performance, and Barron ran a correlation analysis between the overall ratings of the different subjective attributes for eleven different British concert halls. From this analysis, he found that two groups of listening subjects emerged with different preferences. The first group primarily associated ORI with reverberance (and not with intimacy), while the second group associated ORI most strongly with intimacy (and not with reverberance).

The results from both groups also showed a strong correlation between LEV and ORI. When both groups were analyzed separately, LEV was strongly correlated with the main subjective attribute for that group's preference (either reverberance or intimacy) but not the important subjective attribute associated with the other subject group's impression (again, either reverberance or intimacy). Figure 2-1 shows a diagram representing the determined correlations for the different subject groups.

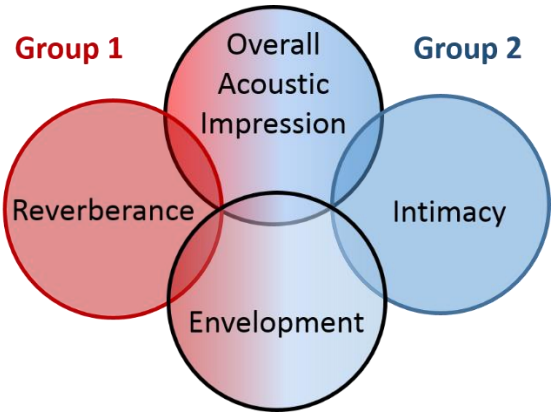


Figure 2-1: Correlations found for the two different subjective groups in Barron's study. Interestingly, two groups, with two different interpretations of LEV emerged. Adapted from Figure 2 in Barron, 1988.[3]

It is important to note that LEV was highly correlated to ORI for all subjects, and not just one of the two specific groups. This points to the overall importance of LEV in

creating a 'good' acoustic environment, no matter what other individual preferences might exist for a specific listener. As well, it is interesting to note that two different interpretations of LEV were found, between the two subject groups. The first group associated LEV with a reverberant, full sound, while the second group associated LEV with a clear, distinct sound. Both sounds are subjectively very different, which points to a clear difference between subjects in interpreting LEV.

Other more recent work by Lokki has also linked various subjective impressions to overall preference.[4] Using a multi-factor analysis, preference mapping was used to help compare all of the overall ratings from his subjective work. In this mapping, a certain number of orthogonal factors were identified, that most highly contributed to explaining the variance in the perceptual ratings of subjects. With these factors, an orthogonal 'preference space' was defined, that allowed a visualization of which individual subjective attributes corresponded to the determined orthogonal factors in the preference map. It should be noted that Lokki employed a method that allowed subjects to select their own attributes with which to rate the concert hall stimuli and to define their own individual anchors for the reference rating scales.[5] A graph of the preference space is shown in Figure 2-2, where different subjective attributes are plotted on the preference space.

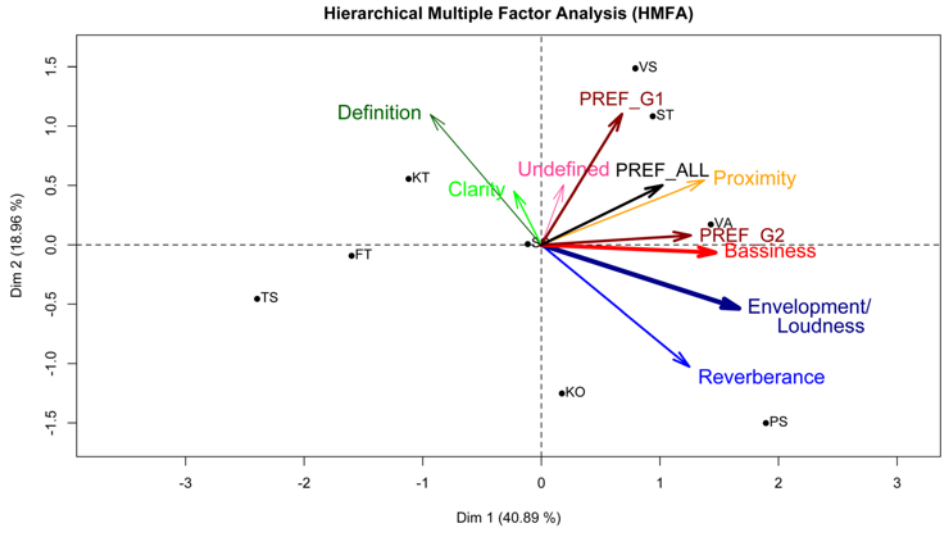


Figure 2-2: Reproduction of Lokki's Figure 10a from [4] using a hierarchical multiple factor analysis. The first dimension, determined by LEV/loudness and bassiness, is important to preference group two (G2), while reverberance, clarity, and definition are related to dimension 2 and are more important to group one (G1).

Again in this study, an interesting breakdown in two groups of subjects emerged. First, both groups of subjects tended to agree upon the first dimension, Dim 1, in the preference space. Most of the subjects fell on the positive half of this axis. This axis was found to correlate most with the sense of LEV or loudness, so that everyone preferred a higher sense of loudness and LEV. However, differences between groups was found for dimension two, Dim 2. From Figure 2-2, it can be seen that this dimension was attributed to the two roughly opposite impressions of reverberance and clarity. One group preferred a clearer, more defined sound, while the other group tended to like a more reverberant sound. Despite these differences in preference, the overall importance of LEV perception was agreed upon by most subjects, in a positive sense, and it provided a link to understanding the overall preference of listeners within a hall.

### 2.1.2: The origins of 'Spaciousness' in Concert Halls

The first work in simulating a directional sound field was done by Reichardt and Schmidt in 1966.[6] Within an anechoic chamber, two loudspeakers were set up in the front direction, to simulate direct sound in a concert hall, and four loudspeakers were placed at the side and back to simulate reverberant energy. Different ratios of direct-to-reverberant energy were played, and 30 subjects were asked to rate the room/spatial impression of each sound field. The concept was further explored by the same researchers in 1967, where individual, isolated reflections were explored. Lateral and ceiling reflections were simulated in separate cases, and paired with a direct sound signal. The lateral wall reflection was found to be imperceptible when it was 10 dB lower in level than the direct sound, and an audible change in the sound field was found with a minimum change in time delay of 7 ms. On the other hand, the ceiling reflection was imperceptible when just 6 dB lower than the direct sound, and a 12 ms change in time delay was needed for a perceptible change in the sound field. Thus, the lateral reflections produced a more noticeable change as compared to the ceiling reflection.

Reichardt and Lehmann made the first effort to combine the important aspects of timing and arrival direction of reflections in their 'Room Impression Index' ($R$), which is translated from the term *Raumeindrucksmass*.[7-8] This metric was found to correlate with the subjective room impression, namely in terms of both spaciousness and liveliness[9] and is defined as:

$$R = 10\log\left\{\frac{\int_{25\,ms}^{\infty} p_k^2 dt - \int_{25\,ms}^{80\,ms} p_r^2 dt}{\int_0^{25\,ms} p_k^2 dt + \int_{25\,ms}^{80\,ms} p_r^2 dt}\right\}\ [\mathrm{dB}]\,, \qquad 2\text{-}1$$

where $p_k$ is the pressure measured from an omnidirectional microphone (*Kugel*) and $p_r$ is the sound pressure recorded with a 'frontally directed' microphone (*Richtmikrofon*). The frontally directed microphone was conceptually defined as a microphone that responded equally to sound within $\pm 40°$ of the frontal direction, and rejected sound outside of that range. This room impression index acts as an energy ratio of all energy after 25 ms, except that arriving from the front direction, to the total energy arriving before 25 ms combined with the frontal energy arriving between 25 and 80 ms. This metric can be seen as a measure of spaciousness, including sound from all directions except the front.

In 1967, around the same time as the first work by Reichart and Schmidt, Marshall first explored the idea of 'spatial responsiveness'.[10] His primary motivation was to determine another room acoustics metric, beyond simply reverberation time, which would provide understanding of the perception of overall concert hall quality. It was his opinion that a certain component of the spatial distribution of reflections impacted the overall impression of having 'good acoustics'. By looking at the cross section of various halls, he concluded that a common criterion for good spatial responsiveness was a narrower cross section, which was exhibited by shoe-box type halls, and not by fan shaped halls.

One of the first pioneers for research in spaciousness was Barron. In 1971, he began to look at the importance of the timing and direction of individual reflections within

a concert hall.[11] By setting up loudspeakers within an anechoic chamber to simulate direct sound and reflections, he was able to establish important directions and time frames for reflections to have an important effect. He concluded that reflections had to occur between 10 and 80 ms in order to impact 'spatial impression' (SI) or a broadening of the source. He also found that lateral reflections from side walls had the most prominent effect on SI, and that ceiling reflections only caused tone coloration. This indicated the primary importance of lateral reflections. Barron's work continued, and he proposed a physical measure for SI after conducting more extensive testing.[12] His new parameter was called early Lateral energy Fraction ($J_{LF}$), and is defined as,

$$J_{LF} = \frac{\int_{5\ ms}^{80\ ms} p^2(t) \cos \emptyset \, dt}{\int_{0\ ms}^{80\ ms} p^2(t)\, dt}, \qquad 2\text{-}2$$

where $p(t)$ is the pressure measured at a receiver location (omnidirectional), and the cosine term applies a directional weighting, emphasizing the sound arriving from the lateral directions (this metric was originally termed LF, but the symbol $J_{LF}$ is used, which appears in the ISO standard[1] for room acoustics measurement). The angle $\emptyset$ is defined as the angle between a reflection and the interaural axis, defined to be zero in both the left and right directions, and measured from the closest direction (either left or right). To measure the cosine term, a figure-of-eight microphone can be used, which has a cosine directivity pattern. The measure can be calculated for each octave band individually, and typically, an overall measure is determined by averaging the 125, 250, 500, and 1000 Hz octave bands. This measure has become somewhat widely accepted as a metric of spaciousness today, and it is included in most room acoustics modeling software packages. It also is included in the ISO standard as the metric for Apparent Source Width (ASW) which will be discussed in section 2.1.2.[1]

It should also be noted that at the same time Barron proposed his metric for early lateral energy fraction, Jordan proposed an almost identical objective measure he termed Lateral Efficiency (LE):

$$LE = \frac{\int_{25\ ms}^{80\ ms} p_F^2(t)\,dt}{\int_{0\ ms}^{80\ ms} p_O^2(t)\,dt}, \qquad 2\text{-}3$$

where $p_F(t)$ is the pressure measured with a figure-of-eight microphone, and $p_O(t)$ is the pressure measured with an omnidirectional microphone. When comparing eqns. 2-2 and 2-3, both are identical, except that the early integration limit is 25 ms, rather than 5 ms as defined in $J_{LF}$. It is interesting to note that Jordan first published his metric LE in 1980 in his book *Acoustical Design of Concert Halls and Theatres*,[13] and this metric is noted in Cremer's *Principles and Applications of Room Acoustics*, as translated by Schultz.[8] Jordan does indicate that other metrics exist, but he claims that his is much easier to measure, since it utilized a figure-of-eight microphone.[14] This statement is unclear, for Barron's $J_{LF}$ also uses a figure-of-eight microphone for the cosine weighting, requiring no difference in the measurement setup. On the other hand, he does include a plot which is from Barron and Marshall's 1981 paper[12] (which at the time was unpublished), and he thanks Barron for allowing him to publish this result from his paper on the topic of SI and $J_{LF}$. As it appears, both seem to have been in discussion over the matter, but Barron's metric truly received much more validation, and overshadowed Jordan's almost identical metric, most likely due to the testing which supported Barron's proposed metric.

### 2.1.3: Apparent Source Width and Listener Envelopment

After Barron's work in the 1970's and 1980's on LEV, more traction for research in the field of LEV began to emerge. After the idea of SI existed in concert hall acoustics, it was determined that two separate perceptions, the perception of the width of a sound source and the perception of LEV, could be distinctively identified within the

term SI. The two terms were separated and individually defined most widely by Bradley and Soulodre in 1995.[15-16] In these studies, it was demonstrated that the Apparent Source Width (ASW) and LEV are both separate spatial perceptions, in which early reflections are integrated with the direct sound, and thus, impact the characteristics of the perceived sound source's size and localization perception. Later sound, which is not integrated by the auditory system with the direct sound, tends to impact the perception of LEV. This phenomenon is highly related to the Haas effect.[17]

These experiments showed that early reflections, as measured using $J_{LF}$, correlated most with ASW, and that late arriving reflections, after around 80 ms, contributed to the sense of LEV. This study was done by varying the amount of early and late energy separately using simulated impulse responses (IR) over a front loudspeaker and a left and right loudspeaker. The reverberant energy was delayed by at least 80 ms, so that early reflections were not influenced by this energy. It was found that although ASW did not correlate with late energy, higher amount of late energy made it more difficult to detect changes in ASW. To better understand the late energy, tests were done using four loudspeakers, at ±35° and ±90°. Reverberant energy was played in different directional combinations of one, three, or five loudspeakers, to gain an understanding of the directional distribution of reverberant energy. From this study, a new metric was proposed, Late Lateral Energy Level ($L_J$) which correlated best with subjective impressions of LEV. This metric is defined as,

$$L_J = 10 \log \left[ \frac{\int_{80\ ms}^{\infty} p_F^2(t)\, dt}{\int_{0\ ms}^{\infty} p_A^2(t)\, dt} \right], \qquad 2\text{-}4$$

where $p_F(t)$ corresponds to the sound pressure measured using a figure-of-eight microphone in a hall, with the null pointed towards the source, and $p_A(t)$ is the sound pressure of the sound source measured at a distance of 10 meters in an anechoic chamber (originally, this metric was represented as $LG_{80}^{\infty}$ and $GLL$). This metric is an adaptation of the strength metric, $G$, in the ISO standard.[1] Morimoto also published concerning the differences between ASW and LEV, before Bradley, but the findings

showed that ASW was impacted by both early reflections and late sound energy.[18-19] Despite this contradictory finding for ASW, the link of ASW to early reflections seems to be the more favorable current opinion.

More recent work has questioned the clear division between ASW and LEV. Bradley has found that while ASW increases with increasing amounts of early energy, increased late lateral energy will cause a decrease in ASW, and conversely, an increase in early energy will cause a decrease in perceived LEV. Despite this relationship, the magnitudes of the decreases in ASW and LEV were found to be smaller than the magnitudes of the increases in the other metric. Thus, typically both ASW and LEV will exist within the same given hall, even despite the proposed destructive interaction of energy. Barron also questioned the exclusion of early sound in LEV ratings as a possible flaw of Bradley and Soulodre's 1995 study.[16,20] Barron points out that since they found a relationship between clarity index and LEV, it might not be as simple as just disregarding early sound energy for LEV. Morimoto also determined that the ratio of front-to-back sound energy in the early part of the IR impacted LEV.[21]

### 2.1.4: The Importance of Lateral Reflections for LEV

The most overarching conclusion from past research in LEV is the importance of lateral reflections. This finding began with Barron's work, showing the importance of early lateral reflections, and was adapted to late lateral reflections to explain the separate sensation of LEV. Again, Bradley and Soulodre first clearly demonstrated this importance with the metric $L_J$, and much research has followed to confirm these findings. Hanyu conducted experiments in which reverberant energy was simulated over a loudspeaker pair on the horizontal plane placed at varying azimuthal directions, from ±22.5° back to ±157.5°, in 22.5° steps.[22] When asked to rate LEV, maximum ratings were found at the 90° placement, and the LEV ratings exhibited a parabolic trend with a maximum at the interaural axis. This result points to the emphasis on lateral reflections, still with importance upon other directions as well. Furuya and Wakuda also conducted experiments in which the most emphasized

direction of importance was found for lateral reflections.[23-25] Soulodre conducted a study in which he validated the original findings from 1995. The setup of the study was highly similar to the original work, but the side loudspeakers were placed at ±30° and ±110°.[26] The same emphasis on lateral reflections was also found with this setup. Overall, the emphasis on lateral reflections is well known, and widely accepted as important to both LEV perception and a positive ORI.

### 2.1.5: The Interaction between Sound Level and LEV

In Bradley and Soulodre's metric, $L_J$, one key aspect which separates it from Barron's $J_{LF}$ is that it is normalized in the same manner as strength ($G$). This normalization term for the strength of a sound source is measured from 10 m in an anechoic chamber, providing a metric that is higher when a higher level of sound is experienced within a given concert hall. This relationship between loudness and LEV was clearly shown by Bradley and Soulodre.[16] Soulodre again confirmed this finding in a follow-up study, with a highly similar setup [26]. Bradley continued to confirm this finding in later work.[27] Many other researchers have confirmed this finding in a very similar fashion to both Bradley and Soulodre.[23-24,28] Some more interesting confirmations of these results were from both Barron[20] and Lokki.[4] In response to Bradley and Soulodre's $L_J$, Barron looked into adjusting his metric of early lateral energy fraction into the Late Lateral energy Fraction (LLF):

$$LLF = \frac{\int_{80\ ms}^{\infty} p^2(t) \cos \emptyset \, dt}{\int_{80\ ms}^{\infty} p^2(t)\, dt}. \qquad 2\text{-}5$$

Barron found that LEV was impacted significantly by overall level, so LLF did not adequately predict the sense of LEV for listeners. In his measurements from 17 British concert halls, he did note that $L_J$ was heavily impacted by the overall level of sound in a particular hall. Barron called into question whether or not Bradley's metric was too skewed towards level, as opposed to the directional sound field properties.

Barron stated that "subjective studies at real concert halls would be welcome to establish whether this simple conclusion is valid."

Another less direct validation of this work was found by Lokki in his individual preference mapping.[5] Lokki had individuals define their own attributes with which to rate different concert hall stimuli. He then performed a clustering analysis, which separated the individually elicited attributes into groups which were interpreted in a similar manner. In essence, this analysis should result in grouping similar impressions together, even if individuals would use different adjectives to describe the impression. After this analysis, one of the six defined groups of attributes was coined the LEV/loudness group, and some of the individually elicited attributes included loudness, fullness, width, presence, and openness. Thus, the two individual perceptions of loudness and LEV appeared to be linked between subjects. It should be noted that the terms LEV and loudness were not specifically rated by all subjects in the group, so no straightforward link of the two can be clearly drawn.

### 2.1.6: The Impact of Non-Lateral Reflections for LEV

The most common criticism of Bradley and Soulodre's metric for LEV, $L_J$, is the exclusion of sound energy arriving directly behind and above a listener. By choosing to use a figure-of-eight microphone, emphasis is given to lateral directions, but by rejecting the frontal sound, the vertical and back arriving energy is not considered. Along with confirming the need for lateral reflections, many studies have also confirmed that reflections from other directions are important as well. Furuya also looked at the influence of vertical and back reverberation, by increasing the relative levels in those directions of reverberant sound. He found that along with the lateral direction, both the vertical and back directions showed a strong positive linear relationship between late directional level and LEV. The vertical and back reverberant energy had 35% and 65% respectively of the contribution to LEV that lateral energy provided.[23-24] Hanyu looked at many different directions, as he moved a pair of loudspeakers from ±22.5° azimuth back to ±157.5°, in 22.5° steps. At each location, he found that reflections from the front right/left and back right/left

increased LEV, even without including direct left-right lateral energy.[22] Barron also questioned Bradley and Soulodre's choice to exclude sound coming from the back and front directions.[20]

Morimoto conducted a study where he varied the front-to-back ratio of reverberant energy. He used six loudspeakers, placed in the front, back, ±45° from the front, and ±45° from the back. Two amounts of reverberant energy were fed into the front three loudspeakers separately from the back three loudspeakers. Thus, different simulations were made by changing this ratio of front-to-back energy. Morimoto found that adding energy from the back, or decreasing the front-back ratio, helped to improve LEV in both the early and late part of the IR. Even with both parts important, it was still found that the late part is more effective at creating a sense of LEV.[21] It should be noted that, although Morimoto claims that reflections from behind a listener play an important role in LEV, he never truly tested reflections that come from purely behind a listener, or just the back loudspeaker.

Thus, some amount of lateral energy, both in the front and the back, is always included in the stimuli, despite the focus of the paper. Morimoto does explain that truly back reflections alone most likely will not create a sense of LEV, but his explanation is slightly misleading. Evjen et al. also found a contradictory result when investigating reflections from above and behind a listener.[29] In all simulations, an additional loudspeaker was placed at a raised elevation or at azimuths of ±35°, ±90°, ±145°, or at 180° (the 180° case did not have an elevation and was located on the horizontal plane). All cases were compared to the case without the additional rear or elevated loudspeaker. No significant increase in LEV was found with the inclusion of any additional loudspeaker positions. Some small artifacts may have been detectible, but it did not seem to change the perception of LEV.

Bradley published his results in 2000 that also support the need for the inclusion of other reflection directions, in his metric ($L_J$).[27] He found that when extending the simulation techniques, adding reverberant energy either in front or behind showed improvement on LEV ratings, even though this energy is not included in $L_J$. Hanyu

also found an interesting result that, when reverberant sound was included from the front loudspeaker, after the direct sound, it caused a change in the subjects' LEV ratings.[22] More energy in the front tended to produce higher LEV ratings when more energy behind a listener was included. Most of the other simulation methods did not include reverberant energy in the front loudspeaker, which might have created a negative impact on certain LEV ratings.

### 2.1.7: Temporal Characteristics and LEV

Another aspect which has been researched is the link between LEV and the temporal characteristics of reflections. Originally, Bradley and Soulodre suggested a cutoff time for late energy starting at 80 ms. Others have found that early energy also creates a sense of LEV, using reflections before 80 ms[21] and questioned if the cutoff time should be later than 80 ms. Soulodre suggested a more appropriate time for the $L_J$ cutoff would be 105 ms, based upon subjective work done in which the onset time of simulated reverberation was varied.[26]

Morimoto also looked into what he called the "Law of the First Wave Front". His interpretation is very similar to the Haas effect,[17] which was explained by Bradley as the reasoning behind separating ASW and LEV with early and late energy.[16] Morimoto claimed that if an early reflection exceeds a certain level, it would no longer be completely integrated with the direct sound, and would create a sense of LEV. Morimoto hypothesized that this threshold would create a division between how much a reflection contributed to ASW versus how much it contributed to LEV. The portion of an early reflection exceeding the limit of the Haas Effect would contribute to LEV, and the portion up to the Haas Effect limit would create ASW. This limit would decrease in level as time from the direct sound increased, so this new division could also be applied to defining late sound energy. In essence, an instantaneous time cutoff is no longer used, but a sliding cutoff based upon the Haas Effect would dictate early and late energy definitions.

Lokki also looked at this phenomena of the integration of reflections, even though his research was less focused on LEV.[30] Lokki claimed that reflections that are more

specular, which he considers temporal envelope preserving reflections, will be best integrated with the direct sound. Other reflections that are more diffusive will not preserve a clear copy of the direct sound, causing a temporal envelope distorting reflection. This phenomena can cause undesirable coloration to the sound, and will not be positively integrated with the direct sound. Lokki found that these distorting reflections can produce a colored, slightly muddier, and less enveloping sound than the temporal envelope preserving reflections. This also points to the impact of early reflections on LEV in concert halls.

### 2.1.8: The Connection between Reverberance, Late Energy Ratios, and LEV

Past work has shown that reverberance has a mixed impact upon LEV. Some work has shown that despite changes in reverberation time, no large change in LEV has been observed.[16,26] These tests were conducted with stimuli presented at the same level, with different Reverberation Times (RT). Morimoto found a strong impact of RT upon LEV ratings in another study.[31] RTs were varied from 1.0 s to 2.0 s, and he found that an increase in both high and low frequency RTs produced an increase in LEV. The contradiction between these two results points to a need for more research between LEV and RT.

### 2.1.9: Other Approaches to the Envelopment Question

Various other approaches have been suggested to quantify the perception of LEV. Hanyu and Kimura suggested a very different metric called the Spatially Balanced Center Time ($SBT_s$):[22]

$$SBT_s = \sqrt{\sum_{i=0}^{n}\sum_{j=0}^{n} a_i a_j \sin\left(\frac{\theta_{i,j}}{2}\right)}, \qquad 2\text{-}6$$

$$a_i = T_{si}\frac{1+\cos\theta_{Li}}{2}, \qquad 2\text{-}7$$

$$T_{si} = \frac{\int_0^\infty t p_i^2(t) dt}{\int_0^\infty p^2(t) dt}, \qquad 2\text{-}8$$

where $T_{si}$ represents the contribution of an individual reflection to the center time of the IR, and $a_i$ weights that reflection's contribution with directional information for that reflection. The angle $\theta_{Li}$ is the angle between the reflection and the interaural axis. $SBT_s$ is calculated by integrating $a_i$ and $a_j$ with respect to all other reflections, shown in Eqn. 2-6, using the angle between the two reflections, $\theta_{i,j}$. This metric was proposed because it had a few properties which differ from $L_J$. First, it compares individual reflections with other reflections in the IR. The sine term in Eqn. 2-6 will reach a maximum when the angle between the two reflections is 180°. This means that when a sound field is more or less symmetrical, and balanced across the interaural axis, it will reach its highest value. It also responds to energy not just in the lateral direction, but also in the front, vertical, and back directions as well. Hanyu found an increase in subjective LEV when front and back reverberance was present, which would not be indicated by $L_J$. On the other hand, $SBT_s$ will have a higher value in this case, due to the symmetry of the sound field. This change causes high ratings of LEV, which was found in subjective studies.[22] Additionally, when reverberant sound was biased towards the right or left side, a decrease in LEV was found. This decrease would not be present in $L_J$, but $SBT_s$ indicates this decrease due to the change in spatial balance of reflections.

Other methods can also be heavily based upon binaural perception. Griesinger has done extensive work connecting the sense of LEV to binaural phenomena.[32-34] Griesinger looked at how the primary localization perception of interaural time delays and interaural intensity differences impact this perception (these localization cues will be described in more detail in Section 2.2.1). When lateral sound reflections are present, especially at low frequencies where the ITD localization cue is dominant, the perceived localization will shift. If using a continuous musical tone, Griesinger claims that this localization shift will create a fluctuation, causing a sense of LEV. If

continuous tones are not present, Griesinger proposes that on fast attacking sounds, these necessary localization fluctuations between reflections result solely from the late arriving energy to the listener, as opposed to between direct sound and reflections.

Hidaka et al. have proposed quantifying LEV with the Interaural Cross-correlation Coefficient (IACC), which can be measured between the two ears of a listener.[2,35] By measuring the IR of a room using a binaural head, two IRs, for the left and right ears, can be obtained, known as a Binaural Room Impulse Response (BRIR). The provided hypothesis is that when reflections are arriving from directions closer to the interaural axis, more masking will take place across the head, and the two signals at the ear will be less correlated. On the other hand, from front-arriving reflections, the IRs will be more correlated. Thus, a lower cross-correlation between the ears should result in a higher perception of spaciousness or LEV. Also, a higher correlation should indicate a less enveloping sound field. The interaural cross-correlation function (IACF) as a function of $\tau$ is given by:[35]

$$IACF_t(\tau) = \frac{\int_{t_1}^{t_2} p_L(t) p_R(t+\tau) dt}{\left[\int_{t_1}^{t_2} p_L^2(t) dt \int_{t_1}^{t_2} p_R^2(t) dt\right]^{\frac{1}{2}}}. \qquad 2\text{-}9$$

To determine a metric for LEV, the maximum value of the IACF is used, using the integration limits of 80 ms to 1,000 ms.[2] $\tau$ is the time step of the cross-correlation, and it typically ranges from -1 to +1 ms, corresponding to the maximum time delay between the left and right ears. By varying $\tau$, and taking the maximum of the IACF over $\tau$, IACC is determined, and it is a good measure for the correlation between the two ear drum pressure signals.

The last binaural method to mention is not directly related to LEV, but was analyzed by Lokki et al.[36] By looking at the binaural characteristics of the human head as a receiver, some insight into lateral reflections can be made. When comparing the HRTFs measured in individual directions, at all frequencies, to HRTF measurements

made in the front direction of a listener, it can be seen that amplification in loudness occurs across many different frequencies when reflections come from a lateral direction. This amplification would imply that a reflection occurring at the same level would have a different apparent loudness, depending upon the direction of arrival. This level difference can be entirely explained by the masking and resonances of the pinnae, head, and reflections from the upper torso. Thus, lateral reflections are more favorable in concert halls, due to an increase in the loudness from a binaural phenomenon, which Lokki termed as the 'binaural loudness'.

### 2.1.10: Concluding Thoughts and Remarks on Envelopment

As has been shown, many different ideas behind LEV exist, and subjective testing is clearly needed to validate what is believed to already be known and to determine what is true in areas where research contradictions exists. Clear importance of lateral energy has been found, but whether or not a cosine weighting function to measure lateral energy is accurate has yet to be determined. Additionally, contradicting evidence on the importance of both vertical and back directions of late energy has been shown, requiring more research to understand this concept. Finally, various other methods proposed rely on binaurally focused phenomena, and links could be made between research focused on directional importance and the binaural properties associated with these directions.

It should be noted that in the majority of the research done for LEV, almost all have been performed using simulated sound fields.[15-16,21-29,31,37-38] For all of these studies, rooms were simulated with direct sound emanating from the front loudspeaker, early reflections from the front and a few side loudspeakers, and then reverberant energy from some subset of the loudspeakers. The number of loudspeakers typically ranged from five to eight, and the reverberant energy was simulated with an artificial reverberator. In all of these cases, the realism of the sound field should be considered. None of the simulations were created with a physical room in mind, but rather, they were highly motivated by perceptual aspects of LEV.

Additionally, this simplistic method of room acoustic simulation was state of the art in the early stages of LEV research, but new auralization techniques are available today that should be utilized for subjective testing. The next section covers the basics of auralization today, and begins to provide information on how loudspeaker arrays can be used to physically recreate a sound field. No longer are the required simulation techniques limited to the methods previously used in LEV research. Subjective studies should be conducted with either simulated sound fields using geometrical acoustics or physically measured sound fields from real concert halls.

## 2.2: Auralization Methods in Concert Hall Acoustics

This section covers the methods that were used in this study to simulate a spatially accurate room impulse response (RIR) for presentation to a listener during subjective listening tests. First, different auralization methods will be provided, discussing both simulation-based and measurement-based auralization. Then, specific methods of loudspeaker-based auralization will be provided, focusing specifically on wave field synthesis and Ambisonics. Finally, the method used in this study, Ambisonics, will be discussed in more fundamental detail.

### 2.2.1: Auralization from Room Measurement

In order to characterize the effects of a room upon a particular sound source present in the room, a RIR is measured. For any given RIR, each specific measurement is directly linked to the excitation source's location and directivity, the room's geometry and material properties, and the receiving transducer's location and directivity. The most common method to measure a room is through the use of an omnidirectional sound source and an omnidirectional diffuse-field microphone. A typical commercially available omnidirectional sound source is a dodecahedron loudspeaker, but most have frequency limitations on omnidirectional behavior around 1000 or 2000 Hz.[39] While an omnidirectional sound source is beneficial as a controlled measurement source, real sound sources begin to exhibit very unique directional behavior at mid and high frequencies. The human voice, musical instruments, loudspeakers, and any other common or natural sound source will have vastly different directivities, which are

highly dependent upon the type, size, frequency and orientation of the sound source. Similar issues concern the receiving transducer, or microphone directivity.

Typically, the characteristics of the room are quantified through room acoustics metrics, which can be calculated from the RIR.[1] Most metrics specify the use of an omnidirectional microphone, which captures the time behavior of room reflections, but loses all directional information carried to a listener in a concert hall. Some metrics, such as $L_J$ and $J_{LF}$, do require the use of a figure-of-eight microphone, but these metrics are less widely-used, and some have very little research behind their development.[12,16]

When creating an auralization, measurements made with an omnidirectional, or even a figure-of-eight microphone, are not sufficient to create a plausible auralization. The human ears, considered as a pair of receivers, exhibit highly directional characteristics, and these characteristics help provide our auditory system with various cues that impact sound source localization in any environment. These cues can include interaural level differences (ILDs), interaural time differences (ITDs), and spectral shaping differences between the ears due to the resonances of the pinnae.[40] These cues are the result of effects from the sizes and shapes of a listener's upper torso, head, and pinnae. In order to recreate these cues in a measurement, a binaural head can be used to measure the BRIR. The binaural head, shown in Figure 2-3, is a replica of a human's upper torso, head, and ears, with omnidirectional microphones placed in each ear at the entrance to the ear canal.

Figure 2-3: The Brüel and Kjær Head and Torso Simulator (HATS) Type 4100-D being used in a BRIR measurement of the Peter Kiewit Concert Hall at the Holland Performing Arts Center in Omaha, Nebraska.

The BRIR consists of both right and left channels, each including the effects of the sound source characteristics, the room, and the binaural head's torso, head shape, and pinnae. With a BRIR measurement, simple but highly plausible auralizations can be made for reproduction over headphones. The left and right ear channels of the BRIR can both be convolved with anechoic music, and the resulting left and right signals can be played over their respective headphone channels. Since the measurement includes the effects of the binaural head, the ILDs, ITDs, and spectral cues will be inherently included within the auralization, creating a spatially plausible reproduction. The main limitation of using a binaural head is that there can be a mismatch between the geometries of the binaural head and the individual listener's torso, head, and pinnae shapes. Although these shape differences might seem small, they can be quite different from person to person, creating the need for individually-tailored spatial hearing cues.

These specific cues can be determined for an individual through measuring an individualized Head-Related Transfer Function (HRTF). An HRTF for an individual consists of a database of measurements made from placing a source at a particular azimuth and elevation on a sphere, and recording the IR with probe microphones

placed at both of a listener's ears. Typically, an arc of loudspeakers is used to vary the elevation of measurement, and the listener's chair is rotated using a turntable to vary measurement azimuth. A typical HRTF measurement setup is shown in Figure 2-4. By taking these measurements aro0und every 5° in elevation and azimuth on a sphere, a complete database for all directions around a listener can be recorded. It has been found that when performing sound localization style tasks, using a non-individualized HRTF can lead to an increase in localization errors and cause internal localization issues, or to the perception of the sound source being inside a listener's head.[41] Thus, auralization made with an average HRTF might not be spatially accurate for every individual.

Figure 2-4: A head related transfer function measurement setup at the Department of Medical Physics and Acoustics at the University of Oldenburg. www.uni-oldenburg.de/en/acoustics/

With the potential difficulty in determining every individual's HRTF, another approach to auralization is to recreate the sound field, as opposed to just the pressures at a listener's ear drums, using an array of loudspeakers. The benefit of this approach is that a listener sitting within the array will naturally have their individualized HRTF applied to the signal, just as would happen if they were listening in a normal concert environment. More specifics on different loudspeaker

array-based auralization methods will be given in Section 2.2.3. A spherical microphone array can be used to acquire the information required for loudspeaker-based auralization methods through measurements.

The most simple and common measurement microphone that has gained traction in the recording world is the B-Format microphone. This type of microphone was originally invented by Gerzon, and was called the SoundField microphone.[42] B-Format microphones are now widely available since manufacturers have produced their own versions of the SoundField microphone, such as the TetraMic by Core Sound (Figure 2-5a). This microphone has the ability to extract up to first-order Ambisonic signals, which will be discussed in more detail in Section 2.3.2. Following the invention of the SoundField microphone are spherical microphone arrays with upwards of 32 microphone capsules, which can extract up to third or fourth order Ambisonic signals from IR measurements, providing a much higher degree of spatial accuracy and resolution. A commercially available spherical microphone array is the Eigenmike em32 by mhAcoustics, shown in Figure 2-5 b.


(a) (b)

Figure 2-5: (a) The TetraMic by Core Sound with a diameter of 13 mm and (b) the Eigenmike em32 by mh acoustics with a diameter of 84 mm.

### 2.2.2: Auralization from Room Simulation

Along with creating auralizations from room acoustics measurements, room acoustics simulation can also be used to create auralizations. Room acoustics simulation programs use various methods and algorithms to simulate the distribution and propagation of reflections within a room. These methods will be discussed in greater detail in Section 4.1. Based upon a specific source-receiver position with a room geometry, the program will calculate and predict the sound field experienced by a listener at a particular location. Many different commercially available room acoustics simulation software exist today such as Odeon,[43] CATT-Acoustic,[44] and EASE.[45] All of the programs are based on the same modeling fundamentals in order to simulate sound propagation within a room.

For each model, the user must supply a room geometry file, which defines the main surfaces of the room. For each surface, the user must also specify absorption and scattering information, which will impact how the reflections from each surface are modeled. Finally, the user must also specify source directivities. All of these elements are analogous to the previously mentioned considerations when measuring a RIR. The end result most often desired from a room acoustics computer model are parameter values for specific room acoustics metrics,[1] such as reverberation time (RT), or the IR of the room. These programs also have the built-in capability to create binaural auralizations, which are created by applying an average HRTF within the program to the RIR, resulting in a left and right channel BRIR. Since the model predicts the individual reflections, complete directional information of the sound field is known, with an infinite degree of directional fidelity. This fidelity depends upon the resolution of the reproduction technique (e.g. loudspeaker array or HRTF for headphone-based), so in practice, this infinite degree of resolution is not achievable.

Most programs allow the user to specify a built-in anechoic recording to use as the musical source, and the software will perform the convolution with the BRIR to create a final auralization. The main method of auralization from these computer models has been historically binaural, but since these programs calculate complete

directional information of individual reflections, many different auralization techniques can be used. For loudspeaker-based auralization, most computer programs provide Ambisonic signals as outputs by the way of multichannel .wav files. For example, Odeon has the capability to output B-format signals (first-order) or second-order Ambisonic signals. Although these software programs have the capability to output Ambisonic signals at even higher orders, often this information is not available. As well, to protect the computational algorithms, they do not provide any means for extracting the exactly simulated directions of arrival and time delays of each individual reflection in the model. This information is imperative when extending the simulations from a room acoustics model to a spatial reproduction method requiring more than second order Ambisonic signals.

Although it does not impact the present study, it should be mentioned that the major concern and issue with room acoustics modeling is the uncertainty and repeatability of results. Many different round robin tests have compared acoustical modeling results in terms of both different simulation programs and different individuals using the same program.[46-49] These studies have shown that significant differences exist between both computer modeling software and modeling across users. Additionally, research has also looked at the uncertainty associated with room acoustics modeling, based upon the uncertainty of the inputs into a room acoustics computer model, such as absorption coefficients.[50] Ultimately, it is important to note the limitations of room acoustical software in simulating results that precisely match physical space measurements.

### 2.2.3: Different Loudspeaker-Based Auralization Methods

As has been mentioned, auralization can be done over either headphones or using loudspeaker-based methods. Headphone-based reproduction is a fairly realistic, cost-effective way of producing auralizations, but limitations do exist. As was stated in Section 2.2.1, unless the HRTF of a subject is used in the binaural processing for the auralization, there are clear limitations in the realistic nature of headphone-based

auralization. Additionally, there are various loudspeaker methods that also employ binaural principles.

The main binaural loudspeaker-based method is cross-talk cancellation. In cross-talk cancellation, two loudspeakers are used, a left and right loudspeaker. The method begins with knowing the two different signals that need to be accurately reproduced at a listener's two ear drums. The left ear drum signal is filtered with the inverse of the Head-Related Impulse Response (HRIR) from the left loudspeaker to the left ear. This is repeated for the right ear and the right loudspeaker. Additionally, both the left and right loudspeakers will create cross-talk, producing sound at the opposite eardrum as well, not intended for the auralization. To remove the cross-talk, the left loudspeaker is also inverse filtered to remove the cross-talk between the left loudspeaker and the right ear. This same process is repeated for the right loudspeaker and the left ear. As long as the signals are presented in a dead room and the listener's ears remain in the correct locations, this method accurately reproduces the left and right signals at the respective eardrums. Although headphones are not used, it still suffers from the same limitations associated with non-individualized HRTFs.

Other loudspeaker-based methods, which are not binaural methods, can be split into two types: perceptually-based methods and physically-based methods. The first method relies mainly on accurately recreating the ITDs and ILDs which help to create correct localization for a listener, but it does not concern itself with recreating the physical wave phenomena or sound field. Examples of such methods include Vector-Base Amplitude Panning (VBAP)[51] and Spatial Decomposition Method (SDM).[52] Other approaches aim at recreating the physical sound field within the reproduction technique. The two most popular and well researched approaches to accomplish this are Wave Field Synthesis (WFS) and Near-Field Compensated Higher-Order Ambisonics (NFC-HOA).[53] From this point forward, Higher-Order Ambisonics (HOA) will be used to refer to near-field compensated higher-order Ambisonics.

When comparing different methods of sound field synthesis, there are multiple factors that play into classifying the effectiveness of different methods. Some of the key factors are mentioned below:[54]

- Timbral fidelity
- Spatial fidelity
- Listening area
- Spatialization parameters
- Number of loudspeakers
- Computational complexity

For the two physically-based methods, WFS and HOA, they can be best compared in terms of timbral fidelity, spatial fidelity, listening area, and number of loudspeakers. WFS is a method that is based upon the wave equation and the free-field Green's function.[55] For WFS, assuming a virtual source, Q, lying outside of a selected volume, V, a wave field, resulting from the source Q can be accurately reproduced within the volume V. This setup is shown in Figure 2-6. This method can be adapted to multiple sources, by simply using the principle of superposition. As well, WFS can be implemented using either 2-D or 3-D arrays. If secondary sources located on the boundary of volume V are driven by signals corresponding to the sound pressure and the directional pressure gradient resulting from the virtual source Q, as found at the locations on the boundary of the volume V, then the wave field within the volume V will be identical to the wave field produced by the virtual source, outside of V.[56] The pressure gradient can also be interpreted as a dipole type source's field, if the main axis of the dipole lies in the direction of the vector n, normal to the surface of V. (Figure 2-6) Thus, the acoustic field within V can be controlled by a sampling of both monopole and dipole-type sources on the surface of V. The sound field would be perfectly reconstructed if a continuous sampling of loudspeakers were used, but this ideal is impossible to realize in practice.

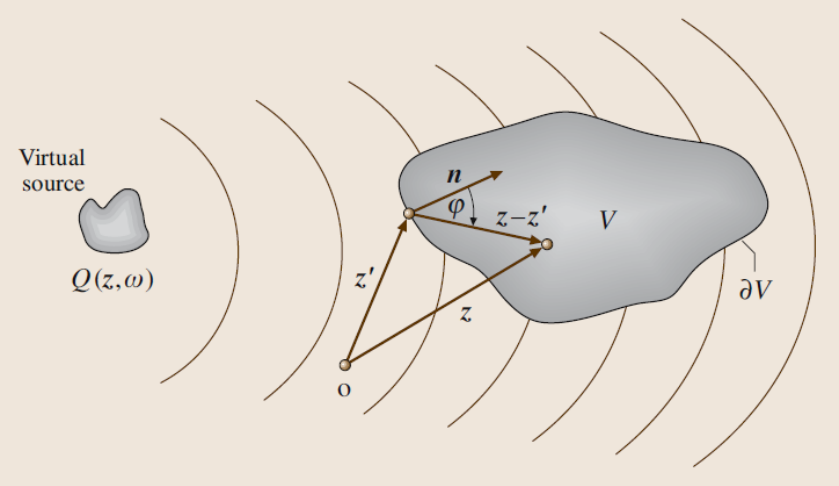


Figure 2-6: The generalized setup for fundamentals of WFS. From *Springer Handbook of Speech Processing*, Chapter 53, Figure 53.2, Rabenstein and Spors, 2008. Editors: Benesty, Sondhi, and Huang.[56]

Due to practical loudspeaker concerns, it is highly desirable to only use monopole-type sources in the theoretical framework, and not use dipole type sources. This is easy to do, and the only tradeoff is improper reproduction of the field outside of the volume, V. In effect, if only monopoles are used, the sound field outside of the volume is simply a mirror image of the inner sound field. As long as the reproduction is only concerned with the sound field inside of the array, the dipole sources can be removed from the processing. The main limitation of WFS results from the spatial sampling of the source distribution across the boundary of V. As a rule of thumb, the frequency at which the half wavelength is equal to the loudspeaker spacing is the highest frequency in which no coloration or increased localization errors will occur. To ensure reconstruction up to 20 kHz, a loudspeaker spacing of 1 cm would be required, which is physically impossible for practical considerations. Realistically, only spacings of around 15 – 20 cm can be achieved with physical loudspeakers. Figure 2-7 shows results from various experiments looking at the localization accuracy of WFS with various loudspeaker spacings for a linear 2-D array.[57] As can be seen, significant localization errors are found for 1.43 m and 0.41 m spacings, but at 0.2 m spacing, localization accuracy tends to be good.

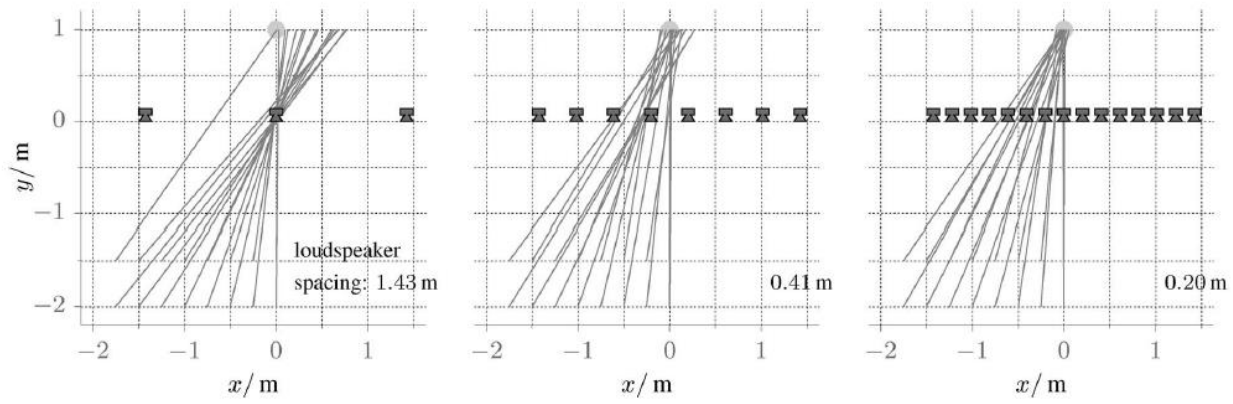


Figure 2-7; Results from localization testing of a WFS system, using a linear source distribution with various loudspeaker spacings. The image is taken from Figure 8 of Spatial Sound With Loudspeakers and Its Perception: A Review of the Current State, S. Spors 2013.[54]

For subjective sound field reconstruction, localization testing does not characterize the entire performance of the array. Even if a broadband type sound source can be correctly localized, it could exhibit very noticeable coloration artifacts, without degradation in localization. Studies have also been conducted where listeners were asked if there was a timbral difference between the reference and the stimulus.[58] All testing was done using binaural synthesis, to provide accurate comparison, and results in Figure 2-8 showed that spacings of 3 cm produced no timbral artifacts, but spacings of 0.12 m or greater produced noticeable timbral changes.

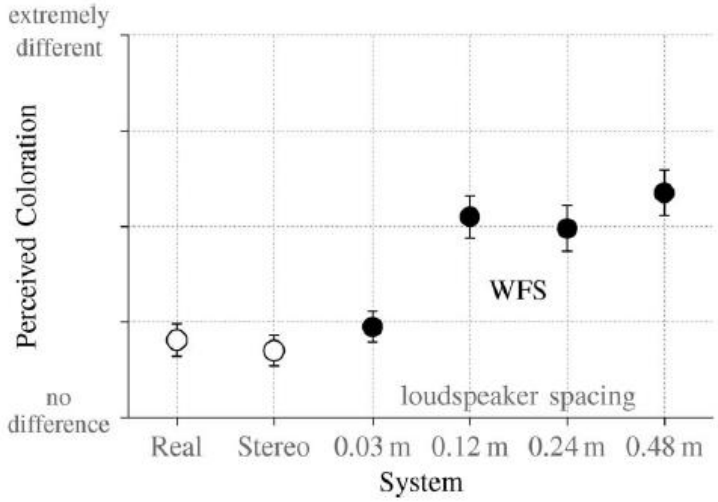


Figure 2-8: Results from an experiment conducted, asking listeners to rate the timbral differences between different WFS reproduction setups and a reference case (real). Image taken from Figure 9 of Spatial Sound With Loudspeakers and Its Perception: A Review of the Current State, S. Spors 2013.[54]

One of the primary benefits of WFS over HOA, which is discussed in the next section, is the fact that WFS recreates the desired sound field over a given volume or area. For applications which require multiple listeners or listening areas not simply limited to one location within the array, WFS is well suited. Other methods, such as HOA, focus the reproduction technique on a specific point within the array, which creates a 'sweet spot', whose size depends upon the loudspeaker array setup and the frequency under consideration. If on the other hand, it is suitable to simply recreate a sound field at one location, HOA could potentially be more suitable. For WFS, a very large number of loudspeakers is needed to realize the resolution and performance which has been discussed to this point. In addition, studies have shown that for similar loudspeaker setups, HOA will have a higher bandwidth of accurate reproduction than WFS at the center of the array, but with a sweet spot that decreases in size with increasing frequency. (Figure 2-9) Additionally, small artifacts after the initial sound in an IR being reproduced over the array are found with WFS. (Figure 2-10) The artifacts are not perceived as audible echoes, for they are occurring quite rapidly, and at a lower level than the initial sound. Despite their low level, they have still been found to produce perceptual differences to the reproduced sound field.

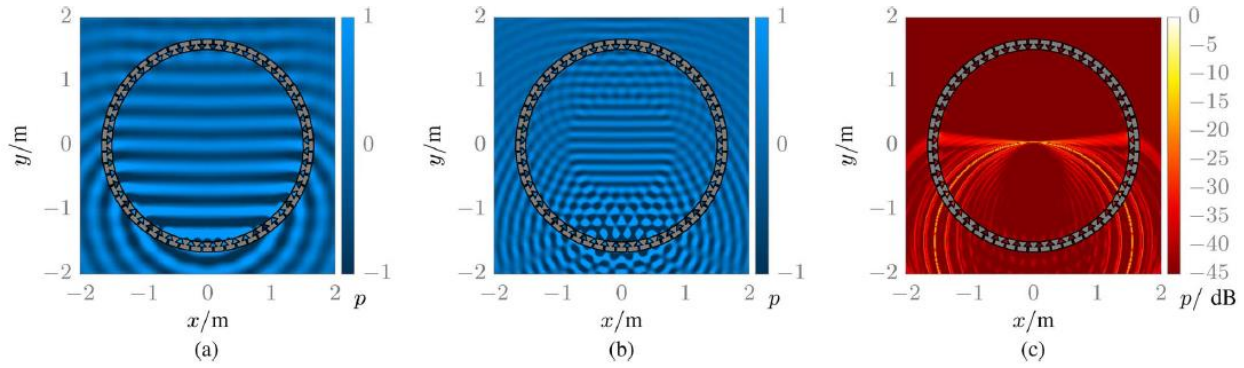


Figure 2-9: Simulations for a 56 element circular distribution using HOA. Shown are a 1 kHz plane wave (a), a 2 kHz plane wave (b), and an impulse response (c). Although the sweet spot is decreasing in size in (b) for a 2 kHz sound, it is still accurately reproducing the sound field at the center of the array. From Figure 5 of Spatial Sound With Loudspeakers and Its Perception: A Review of the Current State, S. Spors 2013.[54]

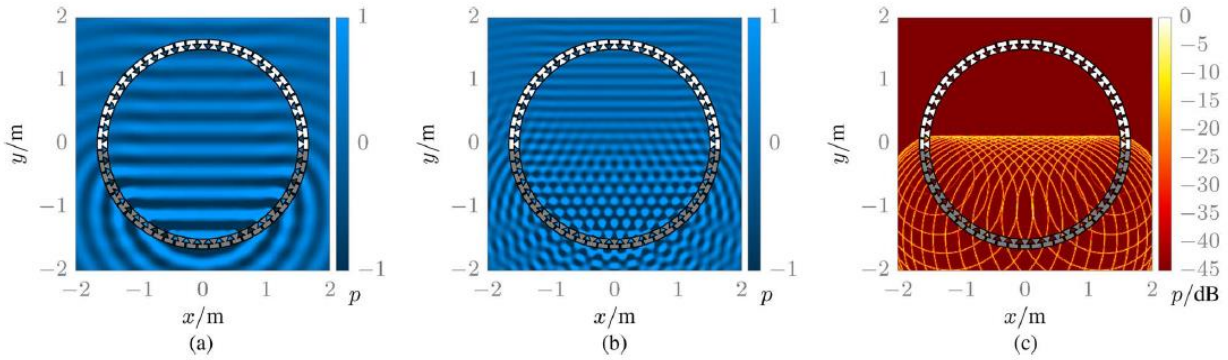


Figure 2-10: The same reproduction found in Figure 2-9, but now with a WFS system. The WFS system begins to break down much more drastically at 2 kHz, but it does not exhibit the same sweet-spot behavior like HOA. Also, the IR has a wake which follows the impulse sound, potentially creating spatial artifacts. From Figure 6 of Spatial Sound With Loudspeakers and Its Perception: A Review of the Current State, S. Spors 2013.[54]

Ultimately, it is not an easy task to compare sound reproduction techniques, because each method has different pros and cons, depending upon application type. HOA creates a very accurate reproduction of the sound field at one location in the array, and it requires a much lower number of loudspeakers, as compared to WFS. For the present application, the highest priority was accurately creating a wide-band sound field at least for one listener (but preferably more). Additionally, cost and space were both strong considerations. For these reasons, HOA was implemented into our loudspeaker array.

## 2.3: Ambisonics

For this study, Higher Order Ambisonics (HOA) was chosen as the reproduction method for various reasons. Ambisonics is a reproduction method which was first pioneered by Michael Gerzon back in the 1970's.[42] The fundamentals behind Ambisonic reproduction relies on breaking the sound field down into spherical harmonic components. Various important properties of spherical harmonics allow any sound field to be expressed as a weighted sum of spherical harmonic components. This sound field can then be reproduced over any arbitrary loudspeaker array, as long as careful signal processing steps are well-followed. Initially, Ambisonics was done using the zeroth and first order components, but it has now been extended into higher orders using HOA. The array can be arbitrary, but the layout of the array will impact

reproduction accuracy. Additionally, although Ambisonics was thought to be a reproduction of the sound field, this goal was not realized until near-field compensation was implemented into the processing.[55] Since the loudspeakers used in creating reproduction arrays are not always sufficiently far from a listener, corrections must be made to ensure the sound field is reproduced accurately.

Ambisonics is typically broken down into two steps: encoding and decoding. Encoding represents expressing a sound field from its spherical harmonic components. The decoding stage can be thought of as spatially sampling the encoded Ambisonic signals (spherical harmonic components) at the loudspeaker locations of the reproduction array. This section provides information on some of the basic concepts behind Ambisonics, and presents how the Ambisonic encoding and decoding is performed. First, the fundamental governing equations in the coordinate system common to HOA will be derived. Then, the basic concepts behind Ambisonics will be discussed including spherical harmonics, Ambisonics formats, and the extension to room acoustics simulation.

### 2.3.1: The Wave Equation in Spherical Coordinates

HOA begins from first considering the homogeneous wave equation:

$$\nabla^2 p = \frac{1}{c^2}\frac{\partial^2 p}{\partial t^2}. \qquad 2\text{-}10$$

The wave equation can be expressed in spherical coordinates, using the Laplacian of the spherical coordinate system defined in Figure 2-11, as:

$$\nabla p^2 = \frac{1}{r^2}\frac{\partial}{\partial r}\left(r^2\frac{\partial p}{\partial r}\right) + \frac{1}{r^2\cos\theta}\frac{\partial}{\partial \theta}\left(\cos\theta\frac{\partial p}{\partial \theta}\right) + \frac{1}{r^2\cos^2\theta}\frac{\partial^2 p}{\partial \varphi^2} = \frac{1}{c^2}\frac{\partial^2 p}{\partial t^2}. \qquad 2\text{-}11$$

The spherical coordinate system used in this study is one that is common to virtual acoustics and Ambisonics, where zero azimuth and zero elevations is defined by the

x-axis, called the look direction (the direction a listener would be looking). This deviates from the typical spherical coordinate system used in other areas of acoustics, where elevation is defined as the angle from the z axis. The resulting difference is that $\cos\theta$ is now used in equation 2-11 (instead of $\sin\theta$ for the other coordinate system), which results in using $\sin\theta$ as the variable for the associated Legendre polynomials, found in upcoming Eqn. 2-24.

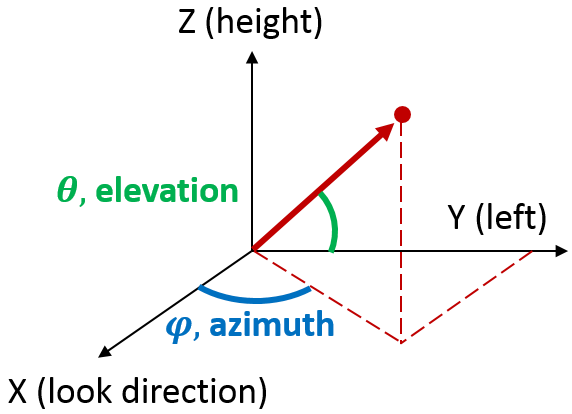


Figure 2-11: Coordinate axes used in this project for loudspeaker placement and Ambisonic processing. Note: this coordinate axes is NOT the same used in other fields of acoustics, but it is typical in the field of Ambisonics.

This equation can be solved by implementing the separation of variables technique.[59] First, it is assumed that the final solution can be in terms of four functions with time dependence, radial dependence, spatial dependence on azimuth, and spatial dependence on elevation:

$$p(r,\varphi,\theta,t) = R(r)\Psi(\varphi)\Theta(\theta)T(t)\,. \qquad 2\text{-}12$$

The time behavior and the spatial behavior can be separated from one another, by substituting Eqn. 2-12 into Eqn. 2-11 and carrying out the derivatives:

$$\frac{1}{r^2R}\frac{\partial}{\partial r}\left(r^2\frac{\partial R}{\partial r}\right)+\frac{1}{r^2\Theta\cos\theta}\frac{\partial}{\partial\theta}\left(\cos\theta\frac{\partial\Theta}{\partial\theta}\right)+\frac{1}{r^2\Psi\cos^2\theta}\frac{\partial^2\Psi}{\partial\varphi^2}=\frac{1}{c^2T}\frac{\partial^2T}{\partial t^2}=-k^2\,. \qquad 2\text{-}13$$

With the time and spatial behavior separated, both sides of Eqn. 2-13 must now be equal to a constant, which has been chosen as the negative of the square of the wavenumber, $k = {}^{\omega}/_{c}$, already shown. Now, isolating only the time behavior,

$$\frac{\partial^2 T}{\partial t^2} + \omega^2 T = 0\,. \qquad 2\text{-}14$$

With this result, our solution for $T(t)$ becomes

$$T(t) = Ae^{i\omega t} + Be^{-i\omega t}\,, \qquad 2\text{-}15$$

with A and B as constants of the complex exponentials. Next, the spatial behavior can be further separated from Eqn. 2-13:

$$\cos^2\theta\left[\frac{1}{R}\frac{\partial}{\partial r}\left(r^2\frac{\partial R}{\partial r}\right) + \frac{1}{\Theta\cos\theta}\frac{\partial}{\partial\theta}\left(\cos\theta\frac{\partial\Theta}{\partial\theta}\right) + k^2r^2\right] = -\frac{1}{\Psi}\frac{\partial^2\Psi}{\partial\varphi^2} = m^2\,. \qquad 2\text{-}16$$

Again, since the azimuthal behavior has been separated from the elevation and radial behavior, we can set both sides equal to a constant, which is chosen to be $m^2$, with $m$ corresponding to the degree of the spherical harmonics equation which will result from this analysis. From Eqn. 2-16, the azimuthal dependence can be isolated from the elevation and radial dependences:

$$\frac{\partial^2\Psi}{\partial\varphi^2} + m^2\Psi = 0\,, \qquad 2\text{-}17$$

which produces the result:

$$\Psi(\varphi) = F\cos(m\varphi) + G\sin(m\varphi)\,. \qquad 2\text{-}18$$

In order to make Ψ a periodic function, with period $2\pi$, $m$ must be limited to integer values. Finally, the dependence on elevation can be determined by separating the $r$ terms from the $\theta$ terms. This is taken from Eqn. 2-16, and results in:

$$\frac{1}{R}\frac{\partial}{\partial r}\left(r^2\frac{\partial R}{\partial r}\right)+k^2r^2=\frac{m^2}{\cos^2\theta}-\frac{1}{\Theta\cos\theta}\frac{\partial}{\partial\theta}\left(\cos\theta\frac{\partial\Theta}{\partial\theta}\right)=C\,. \qquad 2\text{-}19$$

Next, using the separation constant $C$, the dependence upon elevation from Eqn. 2-19 can be isolated:

$$\frac{1}{\cos\theta}\frac{\partial}{\partial\theta}\left(\cos\theta\frac{\partial\Theta}{\partial\theta}\right)+\left(C-\frac{m^2}{\cos^2\theta}\right)\Theta=0\,, \qquad 2\text{-}20$$

and letting,

$$x=\sin\theta \quad \text{so that} \quad \frac{d}{d\theta}=\cos\theta\frac{d}{dx}\,, \qquad 2\text{-}21\text{: a,b}$$

Eqn. 2-21 can be substituted into Eqn. 2-20, and the following relationship is found:

$$(1-x^2)\frac{d^2\Theta(\mathrm{x})}{dx^2}-2x\frac{d\Theta(\mathrm{x})}{dx}+\left(C-\frac{m^2}{1-x^2}\right)\Theta(x)=0\,. \qquad 2\text{-}22$$

Eqn. 2-22 is called the associated Legendre equation, and it will have bounded solutions only if $C=l(l+1)$. With this specification, the following equation results:

$$(1-x^2)\frac{d^2\Theta(\mathrm{x})}{dx^2}-2x\frac{d\Theta(\mathrm{x})}{dx}+\left(l(l+1)-\frac{m^2}{1-x^2}\right)\Theta(x)=0\,. \qquad 2\text{-}23$$

The solutions to Eqn. 2-23 are called associated Legendre polynomials of order $l$ and degree $m$:

$$\Theta(x)=P_l^m(x) \quad \text{or} \quad \Theta(\theta)=P_l^m(\sin\theta)\,. \qquad 2\text{-}24$$

Finally, the radial component can be isolated from Eqn. 2-19, and with some algebraic manipulation,

$$\frac{\partial}{\partial r}\left(r^2\frac{\partial R}{\partial r}\right)+(k^2r^2-C)R=0\,. \tag{2-25}$$

Once the derivative term is expanded, and the term $C=l(l+1)$ is substituted into Eqn. 2-25, we are left with:

$$\frac{\partial^2 R}{\partial r^2}+\frac{2}{r}\frac{\partial R}{\partial r}+\left(k^2-\frac{l(l+1)}{r^2}\right)R=0\,. \tag{2-26}$$

$$R(r)=\begin{cases}h_n^{(1)}(kr)\\ h_n^{(2)}(kr)\end{cases} \tag{2-27}$$

Eqn. 2-26 is also the spherical Bessel equation, whose solutions are spherical Hankel functions, in Eqn. 2-27. Now, combining all of the individual solutions from the separation of variables, we can represent the pressure in Eqn. 2-28, using eqns. 2-12, 2-15, 2-18, 2-24, and 2-27.

$$p(r,\varphi,\theta,t)=\sum_{l=0}\sum_{m=0}A_{m,n}\begin{Bmatrix}e^{i\omega t}\\ e^{-i\omega t}\end{Bmatrix}\begin{Bmatrix}h_n^{(1)}(kr)\\ h_n^{(2)}(kr)\end{Bmatrix}\begin{Bmatrix}\cos(m\varphi)\\ \sin(m\varphi)\end{Bmatrix}P_l^m(\sin\theta) \tag{2-28}$$

By selecting the $e^{j\omega t}$ time convention, and thus choosing the Hankel function of the first kind, corresponding to inward travelling spherical waves:

$$p(r,\varphi,\theta,t)=\sum_{l=0}\sum_{m=0}A_{m,n}e^{i\omega t}h_n^{(1)}(kr)\begin{Bmatrix}\cos(m\varphi)\\ \sin(m\varphi)\end{Bmatrix}P_l^m(\sin\theta) \tag{2-29}$$

This result is the final solution for both outward traveling and inward traveling waves for the spherical coordinate system from Figure 2-11. Again, this coordinate system is not the same as the typically accepted system in other areas of acoustics.

### 2.3.2: Spherical Harmonics

We can also isolate the directional dependence from both azimuth and elevation from Eqn. 2-28. This angular dependence results in the definition of real-valued spherical harmonics,[60]

$$Y_l^m(\varphi,\theta) = N_l^{|m|} P_l^{|m|}(\sin\theta) \begin{cases} \sin(|m|\varphi) & \text{for} \quad m < 0 \\ \cos(|m|\varphi) & \text{for} \quad m \geq 0 \end{cases}, \tag{2-30}$$

$$N_l^{|m|} = \sqrt{\frac{2-\delta_m}{4\pi}\frac{(l-|m|)!}{(l+|m|)!}}, \tag{2-31}$$

$$\delta_m = \begin{cases} 1 & for \quad m = 0 \\ 0 & for \quad m \neq 0 \end{cases}. \tag{2-32}$$

The variable $l$ corresponds to the spherical harmonic order, and the variable $m$ indicates the degree of the spherical harmonic function, which is comprised of integers such that $-n \leq m \leq n$. Additionally, a normalization term, $N_l^{|m|}$, has been added to the relationship. The key aspect of spherical harmonics, which allows them to be used to represent any arbitrary sound field, is their orthogonality.[42] Two functions, $f(\varphi,\theta)$ and $g(\varphi,\theta)$ on the unit sphere are said to be orthogonal if the following holds true,

$$\int f(\varphi,\theta)^* g(\varphi,\theta)\, d\varphi\, d\theta = 0\,, \tag{2-33}$$

where the * implies taking the complex conjugate of a function. The word equivalent of this expression can be stated as well. Considering the energy sums of both functions

$f(\varphi,\theta)$ and $g(\varphi,\theta)$, if both functions are orthogonal, the total energy of the sum of both functions will be equivalent to the sum of the individual total energy in each function. Informally, it means that there is no 'sharing' of energy between spherical harmonic components. Another property which spherical harmonics can possess is orthonormality. Orthonormality occurs if the spherical harmonics are properly normalized, but this property is not required for Ambisonics, and debate still exists over which ways the functions should be normalized. Some semi-normalized forms exist, but these do not exhibit the property of orthonormality. For Ambisonics, the normalization scheme is chosen based upon convenience for audio formats, rather than preserving orthonormality. This study implemented one of those Ambisonics formats, described in Section 2.3.3.

Some other interesting properties of spherical harmonics are noted by Gerzon[42] and provided below:

1. The effect of rotating an $l^{th}$ order spherical harmonic is to obtain another $l^{th}$ order spherical harmonic.
2. Any linear combination of $l^{th}$ order spherical harmonics results in another $l^{th}$ order spherical harmonic. All $l^{th}$ order spherical harmonics may be expressed as a linear combination of rotated versions of any particular non-zero $l^{th}$ order spherical harmonic.
3. Any function on a sphere is expressible, in a unique manner, as the sum of a $0^{th}$ order spherical harmonic, a $1^{st}$ order spherical harmonic, a $2^{nd}$ order spherical harmonic, …, an $l^{th}$ order spherical harmonic, …
4. The number of linearly independent $l^{th}$ order spherical harmonics is $2l+1$, which means any $l^{th}$ order spherical harmonic can be expressed as a linear combination of $2l+1$ specified $l^{th}$ order spherical harmonics.

The third point is the key point that makes spherical harmonics highly useful in expressing sound fields. Taking only the directional dependence from Eqn. 2-28, provided in Eqn. 2-30, any function defined on the surface of a sphere, which in this

case is a sound field, can be expressed as the weighted sum of its spherical harmonic components:

$$p(\varphi,\theta) = \sum_{l=0}^{\infty} \sum_{m=-l}^{l} A_{m,n}\, Y_l^m(\varphi,\theta)\,. \qquad 2\text{-}34$$

### 2.3.3: Ambisonics Formats

In Eqn. 2-30, the spherical harmonics function is shown using the ambiX suggested Ambisonics format.[60] Many different Ambisonics formats exist; the disagreements between formats come from the five following questions:

1. What type of normalization scheme should be used?
2. How should the channels be ordered?
3. Should the Condon-Shortly phase term be included?
4. What variables should represent the order and degree of the harmonics?
5. What data container should be used?

For this study, only the first four questions are of strong importance, for the Ambisonics reproductions are not currently being made available to the public in a common data container. For the ambiX format, the SN3D normalization scheme is used. This scheme does not perform complete normalization, which would ensure that integrating each harmonic over a sphere would result in an answer of 1. These are semi-normalized, where SN3D normalization is used to ensure that as higher order Ambisonic orders are used, no clipping will take place. Furse-Malham normalization creates an orthonormal set of spherical harmonics, but it results in potential clipping of higher order harmonics. For this reason, although the debate is still ongoing, it appears that using the SN3D normalization is most favorable.

Additionally, the Condon-Shortley phase term, a factor of -1 multiplied by the odd order spherical harmonics, is omitted in the ambiX format for simplicity. This term is commonly used in the quantum mechanics literature. Finally, the channels are

ordered using the Ambisonic Channel Numbering (ACN) scheme, which is defined using the indices from the spherical harmonics equation, $m\ and\ l$:

$$ACN = l^2 + l + m\,. \qquad 2\text{-}35$$

With this framework outlined, the current study implemented the Ambisonic processing using the ambiX suggested format (SN3D normalization & ACN ordering), with the coordinate axis from Figure 2-11, for up to third-order spherical harmonic processing. Figure 2-12 shows up to the third-order spherical harmonic components, using these formats. Indices, $m\ and\ l$, are shown on the figure corresponding to each spherical harmonic component. Additionally, Figure 2-13 provides the same graphic, but with numbering shown which corresponds to the ACN ordering scheme, and the Furse-Malham numbering scheme. As can be seen, the ACN method appears much more logically intuitive, and can easily be extended to higher order signals in an algorithmic fashion, from Eqn. 2-35. Since Furse-Malham ordering uses letters as indices, it can only be used up to forth order. After fourth order, the number of spherical harmonics will exceed the number of letters within the alphabet, creating an undesirable limitation to this scheme.

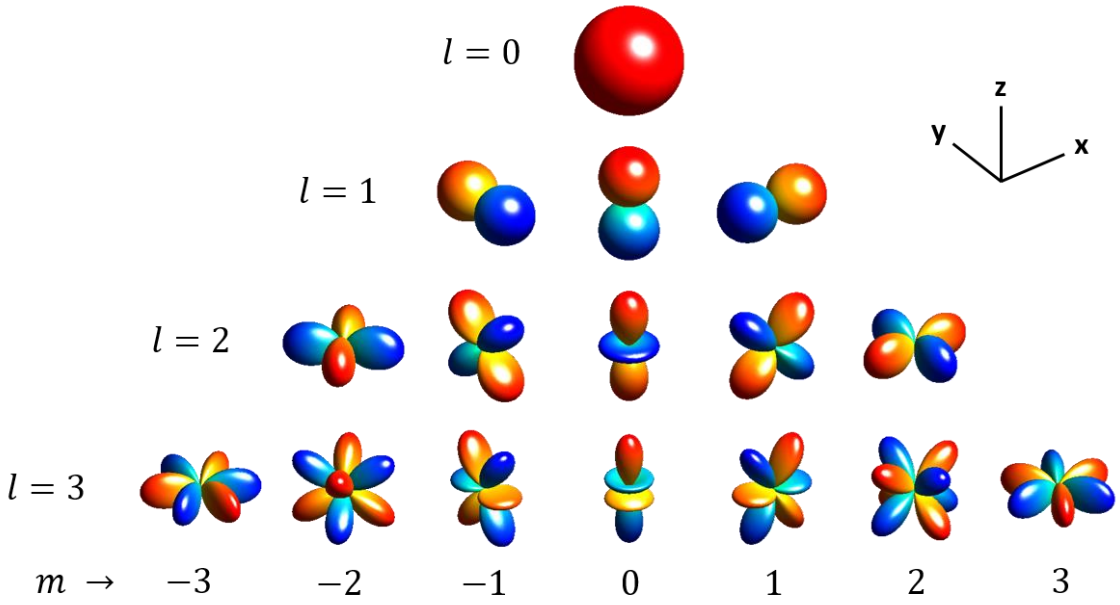


Figure 2-12: Real spherical harmonics, up to the third-order, showing order index (l) and degree (m). The coordinate axis is also provided. Red and blue correspond to a positive and a negative number, respectively.

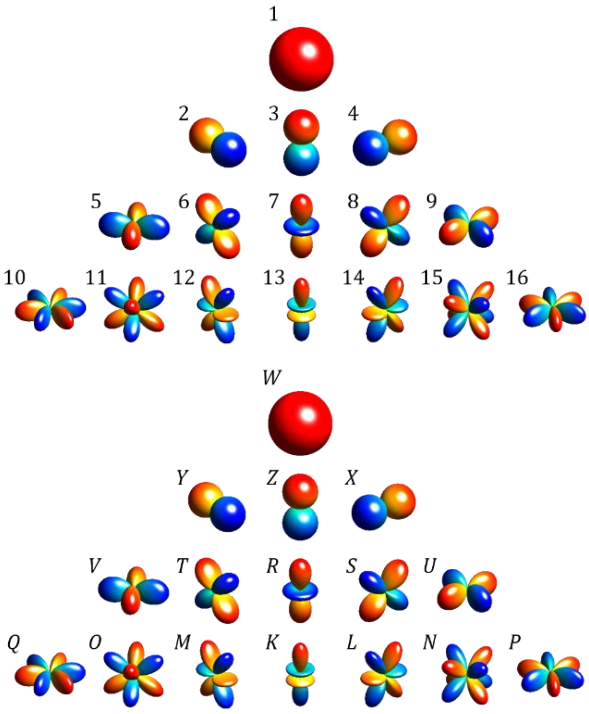


Figure 2-13: A visual representation of the Ambisonic Channel Numbering (ACN) scheme (left) used from the ambiX format and the Furse-Malham numbering scheme (right). The Furse-Malham scheme is limited to only fourth-order spherical harmonics, since the number of Ambisonic components exceeds the number of available letters. Red and blue correspond to positive and negative numbers, respectively.

### 2.3.4: Ambisonics & Room Acoustics Simulation

Ambisonics has been successfully used in auralization for both room acoustics simulations and measurements made using spherical microphone arrays.[61] From spherical microphone array IRs, the extraction of the spherical harmonic sound field components can be quite straightforward. Using a spatial Fourier transform, spherical harmonic components can be extracted from the microphone array, as long as the microphone's number of elements equals or exceeds the number of spherical harmonic components for a particular order and the spatial sampling scheme preserves the orthogonality property of the spherical harmonics. In practice, the diameter of the physical microphone and the spatial aliasing due to microphone element spacing also limits the usable frequency range of the microphone, even if it contains an adequate number of elements.

When performing room acoustic simulation, some assumptions must be made about the sound field. Typically, room acoustic simulation implementing geometrical acoustics will output information about the timing, level, and direction of arrival of individual reflections. In order to determine how the overall sound field can be converted into spherical harmonic components, the radiation of each individual reflection is assumed to follow quasi-plane wave behavior, since the sources are at large distances from the receiver. With this assumption, the individual reflections (considered as far-field sources) with amplitude $S$ from direction $(\varphi, \theta)$ can be encoded into their Ambisonic signals, $B_l^m$:

$$B_l^m = S\, Y_l^m(\varphi, \theta)\,. \qquad 2\text{-}36$$

Since the sound field is being simulated, in effect, up to infinite order spherical harmonic components of the source, $B_l^m$, could be simulated if desired. In room acoustics, the direct and reflected sound energy is typically far from the original source when it reaches the receiver, and the sound field can be approximated by a sum of plane waves. Using this plane wave assumption, a source $S$ can be encoded into its Ambisonic signals by applying the real gains which result from the spherical

harmonics equation. Based upon its time delay, the reflection is populated into Ambisonic IRs, corresponding to each spherical harmonic component. This step would be repeated for every reflection in the simulation. The process of encoding reflections into spherical harmonic components can be found in Section 4.2.5. Up to third-order spherical harmonics were used for this study, based upon the maximum order of the Ambisonic decoder. Eqn. 2-30 was individually solved for each of the 16 third-order Ambisonic components, and the solutions can be found in Appendix D. These functions are provided for convenience, with the correct coordinate axis, using only sine and cosine functions. Also, the second half of Appendix D provides the same functions, but using the more conventional coordinate axes for other areas of acoustics.

### 2.3.5: Ambisonic Decoding and Near-Field Compensation

After the Ambisonic signals have been extracted from the sound field, the signals are then decoded into loudspeaker signals, which can be used to reproduce sound fields. The decoder can be thought of in three separate steps:

1. A decoding matrix, matched to the geometry of the loudspeaker array. This includes time delay and level compensation for non-spherical distributions.
2. Phase-matched cross-over filters, for use of a dual-band decoder.
3. Near-field compensation filters, correcting for the reactive component of the sound field from individual loudspeakers.

First, a decoding matrix must be used, to match the Ambisonic signals to the specific locations of loudspeakers used for the array. The array must contain at least the same number of loudspeakers as there are Ambisonic components, which is $(l+1)^2$. In effect, the decoding matrix spatially samples the spherical harmonic components, matching them to the chosen loudspeaker locations. Thus, the reproduction will achieve its highest possible accuracy with an even loudspeaker distribution. Many different optimization techniques on decoder design can be used, impacting the usable frequency range of implementation.

In spatial hearing, as was discussed in Section 2.2.1, ITD's and ILD's dominate a human listener's localization. Since ILD's are very small at low frequencies, where the wavelength of sound is larger than the human head, the ITD is the dominant cue. At high frequencies, where the ILD is quite dramatic between ears, it becomes the dominant cue for localization performance. Gerzon identified two metrics, the velocity localization vector ($r_v$) and the energy localization vector ($r_e$) which both represent the primary theories behind auditory localization. Looking at these metrics, $r_e$ corresponds to the ILD and $r_v$ corresponds to the ITD. The direction of each vector predicts auditory localization, and the magnitude of each vector, reaching a maximum value of 1, will indicate the quality of the localization. Ideally, these vectors will point in the same direction, both achieving a value of 1, but this ideal is not realizable in practice.

The next component in the decoder are the cross-over filters. This is implemented if a dual band decoder is used for Ambisonic processing. With the competing problems for high and low frequency decoders, good decoder design practice will require two decoders to be designed, one for high and one for low frequencies.[62-63] A decoder is developed for low frequencies, where $r_v$ is ensured to be close to 1 for all frequencies in the optimization of the decoder. Then for mid frequencies, the decoder is designed so that $r_v$ and $r_e$ are always pointing in the same direction for all azimuths and elevations. Finally, at high frequencies, the decoder is optimized such that $r_e$ is maximized across as much of the sphere as possible. Since these criterion are often conflicting and frequency dependent, a dual band decoder is useful.

The cross-over filters are built into each separate decoder, such that the two outputs of the decoders can be added together, for the final reproduction, with split decoding characteristics for low and high frequencies. This helps create the best spatial localization in the decoding process. This concept is analogous to using a cross-over in a two-way loudspeaker. The designer must ensure that the decoder cross-over filters are phase-matched, to prevent unmatched phase characteristic between the decoders, creating a sense of 'phasiness'.[63]

Finally, near-field compensation must be included to ensure that the array is recreating the physical sound field at the center of the array. The exact decoder matrix is constructed assuming that loudspeakers are infinitely far away from the listener within the array. As long as the loudspeakers are at an adequate distance away, the assumption holds. A problem results at low frequencies, where wavelengths are long, and the far-field source assumption for reproduction loudspeakers is not achievable. In the near-field, a reactive, imaginary component from the loudspeakers will be present. In effect, this phenomenon will cause a bass-boosting, very similar to the proximity effect experienced when using directional microphones.[63] To compensate for this bass-boost, a high-pass filter is used, which is applied to the low frequency velocity decoder signals. This is what is referred to as near-field compensation (sometimes called distance compensation).[53] Section 4.2.6 also describes the various tools used to assist in efficiently designing the decoder for this study's loudspeaker array.

# Chapter 3: The AUralization and Reproduction of Acoustic Sound-fields (AURAS) Facility

In order to recreate sound fields which can be presented to listeners for subjective testing in concert hall acoustics, the Auralization and Reproduction of Acoustic Sound-fields (AURAS) facility was created. In its design, the following requirements were considered highly important:

- At least than 16 loudspeakers to reach third-order Ambisonic reproduction
- Two subwoofers to produce low frequency energy
- Even distribution of azimuth & elevation placement of loudspeakers
- Flat frequency response of loudspeakers for listener at the center of the array
- Loudspeaker placement in a fixed, repeatable location
- Easy removal of loudspeakers to preserve use of room as anechoic chamber
- Hardware providing flexible, individual control of each loudspeaker
- Interface for subjects to interact with and rate concert hall acoustic stimuli
- Reliable use with easy implementation for undergraduate & graduate students

With these constraints in mind, the 32 channel AURAS loudspeaker array was setup within the anechoic camber in room 30 of the Hammond Building on the University Park campus of The Pennsylvania State University. This anechoic chamber is used in cooperation with the Center for Acoustics and Vibration (CAV). For the loudspeaker array, 30 two-way loudspeakers and two subwoofers were built and installed in the anechoic chamber. This chapter describe the construction of the loudspeakers, details on the anechoic evaluation of the room, and specifics on the hardware and control.

## 3.1: Loudspeaker Design and Construction

Section 3.1 will cover all of the design specifications and guidelines for the construction of the two-way loudspeakers for the AURAS facility. An overview of the design problem is given, and the design and construction of the loudspeakers is

summarized. The topics covered include driver selection, enclosure and crossover design, construction, validation, and subwoofer design.

### 3.1.1: Loudspeaker Driver Selection

When considering loudspeaker design, a few considerations were set as priorities for the present application. The three most imperative design criteria were frequency range, frequency response shape, and the size of the individual loudspeakers. For the loudspeakers, the main goal was to reproduce the desired signal, at the desired location, over as wide a frequency range as possible. As well, the array was constructed within an anechoic chamber in order to minimize the effects of the listening room upon the recreated sound field, so it was desirable to make the loudspeakers as compact as possible. Reflections will occur between loudspeakers in the room, but by making the loudspeakers as small as possible, these artifacts can be minimized. With these criteria in mind, the design selected was that of a two-way, sealed-box loudspeaker. Although a ported-box enclosure would help to increase the low frequency performance of the loudspeaker, it requires a much higher enclosure volume. The sealed-box enclosure allows for a boost in low frequency performance, while maintaining a compact design.

Another common consideration in loudspeaker design is the off-axis directionality of the loudspeaker. Since the loudspeakers in the final setup are oriented towards the listener, the on-axis frequency response was the main concern. An additional intermediate driver in between the size of the tweeter and woofer could have been used to allow more omnidirectional behavior of the loudspeaker. In the end, the additional cost of building a three-way loudspeaker, considering both money and size, led us to stay with the two-way option. For driver selection, the target was to select a woofer and tweeter which had similar sensitivities, and a combined flat frequency response from around 100 Hz to 20,000 Hz. When selecting the woofer, drivers with a lower compliance equivalent volume were preferred, helping to ensure a compact design. Ultimately, the TangBand W4-1720 4” (10.16 cm) mid-bass driver and the TangBand 25-1166SJ 1” (2.54 cm) neodymium fabric dome tweeter were selected.

Both the woofer and tweeter had the same nominal impedance, similar sensitivities, and could produce the desired frequency response characteristics with a relatively low equivalent volume requirement. The advertised frequency response graphs from the manufacturer, along with pictures of the driver are shown in Figure 3-1. The technical specification sheets for these drivers are provided in Appendix A.


Figure 3-1: Images and advertised frequency responses of the Tang Band W4-1720 4" mid-bass driver (left), and the Tang Band 1" 25-1166SJ Neodymium tweeter (right).

### 3.1.2: Loudspeaker Enclosure and Crossover Design

With the woofer and tweeter selected, the final stage in the loudspeaker design was to design the enclosure and test and design a passive cross-over and L-pad (a combination of resistors, used to lower driver sensitivity). Using a closed box loudspeaker design with heavy fill, and targeting a value of 0.707 for the quality factor of the low frequency roll-off, $Q_{tc}$, a final physical design volume was found to be 2.1 liters (2100 $cm^3$). Accounting for the physical volume of the woofer and tweeter within the box, the final design of the loudspeaker was determined. It was constructed out of 0.75" (1.91 cm) plywood, with outer dimensions 6.5" (16.51 cm) width x 10" (25.40 cm) height x 6" (15.24 cm) depth. Cutouts for the driver and tweeter

were routed into the plywood, so that the faces of the drivers could be flush-mounted with the face of the enclosure. Additionally, the cutout for the woofer was routed on the interior of the box, to ensure that an adequate opening between the magnet of the woofer and the enclosure was provided, preventing any potential turbulent air-rushing type noise.

Next, the passive crossover and various L-pad configurations were tested in the designed loudspeaker enclosure. An initial test enclosure was built, and the woofer and tweeter were temporarily sealed into the enclosure using Mortite (removable caulking). Wires from the tweeter and woofer terminals were run through a small hole drilled in the back of the enclosure, and the hole was again sealed with Mortite. The drivers installed within the test enclosure, with the assembly placed in the anechoic chamber, can be seen in Figure 3-2.

Figure 3-2: Test enclosure used to test various crossover and L-Pad design options.

Second order high and low pass filters were designed for a crossover frequency of 1.8 kHz, and an L-pad was used to match the sensitivity of the tweeter down to that of the woofer. The diagram in Figure 3-3 shows the setup of the passive crossover and L-Pad for the loudspeaker:[64]

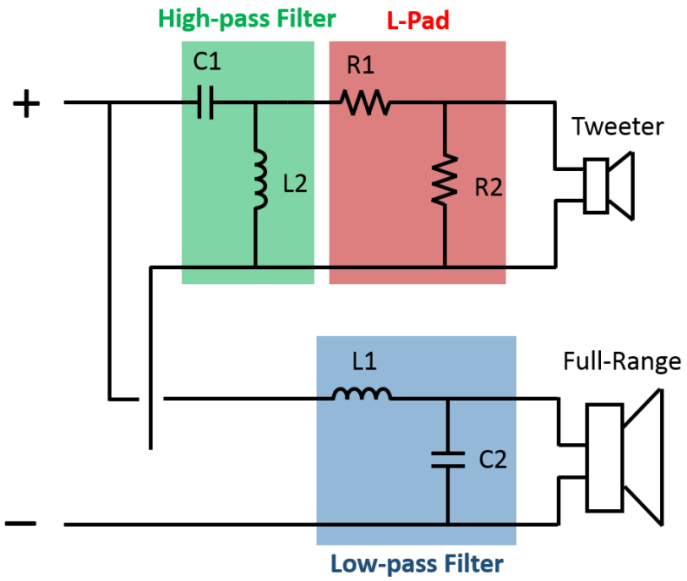


Figure 3-3: Diagram of the selected crossover and L-pad design.

To ensure the sensitivities were best matched, various combinations of resistors in the L-pad were tested in-situ using an IR measurement. The IR measurement program EASERA[45] was used to measure IRs for the loudspeaker for the different L-pad combinations shown in Figure 3-4 below. Ultimately, the final combination of a 3 Ohm resistor in series with the tweeter and a 2 Ohm resistor in parallel with the tweeter was chosen, for it produced the best overall matched sensitivity between the woofer and tweeter.

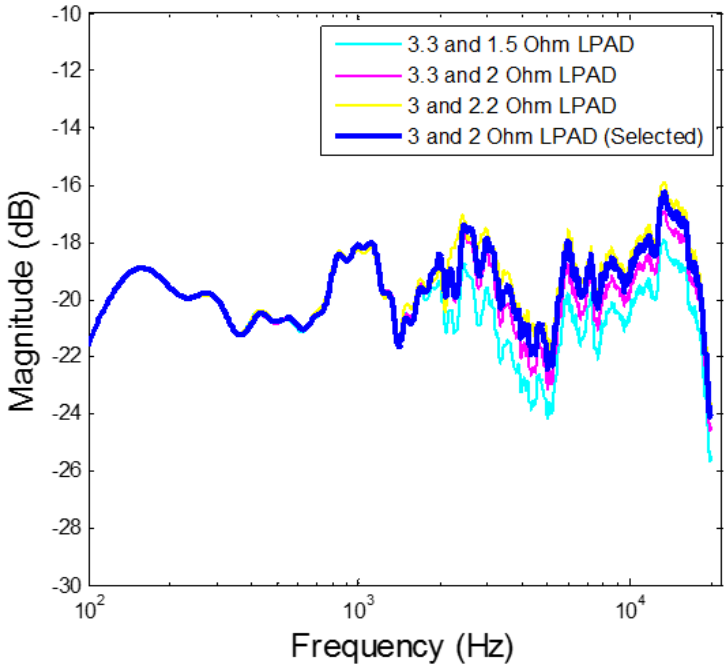


Figure 3-4: Frequency response measurements for the different L-pad configurations, measured with the drivers installed in the test enclosure.

With the final L-Pad selected, the following values were used for the final crossover design, in reference to the diagram in Figure 3-3.

$$C_1 = 15.0\ \mu F$$

$$C_2 = 5.1\ \mu F$$

$$L_1 = 1.5\ mH$$

$$L_2 = 0.5\ mH$$

$$R_1 = 3.0\ \Omega$$

$$R_2 = 2.0\ \Omega$$

As can also be seen in Figure 3-4, the final loudspeaker design resulted in a relatively flat frequency response, within ± 4 dB of a flat response. To further improve the response, digital equalization is performed on the auralization signals sent to the installed loudspeakers, so the non-flat behavior of each individual loudspeaker is compensated for using FIR filters.

### 3.1.3: Final Construction and Loudspeaker Performance Testing

With the loudspeaker design finalized, the final set of 30 loudspeakers were built. A photograph of the construction process is shown in Figure 3-5. A photograph of the final enclosure design, showing the internal wiring and soldered components of the passive crossover and L-pad can be seen in Figure 3-6. All of the enclosures were painted with a black hammered Rust-Oleum finish to provide a professional and uniform end product.

Figure 3-5: A picture of the loudspeaker construction process in the amazing workshop of Andrew Coward!

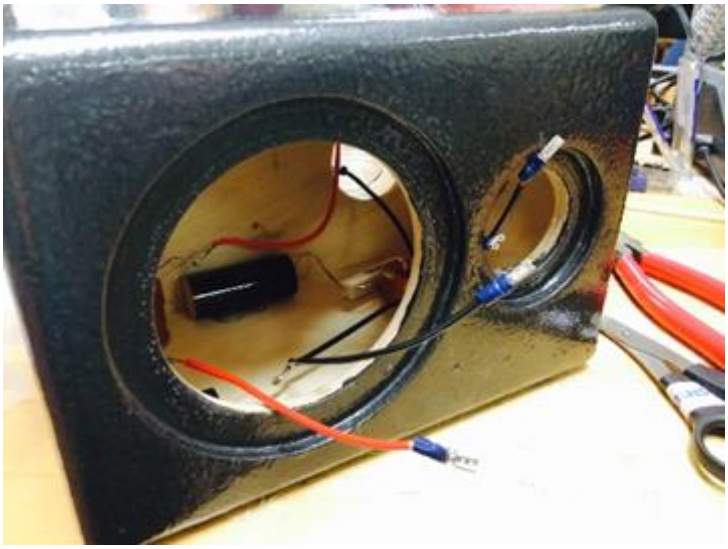

Figure 3-6: Photograph of the finished enclosure for the loudspeaker, showing internal wiring for the passive crossover and L-Pad.

To validate the performance of our loudspeaker, a side by side comparison of the IR of our loudspeaker and a Genelec 8030B was conducted. The 8030B was chosen for comparison, for it is known to exhibit one of the flattest frequency responses of any compact studio grade monitor loudspeaker. The 8030B is also a two-way loudspeaker, and it has a ported enclosure with a 5" (12.7 cm) woofer and a 0.75" (1.91 cm) tweeter. This loudspeaker is often used in virtual acoustics applications, for it has a very flat on-axis frequency response over a large frequency range. The Genelec retails at around $800.00, so the cost is still quite high for an application where many loudspeakers are needed.

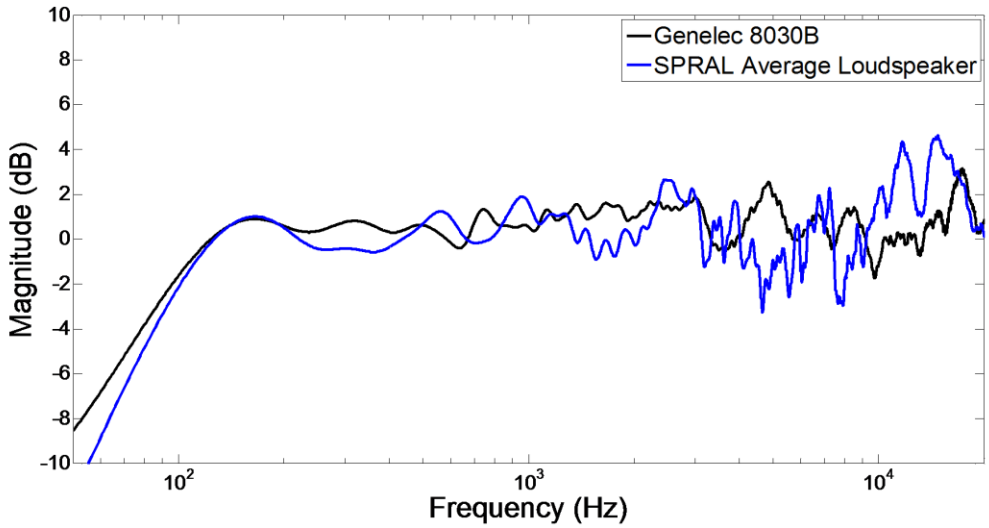


Figure 3-7: Comparison of the Genelec 8030B loudspeaker with the constructed loudspeaker.

As shown in Figure 3-7, the Genelec does perform slightly better, with a ± 2 dB response from around 100 Hz up to 20,000 Hz. Despite the larger deviations, the differences will not be very noticeable or even considerable, since both loudspeakers can be digitally equalized to improve performance. The loudspeaker for this project was not only more compact than the Genelec 8030B, it also cost only around $150.00, including multichannel amplifier costs since the constructed loudspeakers were unpowered. Given the significant cost savings and the additional effort and wiring required to run power to each of 30 powered Genelec loudspeakers in the anechoic chamber, the decision to use custom loudspeakers was a much more cost-effective choice and a better overall solution. Pictures of the final loudspeaker design can be seen below in Figure 3-8 and Figure 3-9.

Figure 3-8: Final construction and finishing of an individual loudspeaker. The physical center between the mid-bass driver and tweeter is indicated by a red dot.

Figure 3-9: Final photo of all 30 loudspeakers, constructed, soldered, and completed!

### 3.1.4: Subwoofer Design.

Additionally, two subwoofers were built to be installed in two corners of the anechoic chamber. The subwoofers were designed by selecting a driver that provided sufficient output power, with as small of a compliance equivalent volume as possible for a sealed-box design. With this requirement, the Tang Band W8-2022 8" (20.32 cm) subwoofer was purchased. It required an extremely low physical design volume of just 6 liters (6000 $cm^3$), when assuming a sealed-box with heavy fill, and with a target value of $Q_{tc} = 0.707$ for the quality factor of the low frequency roll-off. The final subwoofers were built in a similar manner to the loudspeakers, but the outer

enclosure measured 11” (27.94 cm) width x 11” (27.94 cm) height x 6” (15.24 cm) depth A completed subwoofer is shown in Figure 3-10. These two subwoofers were not used for the study presented in this thesis, but the individual loudspeakers were equalized to have a flat frequency response down to 60 Hz, which will provide the necessary low frequency performance for future studies using concert hall auralizations.

Figure 3-10: A completed view of one of the two subwoofers constructed for the anechoic chamber.

## 3.2: Chamber Setup, Design, and Evaluation

This next section highlights how the constructed loudspeakers were installed and implemented within the anechoic chamber in the Hammond Building. Details will be given on the development process of the AURAS facility after the loudspeakers were constructed. Topics that are covered include loudspeaker layout, mounting considerations, signal routing, room characterization, hardware and software control, and a summary of the final facility and its performance.

### 3.2.1: Loudspeaker Layout

Along with the loudspeaker design and room considerations, the loudspeaker layout is an important consideration. Loudspeaker placement and number is highly dependent upon the type of virtual acoustic reproduction which is implemented. The selected method in this study, Ambisonics, has the main requirement of providing as even a distribution of loudspeakers as possible. Ideally, a continuous distribution of

sound sources across a sphere would be used. Due to practical constraints, including space and cost, this ideal is never fully realized. The benefit of Ambisonics is that it can be flexibly extended to any arbitrary loudspeaker arrangement through intelligent design of the Ambisonic decoder. Despite this flexibility, the Ambisonic decoding will always be most accurate when a relatively even distribution of loudspeakers is used. This fact is due to the basic principles behind the process. Ambisonic decoding can be thought of as spatially sampling the spherical harmonic components of the sound field (contained in the Ambisonic signals), at each specific loudspeaker location.

At a minimum, in order for the matrix inversion in the decoding process to take place, the number of loudspeakers must be equal to the number of Ambisonic signals, as explained in Section 2.3.5. Thus, for $n^{th}$ order Ambisonic reproduction, a minimum of $(n+1)^2$ loudspeakers must be used. This number will ensure that the matrix inversion operation can be mathematically carried out, but, depending upon the arrangement, it will not ensure as accurate a directional reproduction as possible. For example, if nine loudspeakers were placed in the left hemisphere (made from bisecting a sphere through the plane of symmetry of a listener's head), mathematically, second order Ambisonic reproduction could be achieved. When considering the spatial sampling of the Ambisonic signals, adequate sampling would occur within the left hemisphere, but no sampling would occur in the right hemisphere. Thus, none of the important information contained in the Ambisonic signals in the right hemisphere could be reproduced. This example arrangement is an extreme and biased case, but it begins to show the importance of loudspeaker placement.

By placing the loudspeakers in a uniform layout, as high a spatial fidelity as possible can be achieved through the spatial sampling of the Ambisonic signals. Also, if more loudspeakers than $(n+1)^2$ are used, a finer resolution in the decoding and spatial sampling process can be achieved, resulting in a higher fidelity of Ambisonic reproduction. For the designed loudspeaker setup, the minimum requirement was to

achieve third-order Ambisonic reproduction. This was heavily dictated by other work within the lab group on Ambisonic reproduction of concert halls, using measurements from the Eigenmike em32, a spherical microphone array containing 32 elements (Figure 2-5, b). With the Eigenmike em32, effective estimates for up to third-order spherical harmonic components of the sound field can be obtained with a wide-band frequency range up to around 8 kHz.[65] Thus, a minimum of 16 loudspeakers was required. In order to gain the higher resolution of reproduction, 30 loudspeakers were constructed to be placed throughout the anechoic chamber. This number was limited by cost and by the maximum of 32 separate output channels on the digital to analog converter, which will be discussed in Section 3.2.5. With two subwoofer channels, a maximum of 30 possible loudspeaker channels remained.

These loudspeakers were then placed as evenly as possible around the listener, with a few practical considerations. The first practical constraint is the room size, which is only 11' (3.35 m) wide by 14' (4.27 m) deep by 8.5' (2.59 m) tall, measured tip to tip. With a smaller space than desirable, it was important to place the loudspeakers as far away as possible from the listener. This constraint meant that the loudspeakers were no longer placed in a perfectly spherical distribution around the listener. To account for this discrepancy, built-in level correction and time-delay adjustments have been added to an Ambisonic decoder VST plug-in, which will be explained in Section 4.2.6. Next, due to the size of the room, it was not possible to place any loudspeakers directly below the listener. Finally, although perfect even angular spacing is ideal, it is more feasible and practical to arrange the loudspeakers as equally distributed at particular elevation rings of loudspeakers. With these requirements, the final loudspeaker arrangement was placed in the following setup shown in Figure 3-11 and Table 3-2, using the coordinate axes specified in Figure 2-11. As shown in Figure 3-11, the two subwoofers are placed in the front-right and back-left corners of the anechoic chamber, and the loudspeakers are distributed, shown in Table 3-1.

.

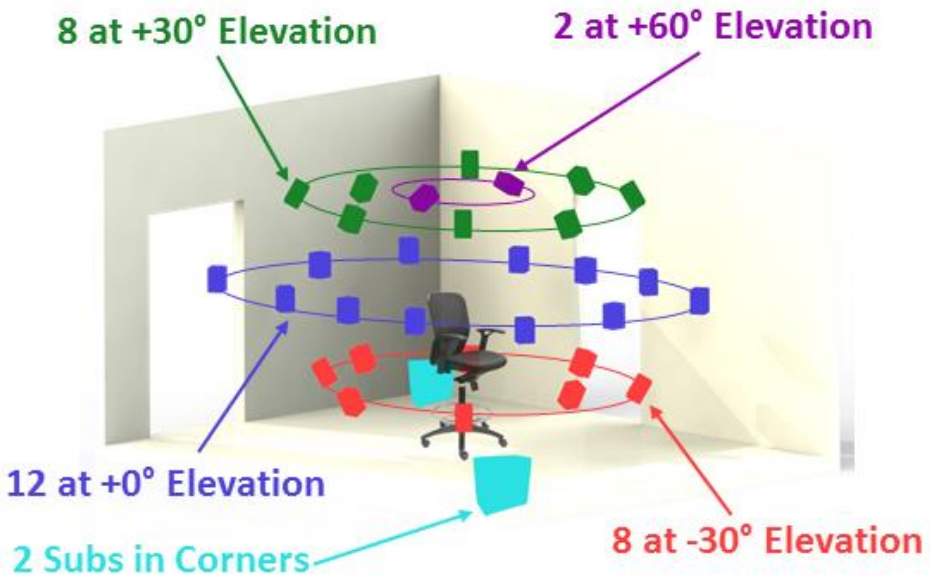


Figure 3-11: Loudspeaker and subwoofer locations inside of the anechoic chamber.

Table 3-1: Loudspeaker ring locations, providing elevations and azimuthal spacings.

| Loudspeaker Ring | Elevation | Number of Loudspeakers | Azimuthal Spacing |
|---|---|---|---|
| Lower Ring | -30° | 8 | 45° |
| Horizontal Ring | 0° | 12 | 30° |
| Upper Ring | 30° | 8 | 45° |
| High Ring – Left and Right | 60° | 2 | 180° |

The placement for the lower three rings was based upon each having a loudspeaker at 0° azimuth, and the two highest loudspeakers were only placed to the left and right of the listener, at +90° and -90° azimuth. This arrangement provided a logical and clear solution for the loudspeaker spacing, while still preserving a uniform and adequate spatial sampling of the third-order Ambisonic signals. A surveying transit level was used to precisely place the loudspeakers at the appropriate azimuth and elevation positions.

To determine the final locations of the loudspeakers, the Eigenmike em32 was also used to measure pink noise bursts played from each loudspeaker. Using beamforming techniques, the precise locations and associated level corrections, were determined

for each loudspeaker. Table 3-2 presents the designed targets for the placement of the center of each loudspeaker, defined as the midpoint between the center of the tweeter and the center of the woofer (see Figure 3-8). This data was extracted from a SolidWorks model created to assist in the coordination of loudspeaker placement within the anechoic chamber. Using the Eigenmike em32 measurements, the errors for azimuth and elevation were all around ±5°, providing the desired relatively even loudspeaker spacing. Loudspeaker 30, with the 14° error is azimuth, appears larger than the actual error since azimuthal errors are smaller in distance at 60° elevation compared to at 0° elevation. This is due to the fact that the arc length associated with a particular change in azimuth decreases as elevation increases.

Looking at a distance deviation, it is around an error of 4.5" to 5" (12.2 cm). It should be noted that the Ambisonic processing was all performed using the actual loudspeaker locations measured with the Eigenmike, so deviations in Table 3-1 will not actually cause degradation in the sound field reproduction. Despite the small deviations, the actual measured locations of the loudspeakers still provide an even spherical distribution, meaning the array performs well for Ambisonic reproduction. The numbering convention for the loudspeakers is also provided in Figure 3-12.

Table 3-2: Modeled physical loudspeaker locations, as determined from the SolidWorks model. These are compared to measurements made using the Eigenmike em32 to determine actual placements of the loudspeakers. Errors in placement are shown in degrees or azimuth and elevations and in meters for distance.

| Speaker Number | Modeled Locations | | | Locations from Eigenmike em32 | | | Placement Errors | | |
|---|---|---|---|---|---|---|---|---|---|
| | Azm. (deg) | Elev. (deg) | Dist. (m) | Azm. (deg) | Elev. (deg) | Dist. (m) | Azm. (deg) | Elev. (deg) | Dist. (m) |
| 1 | 0 | -30 | 1.60 | -0.7 | -25.2 | 1.55 | -0.7 | 4.8 | -0.055 |
| 2 | -45 | -30 | 1.84 | -46.2 | -25.5 | 1.81 | -1.2 | 4.5 | -0.022 |
| 3 | -90 | -30 | 1.71 | -91.3 | -26.1 | 1.68 | -1.3 | 3.9 | -0.026 |
| 4 | -135 | -30 | 1.84 | -135.3 | -29.1 | 1.83 | -0.3 | 0.9 | -0.005 |
| 5 | 180 | -30 | 1.60 | 177.0 | -30.1 | 1.62 | -3.0 | -0.1 | 0.016 |
| 6 | 135 | -30 | 1.83 | 133.4 | -28.2 | 1.85 | -1.6 | 1.8 | 0.013 |
| 7 | 90 | -30 | 1.71 | 88.2 | -27.7 | 1.70 | -1.8 | 2.3 | -0.015 |
| 8 | 45 | -30 | 1.52 | 43.7 | -25.7 | 1.45 | -1.3 | 4.3 | -0.069 |
| 9 | 0 | 0 | 1.96 | -1.8 | 4.4 | 1.92 | -1.8 | 4.4 | -0.039 |
| 10 | -30 | 0 | 2.25 | -32.2 | 2.8 | 2.21 | -2.2 | 2.8 | -0.041 |
| 11 | -60 | 0 | 1.72 | -62.1 | 3.1 | 1.71 | -2.1 | 3.1 | -0.007 |
| 12 | -90 | 0 | 1.50 | -91.5 | 3.1 | 1.57 | -1.5 | 3.1 | 0.068 |
| 13 | -120 | 0 | 1.72 | -120.3 | 1.6 | 1.74 | -0.3 | 1.6 | 0.017 |
| 14 | -150 | 0 | 2.25 | -150.5 | 0.0 | 2.26 | -0.5 | 0.0 | 0.008 |
| 15 | 180 | 0 | 1.96 | 177.6 | 0.4 | 1.99 | -2.4 | 0.4 | 0.031 |
| 16 | 150 | 0 | 2.25 | 147.2 | 0.6 | 2.27 | -2.8 | 0.6 | 0.018 |
| 17 | 120 | 0 | 1.72 | 117.6 | 1.5 | 1.74 | -2.4 | 1.5 | 0.024 |
| 18 | 90 | 0 | 1.50 | 88.7 | 2.6 | 1.51 | -1.3 | 2.6 | 0.006 |
| 19 | 60 | 0 | 1.72 | 58.9 | 2.1 | 1.70 | -1.1 | 2.1 | -0.022 |
| 20 | 30 | 0 | 2.42 | 28.9 | 2.5 | 2.36 | -1.1 | 2.5 | -0.060 |
| 21 | 0 | 30 | 1.56 | -2.2 | 36.1 | 1.53 | -2.2 | 6.1 | -0.036 |
| 22 | -45 | 30 | 1.80 | -48.2 | 35.5 | 1.80 | -3.2 | 5.5 | 0.000 |
| 23 | -90 | 30 | 1.68 | -91.6 | 33.6 | 1.67 | -1.6 | 3.6 | -0.009 |
| 24 | -135 | 30 | 1.76 | -134.4 | 34.6 | 1.81 | 0.6 | 4.6 | 0.049 |
| 25 | 180 | 30 | 1.55 | 178.0 | 32.6 | 1.63 | -2.0 | 2.6 | 0.081 |
| 26 | 135 | 30 | 1.76 | 134.2 | 33.4 | 1.81 | -0.8 | 3.4 | 0.056 |
| 27 | 90 | 30 | 1.68 | 88.4 | 34.4 | 1.70 | -1.6 | 4.4 | 0.021 |
| 28 | 45 | 30 | 1.80 | 42.5 | 33.5 | 1.77 | -2.5 | 3.5 | -0.032 |
| 29 | 90 | 60 | 1.03 | 91.0 | 62.0 | 1.05 | 1.0 | 2.0 | 0.019 |
| 30 | -90 | 60 | 1.03 | -104.0 | 61.0 | 1.04 | -14.0 | 1.0 | 0.011 |

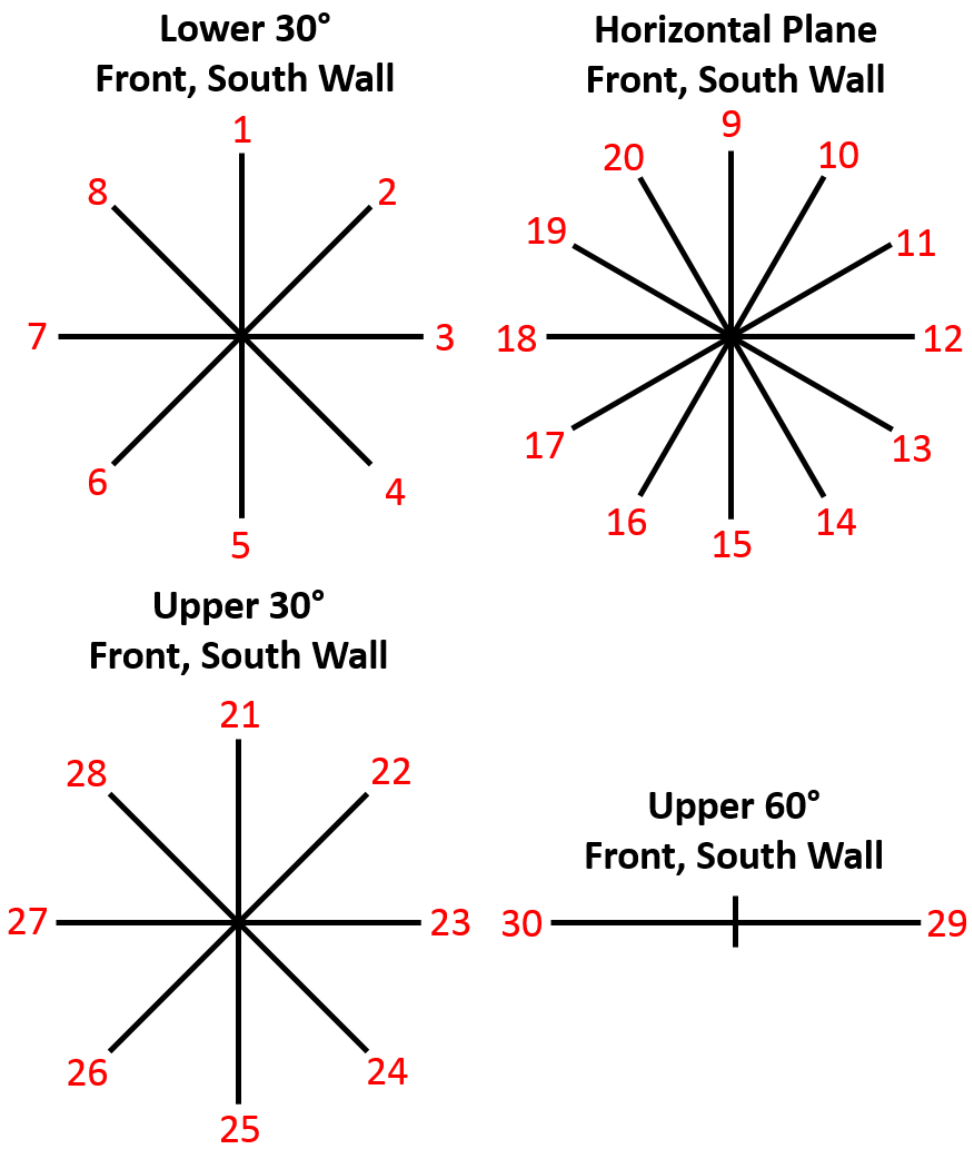


Figure 3-12: Diagram of loudspeaker numbering system, where the top of each figure is facing the front of the array, or the South wall of the anechoic chamber.

### 3.2.2: Loudspeaker Mounting

For this project, loudspeaker mounting options became a very important consideration since both accurate placement is critical (Section 3.2.1) and a need for flexibility in terms of the use of the anechoic chamber was needed. The decoding phase of the Ambisonic processing relies on accurate loudspeaker placement, so any inaccuracy in placement will cause the decoder for the particular array to not perform as expected. The other major consideration was the need for the loudspeakers to be

easily removable, so that the anechoic chamber can be used for other purposes. Since the anechoic chamber is a laboratory space for the Center for Acoustics and Vibration (CAV), the loudspeakers needed to be removable, preserving the anechoic behavior of the room for testing purposes. Thus, a removable, but easily replaceable method was needed for loudspeaker mounting.

A specialized loudspeaker mounting connection was established to meet these requirements. A diagram of the mount is given in Figure 3-13. Fixed pipe flange ends were directly mounted onto the wall, and small 6" (15.24 cm) sections of pipe were secured inside of these pipe. They were specifically designed to be placed at wedge-intersections, so the 6 inch pipe segments would just barely extend past the base of the wedges. Using the expertise of summer laboratory shop students from the Aerospace Engineering Department under the direction of Richard Auhl, quick-release ends were milled into the exposed section of pipe, which contained a slot that would guide the removal and replacement of the loudspeakers. Another section of pipe was designed to tightly fit into the wall mounted section (with a slightly smaller pipe diameter), and it contained a small piece of threaded rod, which was designed to fit with the slot milled into the pipe section attached to the wall.

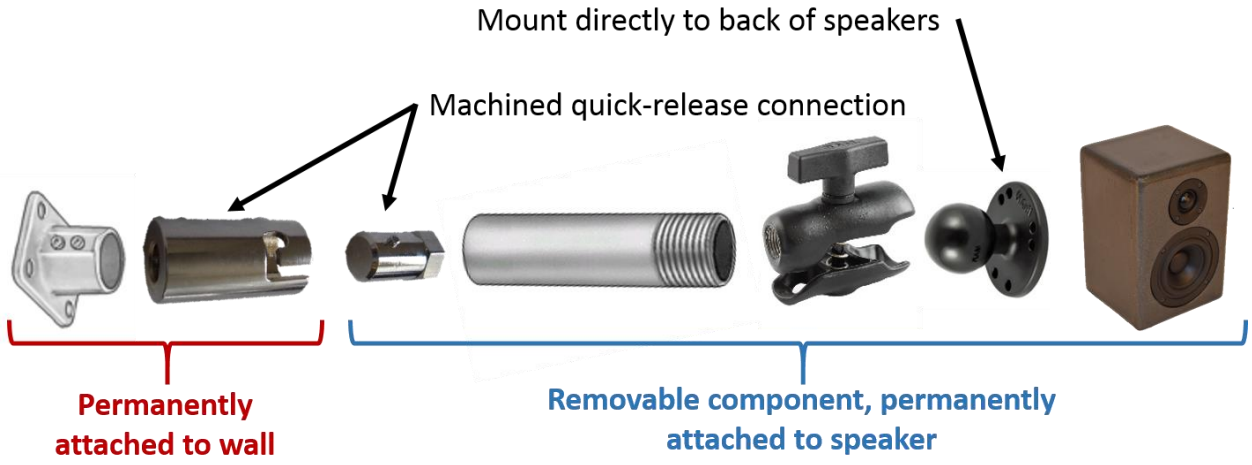


Figure 3-13: Diagram of the mounting system designed for accurate placement and simple removal of the loudspeakers.

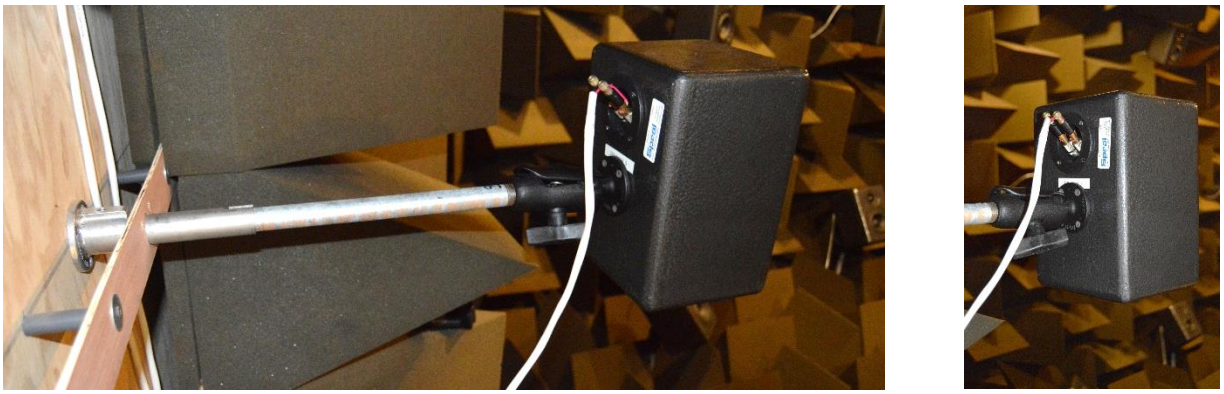

(a) (b)

Figure 3-14: A photo of the loudspeaker mounting wall assembly rod (a), and the ball-clamp joint (b).

The same piece of pipe with the small threaded rod for the quick-release connection was connected to a RAM Mounts ball clamp, using a treaded pipe end connection. This ball clamp was attached to a standard size RAM Mounts ball, and this ball was attached directly to the back of the loudspeaker. This setup allowed for angular adjustments using the RAM Mounts ball and clamp connection, and the placement of the ball on the back of the loudspeaker allowed for translational adjustments to be made as well. After the loudspeaker was accurately placed, all connections were well-tightened. By removing the entire connected unit on the right half of Figure 3-13, the loudspeaker can be removed from the anechoic chamber and replaced into the same location.

The loudspeaker locations were initially sighted using surveying equipment for azimuth and elevation placement, and they were removed and re-installed before performing the location validation measurements which are summarized in Table 3-2. Even after multiple removals and replacements of the loudspeakers, the measured locations were still found to be within ±5° of the target locations. The one location, loudspeaker #30, that was found to exceed this deviation was due to limitations in in the surveying equipment used, and not movement of the mounting assembly (within measurement error).

### 3.2.3: Routing Loudspeaker Signals

To simplify the setup of the array, unpowered loudspeakers were designed, so that individual loudspeakers did not require power to be routed and distributed throughout the anechoic chamber. Instead, only loudspeaker level signals through loudspeaker wire was needed. This was still quite the task, for 32 separate channels of data was required. More details about the hardware located outside of the anechoic chamber can be found in Section 3.2.5. After the loudspeaker signals leave the multi-channel amplifiers, they are run using 12 gauge plenum loudspeaker wire. Plenum loudspeaker wire contains both a positive and negative (red and black) wire, bundled together in a white wire tubing. This effectively reduces the number of stray wires going into and out of the anechoic chamber by a factor of two.

The wires are run to the anechoic chamber wall, where a cable pass-through was constructed to allow signals to be run in and out of the room, while still providing adequate isolation for noise transmission into the anechoic chamber. The pass through consists of 16 four-pin female speak-on connector terminals outside the anechoic chamber, and the same number inside. Each four pin connector is wired to transmit two loudspeaker channels, creating a total of 32 data channels. As well, two 25-pin D-sub connectors are provided inside the anechoic chamber, one of which links to eight male XLR connections outside the anechoic chamber, and the other eight female XLR connectors inside the anechoic chamber. Both are implemented using an eight channel snake cable. This allows for an additional eight inputs and eight outputs of low-level measurement signals into and out of the anechoic chamber. Two USB 3.0 ports are provided inside the room, which can be directly connected to the desktop PC outside of the anechoic chamber. Finally, a single outlet is provided, in which a power strip can be connected to provide power inside of the anechoic chamber. A wooden block was installed within the pass-through, to isolate the power cable from the low level measurement signals, and the loudspeaker level signals within the pass-through as well. A picture of the cable pass-through is shown in Figure 3-15.

Figure 3-15: One side of the cable pass-through installed in the Hammond anechoic chamber.

After the signals are run through the wall, they are routed to an identical panel on the inside of the anechoic chamber. Again, male speak-on connectors are attached into the wall, and two plenum loudspeaker wires (positive and negative wires coupled) extend from the speak-on connectors. These wires are then run vertically upwards and around the upper section of the anechoic chamber wall, to avoid intersecting with either of the room's doors. Once the wires become vertically in-line with the intended loudspeaker, they are run vertically downward to the proper elevation, and then a length of wire is exposed to connect into the loudspeakers. The wires are connected into the loudspeakers using a dual banana plug and a banana plug terminal plate, which was installed in the back of the loudspeakers. Needless to say, this positioning was quite the task! Pictures of the wiring process are shown in Figure 3-16 and Figure 3-17.

Figure 3-16: Picture from the anechoic chamber wiring process. All wiring is attached to the walls using a wire-tacker and the wires are concealed behind the wedges.

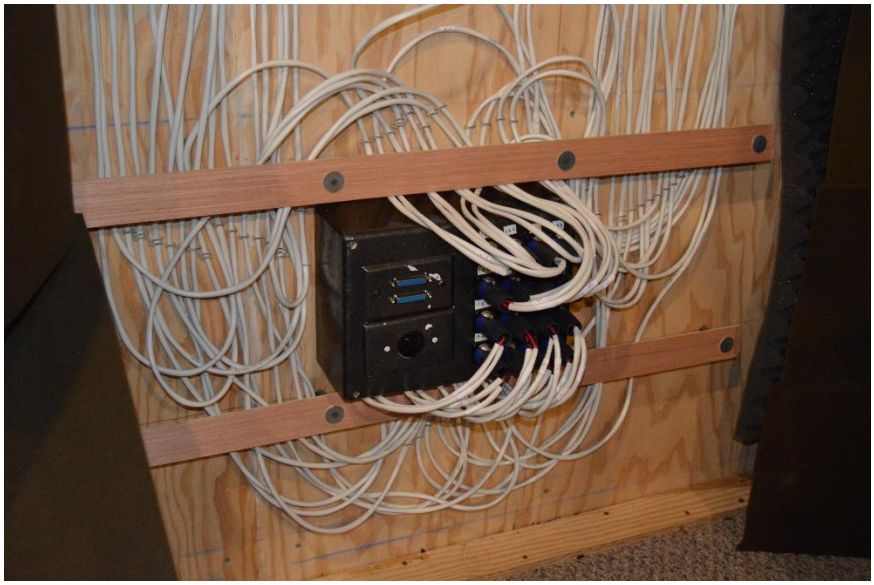

Figure 3-17: The wiring process, routing loudspeaker signals from the pass-through to individual loudspeakers.

### 3.2.4: Free-Field Room Characterization

In order to accurately recreate sound fields over the loudspeaker array, it is important to consider the room in which the auralization is presented and its impact upon the virtual acoustic environment. The anechoic chamber in which the loudspeaker array is built measures 11' (3.35 m) wide by 14' (4.27 m) deep by 8.5' (2.59 m) tall, when measuring from wedge tip to wedge tip with no floor wedges. Dimensions are shown in Figure 3-18. The wedges used in the anechoic chamber are foam wedges, which measure 1' (30.48 cm) x 1' (30.48 cm) wide and long, with a wedge height/depth of 18" (45.72 cm) (4" (10.16 cm) rectangular base depth, and 14" (35.56 cm) of a slowly tapering to a final wedge tip). When the floor is covered with wedges, this setup leaves only 7' (2.13 m) of open space in the height direction, measured from wedge tip to wedge tip.

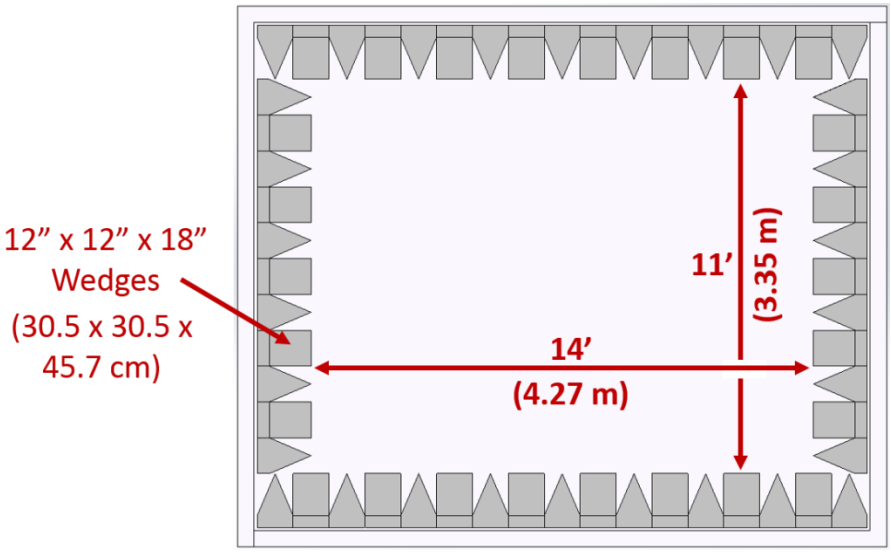


Figure 3-18: Top down view of the Hammond anechoic chamber used for the loudspeaker array construction.

In order to characterize the frequency range over which our anechoic chamber exhibits free-field characteristics, characterization measurements were made. Our measurement setup was based upon the measurements outlined in Annex A of the ISO 3745:2003(E) standard, which provide procedures for qualifying either a hemi-anechoic or anechoic room.[66] It should be noted that although care was taken obtain accurate results, not all specifics of the measurement, as outlined in Annex A, were

followed in terms of the spacing and number of measurements made. For the measurements, an omnidirectional sound source was placed in the center of the anechoic chamber, which was lined with floor wedges.

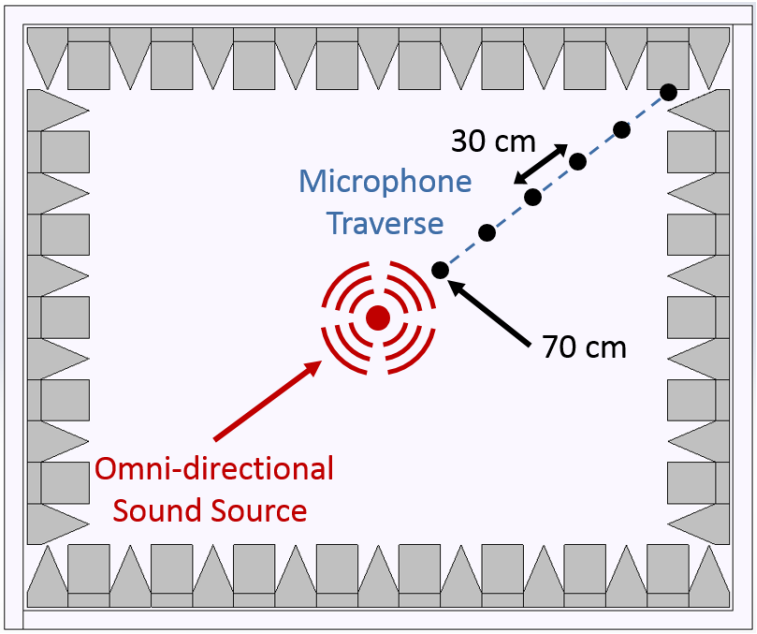


Figure 3-19: Setup of characterization measurement to calculate the room's free-field behavior (top down view).

As shown in Figure 3-19, a microphone traverse was setup extending from the sound source to various corners and sides of the room. IR measurements were taken beginning at a distance of 70 cm from the source, and then taken at 30 cm increments, until the corner of the room was reached. The traverse distance was measured by extending a string from the sound source to the corner of the room, and sliding the microphone along the string to ensure reliable placement (Figure 3-20).

Figure 3-20: A picture of the string, extending from source with adjustable microphone position.

For the measurements, five different microphone traverses were measured, 2, 3, and 5 five to the corners of the room and 1 and 4 to the connection of the ceiling and the side walls shown in Figure 3-21. As well, two different omnidirectional sound sources were used for the measurement. The low to mid frequency source was a Brüel and Kjær OmniPower dodecahedron loudspeaker (< 800 Hz) and the high frequency source was a small dodecahedron loudspeaker (≥ 800 Hz), exhibiting omnidirectional characteristics up to the 5000 Hz third-octave band. The high frequency dodecahedron was constructed by the Sound Perception and Room Acoustics Laboratory (SPRAL), made using twelve 0.75" (1.91 cm) tweeters. Plots of the directivity of this high-frequency source can be found in Appendix H.

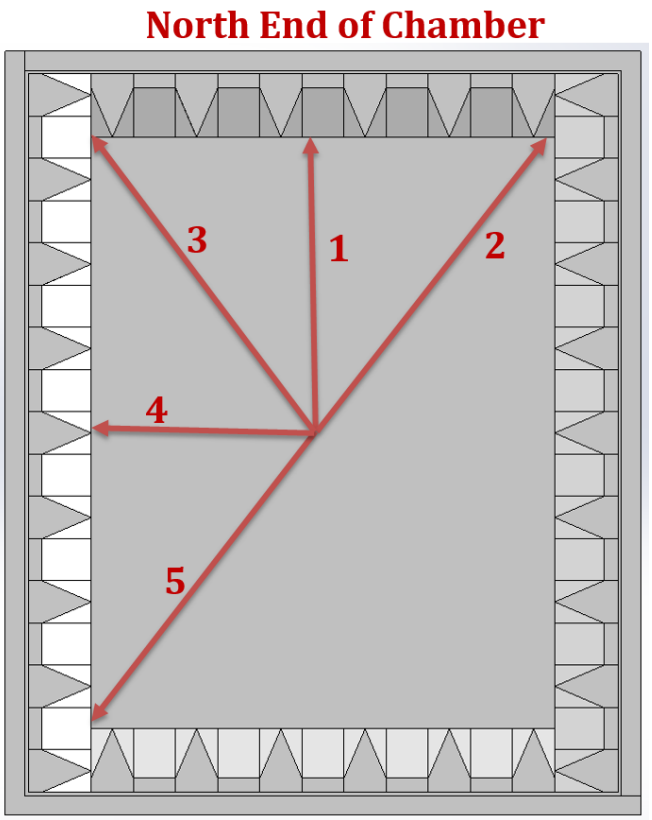


Figure 3-21: Numbered label of traverses for anechoic chamber characterization measurements.

After the IRs were measured, they were post-processed to determine the lowest third-octave frequency bands that no longer exhibited free-field behavior. Each IR was filtered using a one-third-octave band filter, and the relative RMS pressure was calculated for each band, at each location along the five traverses. When plotting these levels against the measurement distance from the source, free-field behavior will exhibit a negative slope of 6 dB per doubling of distance. If the distance is plotted on a log scale against relative level in dB, then a negative linear relationship should emerge. Annex A of ISO 3745:2003(E) provides limits allowing for deviations from this free-field decay linear behavior of ± 1.5 dB for third-octave bands of 630 Hz or less, ± 1.0 dB for third-octave bands between 800 Hz and 5000 Hz, and ± 1.5 dB for third-octave bands greater than 6300 Hz.

To demonstrate the free-field properties of the room, example plots for Traverse 2 (Figure 3-21) are given in Figure 3-22 and Figure 3-23. The plots for the remaining

four traverse measurements are provided in Appendix B. The levels for each third-octave band are plotted in a different color, against distance plotted on a log-scale. The decay of each third-octave band is plotted relative to free-field decay, starting at a relative level of 0 dB at 70 cm. The levels for each third-octave band are shifted so that the sum of squared errors between the free-field decay and the measured decay is minimized. This process in essence centers each decay curve around the ideal free-field behavior. The red thick line shows the estimate for ideal free-field behavior, and the thick black lines show the allowable deviations, as stated in Annex A of ISO 3745:2003(E).

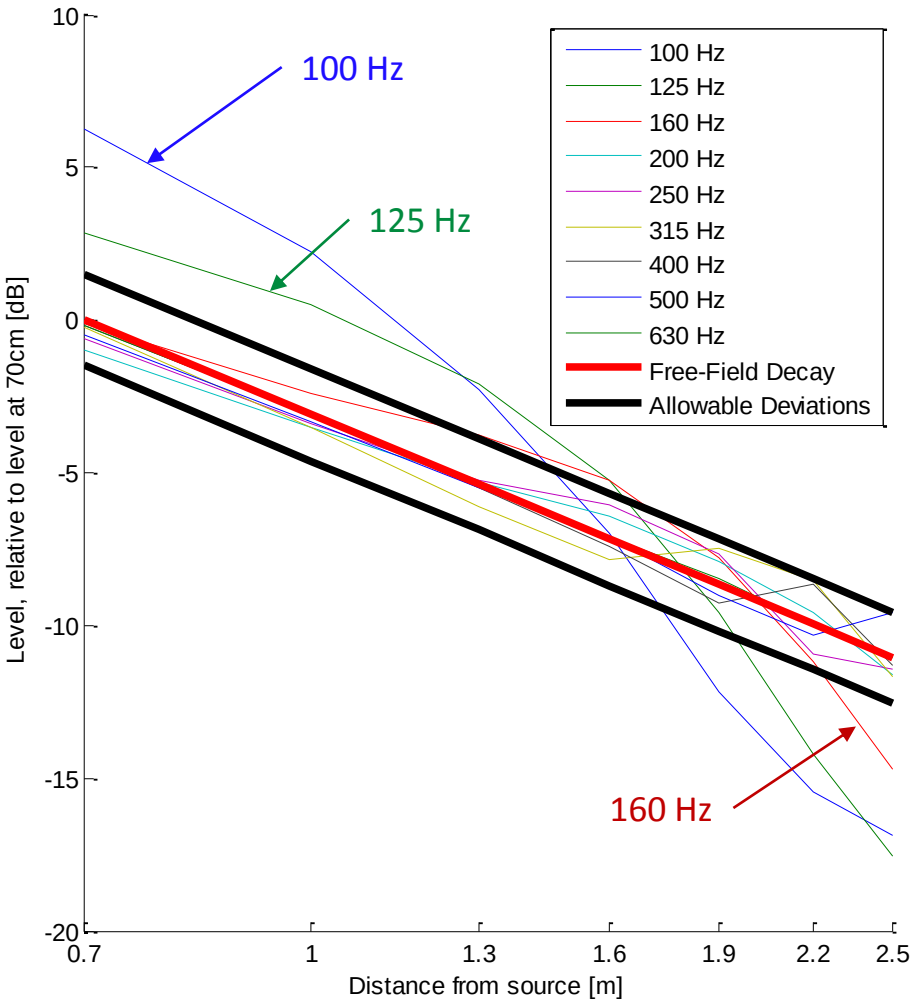


Figure 3-22: Deviations from free-field behavior of the anechoic chamber at low frequencies. Deviations are outside of the allowable range at the 100, 125, and 160 Hz third-octave bands.

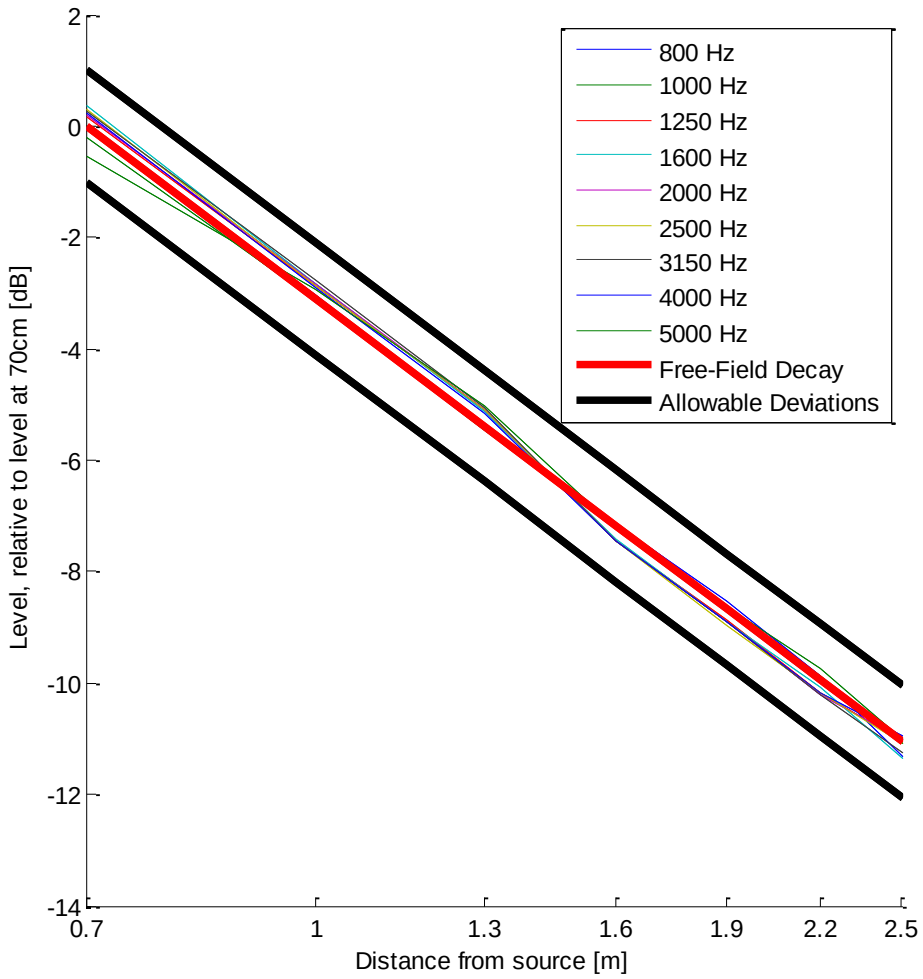


Figure 3-23: Deviations from free-field behavior of the anechoic chamber at mid/high frequencies. No deviations outside of the allowable range are observed at mid/high frequencies.

After analyzing all five traverses, it was found that our anechoic chamber exhibited free-field characteristics down to the 200 Hz third-octave band. Below that, deviations that fell outside of the allowable limits were observed. Figure 3-23 shows that at high frequencies, very small deviations from free-field behavior are observed, which is as expected. Since no reflecting surfaces were present in the anechoic chamber during the measurement (besides the measurement equipment), and since the wedges are highly absorbing at these frequencies, only low frequency limits should exist. As shown in Figure 3-22, the low frequencies exhibit much more significant deviations at most third-octave bands. In the 100 Hz, 125 Hz, and 160 Hz

bands, deviations outside of the allowable limit are observed, which are attributed to the low frequency absorption limit of the 18" deep foam wedges. Thus, below the 200 Hz third-octave band, the effects from the room will impact the overall sound field reproduction accuracy.

### 3.2.5: Hardware and Software Control

Finally, a note should be made about how the array is controlled from an operational standpoint. One of the main goals for the AURAS facility was reliable and user-friendly operation for future undergraduate and graduate student researchers in the Sound Perception and Room Acoustics Laboratory (SPRAL) research group. The well-designed loudspeaker removal and replacement already help to provide this functionality for the physical setup of the loudspeakers, as was mentioned in Section 3.2.2. For the array, a Lenovo K450e high performance tower PC was purchased, for it provided a great balance of a high performance desktop PC with a good price. For the overall setup, the following were needed:

- Individual control of each loudspeaker channel (32 total)
- Power amplifiers for each loudspeaker
- Stationary setup with little to no maintenance concerns

To do so, it was first desired to have a dedicated 32 channel digital to analog converter, which could be connected to the array computer via USB. This was achieved through two pieces of equipment made by RME. The first was RME's MadiFace USB, which takes a USB input, and converts it to the Multichannel Audio Digital Interface (MADI) digital audio format, which can support up to 64 channels of data using a duplex MADI optical cable. The data is then transferred to RME's M32DA via a duplex MADI optical cable. The M32DA is simply a 32 channel digital to analogue converter, which outputs each audio channel separately using a 0.25" (0.64 cm) single channel audio connector. An additional feature of the M32DA is that RME provides a simple extension for up to 64 channels of audio if that is desired in the future. Since the MADI audio format carries up to 64 channels of data, RME built in functionality to connect the MADI output of one M32DA into the MADI input of a

second M32DA, and automatically, channels 1-32 will be sent to the first M32DA and channels 33-64 to the second M32DA. This provides very convenient and simple extendibility for future expansion of the loudspeaker array.

After the signals leave the M32DA through a 0.25" (0.64 cm) jack, a 0.25" (0.64 cm) audio cable with a 0.25" (0.64 cm) to RCA adapter is used to route signals into the multichannel audio amplifiers. For the anechoic chamber, three 12 channel Dayton Audio amplifiers (model #MA 1240a) are used to power the loudspeakers. The first 30 channels are used to power the loudspeakers, and channels 31-34 are used to provide bridged power to the two subwoofers. The audio amplifiers accept RCA input, and output to loudspeaker wire using a Phoenix connector for each separate channel. These wires then connect into the cable pass-through, which was previously described in Section 3.2.3. It should be noted that the amplifier contains rather arbitrary level adjustment dials, so in order to identically calibrate the channel levels, a single tone was played through the setup into the amplifiers. Then, a multi-meter was used to read the current RMS output voltage from the amplifiers. The knobs were each individually tuned to the correct output voltage, all within ± 0.02 V of the target output. All of the knobs were then hot-glued into place. The voltages were all re-measured a few weeks after to ensure levels remained consistent. A simplified diagram of the overall setup is shown in Figure 3-24.

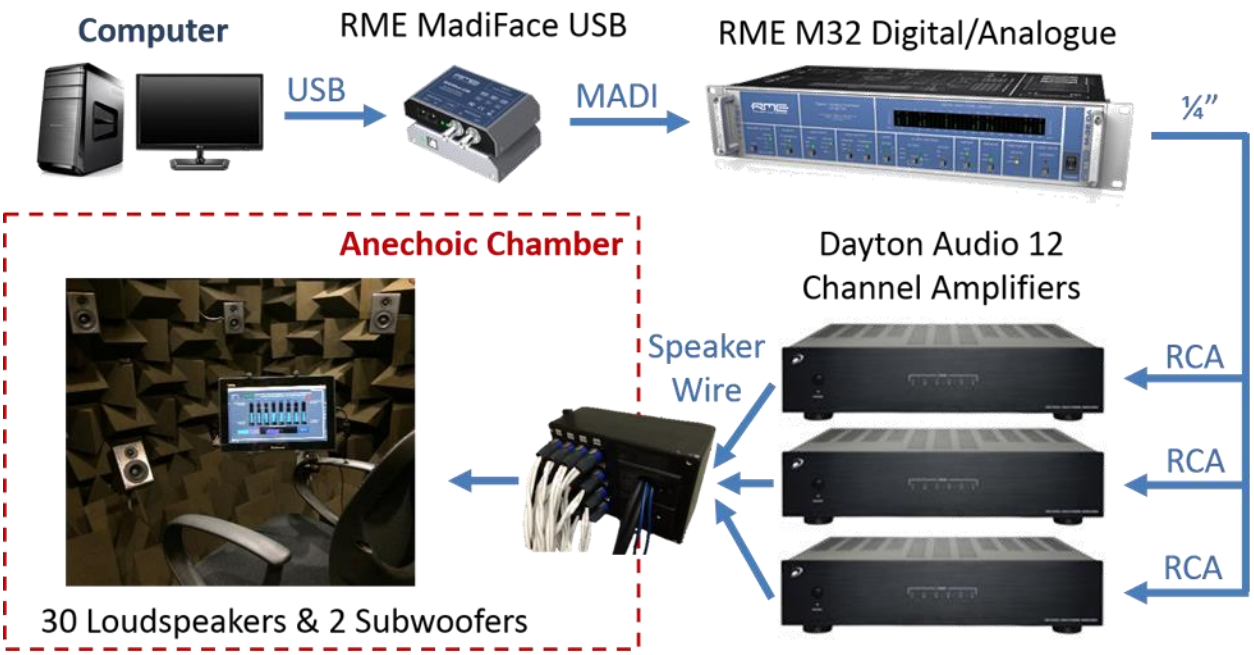


Figure 3-24: Diagram of the hardware setup to control and power the 32 individual channels.

The hardware was installed in an audio rack outside of the anechoic chamber. The setup is easy to operate; once the computer, three amplifiers, and the M32DA are turned on, the array is ready to use. The M32DA stores previous settings, so as long as no changes have been made to the setup, no settings adjustments should be necessary for any of the equipment. The digital audio workstation software REAPER[67] is used to process signals for playback over the loudspeaker array. This can be done in real-time through the use of VST plug-ins. Max 7, the newest version of Max MSP, is a program in which graphic user interfaces with real-time audio processing capabilities can be easily created.[68] Max 7 is a visual programming language made by Cycling74, geared mostly toward the computer music industry. As a visual programming language, it does present some difficulties in more advanced signal processing work, however, it provides an amazingly useful and user-friendly way to make graphic interfaces within the anechoic chamber. Max 7 is designed to operate on a real-time audio processing framework. The anechoic chamber is also equipped with a wireless, battery powered external touch-screen monitor, made by Lenovo (model #LT1423p). The monitor connects via Wi-Fi to the computer, and

allows for user interaction with the anechoic chamber during subjective testing and demonstrations.

Additionally, the University of Huddersfield has developed several externally coded objects (in C), which can be used in Max, and are freely available.[69] One of these tools, the "multiconvolve" object, allows for efficient real-time convolution using any FIR filter stored as a buffer within Max. This creates many different possibilities for application with the loudspeaker array. MATLAB can also be used for preprocessing the signals for playback over the array, but Max 7 is preferred for real-time audio processing, since MATLAB is not well suited to that application.

The digital audio workstation REAPER is used for the Ambisonic processing of signals that are presented over the loudspeaker array. REAPER is sold at a very affordable price to both academic institutions and individual users, and provides an easy environment to work with multiple channels of audio. REAPER is also capable of performing real-time audio processing through the use of VST plug-ins, which can be used in most digital audio. The Ambisonic processing mentioned in Section 2.3 is all implemented into VST plug-ins, made using an Ambisonics decoder toolbox.[70] Ambisonic signals can be opened within the REAPER workstation, and the various plug-ins perform custom Ambisonic decoding. Once the signal chain of plug-ins is set up as effects in REAPER, the Ambisonic signals can be decoded in real time over the array. Additionally, once the plug-in effects are setup, a user can render the final output file as a 30 channel .wav file, which can be directly played over the array in other programs, such as Max 7, with the processing already complete.

Although the current studies using the AURAS facility implement third-order Ambisonic reproduction, the facility provides flexibility, and other methods could be implemented. Studies could be done to determine the reproduction benefit of using different orders of Ambisonic processing and also evaluate perceptually-based methods like Vector-Base Amplitude Panning (VBAP). With the many different simulation and reproduction techniques used in previous LEV research, past studies

and reproduction methods could be recreated using the array. This would allow potential validation and comparison of our methods directly to previous research.

### 3.2.6: Validation of Loudspeaker Performance and Equalization

To determine if a flat frequency response was achieved for all of the individual loudspeakers, IR measurements were taken for each loudspeaker. The individual IR measurements were made with the loudspeakers installed in the anechoic chamber, so that the measurements would contain effects from the low-frequency cutoff of the room, reflections from other loudspeakers in the array, and the non-flat response of each loudspeaker. To make the measurements, bursts of pink noise were played through each individual loudspeaker, and the Eigenmike em32, a 32-channel spherical microphone array, was used to measure the response at the center of the array. The omnidirectional response of the microphone was extracted from the Eigenmike em32 and used for the IR calculation. The measurement was made using four averages, and the final IR was calculated by dividing the frequency domain signal of the averaged measurement by the frequency domain of the source pink noise signal. The measurement was made with digital equalization applied, and then repeated without applying digital equalization.

IRs of all 30 loudspeakers were measured at a distance of 1.5 m on-axis in the anechoic chamber in the Garfield Thomas Water Tunnel building on campus, and these measurements were used to create digital equalization filters for each loudspeaker. This anechoic chamber was used, since it is constructed with 3' (0.91 m) deep fiberglass wedges, allowing for free-field measurements down to a lower frequency than in the Hammond anechoic chamber. Using these IRs, FIR filters were developed by inverting the measured IR individually for each loudspeaker from 60 Hz up to 20 kHz. Below 60 Hz, the equalization filter applied an active high pass filter at 60 Hz to protect the loudspeakers from being overdriven at low frequencies.

Figure 3-25 shows one of the flattest responses achieved out of the 30 loudspeakers (Loudspeaker #4), and Figure 3-26 shows the worst case response of an individual loudspeaker's performance (Loudspeaker #14). For almost all of the loudspeakers,

above 200 Hz, deviations from a flat-frequency response were within a range of ±2 dB to ±3 dB. Low frequency responses for some loudspeakers are affected by modal characteristics of the room, below the free-field cutoff of the room at 200 Hz. This is clearly noticeable for loudspeaker #14. In Figure 3-25 and Figure 3-26, the non-flat response above 9 kHz is due to spatial aliasing from the spacing of the microphones on the Eigenmike em32, and is not a result of the loudspeakers' responses.

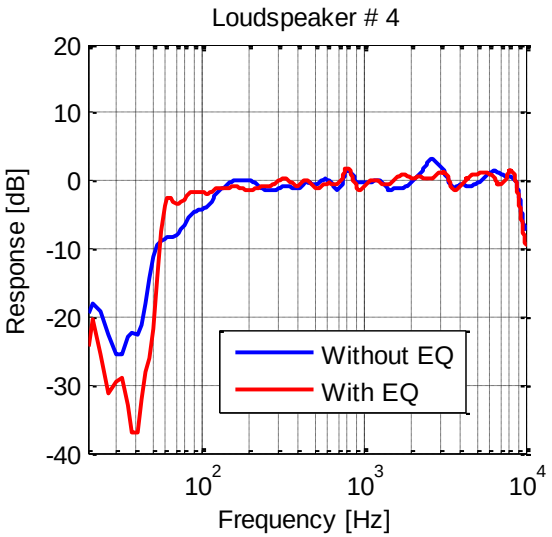


Figure 3-25: Best case showing the un-equalized response of the loudspeaker (blue) versus the equalized response of the loudspeaker (red). The loudspeaker equalization produced a flatter response at mid and high frequencies, and remains flat down the 60 Hz, where the equalization filter cuts off.

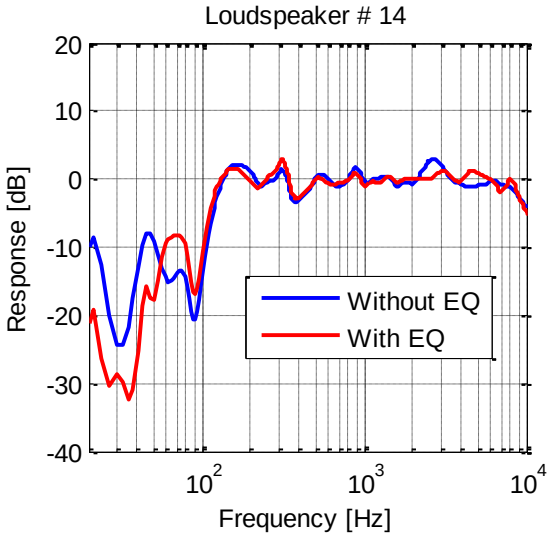


Figure 3-26: Worst case showing that although the loudspeaker equalization produces a flatter response at higher frequencies, modal characteristics from the room negatively impact the response below the room's cutoff frequency of 200 Hz. A clear node in the room can be seen around 90 Hz.

A complete set of comparison frequency response graphics for both equalized and un-equalized loudspeaker responses can be found in Appendix G. Overall, considering the constraints of the room and the low-frequency limit of the loudspeakers, relatively flat responses are observed down to the cutoff frequency of the room, below which some modal room characteristics can negatively impact the frequency response. Without modal characteristics, the loudspeakers produce a flat response down to 60 Hz, as shown in the best-case scenario in loudspeaker #4.

### 3.2.7: Validation of Loudspeaker Array using Binaural Recordings

To test the validity and evaluate the realism of the auralizations being reproduced in the AURAS facility, live recordings were made during the dress rehearsal of the Penn State School of Music's annual MOSAIC concert. The concert features a wide variety of performing ensembles, who perform only a single piece each, and the performers are spaced throughout the hall, which results in a very interesting spatial experience. Specifically, performers are located on stage, in the first row of the hall, in the side walls, and in the balconies. With the variety of performances and spatial characteristics due to the placement of the performers, the recording of this performance provided a method to compare Ambisonic reproductions to actual recordings.

During the performance, binaural recordings were made using a Brüel & Kjær HATS Type 4100-D, and recordings were made using the Eigenmike em32. The recordings were made in adjacent seats, to minimize the perceptual differences between the two slightly different locations of the recording devices. David Dick has developed the processing methods in work done for his Ph.D. dissertation to process the Eigenmike spherical microphone array measurements into Ambisonic signals. The Ambisonic signals are then identically decoded and processed using methods outlined in Section 2.3.5. The recordings from the Eigenmike em32 were then reproduced over the anechoic chamber, and the Brüel & Kjær HATS was again used to make binaural recordings of the Ambisonic reproduction.

Informal listening tests were conducted by David Dick in which an A-B comparison was done between the actual binaural recordings taken during the concert and the binaural recording of the Ambisonic reproduction. Based on the results of this informal test, the only noticeable difference between the two stimuli was the difference in the noise floor. This brief experiment provided a subjective check of the auralization techniques used in this study and provided a first step in validating the perceptual performance of the loudspeaker array. A more formal study is planned for further validation of the Ambisonic reproductions.

### 3.2.8: The Final Product

After six months of loudspeaker building, painting, purchasing, construction, wiring, wedge moving, removing, and replacing, the array was ready to use. The anechoic chamber is equipped with a height-adjustable chair, having an adjustment range of ~10" (25.40 cm), atop of a removable 9" (22.86 cm) tall stand. By adding or removing the stand, the anechoic chamber is capable of accommodating 19" (48.26 cm) of upper body/torso height adjustment, accommodating a wide range of listeners. A custom built tablet holder was implemented into the design. It allows for highly adjustable tablet placement, for ease of use by subjects within the anechoic chamber.

For head positioning, two small copper centering weights have been suspended from the ceiling, which are typically about an inch away from a subject's ears once the chair height has been positioned correctly. This allows subjects to self-correct their head location during testing, ensuring they are located at the center of the room. The disks are about 0.75" (1.91 cm) in diameter, so the frequency in which the half-wavelength of sound is equal to the diameter of the disks is 9,000 Hz. Above this frequency, the disk may have an impact on the perceived sound field. Some informal listening tests done with and without the disks in place showed that no audible differences were caused by the disks.

Finally, a webcam is connected via USB through the pass-through into the array computer, allowing the test administrator to visually monitor the testing process. This helps test subjects to feel comfortable in an acoustically unnatural room since

they are able to speak to the test administrator using the webcam microphone. The webcam also provides the test administrator with the ability to monitor a subject's head location throughout the test. Figure 3-27 shows photographs of the overall, completed loudspeaker array.

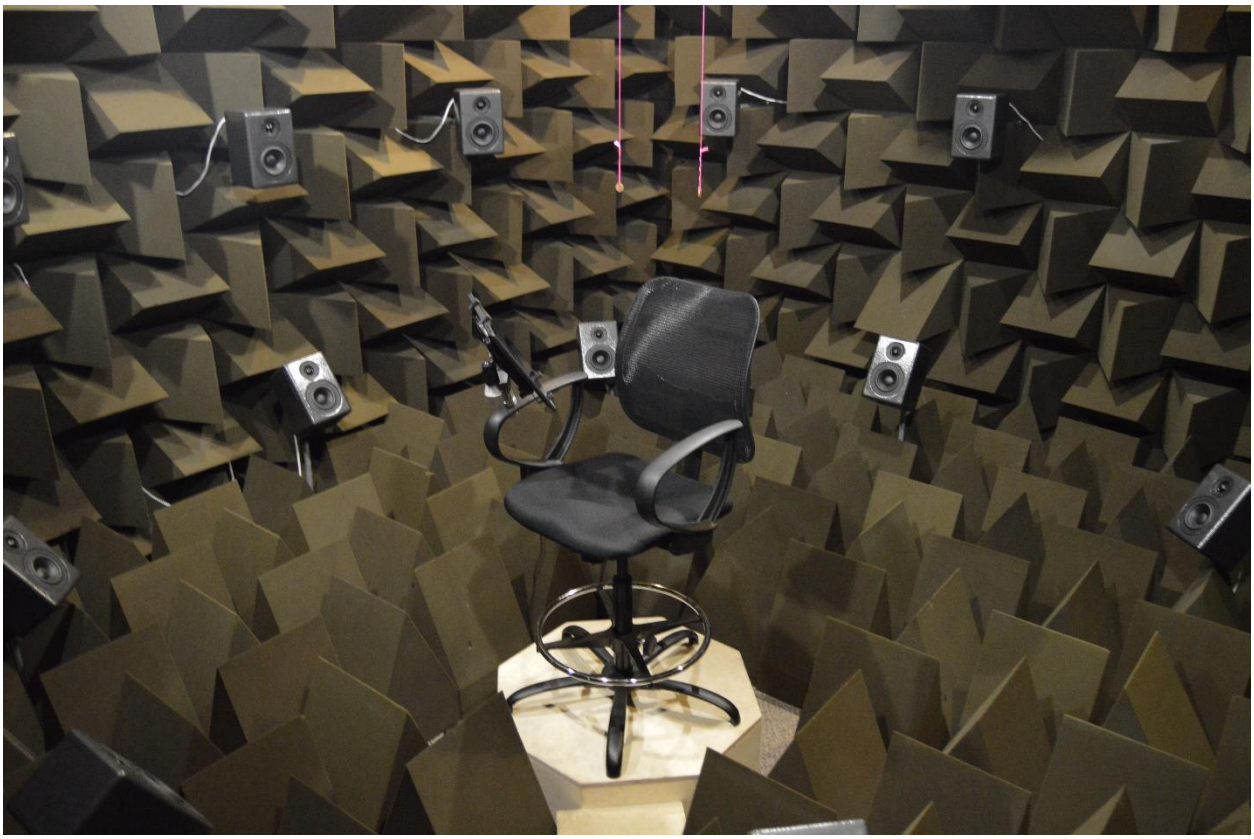

Figure 3-27: Final arrangement of the anechoic chamber, with all elements in place. All we need is a test subject!

# Chapter 4: Room Sound Field Simulation Methods

When considering the perception of LEV or immersion within a sound field, there is still much debate as to what specifically produces such subjective differences. Using the literature summary presented in Chapter 2, the following variables were initially hypothesized to impact LEV:

- Spatial distribution of early reflections within a hall
- Spatial distribution of late reflections within a hall
- Reverberation Time / Early Decay Time of a hall
- The sense of scale or volume of a hall (reflection density)
- Receiver locations within a hall
- Overall shape of the hall
- Perception of loudness of the hall
- Balance of early to late energy

Lacking a clear definition of LEV and understanding on what creates a sense of LEV from previous research, two competing goals arose for the project. The first was the desire to create a physically-based auralization, or one that is reminiscent of a hall which could be built, designed, and realized by an architect and acoustical consultant. The other competing idea was the ability to finely control, manipulate, adjust, and fine-tune aspects of the IR and auralization.

For the overall project, ultimately two methods were adopted. Both simulations and measurements were used for the overall project, based upon their physical basis. David Dick, a fellow graduate student in the Sound Perception and Room Acoustics Laboratory (SPRAL) out of Penn State's Graduate Program in Acoustics, is currently working on and conducting subjective work on the sense of LEV using measurements made with the Eigenmike em32, a 32 element spherical microphone array for his PhD. dissertation. With auralizations from these measurements, it is ensured that the auralization is spatially accurate and also linked to a physically realizable space. The limitation of using measurements of actual halls comes from the time, resources,

and energy required to obtain a wide variety of measurements with this setup. Much coordination is required to gain access to a hall, pack up equipment, travel to a particular hall, and perform measurements, let alone the costs in both time and money associated with the trip. Although physical measurements are the most realistic, they do not satisfy the need for a high degree of controllability to create different auralizations.

For this thesis, simulation was selected as the auralization approach. With a simulation, it is very simple to adjust the room volume, material properties, receiver location, and source location of a particular hall. These simple, but subjectively important changes can make large subjective differences, highly important to the perception of LEV. Computer simulations based upon a particular room geometry also provide a physical significance to the sound field, making a plausible sound field which could be experienced within a real room. The expectation is that the findings of this work, which is simulation-based, will help to direct future studies made using measurements. This way, different halls and receiver locations for measurements can be chosen based upon the results of this work, to ensure a wide range of LEV conditions are found. The next few sections outline the method chosen to simulate room impulses responses, which could be implemented over the anechoic chamber's loudspeaker array.

## 4.1: Different Methods of Room Acoustic Simulation

In room acoustics simulation, many different methods have been determined for how to properly simulate a sound field within a room. Often, they can be broken down into three different categories: wave-based methods, geometrical methods, and artificial methods. These three different methods all have different assumptions or constraints associated with each. Figure 4-1, taken from the book *Auralization* by Michael Vorländer (Fig. 10.2), provides a graphic overview of the different methods of modeling sound propagation within a room.[71]

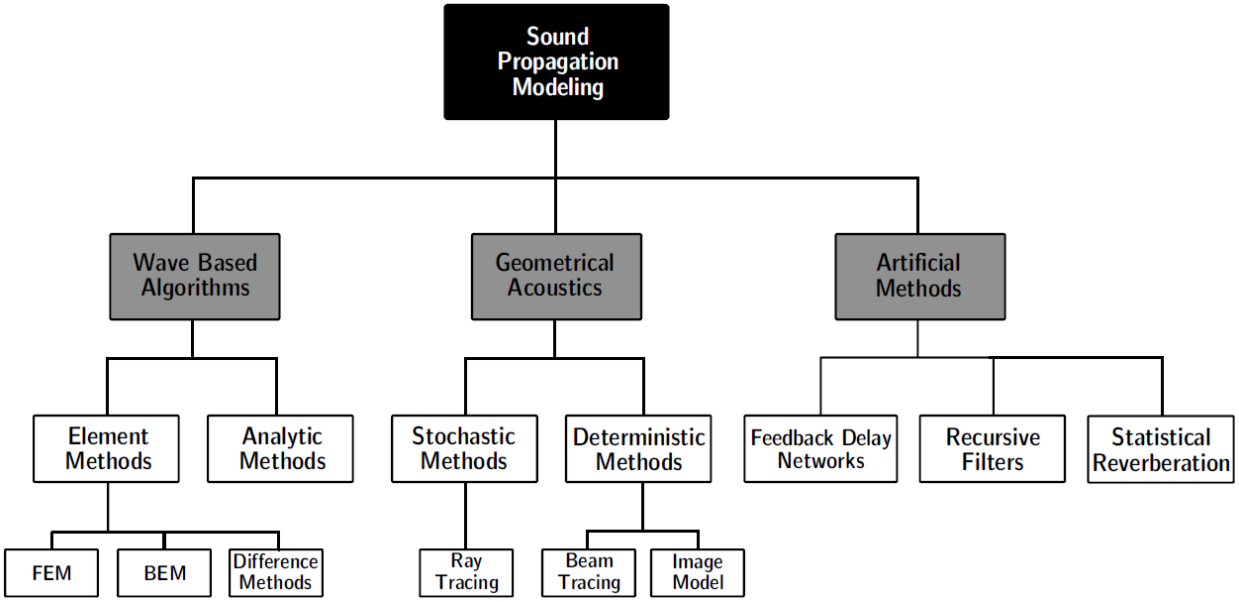


Figure 4-1: Map of room acoustics modeling techniques, from *Auralization* by M. Vorländer, Fig. 10.2.[71]

### 4.1.1: Wave-based (Numerical) Room Acoustics Simulation Methods

The first type are wave-based models, also known as numerical methods. The most commonly used wave-based models for room acoustics are the boundary element method (BEM) and the finite element method (FEM). Both methods require the room to be represented by a meshed grid. FEM requires the room to be represented by a mesh representing the entire volume of the room, while BEM requires a mesh of only the boundary surfaces of the room.[71] Either way, a spatial discretization, or mesh, is required for the solution. For BEM, the number and size of individual mesh elements is highly related to the maximum desired frequency for simulation. This method is related explicitly to a Green's function and employs a discretized form of the Kirchhoff-Helmholtz Integral Equation. Ultimately, the model can be solved at a particular frequency, and depending upon the desired frequency resolution and range, the calculations for this type of model can take up to several hours.

The FEM is another wave-based model for simulating rooms. The fundamental principles behind the calculation for the FEM is different than the BEM, but the calculation time balanced with accuracy is still of concern. Now, the model is broken down into small volume elements, and a typical size for a mesh can be up to 100,000

nodes. Considering models of this size, typical calculation times of around five minutes per frequency are required. Again, this model, depending upon the certainty of model inputs, accurately simulates the wave-based phenomena within a room, but it requires a very high calculation time, again depending upon frequency resolution and range. The other methods, geometrical and artificial models discussed below, don't rely on the fundamental wave-propagation equations, meaning that phenomena such as low frequency diffraction and the seat-dip effect are not correctly modeled; however, this compromise results in significant reductions in computation time, while still providing accurate results.

For the geometric acoustics approach, sound energy is considered as a ray, which travels and is either reflected, refracted, diffracted, or absorbed, and its direction of travel and energy content is adjusted accordingly.[71] A specifically defined receiver point or volume is then set, and energy rays that intersect with that point or within that volume are added up to determine the details of the sound energy experienced at a particular point in space. The surface of the receiver volume is meshed into a grid, in which each mesh element corresponds to a particular directional bin. Rays that intersect within the same direction are grouped together in a bin, and this directional information is used for both auralization and directionally dependent room acoustic parameter calculation. The fundamentals of geometrical acoustics assume ray-like wave propagation, which does not include near-field acoustic phenomenon. Thus, the simulated sound field depends on a long distance approximation, which is approximated using plane wave-like behavior.

### 4.1.2: Hybrid Geometrical Acoustic Simulation

Geometrical acoustic models create acoustic simulations by implementing analogous solutions to those seen in geometric optics. Typically, the IR of a room can be divided into three different categories: direct sound, early reflections, and late reverberation. A simplistic plot of an IR with these three components is shown in Figure 4-2.

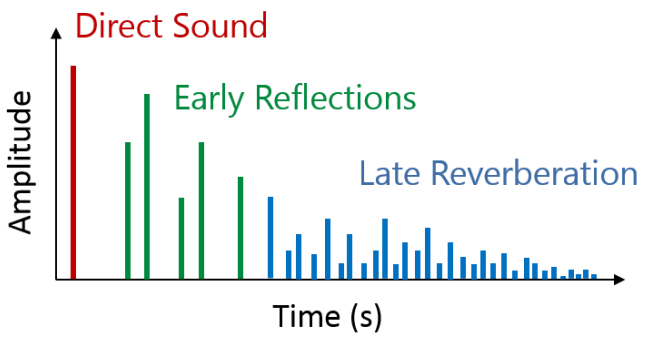


Figure 4-2: Diagram of a typical IR, broken down into three categories: direct sound, early reflections, and late reverberation.

Geometrical acoustics simulates the early reflections with the image-source method, and ray tracing is used to determine the late part of the IR. Current commercial software implements these two methods for room acoustic simulation. For these methods, computational time is significantly reduced from wave-based methods, which results in a more efficient program and algorithm. The image-source method is first used to calculate early specular reflections between a source and receiver. Borrowed from optics, the image-source method was first used in acoustics as a way to efficiently simulate the response of small, rectangular rooms with highly reflective surfaces, such a reverberation chambers.[72] When only considering a rectangular geometry, the locations of image sources can be easily determined based upon the room's dimension and the source's position. A 2-D plot of image source locations is shown for a rectangular room in Figure 4-3.

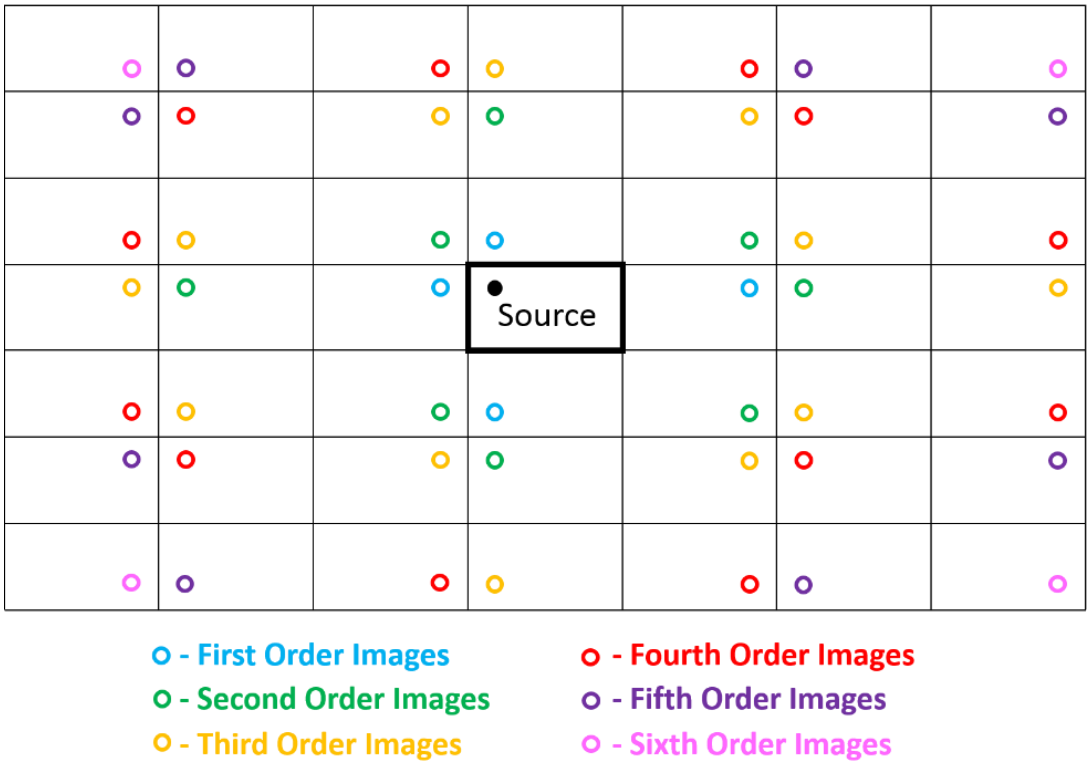


Figure 4-3: A 2-D plot showing image source locations in a rectangular room. Note that the set is incomplete for the fourth, fifth, and the sixth order images.

Later, the image-source method was extended to usage with any arbitrary room geometry, which is how it is currently implemented into computer programs today. First order images are found by reflecting the source perpendicularly across the plane defined by every room surface. For non-rectangular geometries, the possibility of calculating invalid image sources exists. When the desired location of the receiver is considered, if the ray path connecting the image source to the receiver intersects with the last wall over which the image was reflected, then it is considered a valid image source (Figure 4-4a). If the ray path falls outside of the bounds of the last surface of reflection, then it is considered an invalid image source (Figure 4-4b), which will not actually occur within the room, and thus should be removed from the simulation.

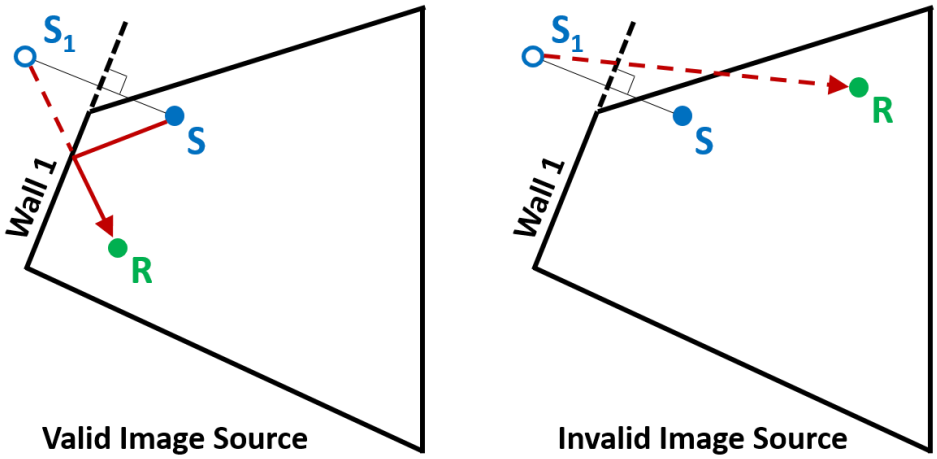


(a) (b)

Figure 4-4: The Wall 1 image source, shown both as (a) valid and (b) invalid, depending upon receiver location.

When non-rectangular geometries are used, a special test by the room acoustics software, called a point-in-polygon test must be performed, which tests to determine if the image source is valid, as described above. This operation must be extended to higher order images as well, to ensure that only valid image sources are included in the model. Since the image source is only valid for specular, early reflections, another method, ray-tracing, must be used to simulate the late energy found in the IR.

In the process of ray-tracing, rays are randomly emitted in all directions from a sound source. A particular source directivity can be added into the model by applying a directional weighting factor to each reflection, depending upon the angle at which each ray was emitted from the source. These rays are propagated through the model, depending upon the boundaries of the room. As the rays propagate, a specific sphere of detection is set up. (Figure 4-5) This sphere records any time a ray passes though, and keeps count of the number of rays arriving in a given direction, over small chunks of time. After the rays have been simulated up to a maximum duration of time in the IR, the count of rays serves as the frequency and directionally dependent energy envelope of the diffuse late reverberation in a RIR. Although this technique provides the energy distribution of the late part of the IR, it does not provide the fine structure of reflections found when many late reflections are all occurring very rapidly. Another method must be used to determine this fine structure.[71,73]

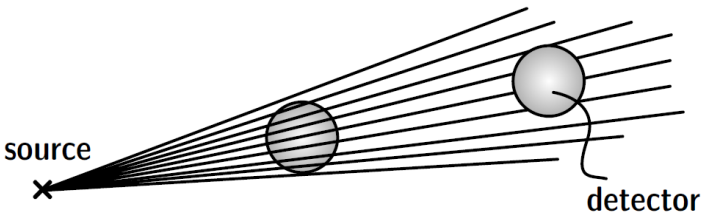


Figure 4-5: A graphic representation of a detector sphere used in the ray tracing algorithm. Image is taken from Figure 11.27 of Vorländer's *Auralization*.[71]

### 4.1.3: Statistical Estimation of Reverberation Fine-Structure

To model this fine structure, a Poisson-distributed noise process can be used.[73-74] A Poisson process is a counting process in terms of time, $N(t)$, which must meet the following criterion:[75]

- $N(0) = 0$
- When $t > 0,\ N(t)$ must have independent increments
- The number of events in any interval of duration $\Delta t$ has a Poisson distribution with mean $\mu\Delta t$. The variable $\mu$ is defined as the rate of the process. The probability of the occurrence of n events over an interval of $\Delta t$, $\gamma_n(\Delta t)$, can also be given by:

$$\gamma_n(\Delta t) = \frac{(\mu\Delta t)^n}{n!} e^{-\mu\Delta t} \qquad \text{for} \qquad n = 0,1,2,\ldots \ \&\ \mu > 0, \Delta t \geq 0\,. \tag{4-1}$$

According to Ross,[75] the time interval between any two consecutive events of a Poisson process can be expressed as an exponentially distributed random variable with mean $1/\mu$. In room acoustics, the event being discussed is the occurrence of a reflection, and $\mu$ is the reflection density of a room. Kuttruff derived the average temporal density of reflections ($\mu$) arriving at time $t$ for a rectangular room of volume $V$ and using sound speed $c$, given by:[76]

$$\mu = \frac{4\pi c^3 t^2}{V}\,. \tag{4-2}$$

with units of reflections per second. Thus, the mean dictating the random time interval has units of seconds per reflection, representing the time between each reflection. We can express $\Delta t_A$, or the time between two consecutive reflections in an IR, using the reflection density of the room and $z$, a uniformly distributed random variable from 0 to 1:

$$\Delta t_A(z) = \frac{1}{\mu}\ln\left(\frac{1}{z}\right) \quad \text{for} \quad 0 < z \leq 1\,. \tag{4-3}$$

He also states that it can be shown that this relationship for the average temporal density of reflections can be extended to any arbitrary geometry as well. This average density of reflections, in reflections per second, is then used in the calculation of our exponentially distributed random time step, $\Delta t_A(z)$. Using eqns. 4-2 and 4-3 we get the final random time step between two reflections:

$$\Delta t_A(t,z) = \frac{V}{4\pi c^3 t^2} * \ln\left(\frac{1}{z}\right) \quad \text{for} \quad 0 < z \leq 1\,. \tag{4-4}$$

It is quite interesting to see that this process can be determined with knowledge of only the room volume, $V$, and the timing index of the current location within the IR, $t$. A defined time for the first event must be made, which represents the minimum time between $t + \Delta t_A$.[73] This starting time, $t_o$, is defined using the speed of sound, $c$, for a room with a volume $V$ as:

$$t_o = \sqrt[3]{\frac{2Vln(2)}{4\pi c^3}} \approx 0.0014\sqrt[3]{V}\,. \tag{4-5}$$

From this algorithm, Dirac-delta functions are placed and spaced within the Poisson noise process based upon the calculated time-steps, $\Delta t_A$ from Eqn. 4-4. Figure 4-6 shows the process of populating individual Dirac-delta functions into a time series that will be shaped into the final reverberant IR. A verbal description of the steps are provided following the diagram.

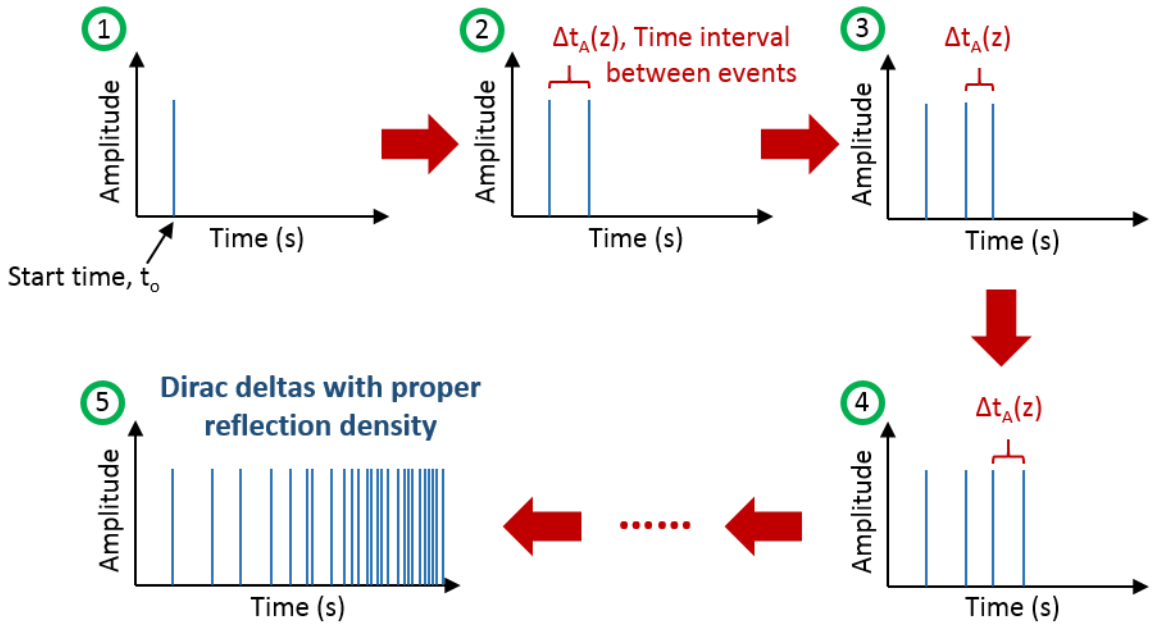


Figure 4-6: A diagram showing the steps required to populate Dirac-delta functions into a time series, which will be shaped into the reverberant energy. Each reflection is placed in time using the exponentially distributed random variable expressed in Eqn. 4-4.

1. The first reflection is placed at the starting time, $t_o$, defined by Eqn. 4-5.
2. The second reflection is placed at a point in time delayed by the time step, $\Delta t_A(z)$, from Eqn. 4-4. This time step is calculated using the time of the previous (first) reflection as $t$ in Eqn. 4-4.
3. The third reflection is placed, delayed in time from the second reflection by a newly calculated random time step, $\Delta t_A(z)$. The time of the previous reflection is now given by the time of the second reflection.
4. The fourth reflection is placed in time, using the previous reflection, the third reflection, as a reference for $t$.
5. This process is repeated, and Dirac-deltas continue to be populated into the time series until a limiting time is reached, and the process is stopped. The limiting time signifies the desired length in time of the simulated RIR.

Each Dirac-delta in Figure 4-6 is randomly assigned either a positive or negative value, depending upon whether they fall into the first or second half of a sample. Finally, the rate, $\mu$, is limited to a maximum value to ensure that no acoustical

artifacts are created, such as rattling, so that the sequence is still perceived as noise.[73-74,77] This criterion is $\mu \leq 10{,}000\ s^{-1}$. Figure 4-7 shows an example of a Poisson distributed noise process created using these relationships.

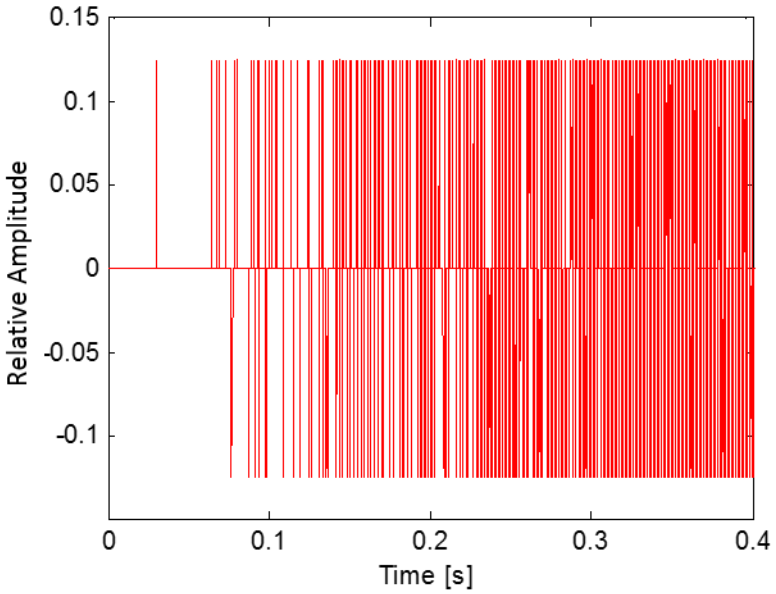


Figure 4-7: A Poisson noise process generated to represent the fine temporal structure of late reverberation.

This energy can then be time windowed, shaped, and filtered for each separate octave band. After separate processing, the energy in each octave band can then be combined back together, creating a final IR with frequency-dependent late reverberant energy, suitable for auralization. The main benefit of using this Poisson noise process is that it creates a temporal distribution that is accurately tied to a physical room size, and includes the fine structure of reverberant energy, creating plausible auralizations. Additionally, it is suitable for use in simulating spectrally neutral, or uncolored reverberant energy in a room, for the random noise process generated has a neutral frequency response. The frequency response of the signal from Figure 4-7 is shown in Figure 4-8.

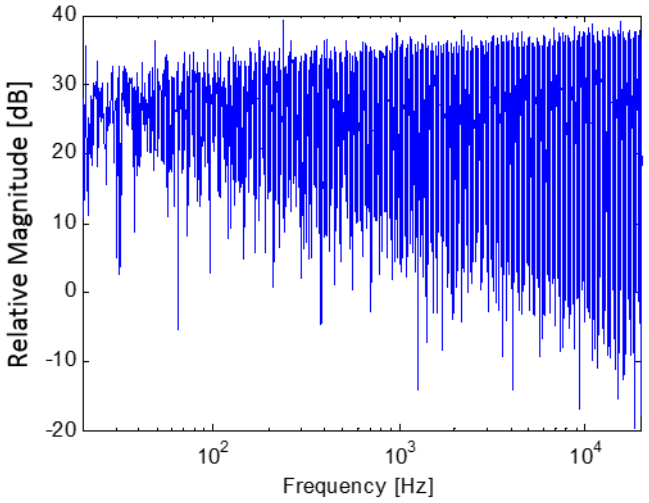


Figure 4-8: The frequency spectrum of the Poisson noise process which is used to generate late reverberant energy. The neutral response allows this noise process to simulate reverberation without coloring the energy.

## 4.2: Simulation Implementation for Current Study

This section describes how the different methods were chosen and implemented into the current study. For simplicity and easy adjustment to the simulation method, a rectangular geometry was assumed for the simulation. Due to the efficiency of the processing time, geometrical acoustics and statistical reverberation were used, as opposed to any wave-based numerical methods. This approach was chosen for a few reasons. First, the processing and adjustments for geometrical acoustics can be entirely determined by room geometry, source-receiver location, and material properties, without the need to create new meshes for every room change. A simple change in room length, width, or height will require new calculation, but they can be implemented rather efficiently.

As well, geometrical acoustics is much more computationally efficient, which makes it possible to create simulations rather quickly for a range of room sizes, and prepare them to be compared over the loudspeaker array. Wave-based methods require much more computation time. Finally, geometrical acoustics was chosen based upon the balance of physical accuracy and controllability for this study. Since LEV is a topic which has received little research in the past, much has yet to be learned. With future LEV research, sound fields used for comparison should be based upon a physical

geometry, but adaptability is of primary concern. In the end, wave-based methods are arguably more accurate, especially at low frequencies, but they do not provide the easy adjustment and adaptability of geometrical acoustics and statically-based reverberation. Thus, the latter were chosen, and are described in Sections 4.2.1 through 4.2.4.

For a final note, in Sections 4.2.2 through 4.2.4, the creation of the room's IR is explained, example plots are given for the different methods, and the combining of the simulation methods into a hybrid method is explained. For all of these examples, the monaural, or omnidirectional RIR is used. In practice, since auralizations are going to be carried out over a loudspeaker array, the IR needs to be encoded into Ambisonic signals, not simply a monaural IR. This process is explained in Section 4.2.5, but for the simulation method discussion, the example of the monaural IR is utilized.

### 4.2.1: Image Source Method – Calculating Image Locations

The image source method, described in Section 4.1.2, was utilized to model the early reflections occurring within the room simulation for this project. Since a rectangular geometry was assumed, all images can be calculated based upon the room's geometry, and image validity can easily be ensured. In a rectangular room, the possibility of overlapping images, a specific type of invalid image source, occurs quite often. For example, in Figure 4-9, if the original source is reflected across wall 1, then the resulting image source is labeled $S_1$. Likewise for wall 2, the resulting image source $S_2$ occurs. Then, to extend the model to a potential second order image source, $S_1$ can now be reflected across wall 2, resulting in the image source $S_{1,2}$ where the order of subscripts represents the order in which the reflections across walls occurred from the original source.

In the same manor, reflecting $S_2$ across wall 1 will result in image $S_{2,1}$ but something strange occurs. Now, both $S_{1,2}$ and $S_{2,1}$ lie directly on top of each other. The check for image-source validity is to determine if the ray connecting the image-source to the receiver location passes through the last wall over which the source was reflected. If

not, the source is invalid, but if it does cross that particular wall, the source is valid. When both overlapping second order images are connected with $R_1$ in Figure 4-9, we see that the ray passes through wall 1, making $S_{2,1}$ valid (last reflected over wall 1), and makes $S_{1,2}$ invalid (last reflected over wall 2). On the other hand, at $R_2$ the ray passes through wall 2, making $S_{1,2}$ valid and $S_{2,1}$ invalid. Expanding potential receiver locations to the entire room, it can be seen that no matter the choice of location, one image, either $S_{2,1}$ or $S_{1,2}$ will always be valid, and the other corresponding image will be invalid.

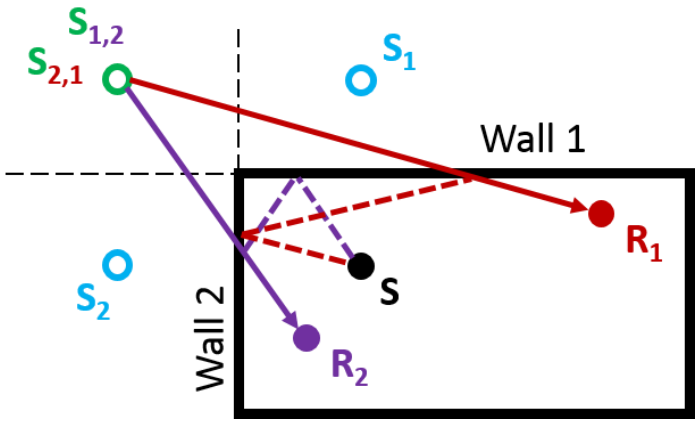


Figure 4-9: For a rectangular geometry, often higher order image sources can create overlapping images, only one of which is a valid image source, depending upon receiver location.

Thus, whenever overlapping images occur for a rectangular geometry, only one of the images should be kept as valid. In the end, since the images are all overlapping, it does not matter which one is conceptually kept for the rectangular geometry case. Thus, image source validity does not require a check to see if it will be valid, for once overlapping images are accounted for, all of the remaining images will always be valid for the rectangular geometry case. Thus, the location of image sources can be entirely determined by simply knowing the source location within the room, and the length, width, and height of the room. For these reasons, this method was implemented into this study. Image sources up to third-order were calculated for a rectangular room, and expressions were developed to determine their locations in terms of source location and room dimensions. The equations for up to third-order image sources are

all provided in Appendix D. The coordinate axes, from which the source, receiver, and all image sources are calculated, along with the wall numbering and room dimensioning system are shown in Figure 4-10.

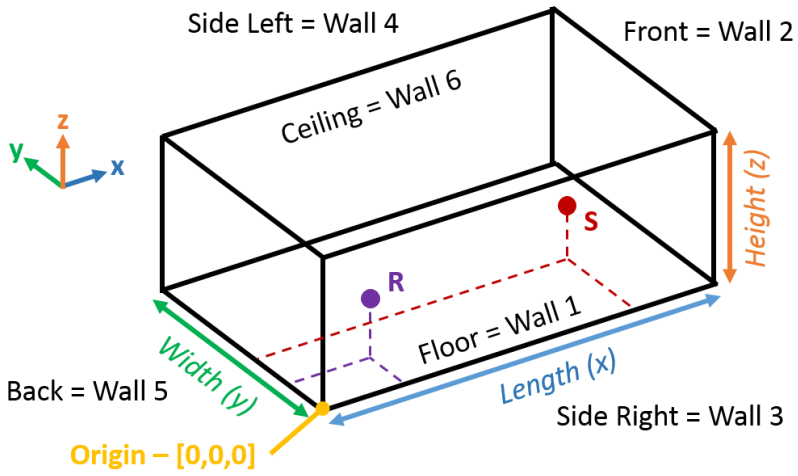


Figure 4-10: The coordinate axes, wall numbering, and room dimensioning used to help calculate image source locations for the rectangular room. Equations are provided in Appendix D.

From these locations, the azimuths and elevations of reflections can be calculated, along with the relative levels of each image source. The azimuths and elevations can be calculated in terms of the receiver locations, using the coordinate axes displayed in Figure 2-11. Then, the locations are adjusted so that the receiver is oriented toward the source ("look direction"). This look direction is achieved by subtracting the original source's azimuth and elevation from each image sources' azimuth ($\varphi$) and elevation ($\theta$), respectively, in the common room x-y-z coordinate axes in Figure 4-10. Effectively, the coordinate axes are being rotated until the x-direction (look direction) is oriented directly towards the source, using the following relationships:

$$\varphi = \frac{180}{\pi} * \left( - \tan^{-1}\left(\frac{i_{n,y} - R_y}{i_{n,x} - R_x}\right) - \tan^{-1}\left(\frac{S_y}{S_x}\right)\right), \quad 4\text{-}6$$

$$\theta = \frac{180}{\pi} * \left( \left(\frac{\pi}{2} - \cos^{-1}\left(\frac{i_{n,z} - R_z}{r_n}\right)\right) - \left(\frac{\pi}{2} - \cos^{-1}\left(\frac{S_z}{r_s}\right)\right)\right), \quad 4\text{-}7$$

where,

$$r_S = \sqrt{(S_x - R_x)^2 + \left(S_y - R_y\right)^2 + (S_z - R_z)^2}\,. \tag{4-8}$$

The inverse tangent used in Eqn. 4-6 must be a four-quadrant inverse tangent function, producing results in which $-180 \leq \varphi \leq 180$ degrees. Time delays associated with the n$^{th}$ image source's propagation distance to the receiver can also be calculated using the simple relationship between the speed of sound in air, $c$, and distance, $r_n$:

$$t_{delay,n} = \frac{r_n}{c} = \frac{\sqrt{\left(i_{x,n} - R_x\right)^2 + \left(i_{y,n} - R_y\right)^2 + \left(i_{z,n} - R_z\right)^2}}{c}\,. \tag{4-9}$$

For the program, the user can specify whether or not to use feet or meters for the room dimensions, which is accounted for in the image source method by simply using appropriate units for the sound speed in air.

### 4.2.2: Image Source Method – Levels

Once the time delays and locations of the image sources are accurately determined, the levels, in each octave band, must be calculated for each individual reflection. For each reflection, the level of the n$^{th}$ image source is given by:

$$L_n(r_n) = \frac{1}{r_n} * \left(1 - \alpha_{abs,wall}(f)\right) * \left(1 - \alpha_{scat,wall}(f)\right) * 10^{-\left(\frac{\alpha_{air}(f) r_n}{20}\right)}. \tag{4-10}$$

The first term accounts for the spherical spreading of the IR, by dividing by the propagation distance from the image source to the receiver. The next two terms are the attenuation from absorption and scattering of the wall surfaces, after reflection. Eqn. 4-10 represents what would occur for a first order image source. If second or third-order image sources are calculated, additional $(1 - \alpha)$ multiplication terms would be needed for each additional wall reflection, for both absorption and

scattering. Both absorption and scattering coefficients are implemented as frequency dependent quantities, specified in terms of octave bands.

The final term accounts for air absorption, which was calculated and validated against the ISO 9613-2:1996 standard.[78-80] From the standard, air absorption coefficients are provided on an attenuation in dB per reference distance, for a specific temperature, pressure, relative humidity, and frequency – designated as $\alpha_{air}(f)$. This value is calculated on either a dB/m or a dB/ft basis, depending upon the input units for the room dimensions. For this project, standard room conditions were assumed of 20 °C, 50 % RH, and atmospheric pressure (101.325 kPa). As well, values were calculated at octave-band center frequencies to account for processing at different frequencies. Ultimately, it would be desirable to have the air absorption reported in a manner similar to absorption or scattering coefficients of materials. To meet this goal, the value needs to be algebraically manipulated, creating an attenuation coefficient that represents the attenuated sound pressure over the original sound pressure.

The final term was derived as follows: from the equation for sound pressure level,

$$L_P = 20\log_{10}\left(\frac{p_{rms}}{p_{ref}}\right), \qquad \text{where} \qquad p_{ref} = 20 * 10^{-6}\ \text{Pa}, \tag{4-11}$$

an expression for the difference in dB, between the original level and the attenuated level, is obtained using logarithmic subtraction rules:

$$\Delta L_P = 20\log_{10}\left(\frac{p_{original}}{p_{ref}}\right) - 20\log_{10}\left(\frac{p_{attenuated}}{p_{ref}}\right) = 20\log_{10}\left(\frac{p_{original}}{p_{attenuated}}\right). \tag{4-12}$$

Knowledge of the change in dB, $\Delta L_P$, is equivalent to the ISO standard's air attenuation coefficient times the n$^{th}$ image source's propagation distance, $r_n$, in feet or meters, and we find:

$$\Delta L_P = \alpha_{air}(f) * r_n = 20 \log_{10}\left(\frac{p_{attenuated}}{p_{original}}\right). \quad 4\text{-}13$$

And with a bit of algebraic manipulation, we get the final attenuation multiplier, written as a ratio of the attenuated sound pressure to the original sound pressure:

$$\frac{p_{attenuated}}{p_{original}} = 10^{-\left(\frac{\alpha_{air}(f) r_n}{20}\right)}. \quad 4\text{-}14$$

It should be noted that the following relationship for air absorption is given for an individual reflection from the $n^{th}$ image source. The final result is obtained by performing this calculation separately for each image source, in each octave band, and summing the individual results together. Thus, the levels of the specular early reflections within the room can be calculated from the image source method. Finally, using the time delays and levels from spherical spreading, wall absorption, wall scattering, and air absorption, the omnidirectional RIR for the early reflections were calculated for the room. The RIR was then used to calculate common room acoustics metrics, i.e. T30 and EDT. T30 and EDT represent the time it takes sound to decay by 60 dB in a room. T30 is calculated by extrapolating the decay from -5 dB to -35 dB (normalized to direction sound energy at 0 dB), and EDT is calculated by extrapolating the decay from 0 dB to -10 dB, looking primarily at early reflections within the room.

First, the reflections of the RIR are created and input at the correct time by placing a Dirac delta function at the correct time delay. For the IRs, the zero time reference refers to the moment that sound was initially played from the source. This creates a natural propagation delay that is included in the IR. Once the time structure is created, the levels of each reflection are attenuated according to Eqn. 4-10. This is now done separately for each octave band since air absorption and wall absorption and scattering are all frequency dependent quantities. The IR for each given octave band is then band-pass filtered for its respective octave band. Finally, the band-pass

filtered IRs are then added together, creating the final, full frequency IR for the early reflections in the room. This process is shown below in Figure 4-11.

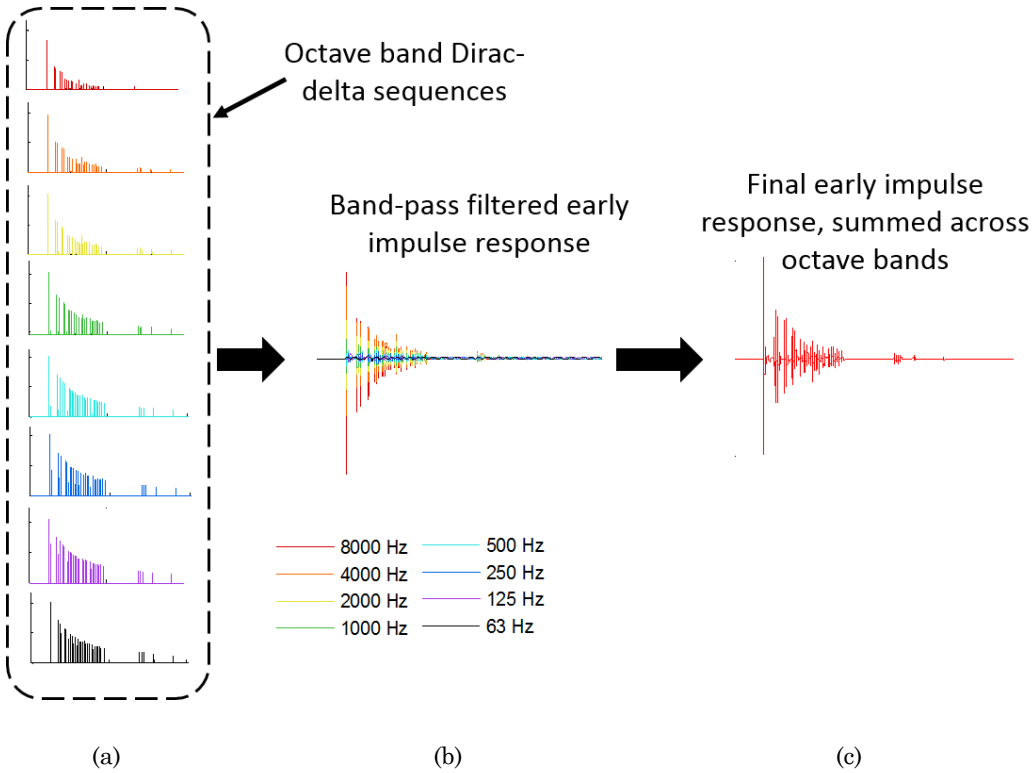


Figure 4-11: The process of populating times and level delays into a final IR. From left to right, (a) Dirac-delta functions are populated into an IR based upon image time delays and attenuated separately in each octave-band. Then, (b) they are band-pass filtered and (c) summed for the final IR.

### 4.2.3: Reverberation Synthesis

With the image source accounting for the early reflections present within the room, the late part of the IR must also be simulated. Due to the fact that not all surfaces in a room generate perfectly specular reflections, over time, the properties of reflections within a room change as time increases. Again, referring to the simplified diagram of the IR in Figure 4-2, reflections become much smaller in amplitude, but more closely spaced in time. Due to the diffusive material properties within a room, as time increases, at some point all reflections should end up arriving from all directions in a somewhat random pattern. Some rooms that may inherently create a non-diffuse sound field, not reaching this point, result from very long, flat, or coupled spaces.[71,76]

For the late energy, the temporal structure can be modeled using the Poisson process described in Section 4.1.3. First, the initial structure is created, based specifically on the room volume, the current time index in the IR, and the total target length of the IR. This process is done according to eqns. 4-3 through 4-4, and an example of the resulting distribution is shown in Figure 4-7. Once this structure is created, the levels need to be adjusted to account for spherical spreading, air absorption, and wall reflections. The levels are calculated from:

$$L_n(t) = \frac{1}{ct_n} * \left(1 - \alpha_{abs,reverb}(f)\right)^{t_n * n_{rfl,avg}} * 10^{-\left(\frac{\alpha_{air}(f) c t_n}{20}\right)}. \qquad 4\text{-}15$$

Eqn. 4-15 is very similar to Eqn. 4-10, with a few adjustments. Now, every reflection generated by the Poisson process is adjusted based upon its time of occurrence, or time delay, $t_n$. This time of arrival is used to calculate the propagation distance by simply multiplying $t_n$ by the speed of sound, $c$ (this replaces $r_n$ from the previous Eqn. 4-10). Scattering attenuation is no longer included, since this diffuse late reverberation is highly composed of scattered sound. Finally, since we no longer have specific image sources, we don't know what wall each reflection will have occurred from, or even how many reflections each sound event has undergone. To estimate this number, a relationship derived by Kuttruff is used for the average number of wall reflections per second experienced by a diffuse reflection within a rectangular geometry. This relationship is provided below, where $S$ is the total wall area of the room:[76]

$$n_{rfl,avg} = \frac{cS}{4V}. \qquad 4\text{-}16$$

This quantity is directly related to the mean free path, a typical concept in room acoustics. Eqn. 4-16 could also be found by dividing the speed of sound, $c$ (in meters per second), by the mean free path (in meters per reflection), resulting in the number of reflections occurring after a given time in seconds. It should be noted that this simple relationship is defined assuming a diffuse sound field, with reverberant

energy evenly distributed throughout a space and reflections arriving to individual listeners randomly, from all directions. This allows averaging of the number of reflections over all propagation directions. The main benefit of using this relationship is that it provides something that is only dependent upon the time delay of the reflection. As well, the absorption coefficient for the wall reflections, $\alpha_{wall,reverb}(f)$, is taken as a weighted average, based upon surface area and the absorption coefficients assigned to the room surfaces.

In summary, the following steps were used to simulate the final reverberant tail:

1. The Poisson noise process was generated, as seen in Figure 4-7.
2. The reflections in the Poisson noise process were shaped based upon eqns. 4-15 and 4-16, including the frequency dependence for different octave bands. This resulted in eight separate IRs.
3. A band-pass octave-band filter was applied to each corresponding shaped Poisson noise process. This extracted only the desired energy from each shaped noise signal for its corresponding octave band.
4. The octave-band IRs were summed, to create the frequency dependent reverberant energy for the room. This will then be combined with the image source method for the final IR, discussed in Section 4.2.4.

With these steps, the reverberant energy can be simulated for the sound field. This process was used to construct the omnidirectional IR for the room's diffuse late reverberation, and it is summarized in Figure 4-12.[73] The numbers in Figure 4-12 correspond to the numbered steps 1-4 described in the process above.

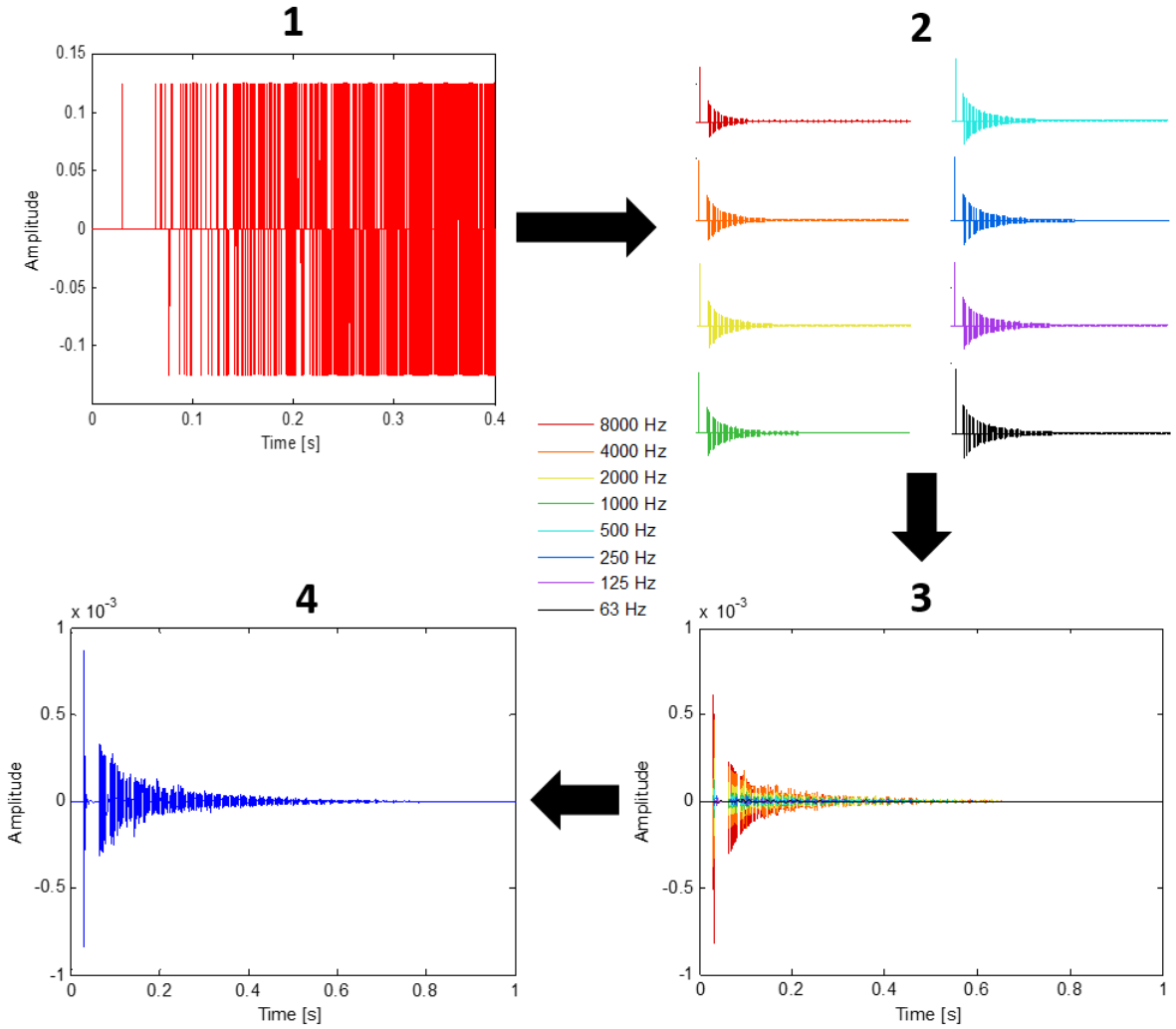


Figure 4-12: The steps used to generate and shape the Poisson noise process into late reverberant energy. This figure is based off of Figure 5.18 from Dirk Schröder's dissertation, RWTH University, Aachen, 2011.[73]

### 4.2.4: Hybrid Simulation – Combining Image Sources with Reverberation

Once both the image-source method and the statistical reverberation method were used to simulate energy for the RIR, the energy from both simulations were combined into a final RIR. This is the step in which both separate simulation methods were combined together into one hybrid method. For the IR within a room, it is not a simple task to specify the time in which energy transitions from early to late energy. This distinction is a property of the room size, room geometry, and human auditory perception. For this reason, flexibility in specifying this transition point was desired. The simulation required an input of a transition time, and a transition length. The

transition time is the time, in seconds, that the transition between the image-source method and the late reverberant simulation occurred. The transition length is the interval of time, in seconds, over which the image-source method was "turned off". This same length of time was used for the time it took to "turn on" the reverberant energy. A time windowing technique was used to accomplish this transition. For both methods a time window was constructed using half of a Hann window, to create a smooth transition between the two. The Hann window was created to be twice the width of the transition time so that half of the window would be equal to the transition time. Figure 4-13 shows a 10 millisecond Hann window, which was used to construct windows for a transition time of 5 milliseconds.

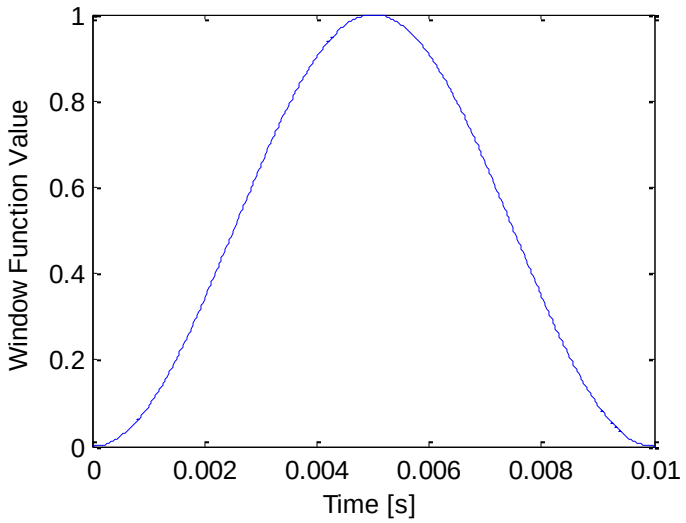


Figure 4-13: A Hann window of length 10 ms, constructed for a transition time of 5 ms for hybrid simulation.

For the image-source window, a vector of ones equal to the IR length was used, and the second half of the Hann window inserted so that the midpoint of the Hann window was placed at the specified transition time. Once this segment of the Hann window returned to zero, the ones in the image-source window were replaced with zeros. Similarly, for the reverberant window, the first half of the window was placed within a vector of zeros, placing the midpoint of the Hann window at the specified transition time. Then ones were inserted into the reverberant window, after the window had

reached a value of 1, which resulted in the final reverberant energy time window shown in Figure 4-14.

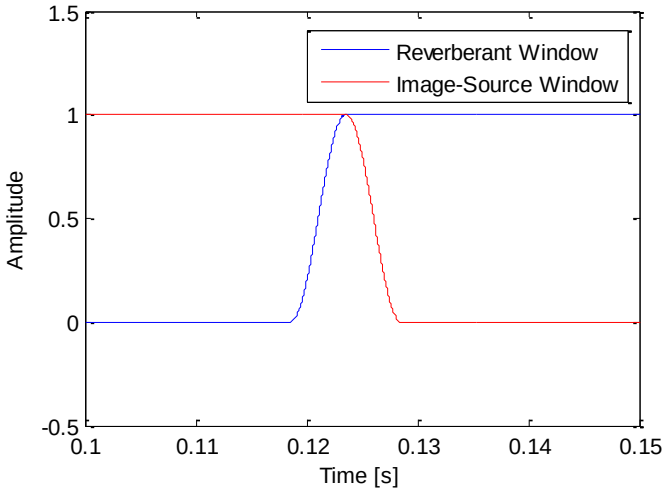


Figure 4-14: A plot showing both of the time windows used to combine the image-source simulation with the reverberant energy simulation. A transition time of 0.005 s was used

To create the final IR, both simulated IRs were multiplied with each corresponding element of the time windows. Then a final summation of the two simulations created the final monaural RIR for a particular source-receiver combination in the simulated room (see example in Figure 4-15).

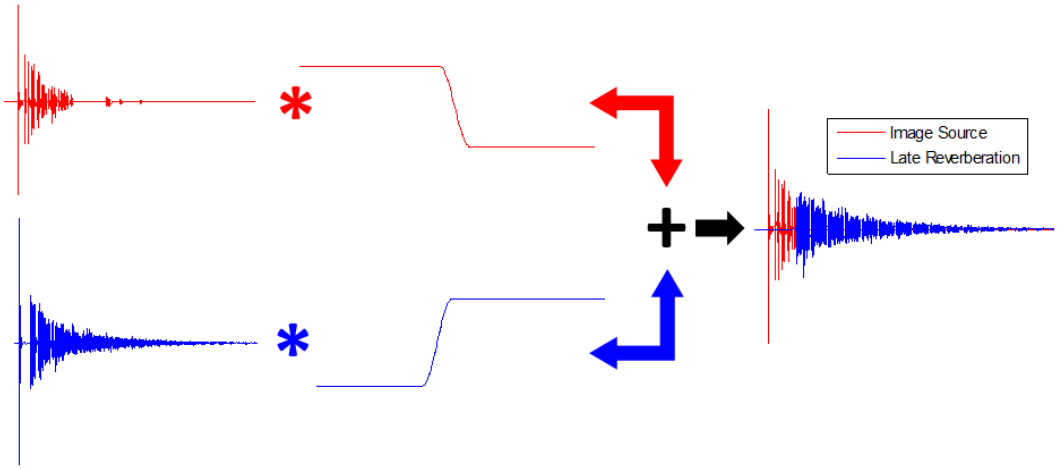


Figure 4-15: Time-windowing both the image source and the late reverberation impulse responses and summing to create the final RIR.

A method to expedite the selection of the transition point in this simulation was explored. When creating auralizations, individually specifying the room's transition time can be quite tedious, and an automated process is desirable. After multiple methods were tested, the best method to automate the process was to specify this point as the average of the first, second, and third-order image sources' time delays. For the simulated process, a visual inspection was always used to ensure that this transition time occurred when the image-source method reflections were closely spaced in time. As well, the specification of this transition time could be used as a variable to manipulate in creating stimuli for subjective studies.

### 4.2.5: Encoding in Spherical Harmonics

To this point, the monaural IR has been used as an example to illustrate the simulation process, but this information alone is not enough information for a detailed third-order Ambisonic auralization to be reproduced over the loudspeaker array. The IR must be encoded into Ambisonic signals instead of a simple omnidirectional IR. The Ambisonic signals, as explained in Sections 2.3.3 through 2.3.5, are the spherical harmonic components of a signal, up to a specified order $n$. For this study, third-order Ambisonics was used for encoding into Ambisonic signals and decoding into the 30 loudspeaker signals required for reproduction. The same processing for populating the final monaural IR described in Sections 4.2.1 – 4.2.4 is used. The difference is that instead of populating one monaural IR, 16 Ambisonic IRs are populated, corresponding to the 16 spherical harmonic components shown in Figure 2-12. To encode the signals into each component, the levels of each reflection have one more level adjustment applied, which are adjusted forms of previously shown eqns. 4-10 and 4-15:

$$L_n(r_n, l, m, \varphi, \theta) = \frac{1}{r_n} * \left(1 - \alpha_{abs,wall}(f)\right) * \left(1 - \alpha_{scat,wall}(f)\right) * 10^{-\left(\frac{\alpha_{air}(f) r_n}{20}\right)} * Y_l^m(\varphi, \theta)\,, \qquad 4\text{-}17$$

$$L_n(t_n, l, m, \varphi, \theta) = \frac{1}{c t_n} * \left(1 - \alpha_{abs,wall}(f)\right)^{n_{rfl,avg}} * 10^{-\left(\frac{\alpha_{air}(f) c t_n}{20}\right)} * Y_l^m(\varphi, \theta)\,. \qquad 4\text{-}18$$

The additional term in both equations is from the definition of the real parts of the spherical harmonics, provided in Eqn. 2-30. Based upon the direction of the reflection, this term adjusted the level for each reflection, as it was encoded into the Ambisonic signals. With this new adjustment, each reflection was populated into a separate IR for each octave band, and each Ambisonic component, resulting from the spherical harmonics term. This produced $8 * 16 = 128$ separately populated directional IRs. Then, the IRs were filtered with their respective band-pass octave-band filters, to retain the energy which corresponded with the desired octave-band (for all octave bands within each Ambisonic signal). After this operation was performed, the filtered IRs were summed across all octave-bands, resulting in the 16 Ambisonic IRs. Again, this processing is identical to the monaural IR processing, but now done separately for each of the 16 Ambisonic signals, including the spherical harmonics term as a directionally dependent amplitude adjustment.

For simple implementation, the spherical harmonics term and the corresponding Legendre polynomials have been worked out, according to Eqn. 2-30, and represented in terms of sine and cosine functions of the azimuth and elevation angles. These functions can be found in the first half of Appendix D, evaluated using the definition of elevation as the angle between the direction vector and the horizontal plane, shown in the coordinate aces in Figure 2-11. Often times, other references will use the more common definition of elevation, where it is defined as the angle between the direction vector and the vertical (z) axis. For this reason, the same function has also been evaluated using that definition of elevation, and the solutions are provided in the second half of Appendix D.

### 4.2.6: Auralizations: Decoding Ambisonic Signals to Loudspeakers Signals

Once the final Ambisonic signals had been simulated, the Ambisonic processing required for playback over the loudspeaker array is implemented. This step is referred to as the decoding phase of the Ambisonic processing. To implement the decoding, the digital audio workstation REAPER was utilized.[67] Using VST plug-ins, a series of effects were added into the signal chain within REAPER. A 16 channel

Ambisonic file of the auralization was loaded into REAPER, and once the effects were in place, the Ambisonic file can either be decoded and processed in real-time over the array, or it can be rendered into a final 30 channel .wav file for playback over the 30 loudspeakers.

An overview of the VST plug-ins implemented in REAPER is shown in Figure 4-16. The first step in the signal chain is the Ambisonic format converter.[81-82] When using an Ambisonic decoder, it is vital to ensure the Ambisonic signals are in the correct format, which the decoder expects to read from.[60] The different formats were briefly discussed in Section 2.3.3. The Ambisonic signals are encoded into the ambiX format, which uses the SN3D normalization scheme with ACN channel numbering (see Section 2.3.3). The SPRAL loudspeaker array decoder, developed by Dave Dick for his Ph.D. project, was made using the Ambisonics decoder toolbox based in MATLAB.[70] This decoder expects Furse-Malham Ambisonic signals, so the Ambisonics converter must be used. Then, the signals are decoded into the loudspeaker signals using a dual-band decoder, described in the next paragraph.

Finally, the loudspeaker signals are sent through the last VST plug-in, which is a simple convolution block, performing digital equalization for the non-flat loudspeaker responses.[82-83] Each of the loudspeakers was measured in the anechoic chamber in the Garfield Thomas Water Tunnel Building, which has a much lower free-field cutoff than the anechoic chamber in the Hammond Building (it has 3' (0.91 m) deep fiberglass wedges). The IR was measured for each loudspeaker individually, and this IR was inverted, with a low frequency cutoff at 60 Hz. This inverted IR was used to generate an FIR filter, individually designed for each loudspeaker.


Figure 4-16: A schematic layout of the processing steps setup within REAPER, creating the final loudspeaker signals. This includes format conversion, decoding, level compensation, time delay compensation, and loudspeaker equalization.

The general design philosophy outlined in Section 2.3.5 was used for the design process. The loudspeaker locations used were the locations measured with the Eigenmike em32, shown in Table 3-2. Since the decoder performance is much more sensitive, and breaks down at high frequencies, for simplicity, the locations measured were the tweeter locations. Near-field compensation is also performed, which is based upon the physical distance between the listener and the loudspeaker array. A dual-band decoder was created, with a crossover point at 400 Hz. The low frequency decoder is computed to ensure that the velocity localization vector, $r_v$, is maximized in all directions.[70] The method is further optimized to ensure that the minimum required power solution is used.

For the high frequency decoder, when an unevenly spaced loudspeaker array is used, the localization vectors, $r_v$ and $r_e$, are not required to point in the same direction.[70] To balance the tradeoff between maximizing the two vectors, and ensuring they point in the correct direction, optimization tools are used. In the toolkit, users are provided with different criteria in decoder design, such as angular accuracy, performance in specific directions, and uniform energy gain. The user than applies weights, specifying the overall importance of the different criterion for their specific application. All criterion are combined together, and optimization techniques are used to design a decoder for the specific application. Many different solutions can result, so it is up to the user to know the project's needs, and balance performance trade-offs in decoder design. To combine the two decoders together, the relative levels of each signal are adjusted to ensure that the original RMS level is preserved in the decoding process. The developed decoders also include level and time delay compensation for non-spherical loudspeaker arrays, based upon the input loudspeaker locations into the toolbox.

## 4.3: Measurement Validation of Simulations

To determine the accuracy of the simulations being reproduced over the array, comparisons were made between the simulated IRs and reproduced IRs, as measured in the anechoic chamber after Ambisonic reproduction. Eight different hall

simulations, of widely varying room conditions, were simulated for the validation process. The eight simulations correspond to the first set of room simulations made for the subjective study (set 1), which will be described in Section 5.3. To measure the IRs in the anechoic chamber, the simulated Ambisonic IRs for each stimuli were convolved with a sine sweep signal, containing six separate sine sweeps from 20 Hz to 22 kHz, with 1 second of silence in between each sweep. The resulting signal was then processed using the VST plug-ins for the decoding, near-field compensation, time and level adjustment, and loudspeaker equalization.

The final signal represented a simulation of an omnidirectional loudspeaker playing a sine-sweep on stage in the simulated room. The Eigenmike em32 was used to record the simulated sine-sweep auralizations. The measured sine sweeps were averaged, using the last five sweeps and discarding the first sweep as a measurement pre-send. After averaging in the time domain, the average measured signal and the original sweep signal were converted to the frequency domain, divided to obtain the transfer function, and converted back to the time domain to extract the measured RIR. Figure 4-17 and Figure 4-18 compare the IR for two of the eight simulations. In both cases, the overall shape of the IR and the timing and levels of early reflections match very well, validating the IR simulation and reproduction.

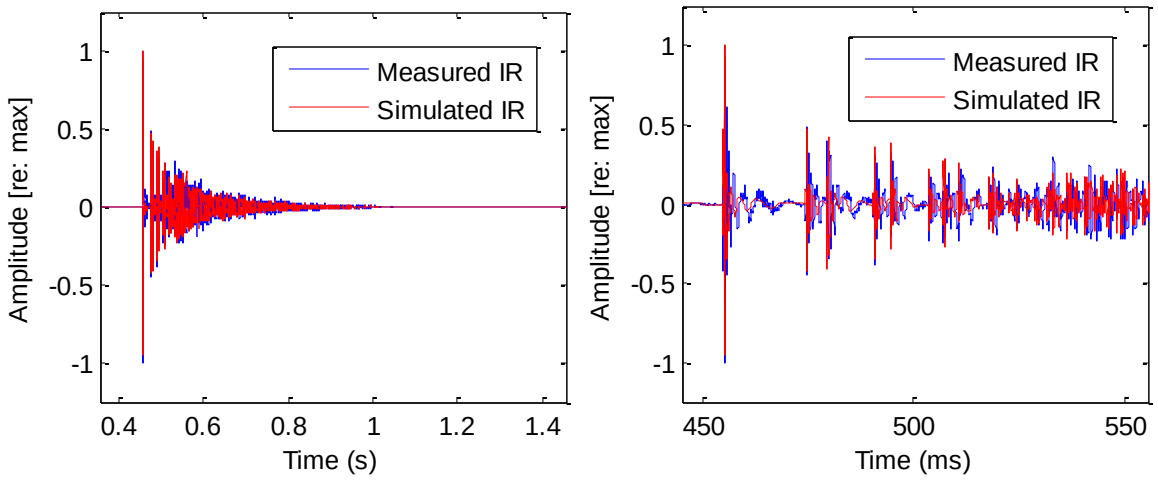


Figure 4-17: (a) A comparison between a sample simulated IR (red) and measured IR (blue) which is the Ambisonics reproduction of the simulated IR. (b) A zoomed in view of the early part of the IR in (a), showing how well the early, individual reflections line up in time for the both the measured and simulated IRs.

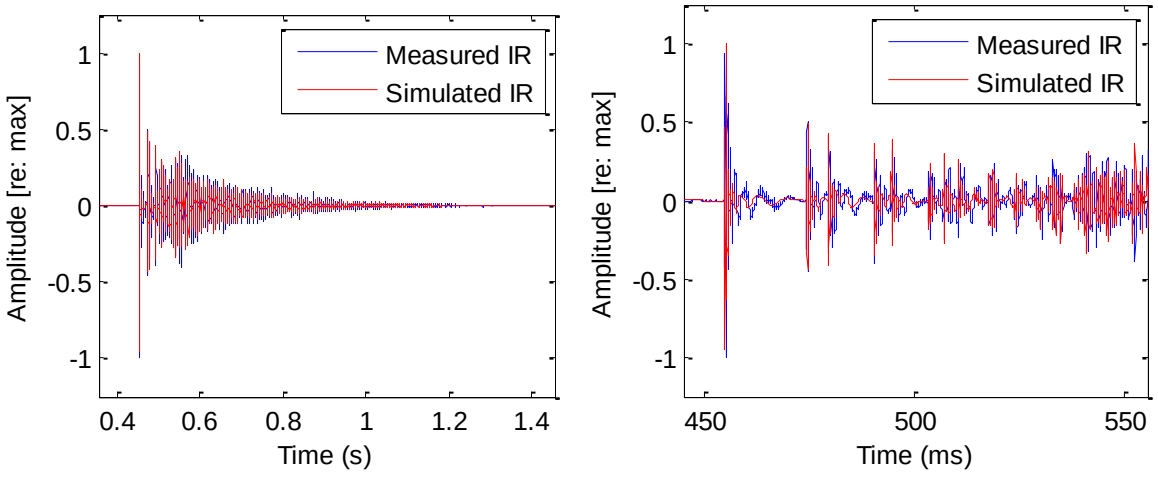


Figure 4-18: (a) An overall comparison between a sample simulated IR (red) and measured IR (blue) which is the Ambisonics reproduction of the simulated IR. (b) A zoomed in view of the early part of the IR, showing how well the early, individual reflections line up in time for both the measured and simulated IRs.

Additionally, common room acoustics metrics were calculated and compared between the simulated and the measured IRs, validating the simulations in another manner. To quantify this comparison, Reverberation Time (T30) and Early Decay Time (EDT), were used. T30 is a measurement calculated from the decay of the RIR from -5 to -35 dB (normalized to 0 dB for the direct sound), and provides a representation of the

overall energy in the IR. EDT is calculated from the decay of the IR from 0 to -10 dB, characterizing deviations that occur in the early part of the IR. Figure 4-19 shows comparisons between measured and simulated values for T30 for four of the eight simulations; the curves are nearly identical. Figure 4-20 shows the differences between measured and simulated results for EDT, again for four of the eight simulations. For the case of EDT, results between simulations and measurements agree within ±0.2 s for most cases.

Although the differences in EDT are larger than the differences for T30, this result is expected due to the sensitivity of EDT. Since EDT is dependent on the early reflections in the IR, small changes in microphone placement or amplitudes of reflections will cause much larger changes in the measured values. Additionally, percentages deviations comparing measured results to simulations for T30 and EDT are given in Table 4-1 and Table 4-2 respectively. With a just-noticeable difference (JND) value of 5% for both T30 and EDT,[1] all of the deviations except at one octave band fall within 1 JND. The significant deviations for EDT range from 1 to 3 JNDs. Although this difference is larger, studies have shown that measurement uncertainty can be extremely high for this metric.[84] One study in particular showed that EDT measurement variations were well over 20% in certain octave bands.[48] The deviations found in this work are smaller than variations in other studies, so the differences in the measured and simulated IRs are considered within measurement error.

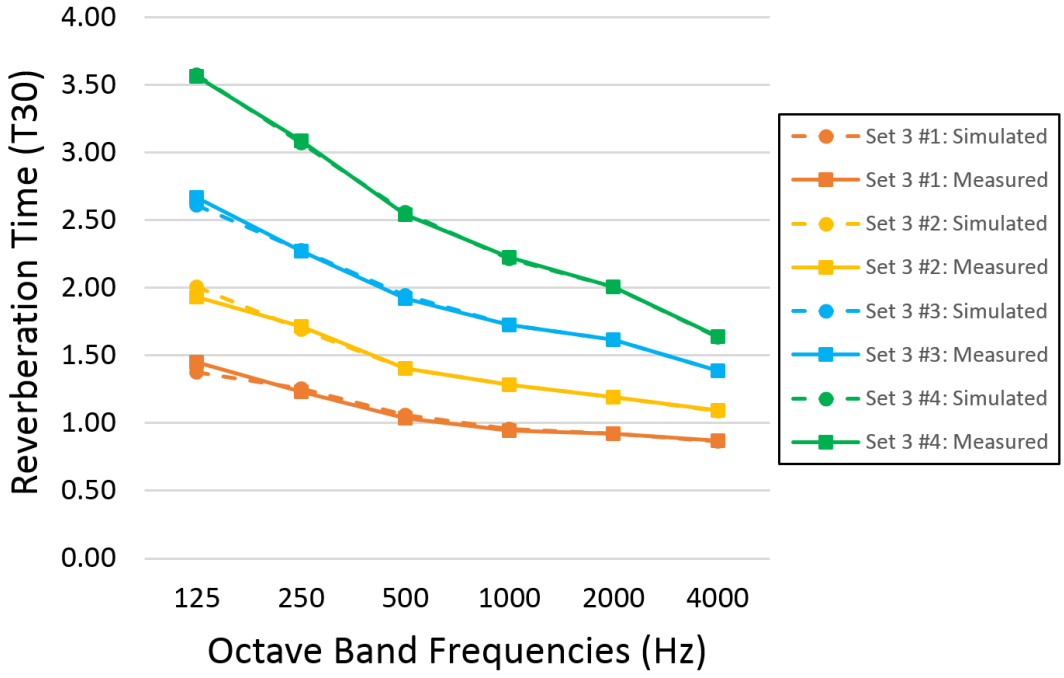


Figure 4-19: A comparison between measured RT values (solid lines) and simulated RT values (dashed lines) for four different simulated rooms. The graphs show nearly identical results between the two.

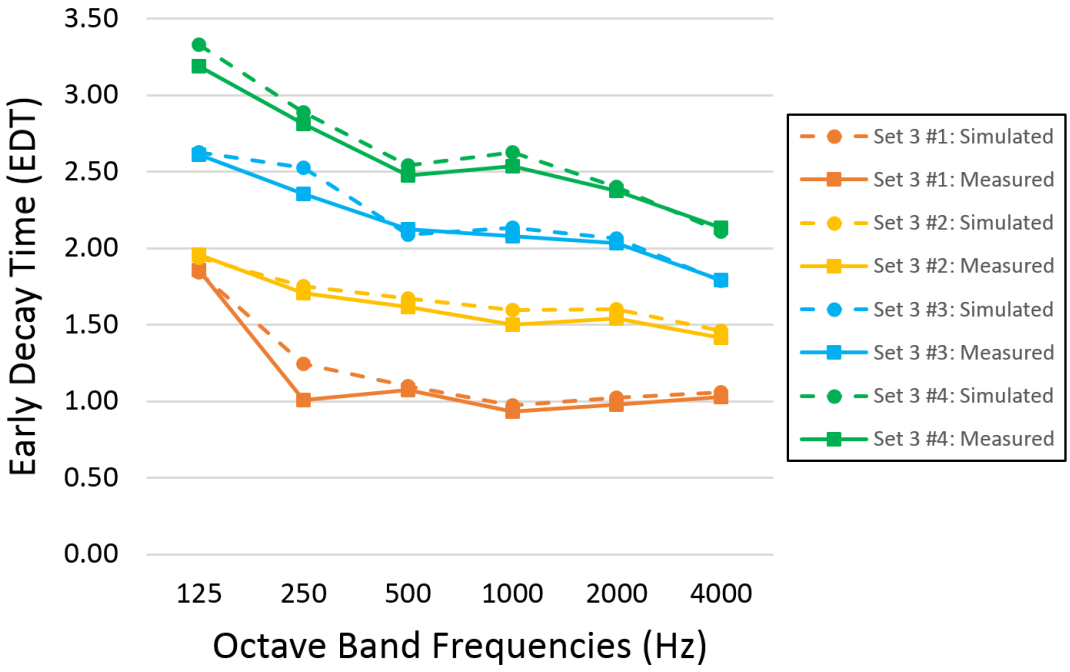


Figure 4-20: A comparison between measured EDT values (solid lines) and simulated EDT values (dashed lines) for four different simulated rooms. The graphs show a high amount of agreement between the two.

Table 4-1: A summary table showing the percentage deviations of T30 comparing the measured values to the simulated values. Deviations are all within one JND for T30 (5%), except for one case highlighted in red.

| Set # | Audio # | T30 Differences (%) | | | | | | |
|---|---|---|---|---|---|---|---|---|
| | | Avg. | 125 Hz | 250 Hz | 500 Hz | 1000 Hz | 2000 Hz | 4000 Hz |
| 3 | 1 | -1.5% | **5.5%** | -2.2% | -2.1% | -1.2% | 0.0% | 0.5% |
| 3 | 2 | 0.4% | -3.7% | 1.2% | -0.4% | 0.3% | 0.0% | 0.4% |
| 3 | 3 | -0.4% | 2.2% | -0.3% | -1.3% | 0.2% | 0.0% | -0.2% |
| 3 | 4 | 0.1% | -0.2% | 0.4% | -0.7% | 0.5% | 0.2% | 0.3% |
| 3 | 5 | -0.6% | 3.5% | 0.5% | -1.6% | -1.1% | -0.2% | 0.0% |
| 3 | 6 | -1.0% | 1.5% | -3.1% | -0.8% | 0.0% | 0.4% | 1.3% |
| 3 | 7 | -0.7% | -0.2% | -2.6% | -0.5% | 0.7% | 0.3% | 0.2% |
| 3 | 8 | -0.1% | -1.1% | -0.1% | -0.9% | 1.3% | -0.6% | 0.1% |

Table 4-2: A summary of the percentage differences in EDT between measured and simulated values for the eight test-case IRs. 12 of the 48 octave bands are larger than 1 JND for EDT (5%), highlighted in red. However, these results are still smaller than published results on the measurement uncertainty of EDT.[48,84]

| Set # | Audio # | EDT Differences (%) | | | | | | |
|---|---|---|---|---|---|---|---|---|
| | | Avg. | 125 Hz | 250 Hz | 500 Hz | 1000 Hz | 2000 Hz | 4000 Hz |
| 3 | 1 | **-7.9%** | 1.0% | **-18.8%** | -2.2% | -4.2% | -4.4% | -3.0% |
| 3 | 2 | -3.9% | 1.1% | -2.7% | -3.3% | **-5.8%** | -3.8% | -3.1% |
| 3 | 3 | -2.5% | -0.5% | **-6.7%** | 1.8% | -2.7% | -1.4% | 0.3% |
| 3 | 4 | -2.5% | -4.1% | -2.7% | -2.6% | -3.5% | -1.1% | 1.2% |
| 3 | 5 | **-7.5%** | **-12.0%** | **-9.0%** | -3.7% | **-8.8%** | **-8.6%** | **-14.7%** |
| 3 | 6 | -4.6% | -1.2% | -3.4% | **-6.5%** | -4.4% | -4.2% | -3.6% |
| 3 | 7 | -2.1% | 0.0% | -1.8% | -4.1% | -2.6% | 0.2% | -0.4% |
| 3 | 8 | 3.0% | 1.4% | **9.6%** | 4.3% | -1.9% | -1.5% | 2.9% |

Final measurements of many different room acoustics metrics, for each of the stimuli used in this test, is given in Appendix I. In this appendix, the provided parameters are based upon measurements made using the Eigenmike em32. A wide variety of room acoustics parameters are given for the stimuli for the reader's reference and discussion of future work and results from future studies. All metrics are provided from the 125 Hz to the 4000 Hz octave bands. Again, these metrics are not simulated, but rather, measured in the array, so they correspond directly to what the listener experienced during the test.

# Chapter 5: Subjective Testing Methods

The AURAS facility discussed in Chapter 3 and the simulation methods discussed in Chapter 4 were implemented in an initial study looking at the perception of LEV in concert halls. This chapter will discuss the subjective testing performed, and how these newly developed resources were utilized. Participation requirements, methods, and the structure of the test will be discussed. Finally, the individual stimuli created using the simulation methods from Chapter 4 will be provided. Results from this subjective test are presented in Chapter 6.

## 5.1: Participation Requirements

When selecting participants for any listening test, subjects should represent a complete subset from the target audience you are trying to learn and understand about. For our testing, the target subject sample was concert-goers and musicians who would listen to and enjoy performances in concert halls. To achieve an accurate representation of this group, musicians were chosen as the target participant group. When musicians are used for listening tests in concert hall acoustics, fewer subjects are typically required to find statistically significant results. This is due to their experience and ability of musicians to hear smaller differences than non-musicians without listening experience. Since the term musician is not specific, our test had the following musical requirements:

1. The participants had to be currently taking private lessons and/or participating within a musical ensemble.
2. The participants had to have at least five years of combined formal musical training.[85-86] This could be achieved with combined experiences in private study and ensembles.

These criteria provide a good screening method for selecting participants with adequate musical training. Subjects were pre-screened with these questions via email to ensure that they met our musical training requirements. It should be noted that some very qualified potential test subjects will not meet these requirements, namely

if they are not currently participating actively in formal musical training or playing in an ensemble. If potential candidates had a very strong musical background, but had recently stopped formal training, exceptions were rarely allowed. This was only done if their training experience was clear (15+ years) and they were still actively playing and/or listening to music on a regular basis.

Subjects were also required to pass a hearing screening, and have a minimum hearing threshold of at least 15 dB HL[87] in the 250, 500, 1000, 2000, 4000, and 8000 Hz octave bands. If any participant did not meet these minimum hearing threshold requirements, the study was terminated after the hearing screening. For taking the time to sign up for the test, these participants were compensated with a $5 gift card. If participants passed the screening requirements, they were allowed to participate in the study, and they were compensated for their time with a $15 gift card. Musicians were recruited to the study using the email list servers for undergraduate and graduate School of Music students, school of music ensembles, and the Graduate Program in Acoustics. All testing was submitted and approved through the Internal Review Board (IRB) at Penn State (IRB protocol #41733).

## 5.2: Testing Method

Various testing methods could be considered when conducting listening tests in concert hall acoustics. The most common method requires the participants to individually rate each stimuli, one at a time. In this method, subjects listen to one concert hall stimuli at a time, and then rate that one stimuli in terms of a subjective attribute, such as LEV, reverberance, clarity, etc. Each question is presented separately, and accurate comparison relies on the participant's auditory memory between stimuli, and statistical averaging between subjects. Typically, order of questions within sets and the order of question sets is completely randomized, so that any effects from presentation order is removed as more and more participants are tested.

This method has limitations, which appear when more subtle differences are being tested. If a subject's auditory memory cannot distinguish differences between successive questions, comparisons will not be heard properly. When differences between stimuli are large, this issue is typically not a problem, for our auditory memory can make these comparisons. When differences are smaller and more subtle, it is very hard for a listener to make adequate judgments and comparisons using this method. Even though successive stimuli could be heard within a matter of around 10 seconds of each other, the auditory memory needed to compare such differences is not adequate. To help reduce the load on auditory memory, stimuli could be presented in a comparative way, where listeners can freely switch back and forth between any number of stimuli. One specific type of test that implements this style of questions is the Multiple Stimulus test with Hidden Reference and Anchor (MUSHRA).[88-89] This type of test is commonly used in audio quality testing, and an example user interface is shown in Figure 5-1.

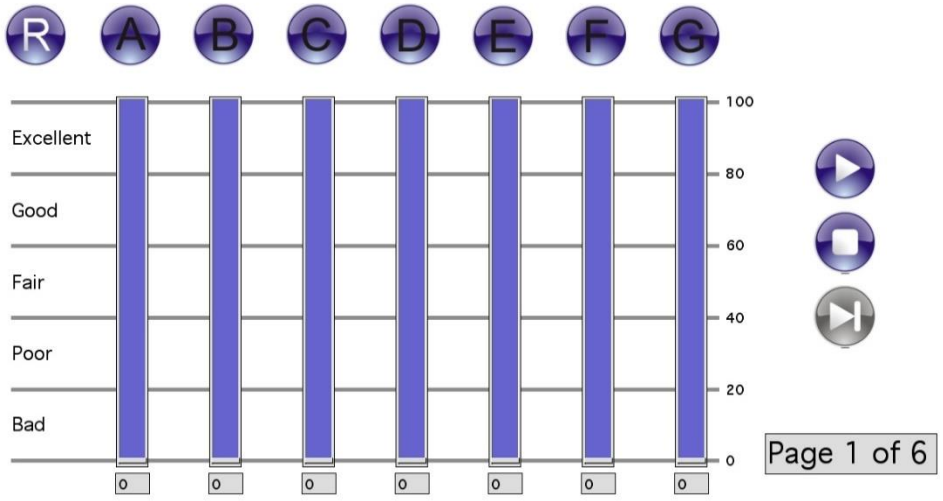


Figure 5-1: An example of a typical graphic user interface used for a MUSHRA style audio quality test.

In audio quality testing, often it is desirable to know if certain processing schemes have a noticeably negative impact upon perceived quality of an audio signal. The R button in Figure 5-1 is the reference, which can be thought of as the gold standard. Subjects are asked to compare every other stimuli, A through G, to the reference. A high rating of excellent, or 100, means that the stimuli are identical to the reference,

with no noticeable distortion or artifacts present in the compared letter stimuli. A lower rating results from the audibility of distortions or artifacts in the signal. Participants will rate all of the stimuli, comparing each to the reference, and may switch back and forth between stimuli freely during the comparison process.

Once the subject is done, answers are submitted with the next question set button on the right. Then, the same test can be done with new stimuli. Additionally, inside of the lettered stimuli, two of the signals provide a hidden reference and anchor. The hidden reference is simply an identical copy of the known reference, to help determine reliability. The hidden anchor is a file of known obvious distortion, which should receive the lowest rating. This helps provide a low end to the scale, and helps with subject comparison. The benefits of such a method are quite clear. If a participant is allowed to compare stimuli one next to the other, the subtle differences that might not be identified with a successive stimuli type test might be identified with a MUSHRA style test. For the study in this project, a MUSHRA style test was adapted for use, and it is described in Section 5.3.

## 5.3: Final Subjective Stimuli

For the test, four different groups of eight stimuli were created, all with a different focus. In each set, specific variables were changed, which were initially expected to produce noticeable differences in LEV for subjects. This section describes each of the four sets, and the factors used to simulate each of the different test cases. Eight stimuli were paired together, balancing the desire for variety in comparisons with the difficulty of the test. For all of the stimuli, an anechoic motif from the Denon anechoic orchestral recordings CD was used.[90] The excerpt was from the overture of the Opera *Ruslan and Lyudmila*, which was listed as track 5 on the CD. A 60 second segment of the piece was identified, selected, and edited for final use in the study. To create the simulations, the anechoic music was convolved with each of the 16 third-order Ambisonic IRs described in Section 4.2.5. These were then decoded over the loudspeaker array in REAPER, using the VST plugins which were developed by Dave Dick for the loudspeaker array. This processing is briefly described in Section 4.2.6.

Table 5-1: Summary of the different independent variable for each set of stimuli.

| Stimuli Set Summary Table | | | | |
|---|---|---|---|---|
| Stimuli Set | Primary Variable | | Secondary Variable | |
| | Variable | Cases | Variable | Cases |
| 1 | RT | 1.05 s - 2.87 s | Room Size | 80% & 120% |
| 2 | Late Energy Scaling | 0.5, 0.7, 1.0, 1.5 | Receiver | R1 & R2 |
| 3 | Room Size | 80%, 100%, 110%, 120% | RT | 1.4 s & 2.1 s |
| 4*** | Room Size | 80%, 100%, 110%, 120% | RT | 1.4 s & 2.1 s |

***Indicates stimuli set was not level equalized

Overall, the breakdown for the stimuli sets is provided in Table 5-1. In the table, the two main independent variables changed in each set are shown. As will be described, RT, hall size, receiver location, and the late energy scaling factor were adjusted for the different sets. The primary and secondary variables chosen for each stimuli set are shown, and the different levels of each of these variables are listed. The remainder of this section provides details of how each set was created specifically, using the simulation program.

The first set of stimuli looked to identify differences in LEV produced by different sizes of rooms. Two different sized room were created, all based upon the published size of Boston Symphony Hall (BSH) – 160' (48.8 m) length x 75' (22.7 m) wide x 61' (18.6 m) tall.[2] The two hall sizes that were used were set to be simple scales of BSH, with multipliers of 80% – 128' (39.0 m) x 60' (18.3 m) x 48.8' (14.9 m) – and 120% – 192' (58.5 m) x 90' (27.4 m) x 73.2' (22.3 m). For both of the hall sizes, the source remained at a constant location, in reference to the front of the room, and the receiver location remained constant relative to the source. The source-receiver location for both halls, along with the relative sizes of the halls, are shown in Figure 5-2, where the smallest dashed line represents the 80% hall, and the largest is the 120% hall. For (x,y,z) source-receiver locations, please refer to Appendix E. To make the eight different stimuli, along with hall size, the rooms' RTs were adjusted such that the average mid-frequency RT values fell within a range of 1.0 s and 2.9 s, producing four different RT settings within each size of hall. After altering material properties in the large hall, the range of RTs achieved was from around 1.4 s to 2.9 s. For the small hall, after adjusting materials, a range of RT was found from 1.0 s to 2.5 s. Since the

volume was much lower for the 80% hall, it was much easier to achieve a low RT in the hall, shown in the 1.0 s case. For the 120% hall, with its large volume, the RT could not reach a value around the 1.0 s RT curve, so instead, a higher RT curve of 2.9 s was added for the larger hall. The RT values for both halls were still overlapping in the range from 1.4 s to 2.5 s. Plots of RT across octave bands for each room size and absorption setting are shown in Figure 5-3.

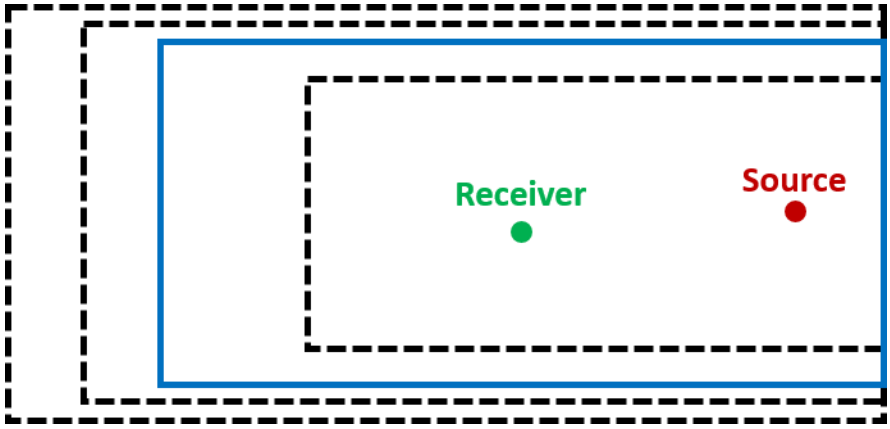


Figure 5-2: A plan view of the modeled source-receiver location for set 1 auralizations. The 100% BSH is shown in blue, and other hall sizes are shown as dashed lines. These represent the 80%, 110%, and 120% cases.

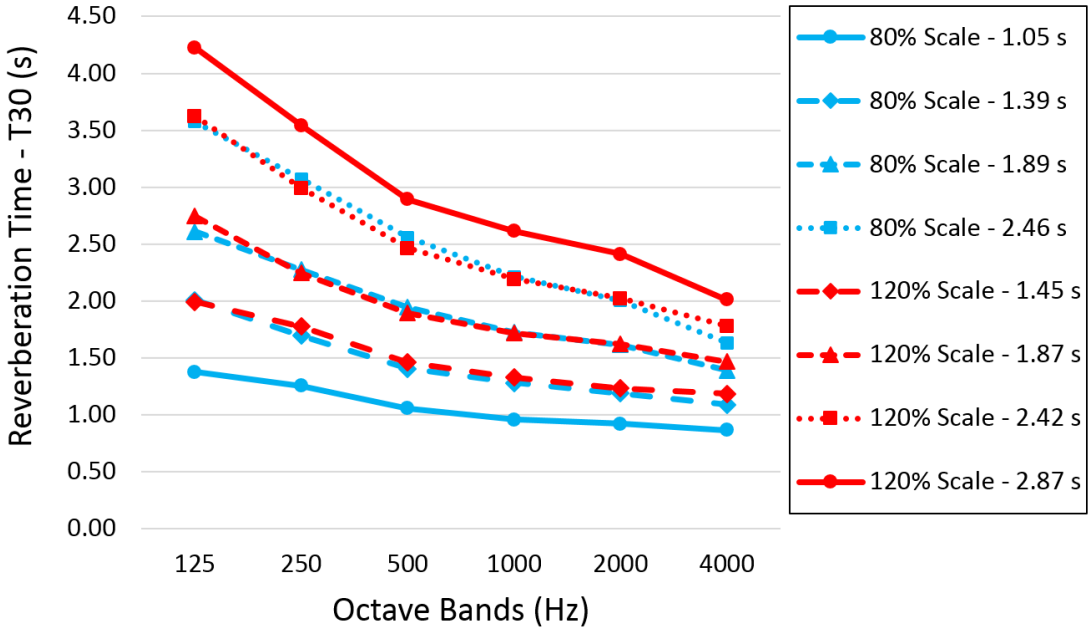


Figure 5-3: Reverberation times (T30) for the different simulations for set 1 (2 scales, 4 absorption values).

To create different absorption settings, initial hall scattering coefficient values and absorption coefficients were taken to represent a hall with medium upholstered seating and fairly reflective surfaces on all other walls. Then, to create the different absorption settings, a simple scaling factor was applied to the absorption coefficients, separately for each octave band. In most cases, one overall multiplier provided was needed to match the RT curves between hall sizes, but a close match required slight adjustments to individual octave band coefficients. In any of the weighting adjustments, the absorption coefficients were always limited between the values of 0 and 1. Specifics on all of the inputs to the simulation models for auralization sets 1 through 4 can be found in Appendix E, along with input data for the remain three sets of auralizations.

A different approach was used in the second set of questions. For this set, the main variable was controlling the balance of early-to-late energy within the hall. Such a comparison is commonly used in developing various metrics in concert hall acoustics, e.g. Clarity Index (C80). Typically, this parameter is determined by the distance a receiver is located from a source. When a listener is closer to a source in a room, the direct sound energy and early reflections will be stronger, and be more prominent, compared to the reflected energy. The further a listener moves from a source, the prominence of direct sound and early reflections will decrease. This is primarily due to the effects of both spherical spreading, and air absorption at higher frequencies. Since both late and early sound have been proposed to impact the sense of LEV in a hall, balancing this ratio between late and early sound is of interest.

An initial simulation was carried out in the 80% BSH-sized room. This was the only room used for the second set of auralizations. Two receiver locations were selected, whose locations can be found in Figure 5-4.

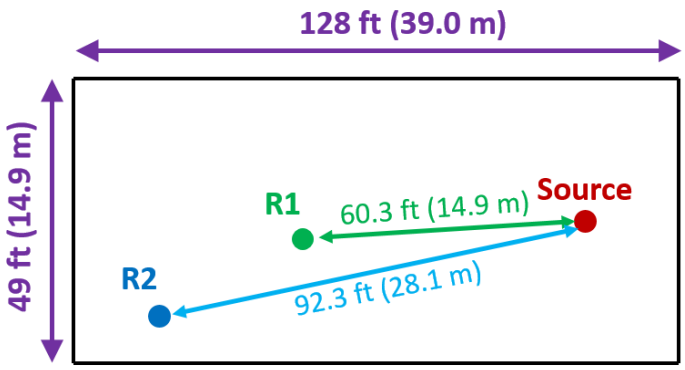


Figure 5-4: Relative locations of the source and two receiver position, R1 and R2, for the scaled late reverberation auralization set (set 2).

For exact (x,y,z) receiver and source locations, please refer to Appendix E. Initially, the first stimulus was made using the baseline hall materials, and the resulting mid-frequency average RT was 1.42 s. To change the stimulus, the simulated reverberation was scaled in amplitude before combining with the direct sound and early reflections. Four scale factors were applied to the reverberant energy wall absorption coefficients to adjust the stimuli: 0.5, 0.7, 1.0, and 1.5. A smaller scaling factor resulted in lower absorption coefficients, increasing the amount of reverberant energy. As well, the scaling factors were only applied to the wall absorption coefficients for late reverberation simulation, which did not impact the absorption coefficients used for early reflection simulation. This produced identical direct and early energies for the same source-receiver location. Once this process was completed for R1, the same process was repeated for R2, with the same scaling factors. Large scaling factors resulted in a lower amount of reverberant energy. The scaled late energies can be seen in the IRs shown in Figure 5-5.

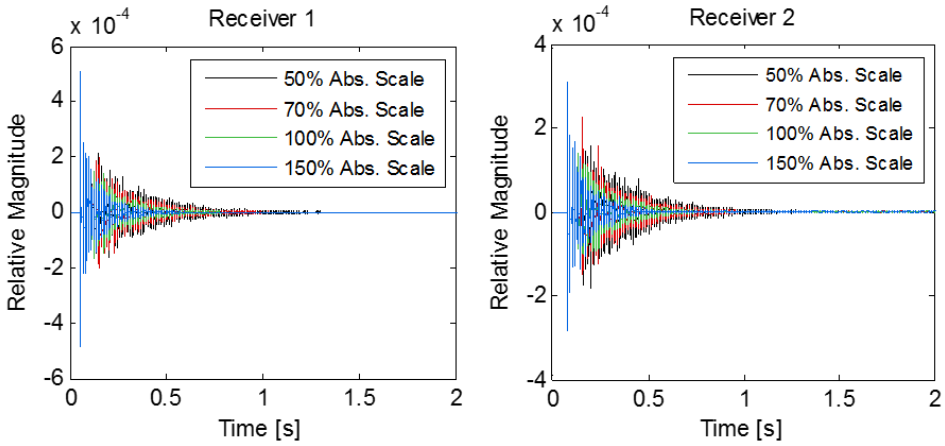


Figure 5-5: IRs generated using different scaling factors on the reverberant energy for both receiver locations. Note how the late energy changes due to the different scaling factors.

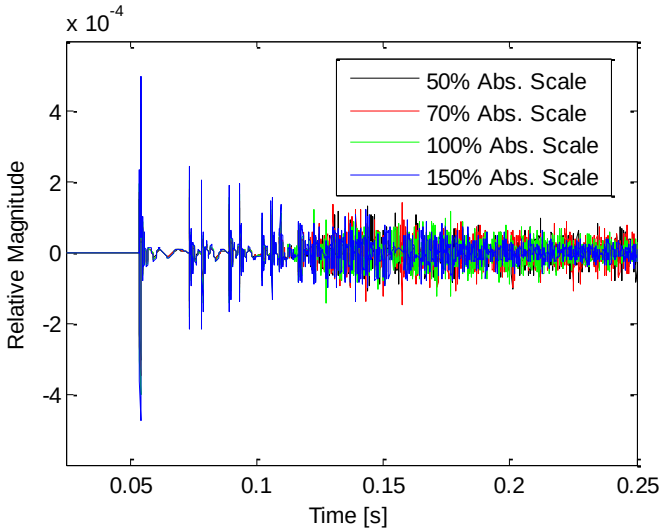


Figure 5-6: A zoomed-in view of the early part of the receiver 1 IRs from Figure 5-5. In the early part of the IR, up until around 70 ms after the direct sound, early reflections are identical in time and spatial location,

The effects of the scaling factors on the late part of the IRs can be clearly seen in Figure 5-5. The colors correspond to the different scaling factors, which change the late reverberation characteristics. As can be seen in Figure 5-6, the direct and early reflections between the IRs at the same receiver location do not change between scaling cases. Since we are looking at the balance between early and late energy in the IR, the best room acoustic's metric to quantify this relationship is the Clarity Index for music (C80). C80 is a decibel measure of the ratio of the early sound energy to the late sound energy, with a cutoff time between early and late energy of 80 ms.

Figure 5-7 shows plots of the C80 values versus octave band, resulting from the scaling process. For this set of stimuli, a range of broadband C80 values of around 8 dB was achieved.

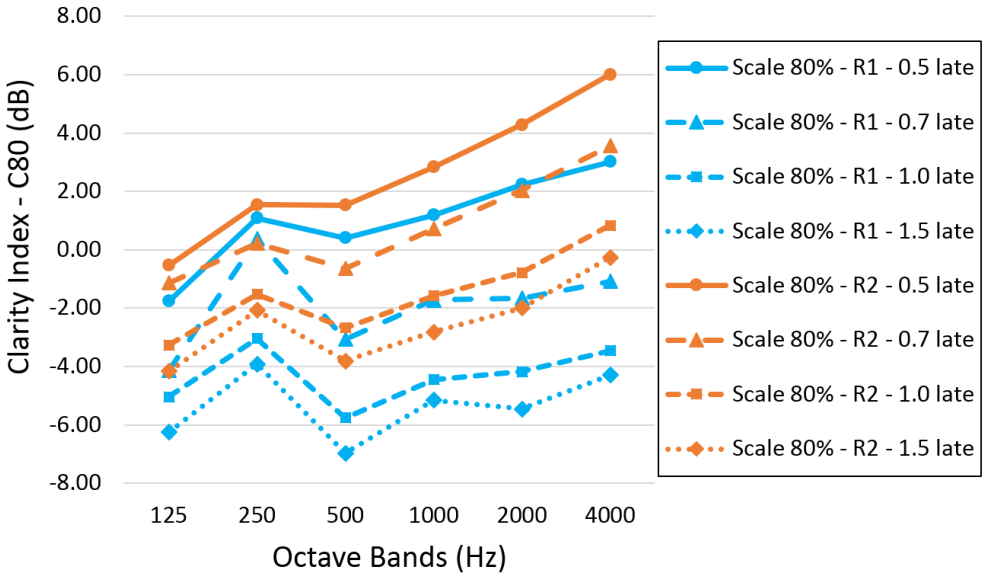


Figure 5-7: The calculated C80's of the different stimuli used in set 2 (2 receivers, 4 absorption values), where late energy was scaled with a particular factor. A range of around 8 dB was achieved for C80.

Again it should be noted that all of the different stimuli were level equalized to the level of the loudest stimuli. This means that the final presented auralization levels of the direct sound in each auralization was not the same, even though they were simulated with identical direct sound and early reflections. Differing late energy amounts created different overall levels, and required unique level equalization amounts for each auralization, based upon the total energy in the IR.

For stimuli set 3 from Table 5-1, a very similar test consideration to set 1 was used. Instead of using two hall sizes and four RTs for the cases, two RTs and four hall sizes were used. The same method from set 1 for controlling the source-receiver distance was implemented in this set. The diagram for source-receiver distance in different hall scales, again, is found in Figure 5-2. For this set, halls sizes were scaled to be 80%, 100%, 110%, and 120% of BSH, and four RTs were used for each scale, ranging from an average value from 250 – 2000 Hz of 1.4 s and 2.1 s. The plots of these different RTs across octave bands is provided below in Figure 5-8. Again, level

equalization was performed to ensure all stimuli were presented at the same level as the highest level stimuli.

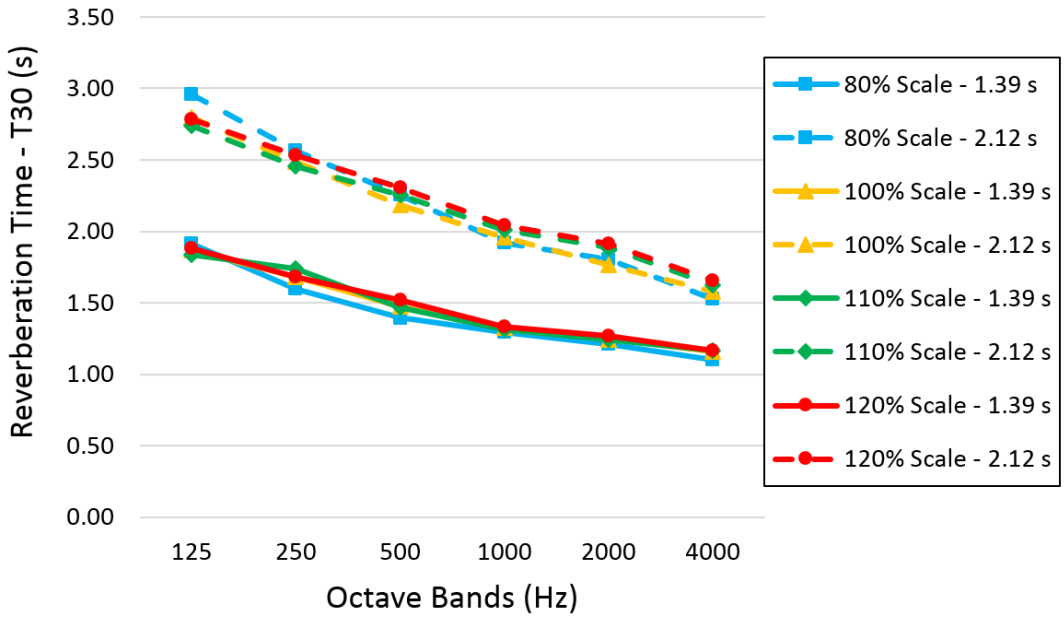


Figure 5-8: A plot showing RTs in each octave band of the stimuli for sets 3 & 4 (4 scales, 2 absorption values).

The final set, found in Table 5-1 (set 4) was identical to set 3, but no level equalization was performed. Without level adjustment, the direct sound energy level was identical in all cases, but due to the early reflection and late reverberation energy differences, the overall levels changed quite drastically. Since the only difference between set 3 and set 4 is level equalization, RTs will be the same, and they are, again, presented in Figure 5-8. After simulations were made, the overall A-weighted levels for the eight different stimuli ranged from values of 56.3 dBA to 63.1 dBA. These values were measured using a Brüel & Kjær 2250 sound level analyzer. This final set helped to also understand the highly audible impact of sound level and loudness on the perception of LEV.

## 5.4: Testing Interface

The interface for testing was operated by the subject using a wireless touch screen external monitor, located inside of the anechoic chamber. The MUSHRA style test was adapted into an interface where LEV could be rated by the musicians. A few

points needed to be addressed to adapt the test, which created differences between a MUSHRA test and our testing design.

- No clear known reference existed to test all stimuli against
- Rating scale labels are not well suited to LEV
- No widely accepted anchor known to hide within the stimuli

To address these concerns, various adjustments were made. First since no clear reference existed, no reference was provided to the subjects. They rated each stimuli individually, but compared the stimuli with all other stimuli within the set. Again, no anchor was included. Since LEV is an under-researched topic, there is no clear agreement upon what sound field is considered fully enveloping. Finally, the scale was adjusted to a range from 0 to 100, with 0 defined as "Not At All Enveloped" and 100 defined as "Completely Enveloped". This description was provided directly on the Graphical User Interface (GUI), and it was defined in a training session, which taught test participants how to use and operate the GUI to provide LEV ratings. The GUI was implemented in Max 7, for this program allowed real time control of audio signals, making real time switching between stimuli possible. Other existing GUI's used by our lab group were not able to operate with a 30 channel audio file, and could not be updated to include the ASIO drivers required for our hardware setup. This was another reason why Max 7 provided a good platform for GUI development from a graphic interface and an audio control standpoint. A picture of the GUI is shown in Figure 5-9.


Figure 5-9: The GUI which subjects used for the subjective study.

Using this interface, subjects could press any of the different play buttons, A through H, which all represented different hall simulations. The simulation playing over the array would then switch, in real-time, to the desired stimuli, where the musical passage would continue uninterrupted as the switching occurred. This provided instant comparison between any stimuli presented in the set of eight. At any time, users could also mute the simulation, to stop any sound from playing over the array. Then, the program could be unmuted by selecting any file and pressing its respective play button again. Blue indicator lights below the play buttons indicated which file was currently playing over the array.

For each file, a slider bar was also provided to allow the subjects to change and compare their ratings between stimuli. The stimuli were presented in a randomized order to musicians, and the order of the sets of questions was randomized for every participant as well. This provided a completely randomized testing design. Boxes below the slider bars also indicated the current value at which the slider bars were located, for fine adjustments as needed. The numbered labels and anchors were also placed on either side of the eight stimuli.

The final control allowed the subjects to limit the range of the passage in which they were listening. Using the horizontal purple bar at the bottom center of the screen, a listener could adjust the start and end of the section of the passage in which they were listening. The small bar above it would also indicate the current position in time of the sound file being played. After the horizontal purple bar was adjusted as desired, subjects could then press "Limit Passage" to limit the play range of the passage to the specified selection. The sound field was constantly looping, and the loop would always start, end, and restart at the currently selected passage range. If participants wanted to return to playing the full passage again, they could do so by simply pressing the "Full Passage" button. Also, to restart the passage from the beginning of the current time selection, musicians could do so by simply pressing "Restart Passage", the light blue button in the bottom left hand corner.

With all of these options, the interface is easy to use, and it seemed to assist in making the comparisons between the stimuli. Once subjects were done, they could press the "Next" button, which would reset the GUI, now with eight new sound files, and all slider bars would be returned to their original position of 50. This button was only activated after the play button for each file had been selected at least once. After the second set of eight stimuli and ratings were completed, the Next button now read "Finish", and it would send a message stating that the listener was done with the round of question sets, and could now take a short break. When the finish button was pressed, subjective ratings, including audio file number, randomization order, and subject number were exported to a .txt file. This provided easy data access for input into statistical analysis software.

## 5.5: Testing Layout and Structure

The overall testing included many different steps. The various steps, along with the relative range of time they took, are presented in Table 5-2. Overall, the testing took approximately one hour to complete, which was within the range listed in the participation recruitment materials.

Table 5-2: A breakdown of testing order, along with the overall timing of the test.

| Test Element | Time Range |
|---|---|
| Initial Forms | 5 minutes |
| Audiogram | 5 - 10 minutes |
| Tutorial | 5 - 10 minutes |
| Block 1: Training and Hidden Practice Sets | 5 - 10 minutes |
| Short Break | 5 minutes |
| Block 2: Stimuli Sets A & B | 7 - 10 minutes |
| Short Break | 5 minutes |
| Block 3: Stimuli Sets C & D | 7 - 10 minutes |
| Final Forms & Feedback | 5 minutes |
| **Total:** | 50 - 70 minutes |

Initially, an informed consent form and a musical background form were filled out by the listening test participant. Immediately after forms, the audiogram was administered within the anechoic chamber. If the subject passed the hearing screening, a tutorial was given in the form of a PowerPoint presentation in which the musicians clicked through using the wireless tablet interface inside of the anechoic chamber. This tutorial introduced them to the general goal of the study, the definition of what attribute they would be rating (LEV), how to use the testing interface, and general guidelines for the testing. Once the tutorial was complete, the alignment of the subject's ears with the copper markers was checked, to ensure that they were positioned within the center of the array.

The test consisted of a total of 3 blocks, with two questions sets in each block (Table 5-2). The first block contained two sets of questions with four and eight stimuli respectively. The subjects were told that the first set of four questions were for training purposes, so that the participants would get used to using the interface and rating auralizations for LEV. Although the subjects were told the next set of eight stimuli was no longer training (not practice), it was actually used as a hidden practice round, to ensure adequate time and adaptation to the given test method. Once done with the hidden practice set, the musicians received a five minute break.

After the break, the first non-training stimuli sets were rated for LEV. Block two consisted of two sets of questions sets A & B, randomly ordered for each subject. Here

they are provided as letters, for the order of sets 1 through 4 described previously was randomized. The block of questions took roughly 7 to 10 minutes to complete. Again, another short break was administered, and the final blocks of stimuli, sets C and D, were rated (random order). When done with the final block, participants filled out a feedback form for the test, a form for future testing interest if desired, and received their payment, a $15 gift card.

# Chapter 6: Results

This chapter discusses the results of the subjective study conducted, analyzing the effects of hall size, RT, early-to-late energy scaling, and level on LEV ratings. The entire process and testing methods are described in the previous chapter. First, the initial data were analyzed as a whole, to determine if trends emerged. From this analysis, results from each set of eight stimuli are presented, and overall trends across the data are summarized. Note that in sets 1 – 3, all stimuli were all "level equalized", meaning that after the simulations were made, all stimuli were scaled so that the overall A-weighted levels of the stimuli were identical.

## 6.1: Initial Results of LEV Study

For the subjective study, 21 participants who met both the musical background and hearing threshold requirements participated. The subjective breakdown of gender was 47.6% male and 52.4% female, with a mean age of 24.7 years. The average amount of musical training and experience was 15.4 years, and musicians from a wide range of musical backgrounds participated. The ensemble backgrounds, starting with the most common, included choral, band, and orchestral ensembles. After all subjects had been tested, the ratings data were concatenated and organized by stimuli set number. Each different auralization was assigned a reference number, coded 1 through 8. Initially, a one-way ANOVA analysis was run on each dataset, to determine if overall significant differences were found between the different stimuli.

A two-way repeated measures ANOVA was then run, using the primary and secondary variables from Table 5.1, reproduced here as Table 6.1, as the main effects for each stimuli set. An interaction term was included in each analysis, and Mauchley's test of sphericity was checked to determine if the variances of the differences between all possible pairs were equal.[91] If violated, the degrees of freedom were corrected using the Greenhouse-Geisser estimates. The next four sections demonstrate and plot the results of those different subjective results.

Table 6-1: Summary of the different independent variable for each set of stimuli.

| Stimuli Set Summary Table | | | | |
|---|---|---|---|---|
| Stimuli Set | Primary Variable | | Secondary Variable | |
| | Variable | Cases | Variable | Cases |
| 1 | RT | 1.05 s - 2.87 s | Room Size | 80% & 120% |
| 2 | Late Energy Scaling | 0.5, 0.7, 1.0, 1.5 | Receiver | R1 & R2 |
| 3 | Room Size | 80%, 100%, 110%, 120% | RT | 1.4 s & 2.1 s |
| 4*** | Room Size | 80%, 100%, 110%, 120% | RT | 1.4 s & 2.1 s |

***Indicates stimuli set was not level equalized

### 6.1.1: Set 1: Two Hall Sizes and Four Reverberation Times

For set 1, the major factor under consideration was the RT of the hall. Additionally, for each of the reverberations times, hall size was also changed, to consider it as a secondary effect. RTs were tuned to have similar values between hall cases, for comparison between the two. A one-way repeated measures ANOVA was run on this dataset to determine if significant differences were found among any of the stimuli.[92] The treatment input into the model was simply stimulus number, arbitrarily assigned 1 through 8. From this analysis, significant differences were found among the stimuli ($p = 0.007$). Figure 6-1 shows the mean of the LEV ratings of each stimuli, along with bars representing the standard error of the mean ratings. The mean of the LEV ratings versus mean mid-frequency RT are shown in Figure 6.1, with each hall size represented in a different color.

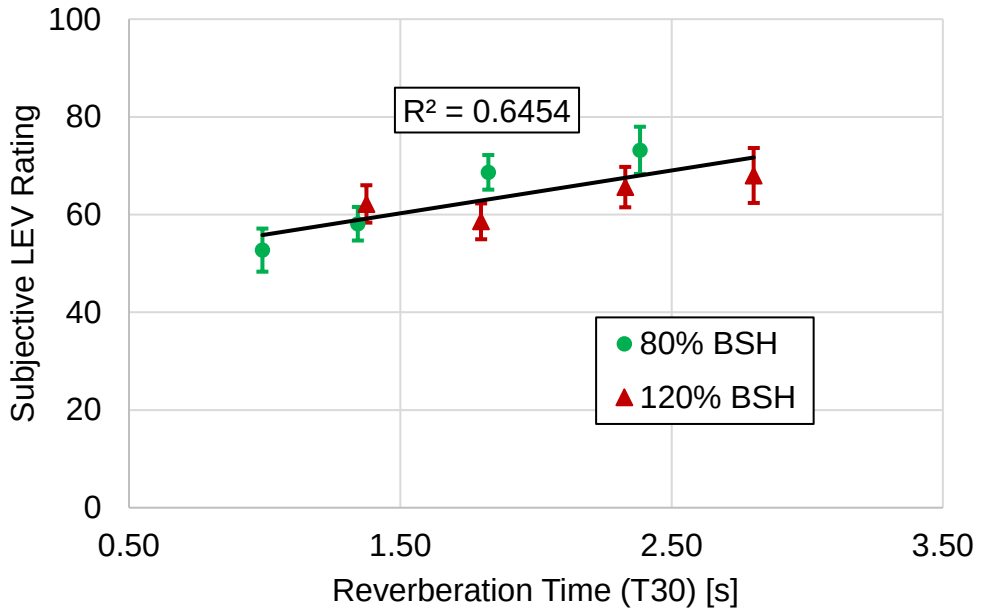


Figure 6-1: The mean of the LEV ratings for set 1 across all subjects. Standard errors of the mean ratings are shown using the error bars in the plot. Colors represent different scales of halls used. The main effect of RT from the ANOVA is significant at p = 0.013.

With significant differences found between stimuli, a two-way repeated measures ANOVA was run, with hall size and RT as the main effects. RT was found to have a significant effect upon the mean of the LEV ratings ($p = 0.013$), but hall size ($p = 0.783$) and the interaction effect between RT and hall size ($p = 0.086$) did not cause significant changes in the LEV ratings. Since all stimuli were adjusted to be played at the same level, this significant finding in this set is not due to overall level differences but to differences in the amount of reverberant energy. A regression analysis was then run with the data between RT and mean of the LEV ratings. The regression was found to be significant ($p = 0.016$) with an $R^2 = 0.6454$. It should be noted that the stimuli used in this study cover a large range of RT (1.05 to 2.87 s), with a total difference of around 1.8 seconds. Despite contradictory results in the literature, it appears that RT does impact LEV perception, but the connection might not be as strong as some have previously shown.[31]

### 6.1.2: Set 2: Early-to-Late Reverberation Scaling

The second set included stimuli in which the absorption coefficients simulating the reverberant energy were scaled with different scaling factors. This technique produced stimuli that had the same relative amplitude and time delays in the direct sound and early reflections, but different amounts of reverberant energy. This set also included level equalization for all stimuli. Two different receiver locations within the same simulated room (80% BSH case) were used, and if no level equalization had been performed, the direct sound energy and early reflection levels for each auralization would have been identical. Since level equalization was applied to the stimuli, each auralization had to be individually scaled, to account for the different levels resulting from differences in the late reverberant energy. For all stimuli, again, a one-way ANOVA was run with stimulus number as the treatment. A significant difference between stimuli was found ($p < 0.001$), so a two-way repeated measures ANOVA was performed, with early-to-late energy scaling and receiver as main effects.

The effect from early-to-late energy scaling factor was found to be significant ($p < 0.001$), but receiver ($p = 0.349$) and the interaction effect ($p = 0.559$) were not found to significantly impact mean of the LEV ratings. To illustrate the results from this set, the mean of the LEV ratings have been plotted against the clarity index (C80) of each stimuli. Since C80 is the ratio of early to late sound energy in the IR, a lower C80 will show a higher late energy scaling factor, and vice-versa. Figure 6-2 shows that a higher amount of late energy correlates to an increased sense of LEV. A regression analysis between the mean of the LEV ratings and C80 was also performed and was found to be significant ($p = 0.006$) with an $R^2 = 0.741$.

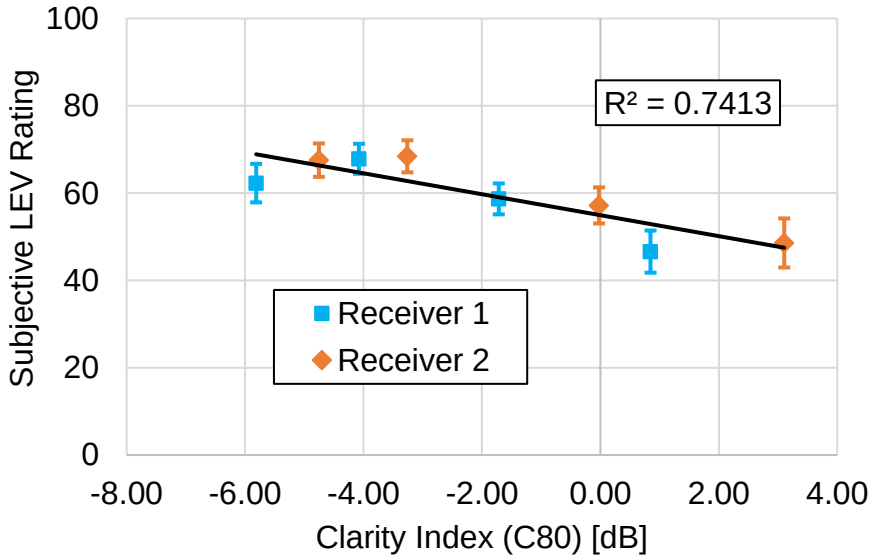


Figure 6-2: The mean of the LEV ratings for all subjects for auralization in set 2. Bars showing standard errors of the mean ratings are provided. The colors represent different receiver locations, shown previously in Figure 5-4. The main effect of early-to-late energy scaling from the ANOVA was significant at $p < 0.001$

Another interesting observation is that the differences in the mean of the LEV ratings are much larger when late energy scaling was lower (higher C80), shown in Figure 6-2. Also, when late energy scaling was higher, differences in LEV were not as apparent. This might point to a non-linear relationship between early-to-late energy scaling and LEV. When enough late energy is present, a limiting case may exist where additional late energy will not increase perceived LEV. Since this study did not include higher amounts of late energy, more work should be conducted to examine the effects of even higher amounts of late energy on LEV ratings.

### 6.1.3: Set 3: Four Hall Sizes and Two Reverberation Times

This test was very similar to the set 1 in both setup and results. The stimuli varied as a function of four different hall sizes and two RTs. The auralization levels were equalized, removing the expected increase in sound level due to smaller hall sizes or a higher RT, if source-receiver location remains constant. Significant differences were found between all eight stimuli ($p = 0.028$), so a two-way repeated measures ANOVA was performed, with RT and hall size as the main effects. The mean ratings for each

stimuli, along with standard error bars are plotted against RT in Figure 6-3. The four different hall sizes are represented by four different colors of points.

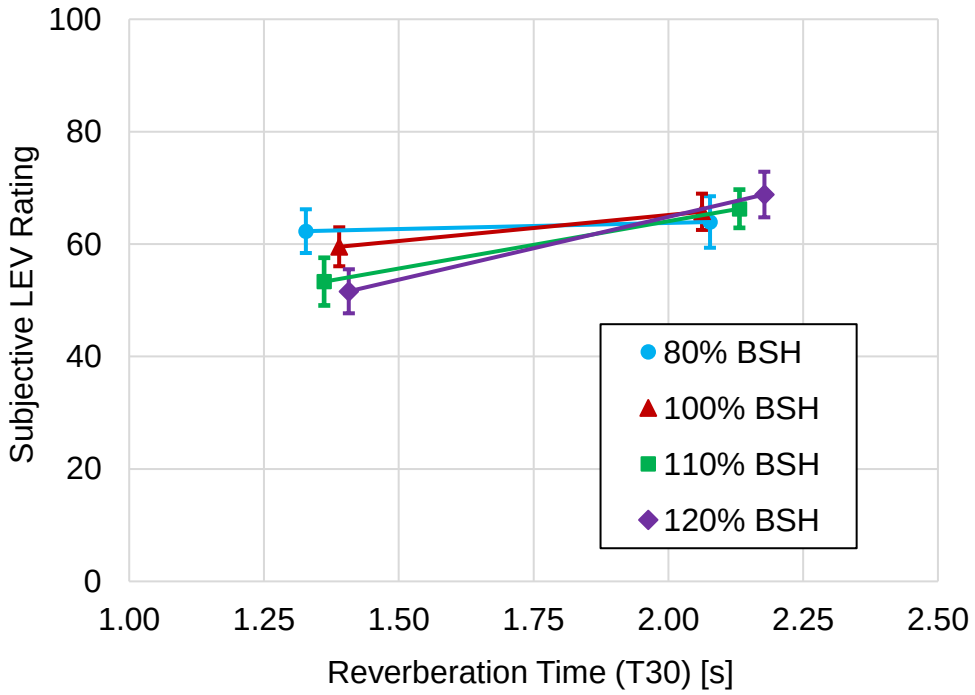


Figure 6-3: The mean of the LEV ratings across all subjects for set 3. Standard errors of the means are shown as bars. Individual colors represent different scales of halls used. The effect of RT from the ANOVA was significant at $p = 0.017$, and the effect of room size was not significant at $p = 0.676$.

Again, as was found in set 1, RT correlated to a significant difference in the mean of the LEV ratings ($p = 0.017$), but the effects of room size ($p = 0.676$) and the interaction effect ($p = 0.068$) were not found to be significant. For all hall sizes, a trend showing an increase in LEV with increasing RT was observed. Although the interaction effect was not found to be significant at a significance level of 0.05, the interaction term still shows potential of being significant, if more subjects were tested. From Figure 6.3, it appears that larger LEV differences with changing RT are found when a hall is larger. Again, this trend was not significant at a 0.05 level, so more research is needed to further examine if hall size might change the relationship between LEV and RT. Additionally, the results from set 1 showed that a larger range of LEV ratings was found in the smaller hall, which is contrary to the trend observed in this data set.

### 6.1.4: Set 4: No Level Equalization Applied to Set 3

The final set of auralizations was identical to set 3, but the level equalization was removed from the simulations. The resulting stimuli contained identical levels of direct sound in every auralization, but included different levels and directions of early reflections and late reverberation, dependent upon hall size and materials. In a similar fashion to the other sets, a one-way ANOVA was run and revealed that significant differences were found between stimuli ($p < 0.001$). With significant differences present, a two-way repeated measures ANOVA was performed with hall size and RT as main effects.

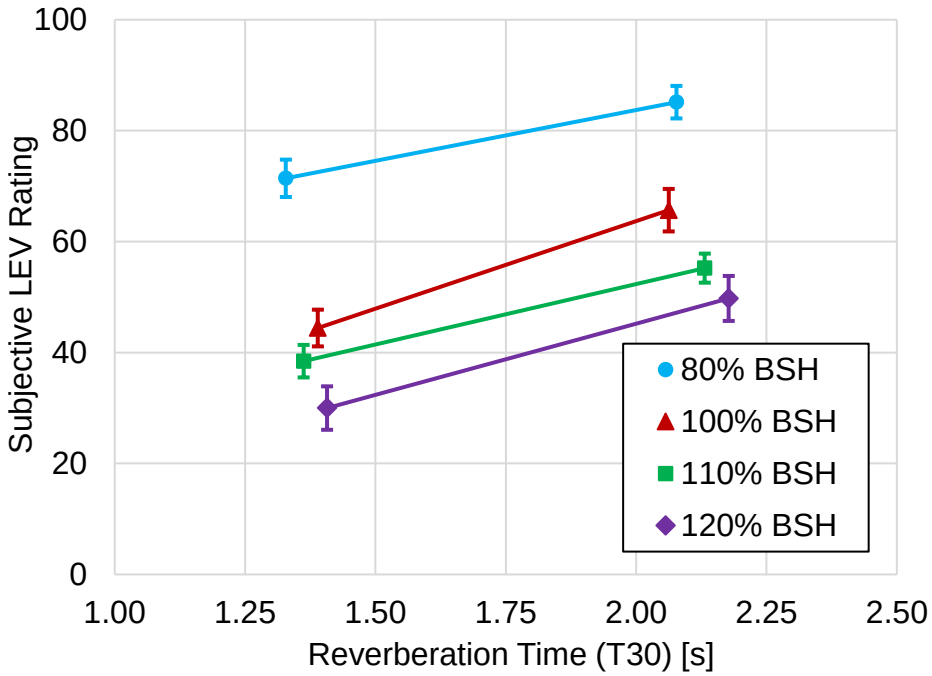


Figure 6-4: The mean of the LEV ratings for auralization set 4 across all subjects, with standard errors of the means shown using the bars provided. The main effects of RT and room size from the ANOVA were found to be significant with $p < 0.001$ and $p < 0.001$, respectively.

From the two-way ANOVA analysis, RT ($p < 0.001$) and hall size ($p < 0.001$) both significantly affected the mean of the LEV ratings of this stimuli set. The interaction term did not correlate with significant changes in LEV ($p = 0.475$). As Figure 6.4 demonstrates, halls with a higher RT were rated with a higher sense of LEV, and smaller halls were rated with a higher perceived LEV. With the effect of level

equalization not included in this set of stimuli, the results are drastically different than in set 3. Still, halls with higher RTs are rated as more enveloping. Another main difference between sets 3 and 4 is the magnitude of the differences in LEV ratings found overall. Subjects showed much higher differences in LEV ratings in set 4, compared to set 3, which suggests that differences in set 4 were much more apparent than in set 3. Despite the clear significance from the effect of hall size and RT, it was clear that changing both hall size and RT each have an impact on the overall level of the simulations. Since clear multicollinearity was present between level and both hall size and RT, a regression analysis was needed.

## 6.2: The Effect of Overall Level on LEV

When both hall size and RT in the room was changed, each individually, the overall level of the auralization was also impacted, quite significantly. Since the stimuli in set 4 were not level equalized, these differences in level, resulting from changes in room size and in RT, were apparent to subjects. With a lack of independence among other possible predictor variables for LEV, it cannot be assumed that RT and hall size are both the sole variables that explain differences in LEV. To investigate this possibility, the effect of level was first isolated from any other effects. In this data set, there was an overall deviation of around 7 dBA between all stimuli. To determine if the differences in LEV could also be predicted by level, a one-way ANOVA, with overall A-weighted sound pressure level as the main effect upon the mean of the LEV ratings, was run for set 4. Level was found to significantly affect the mean of the LEV ratings ($p < 0.001$). Figure 6.5 shows a linear trend between the A-weighted level and the mean of the LEV ratings.

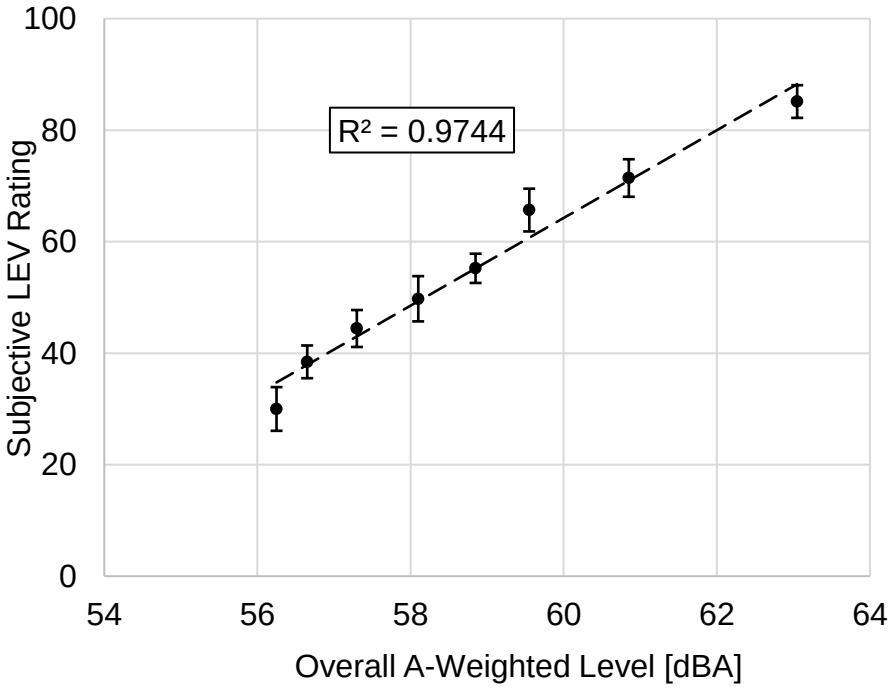


Figure 6-5: The mean of the LEV ratings from set 4 plotted against overall A-weighted level. Standard errors of the mean ratings are provided using bars. As shown, a strong, linear relationship exists between LEV and level.

To determine the strength of the relationship between overall A-weighted levels and the mean of the LEV ratings, a linear regression analysis was also run between level and LEV. The regression analysis was found to be significant ($p < 0.001$). The regression, shown in Figure 6.5, had an $R^2 = 0.974$, indicating that A-weighted level accounted for 97.4% of the variance found in LEV ratings from set 4. This same strong, linear relationship between LEV ratings and level has also been found in previous LEV research[16].

To determine which factors or combination of factors best predicted the mean of the LEV ratings, a step-wise multiple-linear regression, predicting LEV ratings from level, RT, and hall size, was conducted. This step-wise multiple-linear regression had an entry criterion of $p < 0.05$. When run, the model that best predicted LEV ratings included overall A-weighted level as a predictor, and excluded both RT and hall size from the model. This result shows that level was the best predictor of LEV, and

neither RT or hall size accounted for a significant additional amount of the variance in LEV ratings.

It is interesting to compare the findings between sets 3 and 4, where the only difference between the two stimuli sets was whether or not level equalization was applied. When the stimuli levels were equalized, the effect of RT upon a subject's perception of LEV was significant, which was also the case in set 1. On the other hand, when level differences, covering a range of 7 dBA, were added into the stimuli, level best predicted the mean of the LEV ratings, with no added significance from including RT in the model was found. As well, the differences in LEV ratings of stimuli were much larger when level differences were also introduced. This difference points to a conclusion that level differences, when perceptible, dominate a listener's perception of LEV. Despite the dominance of level in LEV perception, when levels between stimuli are similar, a more subtle, yet still significant effect of RT can be found upon LEV perception.

A summary table of the statistical findings of these four different sets within the subjective study is provided in Table 6-2. Results for the ANOVAs and regression models are provided for each set when the test was performed.

Table 6-2: A summary table of the ANOVAs run for each dataset. Tests of main effects are shown, and linear regression significance p-values and $R^2$ are provided when performed.

| Set | ANOVA Main Effect Results | | | Linear Regression | |
|---|---|---|---|---|---|
| | Main Effect | p-Value | Level EQ? | p-Value | $R^2$ Value |
| 1 | RT | 0.013 | Yes | 0.016 | 0.6454 |
| 1 | Room Size | 0.783 | Yes | N/A | N/A |
| 2 | Early-to-Late Scaling (Regression with C80) | < 0.001 | Yes | 0.006 | 0.7413 |
| 2 | Receiver | 0.349 | Yes | N/A | N/A |
| 3 | Room Size | 0.676 | Yes | N/A | N/A |
| 3 | RT | 0.017 | Yes | N/A | N/A |
| 4 | A-weighted Level | < 0.001 | No | < 0.001 | 0.9744 |

## 6.3: Consideration of Non-diffuse Reverberant Energy

One major limitation with the current simulation technique, based upon assumptions of the simplified simulation method, is perfectly diffuse reverberant energy. In an attempt to create realistic auralizations, it was not desired to directionally alter or bias the late, reverberant energy in the initial study. Despite this assumption, studies in the past have highly linked the perception of LEV with the directional character of the late sound field. To determine whether or not a non-diffuse late energy distribution contributed to perceived LEV, adjustments were made to the simulation program to provide an additional directional weighting input for late sound energy simulation. These reverberant energy weights allowed focusing of the late sound reflections to particular directions.

A randomization process was created that continued to randomly place reflections around a listener, but the reflections had a greater chance of falling within the directional ranges which had higher weighting factors. The specific directional ranges are provided below in Figure 6-6. (Directional groups not shown in Figure 6-6 include the right-top, left top, right-bottom, and left bottom.) For example, if a 20% weight was applied to the left direction, 20% of the late reflections would be assigned to a direction specified within the ranges of the left direction (+67.5° to +112.5° azimuth). Table 6-3 shows each directional group in its corresponding azimuth and elevations limits.

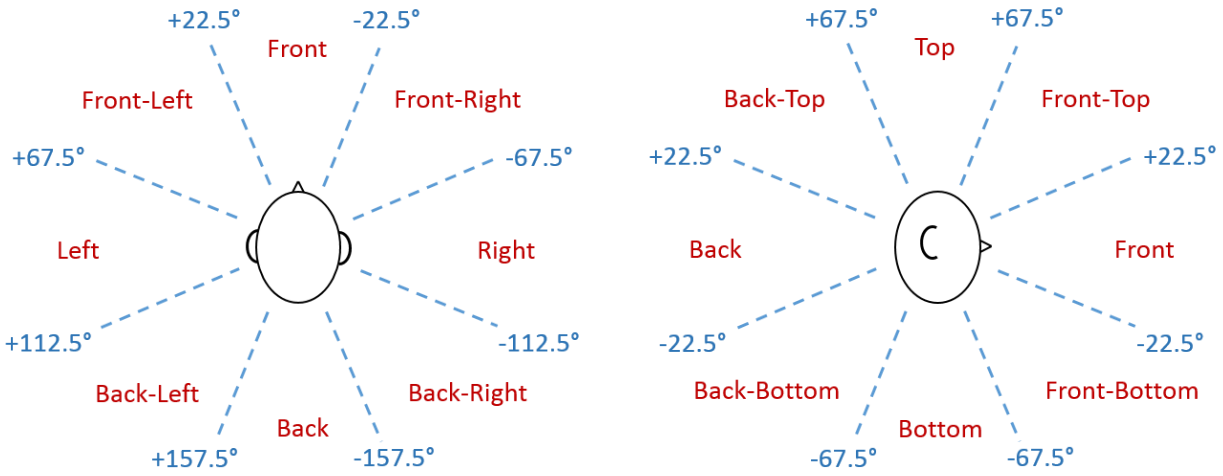


Figure 6-6: A diagram showing the layout of the directional weighting ranges. The (a) azimuthal and (b) elevation ranges for each of the directional categories are shown in a (a) top view and (b) side view.

Table 6-3: A complete list of the azimuth and elevation ranges for each of the directional weighting categories for the reverberant energy.

| Direction | Azimuth Range | Elevation Range |
|---|---|---|
| Omni | $-180 \le \phi \le 180$ | $-90 \le \theta \le 90$ |
| Front | $-22.5 \le \phi \le 22.5$ | $-22.5 \le \theta \le 22.5$ |
| Front-Right | $-67.5 \le \phi \le -22.5$ | $-22.5 \le \theta \le 22.5$ |
| Right | $-112.5 \le \phi \le -67.5$ | $-22.5 \le \theta \le 22.5$ |
| Back-Right | $-157.5 \le \phi \le -112.5$ | $-22.5 \le \theta \le 22.5$ |
| Back | $157.5 \le \phi$ & $\phi \le -157.5$ | $-22.5 \le \theta \le 22.5$ |
| Back-Left | $112.5 \le \phi \le 157.5$ | $-22.5 \le \theta \le 22.5$ |
| Left | $67.5 \le \phi \le 112.5$ | $-22.5 \le \theta \le 22.5$ |
| Front-Left | $22.5 \le \phi \le 67.5$ | $-22.5 \le \theta \le 22.5$ |
| Front-Top | $-45 \le \phi \le 45$ | $22.5 \le \theta \le 67.5$ |
| Right-Top | $-135 \le \phi \le -45$ | $22.5 \le \theta \le 67.5$ |
| Back-Top | $135 \le \phi$ & $\phi \le -135$ | $22.5 \le \theta \le 67.5$ |
| Left-Top | $45 \le \phi \le 135$ | $22.5 \le \theta \le 67.5$ |
| Top | $-180 \le \phi \le 180$ | $67.5 \le \theta$ |
| Front-Bottom | $-45 \le \phi \le 45$ | $-67.5 \le \theta \le -22.5$ |
| Right-Bottom | $-135 \le \phi \le -45$ | $-67.5 \le \theta \le -22.5$ |
| Back-Bottom | $135 \le \phi$ & $\phi \le -135$ | $-67.5 \le \theta \le -22.5$ |
| Left-Bottom | $45 \le \phi \le 135$ | $-67.5 \le \theta \le -22.5$ |
| Bottom | $-180 \le \phi \le 180$ | $\theta \le -67.5$ |

Informal listening tests were performed within the SPRAL research group (four people) to explore the effect of directionally controlled late energy. Reverberant energy was focused separately in six directional groups: (i) the front, (ii) the front-left and front-right, (iii) the left and right, (iv) the back-left and back-right, (v) the back, and (vi) the top directions. Energy was focused in each of these directional groups separately, and LEV was rated. A 40% directional weighting factor was used for the one direction, or divided between the groups of two directions. The additional 60% of the late energy was weighted as diffuse reverberation.

Although differences seemed more noticeable, a quite prominent directional weighting of 40% was needed in order to create clear LEV differences. Therefore, the amount of directional emphasis required to create a perceptual change was potentially much greater than what would be expected within a real room. Although only a few subjects within the lab were tested, some overall trends began to emerge. The most highly rated condition for LEV was case (iii), where 40% of the energy was weighted in the left and right directions. Cases (ii), (iv), and (vi) also had higher LEV ratings than the perfectly diffuse condition, but not as highly as case (iii). This finding does suggest that purely lateral energy is most important for LEV, but energy from somewhat lateral directions promotes a sense of LEV as well. More research, with finer directional resolution, should be used to help determine and refine the cutoffs of what is considered lateral energy. Currently, the lateral energy is defined by a dipole field, used for the present metrics of $J_{LF}$ and $L_J$, but the increasing availability of spherical microphone arrays allows for a greater flexibility in the definition of this pattern.

For case (v), where directional reverberant energy was weighted towards the back, LEV ratings were similar to or lower than the ratings for the perfectly diffuse, reverberant energy. This result indicates that energy from the back, when made more prominent than the other directions, potentially decreases the sense of LEV. This sense could be caused by front back confusion by the listener, when energy from directly behind a listener may sound as if it is coming from directly in front, creating

a more frontally-biased sound field. This effect should be further studied, with finer directional resolution, to determine the effect of weighting the reverberant energy in the directional range behind a listener which appears to reduce LEV. As well, the effect of weighting the rear reverberation with less energy, as compared to all other directions, should be studies, to see if LEV perception increases when rear-reverberance is reduced.

The impact of non-diffuse reverberant energy is a point of further research for the SPRAL research group, and the directional reverberation simulation method will continue to be adjusted and refined. For reverberant energy, it is typical to assume that a diffuse field is reached within a hall after a certain time, but this point in time is heavily determined by the overall size, geometry, and material properties of the room. With measurements made using the Eigenmike em32 in a number of different halls, analyses will also be conducted to determine if non-diffuse sound fields exist in physical halls, and at what time a diffuse field is reached in different sizes and shapes of halls. These measurements will provide insight into the validity and application of using directionally weighted reverberant energy in simulations for subjective testing. As well, these measurements will help provide an understanding of exactly how non-diffuse reverberant energy can be within a hall at different time windows in the impulse response.

# Chapter 7: Conclusions

A state-of-the-art 30 channel loudspeaker array was constructed for concert hall acoustics subjective testing, ensuring a highly accurate spatial reconstruction of sound fields. The AURAS facility provides a level of accuracy in sound field simulation which has rarely been used in previous research on LEV. Loudspeakers were constructed and designed specifically for the anechoic chamber in the Hammond Building on Penn State's campus. Using the designed loudspeakers and digital equalization, a flat frequency response was achieved within ±3 dB for most loudspeakers down to 200 Hz. The anechoic chamber in which the array was installed exhibits free-field characteristics down the 200 Hz one-third octave-band. Loudspeakers were evenly distributed around a listener location, which was located in the center of the room. Third-order Ambisonic reproduction was implemented using VST plug-ins in the digital audio workstation REAPER. These plug-ins also provided real-time Ambisonic format conversion, level and time-delay compensation, and digital loudspeaker equalization.

To provide a high level of control over the auralizations being reproduced in the anechoic chamber, a simulation program was designed in MATLAB. This simulation program assumed a simple rectangular geometry, creating physically-based auralizations. A wide-range of auralizations can be created by adjusting room dimensions, source-receiver locations, and material properties. The simulation program outputs the required 16-channel third-order Ambisonic signals, which can be processed in real-time or rendered into loudspeaker signals using REAPER. The simulation program was then utilized in an initial subjective study on LEV in concert halls. The study aimed at determining the effects of RT, room size, early-to-late energy scaling factors, and level upon the perception of LEV. Four sets of eight stimuli each were rated by 21 musicians, and these ratings were analyzed to determine the impact of these variables upon LEV.

## 7.1: Summary of Findings

This study was designed, based upon previous research, showing the following variables had significant effects on perceived LEV: level, RT, and early-to-late energy scaling. Some additional effects, such as room size, were also included, which have not been studied in previous research. From these results, the strongest relationship was found between LEV ratings and overall A-weighted level, accounting for 97.4 percent of the variance in LEV ratings from stimuli set 4. This result has also been found in previous literature[16], showing the same strong connection between LEV and level. Despite this strong connection, other factors were also found to have significant, but more subtle effects than overall level.

When level equalization was performed on the room stimuli, RT was found to have a significant effect upon the mean of the LEV ratings. Although this effect was significant, it appeared to be a much smaller effect on LEV perception than level. The effect of RT on LEV has been contradictory in previous literature.[16,31] This discrepancy could be due to the masking of the effect of RT on LEV by more striking differences related to level.

Additionally, the impact of the early-to-late energy scaling was found to correlate with significant differences in LEV. As the late energy was scaled, relative to the early energy in the IR, an increase was found in the mean of the LEV ratings. This increase in LEV with scaling factor was clear at the lower scaling factors, where less late energy was present. At the highest late energy scaling factors, however, the increase in LEV ratings with scaling factor was not as clear, pointing to a potential non-linear relationship. This trend may indicate that once a certain ratio between early and late energy is achieved, increasing the amount of late energy may not create an increased sense of LEV. This increased amount of late energy would also potentially lead to a muddy sound, causing overall negative impacts on the overall impression of a room's sound field. To determine if this non-linear relationship exists, a wider range of scaling factors should be considered in future work. This future study

would help identify if LEV increases from added late energy reach a limiting case at a certain energy ratios.

The other factors considered in these studies, both receiver location and hall size, did not reveal any significant differences. Although hall size was found to be significant in set 4, it was determined that the differences were explained best by the effect of level upon LEV perception, and not hall size. This explanation is reinforced by the lack of any significant effects in set 3, when levels were equalized between stimuli. Hall size is a large factor affecting both reverberance and level, but the more subtle characteristics of an IR impacted by hall size, such as reflection density, did not impact LEV perception in this study.

When receiver location was changed in set 2, no significant differences were observed due to this effect. Using the present simulation method, altering receiver location would change the structure of the early reflections in the IR, but if materials and room dimensions were not changed, the late part of the IR was perceptually similar. This result suggests that the early part of the IR may not play an important role, in itself, based upon differences from moving locations within the same room. This conclusion is not justified to extend to a general conclusion because this study used a limited range of receiver locations and hall shapes. In the present study, only one shape of hall was used, a simple rectangular hall, which is known to produce a good sense of LEV. This question would be better answered in a study with a variety of hall shapes and sizes, along with multiple receiver locations in these halls. Such a study would allow a more realistic, and holistic look into the effect of hall size and receiver, along with hall shape effects.

The final area under consideration was the directional character of the late sound field. Although this variable was not included in the simulation method for the formal studies, this capability was added for pilot research within the lab group. The idea of directional late energy has been included in most previous LEV work,[16,20-24,27-29] but in almost all cases, it is altered, essentially, by including or excluding late reverberant energy in individual loudspeaker channels. To create a more adaptable, realistic

sense of reverberant energy, a randomization process was developed, which produced randomly arriving late reflections based upon weighting factors for different directional zones. After the reflections were assigned a direction, producing the desired directional character, they were encoded as plane-waves into the Ambisonic IR. This technique allowed the reflections to be simulated as plane-waves arriving at a listener, as opposed to reverberant effects applied to speaker channels. The result of this algorithm was directionally controlled late energy, without completely removing all late energy from a particular direction.

With a more advanced method for simulating directional reverberation, initial pilot testing revealed that a relatively significant bias, on the order of around 40%, was required to create a perceptible difference in LEV. It should be determined how much directional bias of the late energy is needed to create a higher sense of LEV, along with the importance of specific directions. Once this is known, it is also important to understand how much directional bias actually exists in the late sound field of real halls. Even if altering late energy can impact LEV perception, it is only important if this change can be created in real halls.

## 7.2: Future Work

Much future work could be done to further understand the question of LEV in concert hall acoustics. First, different testing methods should be used to study LEV, to determine if other test methods might help listeners to identify smaller differences between stimuli. Although the real-time switching in this test helped to reduce the load on auditory memory, the presentation of eight stimuli simultaneously might have been overwhelming and/or distracting to rate. Other methods like paired-comparison studies should be used, which allow listening test participants to focus on only one comparison at a time. This method could help participants hear smaller differences between stimuli, and determine, with more certainty, which factors impact the perception of LEV.

To confirm the most significant finding, the impact of level, reverberation, and early-to-late energy scaling factors upon LEV ratings should be analyzed with not only simulated, but measured data. Most studies to date have been based upon auralizations either not tied to any specific room geometry, or they have only used a small subset of hall conditions in the perceptual testing. In this study, although auralizations did have a geometric basis for simulation, still only one hall geometry was considered. While these methods help to identify key factors, it should be determined how each of these factors can be created in real halls, through spherical microphone array IR measurements, and virtual acoustic sound field simulation techniques. By using measured data, the values of these important, yet interrelated parameters can be analyzed across a wide variety of hall shapes and sizes. Then, the results of this study, and prior results in the literature, can be confirmed against a wide variety of realistic sound fields. The connection between these factors and LEV would be further refined, and potential metrics to predict the sense of LEV across a wide variety of concert halls could be proposed.

Another factor, which was not studied in the present work, was the arrival direction of late sound energy within the hall. Due to the assumptions used to simulate the reverberant energy, the late sound field was assumed to be diffuse, or arriving at the listener randomly, from all directions. Other LEV studies have not included this assumption, and it is known that directional late energy, especially lateral, will have an impact upon LEV. Future work should be done using the directional weighting techniques described in Section 6.3. Additionally, it would be interesting to apply a time-based transition between directionally weighted reverberant energy and diffuse reverberant energy. This approach would effectively split the late impulse response into two parts: a directional part and a diffuse part. The onset time of both parts could be adjusted, and the timing and direction of the late directional energy could be analyzed as it relates to the perception of LEV.

More work also needs to be done to determine the physical validity of directional late energy, even though it has been widely used in past LEV research. Using the

Eigenmike em32, measurements of a wide variety of concert halls should be made, including rooms of very different sizes, shapes, and material property characteristics. Beamforming techniques could then be applied to specific time windows of the spatial RIR. Looking at spatial behavior of the RIR at specific times, it could be determined if directional late energy exists in real rooms, and also if there is a point in which real sound fields become statistically diffuse. Understanding this part of the IR will help ground and validate future work in directionally weighted simulations used for LEV research.

A final area of future work, which is currently being studied in our lab group, is the perception of LEV using auralizations made from spherical microphone array measurements in real halls. Although simulation is extremely helpful, cost effective, and time efficient in creating a wide variety of sound fields, the auralization will only be as plausible as the limitations of the simulation and reproduction methods. The current study was limited to early reflection characteristics arising from a shoe-box style hall, which is known to exhibit favorable LEV characteristics. In a study with measurements from real halls, with various hall shapes, including fan and vineyard, the effect of hall geometry could be explored, which was not evaluated in the present work. This study would provide evidence using physically justifiable auralizations, which is much needed in light of the previous simulation methods surrounding almost all LEV research.

If clear conclusions can be drawn from future studies, an important outcome would be an objective measure of LEV. This metric would provide an important link, necessary to bridge the gap between the acoustical consulting and the concert hall acoustics research communities. With such a metric, architectural acousticians could implement this new knowledge in future concert hall designs, with a better understanding of how to create halls that exhibit a sense of spatial impression and LEV.

# References

[1] ISO 3382:2009, “Acoustics – Measurements of room acoustics parameters – Part 1: Performance spaces".

[2] L. Beranek, Concert Halls and Opera Houses, New York: Springer-Verlag, 2004.

[3] M. Barron, "Subjective Study of British Symphony Concert Halls," Acustica, vol. 66, no. 1, pp. 1-14, 1988.

[4] T. Lokki, J. Pätynen, A. Kuusinen and S. Tervo, "Disentangling preference ratings of concert hall acoustics using subjective sensory profiles," J. Acoust. Soc. Am., vol. 132, no. 5, pp. 3148-3161, November 2012.

[5] T. Lokki, J. Pätynen, A. Kuusinen, H. Vertanen and S. Tervo, "Concert hall acoustics with individually elicited attributes," J. Acoust. Soc. Am., vol. 130, pp. 835-849, 2011.

[6] W. Reichardt and W. Schmidt, "Die hörbaren Stufen des Raumeindruckes bei Music (in German)," Acustica, vol. 17, pp. 175-179, 1966.

[7] W. Reichardt and U. Lehmann, "Definition of the room impression index R by determining the room impression of the basis of subjective examination of musical performance (German)," Appl. Acoust., vol. 11, no. 2, pp. 99-127, April 1978.

[8] L. Cremer, H. Muller and T. Schultz, Principles and Applications of Room Acoustics, vol. 1, London and New York: Applied Science Publishers, 1978.

[9] W. Reichardt and U. Lehmann, "Room impression as an overall concept of spaciousness and liveliness. Examples of room measurement factor (German)," Acustica, vol. 40, no. 5, pp. 277-290, September 1978.

[10] A. Marshall, "A Note on the Importance of Room Cross-Section in Concert Halls," J. Sound & Vib., vol. 5, no. 1, pp. 100-112, 1967.

[11] M. Barron, "The subjective effects of first reflections in concert halls - the need for lateral reflections," J. Sound and Vib., vol. 15, pp. 475-494, 1971.

[12] M. Barron and A. Marshall, "Spatial impression due to early lateral reflections in concert halls: The derivation of a physical measure," J. Sound & Vib., vol. 77, pp. 211-232, 1981.

[13] V. Jordan, Acoustical Design of Concert Halls and Theatres, London: Applied Science Publishers Ltd., 1980, p. 159 and 191.

[14] V. Jordan, "A Group of Objective Acoustical Criteria for Concert Halls," Appl. Acoust., vol. 14, pp. 253-266, 1981.

[15] J. Bradley and G. Soulodre, "The influence of late arriving energy on spatial impression," J. Acoust. Soc. Am., vol. 97, no. 4, pp. 2263-2271, April 1995.

[16] J. Bradley and G. Soulodre, "Objective measures of listener envelopment," J. Acoust. Soc. Am., vol. 98, pp. 2590-2597, 1995.

[17] H. Haas, "On the influcence of a single echo on the audibility of speech," Acustica, vol. 1, pp. 48-58, 1951.

[18] M. Morimoto and Z. Maekawa, "Auditory spaciousness and envelopment," Proc. of the 13th Int. Cong. on Acoust., Belgrade, pp. 215-218, 1989.

[19] M. Morimoto, H. Fujimori and Z. Maekawa, "Discrimination between auditory source width and envelopment (Japanese)," J. Acs. Soc. Japan, vol. 46, no. 6, pp. 449-457, June 1990.

[20] M. Barron, "Late lateral energy fractions and the envelopment question in concert halls," Appl. Acoust., vol. 62, pp. 185-202, 2001.

[21] M. Morimoto, K. Iida and K. Sakagami, "The role of reflections from behind the listener in spatial impression," Appl. Acoust., vol. 62, no. 2, pp. 109-124, 2001.

[22] T. Hanyu and S. Kimura, "A new objective measure for evaluation of listener envelopment focusing on the spatial balance of reflections," Appl. Acoust., vol. 62, no. 2, pp. 155-184, 2001.

[23] H. Furuya, K. Fujimoto, A. Wakuda and Y. Nakano, "The influence of total and directional energy of late sound on listener envelopment," Acoust. Sci. & Tech, vol. 26, pp. 208-211, 2005.

[24] H. Furuya, K. Fujimoto, C. Ji and N. Higa, "Arrival direction of late sound and listener envelopment," Appl. Acoust., vol. 62, pp. 125-136, 2001.

[25] A. Wakuda, H. Furuya, K. Fujimoto, K. Isogai and K. Anai, "Effects of arrival direction of late sound on LEV," Acoust. Sci. & Tech., vol. 24, no. 4, pp. 179-185, 2003.

[26] G. Soulodre, M. Lavoie and S. Norcross, "Objective measures of listener envelopment in multichannel surround systems," J. Audio Eng. Soc., vol. 51, no. 9, pp. 826-840, 2003.

[27] J. Bradley, R. Reich and S. Norcross, "On the combined effects of early- and late-arriving sound on spatial impression in concert halls.," J. Acoust. Soc. Am., vol. 108, pp. 651-661, 2000.

[28] M. Morimoto, K. Nakagawa and K. Iida, "The relation between spatial impression and the law of the first wavefront," Appl. Acoust., vol. 69, pp. 132-140, 2008.

[29] P. Evjen, J. Bradley and S. Norcross, "The effect of late reflections from above and behind on listener envelopment," Appl. Acoust., vol. 62, no. 2, pp. 137-153, 2001.

[30] T. Lokki, J. Pätynen, S. Tervo, S. Siltanen and L. Savioja, "Engaging concert hall acoustics is made up of temporal envelope preserving reflections," J. Acoust. Soc. Am., vol. 6, pp. EL223-228, 2011.

[31] M. Morimoto, M. Jinya and K. Nakagawa, "Effects of frequency characteristics of reverberation time on listener envelopment," J. Acoust. Soc. Am., vol. 122, no. 3, pp. 1611-1615, 2007.

[32] D. Griesinger, "General overview of spatial impression, envelopment, localization and externalization.," Audio Eng. Soc. 15th Int. Conf., Vols. Paper # 15-013, 1998.

[33] D. Griesinger, "Objective measures of spaciousness and envelopment," Audio Eng. Soc. 16th Int. Conf., Vols. Paper # 16-003, 1999.

[34] D. Griesinger, "The Psychoacoustics of Apparent Source Width, Spaciousness and Envelopment in Performance Spaces," Acta Acustica, vol. 83, pp. 721-731, 1997.

[35] T. Hidaka, L. Beranek and T. Okano, "Interaural cross-correlation, lateral fraction, and low- and high-frequency sound levels as measures of acoustical quality in concert halls," J. Acoust. Soc. Am., vol. 98, no. 2, pp. 988-1007, 1995.

[36] T. Lokki and J. Pätynen, "Lateral reflections are favorable in concert halls due to binaural loudness," J. Acoust. Soc. Am. EL, vol. 130, no. 5, November 2011.

[37] M. Morimoto and Z. Maekawa, "Effects of low frequency components on auditory spaciousness," Acustica, vol. 66, pp. 190-196, 1988.

[38] W. Reichardt and W. Schmidt, "Die wahrnehmbarkeit der veränderung von schallfeldparameternbei der darbietung von music (in German)," Acustica, vol. 18, pp. 274-282, 1967.

[39] T. Leishman, S. Rollins and H. Smith, "An experimental evaluation of regular polyhedron loudspeakers as omnidirectional sources of sound," J. Acoust. Soc. of Am., vol. 120, no. 3, 2006.

[40] J. Blauert, Spatial Hearing – The Psychophysics of Human Sound Localization, revised edition., Cambridge: MIT Press, 1996.

[41] H. Möller, M. Sörensen, C. Jensen and D. Hammershöi, "Binaural Technique: Do We Need Individual Recordings?," J. Audio Eng. Soc., vol. 44, no. 6, pp. 451-469, June 1996.

[42] M. Gerzon, "Periphony: With-Height Sound Reproduction," J. Audio Eng. Soc., vol. 21, no. 1, pp. 2-10, January/February 1973.

[43] "Odeon Room Acoustics Software," [Online]. Available: www.odeon.dk.

[44] "CATT-Acoustic," [Online]. Available: www.catt.se.

[45] "EASE - Enhanced Acoustic Simulator for Engineers," [Online]. Available: ease.afmg.eu.

[46] M. Vorländer, "International Round Robin on Room Acoustical Computer Simulations," 15th Int. Cong. on Acoust., 26 - 30 June 1995.

[47] I. Bork, "A Comparison of Room Simulation Software - The 2nd Round Robin on Room Acoustical Computer Simulation," Acustica, vol. 86, pp. 943-956, 2000.

[48] I. Bork, "Report on the 3rd Round Robin on Room Acoustical Computer Simulation – Part I: Measurements," ACTA Acustica United with Acustica, vol. 91, pp. 740-752, 2005.

[49] I. Bork, "Report on the 3rd Round Robin on Room Acoustical Computer Simulation – Part II: Calculations," ACTA Acustica United with Acustica, vol. 91, pp. 753-763, 2005.

[50] M. Vorländer, "Computer simulations in room acoustics: Concepts and uncertainties," J. Acoust. Soc. Am., vol. 133, no. 3, pp. 1203-1213, March 2013.

[51] V. Pulkki, "Virtual sound source positioning using vector base amplitude panning," J. Audio Eng. Soc., vol. 45, no. 6, pp. 456-66, June 11997.

[52] S. Tervo, J. Patynen, A. Kuusinen and T. Lokki, "Spatial Decomposition Method for Room Impulse Responses," J. Audio Eng. Soc., vol. 61, no. 1-2, pp. 17-28, Jan-Feb 2013.

[53] J. Daniel, "Spatial Sound Encoding Including Near Field Effect: Introducing Distance Coding Filters and a Viable, New Ambisonic Format," Audio Eng. Soc. 23rd Int. Conference, 23-25 May 2003.

[54] S. Spors, H. Wierstorf, A. Raake, F. Melchior, M. Frank and F. Zotter, "Spatial Sound With Loudspeakers and Its Perception: A Review of the Current State," Proceedings of the IEEE, vol. 101, no. 9, pp. 1920-1938, September 2013.

[55] J. Ahrens, Analytic Methods of Sound Field Synthesis, New York, Dordrecht, London: Springer Heidelberg, 2012.

[56] R. Rabenstein and S. Spors, "Chapter 53: Sound Field Reproduction," in Springer Handbook of Speech Processing, Berlin, Springer-Verlag Berlin Heidelberg, 2008, pp. 1095-1114.

[57] H. Wierstorf, A. Raake and S. Spors, "Localization of a virtual point source within the listening area for wave field synthesis," Proc. of the 133rd Con. of the Audio Eng. Soc., October 2012.

[58] H. Wittek, "Perceptual differences between wavefield synthesis and stereophony," Ph.D. dissertation, University of Surrey, 2007.

[59] E. Williams, Fourier Acoustics: Sound Radiation and Nearfield Acoustic Holography, Academic Press, 1999.

[60] C. Nachbar, F. Zotter, E. Deleflie and A. Sontacchi, "AmbiX - A Suggested Ambisonics Format," Ambisonics Symposium, 2-3 June 2011.

[61] S. Clapp, A. Guthrie, J. Braasch and N. Xiang, "Using Ambisonics to Reconstruct Measured Soundfields," Audio Eng. Soc. Convention, vol. Paper 9002, 17-20 October 2013.

[62] M. Gerzon and G. Barton, "Ambisonic Decoder for HDTV," 92nd Audio Eng. Soc. Convention Preprints, no. Number 3345, March 1992.

[63] A. Heller, R. Lee and E. Benjamin, "Is My Decoder Ambisonic?," Proc. of 125th Conv. of the Audio Eng. Soc., 1-5 October 2008.

[64] V. Dickason, The Loudspeaker Design Cookbook, 4th Edition ed., Peterborough, New Hampshire: Audio Amateur Press, 1991.

[65] "em32 Eigenmike microphone array release notes (v17.0)," [Online]. Available: www.mhacoustics.com/sites/defaul/files/ReleaseNotes.pdf.

[66] ISO 3745:2003(E), "Acoustics- Determination of sound power levels of noise sources using sound pressure- Precision methods for anechoic and hemi-anechoic rooms".

[67] "REAPER - Digital Audio Workstation," [Online]. Available: www.reaper.fm.

[68] "Cycling '74 Max," [Online]. Available: www.cycling74.com/max7/.

[69] A. Harker and P. Tremblay, "The HISSTools Impulse Response Toolbox: Convolution for the Masses," Int. Comp. Music Conf., pp. 48-55, 9-14 September 2012.

[70] A. Heller, E. Benjamin and R. Lee, "A Toolkit for the Design of Ambisonic Decoders," Linux Audio Conference, 12-15 April 2012.

[71] M. Vorländer, Auralization, Berlin: Springer - Verlag, 2008.

[72] J. Allen and D. Berkley, "Image Method for Efficiently Simulating Small-Room Acoustics.," J. Acoust. Soc. Am., vol. 65, p. 943, 1979.

[73] D. Schröder, "Physically Based Real-Time Auralization of Interactive Virtual Environments," Dissertation, RWTH Aachen University, 2011.

[74] R. Heinz, "Binaural Room Simulation Based on an Image Source Model with Addition of Statistical Methods to Include the Diffuse Sound Scattering of Walls and to Predict the Reverberant Tail," Appl. Acoust., vol. 38, pp. 145-159, 1993.

[75] S. Ross, Applied Probability Models with Optimization Applications, San Francisco, California: Holden-Day, 1970.

[76] H. Kuttruff, Room Acoustics, 4th Edition, Elsevier Science Publisher, 2000.

[77] S. Pelzer, "Interactive real-time auralization of complex virtual environments," Master's Thesis, RWTH Aachen University, 2007.

[78] ISO 9613-1:1993, "Acoustics - Attenuation of sound during propagation outdoors - Part 1: Calculation of the absorption of sound by the atmosphere".

[79] ISO 9613-2:1996, "Acoustics - Attenuation of sound during propagation outdoors - Part 2: General method of calculation".

[80] E. Salomons, Computational Atmospheric Acoustics, Springer, 2001.

[81] M. Kronlachner, "ambiX v0.2.3 – Ambisonic plug-in suite," [Online]. Available: http://www.matthiaskronlachner.com/?p=2015. [Accessed 05 07 2015].

[82] M. Kronlachner, "Plug-in Suite for Mastering the Production and Playback in Surround Sound and Ambisonics," 139th Conv. of the Audio Eng. Soc., April 2014.

[83] M. Kronlachner, "mcfx v0.3.2 – multichannel audio plug-in suite," [Online]. Available: http://www.matthiaskronlachner.com/?p=1910. [Accessed 05 07 2015].

[84] A. Lundeby, T. Vigran, H. Bietz and M. Vorländer, "Uncertainties of measurements in room acoustics," Acustica, vol. 81, no. 4, pp. 344-355, 1995.

[85] C. Micheyl, K. Delhommeau, X. Perrot and A. Oxehham, "Influence of musical and psychoacoustical training on pitch discrimination," Hear. Res., vol. 219, pp. 36-47, 2006.

[86] Oxenham, AJ, Fligor, BJ, Mason, CR and Kidd, G, "Informational masking and musical training.," J. Acoust. Soc. Am., vol. 114, no. 3, pp. 1543-1549, 2006.

[87] S. Bech, "Selection and training of subjects for listening tests on sound reproducing equipment," J. Audio Eng. Soc., vol. 40, no. 7/8, pp. 590-610, 1992.

[88] ITU-R BS.1116-1 (1994-1997), "Methods for the subjective assessment of small impairments in audio systems including multichannel sound systems".

[89] ITU-R BS.1534-1 (2001-2003), "Method for the subjective assessment of intermediate quality level of coding systems".

[90] Denon, Anechoic Orchestral Music Recording, Audio CD, 1988.

[91] A. Field, Discovering Statistics using SPSS, 3rd Edition, Sage Publications Inc., 2009.

[92] M. Kutner, C. Nachtsheim, J. Neter and W. Li, Applied Linear Statistical Models, 5th Edition, McGraw Hill Education, 2005.

# Appendix A: Loudspeaker Driver Specifications

This appendix contains the manufacturer technical specifications for the Tang Band 4" Underhung mid-bass driver and the Tang Band 1" Neodymium Tweeter, both used in the construction0 of the loudspeakers for the spherical loudspeaker array. Also, the information for the Tang Band 8" RBM Subwoofer is included as the third specification sheet. All products were purchased through Parts Express at http://www.parts-express.com/.

Mid-bass driver:
http://www.parts-express.com/tang-band-w4-1720-4-underhung-midbass-driver--264-872

Tweeter:
http://www.parts-express.com/tang-band-25-1166sj-1-neodymium-tweeter--264-834

Subwoofer:
http://www.parts-express.com/tang-band-w8-2022-8-rbm-subwoofer-8-ohm--264-955

# WF SERIES

# W4-1720

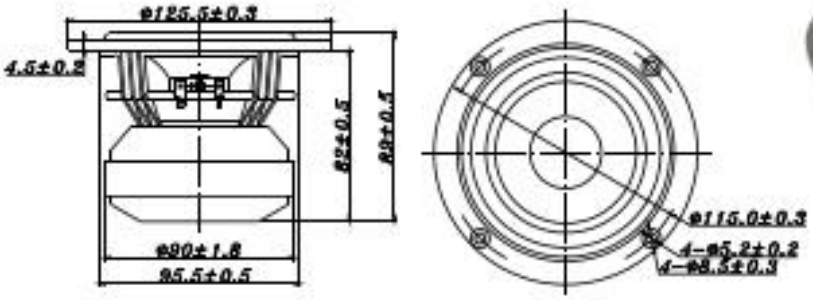


- HUGE FERRITE MAGNET, UNDER HUNG MOTOR DESIGN
- SHORT RING ON POLE PIECE, VC = 32mm
- VERY LOW 2nd AND 3rd DISTORTION (LOW THD)
- LONG THROW, HIGH POWER LOADING, Xmax = 5mm
- ALUMINUM BASKET


## 4" MID BASS

| | |
|---|---|
| DIAPHRAGM MTL | Paper |
| SURROUND MTL | Rubber |
| NOMINAL IMPEDANCE | 4 Ω |
| DCR IMPEDANCE | 3.8 Ω |
| SENSITIVITY 1W/1M | 86 dB |
| FREQUENCY RESPONSE | 60Hz-8K Hz |
| FREE AIR RESONANCE | 60 Hz |
| VOICE COIL DIAMETER | 32 mm |
| AIR GAP HEIGHT | 17 mm |
| RATED POWER INPUT | 30 W |
| MAXIMUM POWER INPUT | 60 W |
| FORCE FACTOR, BL | 3.82TM |
| MAGNET WEIGHT ( oz) | Neodymium |
| MOVING MASS | 5 g |
| FERROFLUID ENHANCED | No |
| SUSPENSION COMPLIANCE | 1284 $MN^{-1}$ |
| EFFECTIVE PISTON AREA | 0.0057 $M^2$ |
| Levc | 0.037 mH |
| Zo | 22 ohm |
| Xmax | 5 mm |
| Vas | 5.92 Litr |
| Qts | 0.42 |
| Qms | 2.33 |
| Qes | 0.51 |

TB SPEAKERS

VOICE: 886.2.26570282 FAX: 886.2.26580166
E-MAIL:info@tb-speaker.com

# NS SERIES 25-1166SJ

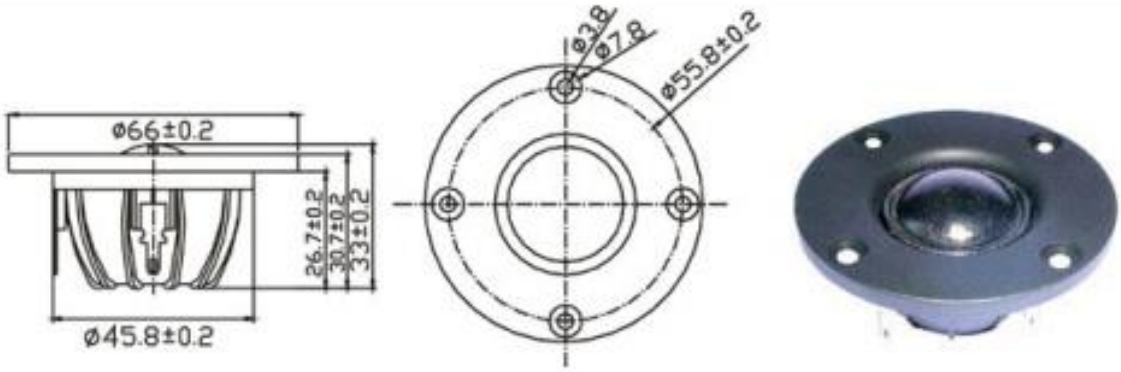


## 1" FABRIC DOME/NEODYMIUM

- **SOFT FABRIC DOME DIAPHRAGM COATING WITH HIGH LOSS MATERIAL**
- **FERROFLUID COOLED**
- **WOOL IN CAVITY OF POLE PIECE**
- **ABS FRONT PANEL**
- **NEODYMIUM DESIGN WITH BACK CHAMBER**

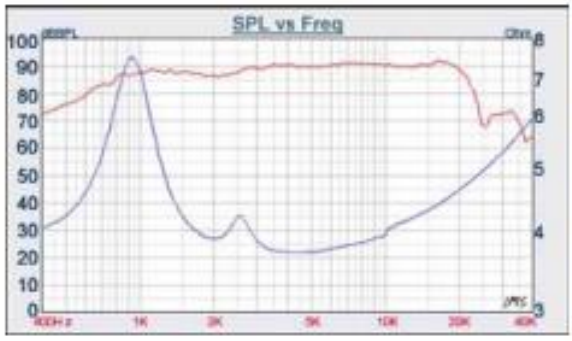


| | |
|---|---|
| **DIAPHRAGM MTL** | Fabric |
| **SURROUND MTL** | N/A |
| **NOMINAL IMPEDANCE** | 4 Ω |
| **DCR IMPEDANCE** | 3 Ω |
| **SENSITIVITY 1W/1m** | 90 dB |
| **FREQUENCY RESPONSE** | **920-22K** Hz |
| **FREE AIR RESONANCE** | 920 Hz |
| **VOICE COIL DIAMETER** | 25.4 mm |
| **AIR GAP HEIGHT** | 2 mm |
| **RATED POWER INPUT** | 8 W |
| **MAXIMUM POWER INPUT** | 80 W |
| **FORCE FACTOR, BL** | N/A |
| **MAGNET WEIGHT ( oz)** | Neodymium |
| **MOVING MASS** | N/A |
| **FERRO FLUID ENHANCED** | Yes |
| **SUSPENSION COMPL.** | **N/A** |
| **EFFEC.PISTON AREA** | N/A |
| **Levc** | 0.006 mH |
| **Zo** | 7.40 ohm |
| **X-max** | N/A |
| **Vas** | N/A |
| **Qts** | 0.87 |
| **Qms** | **2.13** |
| **Qes** | **1.45** |

TB SPEAKERS
VOICE:886.2.26570282 FAX:886.2.26580166
E-MAIL :info@tb-speaker.com

# PM SERIES W8-2022

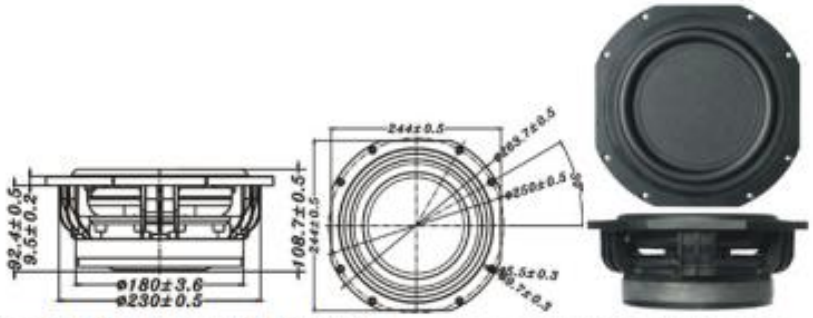


- **UNIQUE, PATENTED SUSPENSION SYSTEM PROVIDES EXTREMELY LINEAR EXCURSION.**
- **HIGH POWER HANDLING DESIGN, 75mm OF VOICE COIL**
- **LIGHT WEIGHT AND HIGH STIFFNESS OF FLAT COMPOSITE CONE BODY**
- **PATENTED ALUMINUM BASKET DESIGN**
- **EXTREMELY LOW DISTION(THD), EVEN<100Hz.**
- **GOOD FOR WOOFER OR SUBWOOFER APPLICATION**

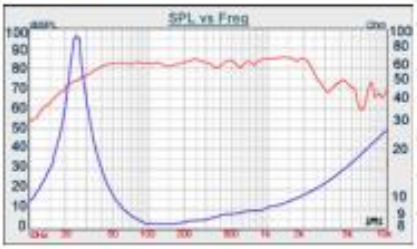


8" PP SANDWICH FOAM WOOFER

| | |
|---|---|
| DIAPHRAGM MTL | PP Sandwich foam |
| SURROUND MTL | Rubber |
| NOMINAL IMPEDANCE | 8 Ω |
| DCR IMPEDANCE | 6.6 Ω |
| SENSITIVITY 1W/1m | 83 dB |
| FREQUENCY RESPONSE | 25-1 K Hz |
| FREE AIR RESONANCE | 25 Hz |
| VOICE COIL DIAMETER | 75.5 mm |
| AIR GAP HEIGHT | 8 mm |
| NOMINAL POWER | 60 W |
| MUSIC POWER | 120 W |
| FORCE FACTOR, BL | 15.77 TM |
| TYPE OF MAGNET | Ferrite |
| MOVING MASS | 99.78 g |
| FERROFLUID ENHANCED | No |
| SUSPENSION COMPLIANCE | 417.52 $uMN^{-1}$ |
| EFFECTIVE PISTON AREA | 0.023 $M^2$ |
| Levc | 0.21 mH |
| Zo | 90 ohm |
| X-max | 8 mm |
| Vas | 31.36 Litr. |
| Qts | 0.38 |
| Qms | 5.24 |
| Qes | 0.41 |

TB SPEAKERS
VOICE:886.2.26570282 FAX:886.2.26580166
E-MAIL:info@tb-speaker.com

# Appendix B: Chamber Characterization Results

The plots in this section show the free-field behavior of the CAV's anechoic chamber in the basement of the Hammond Building. Plots are shown from 100 Hz up to 5000 Hz. It should be noted at after the measurements, the high-frequency dodecahedron loudspeaker was found to have one driver wired out-of-phase with the rest of the drivers. This sound was only used for frequencies at 800 Hz and above, so no errors are found in the low frequency plots. Deviations at high frequencies should not be expected, since no significantly reflection surfaces were placed within the anechoic chamber. Thus, deviations shown in the plots for 800 Hz and higher, for only specific traverses, most likely are due to interactions with the out-of-phase driver.

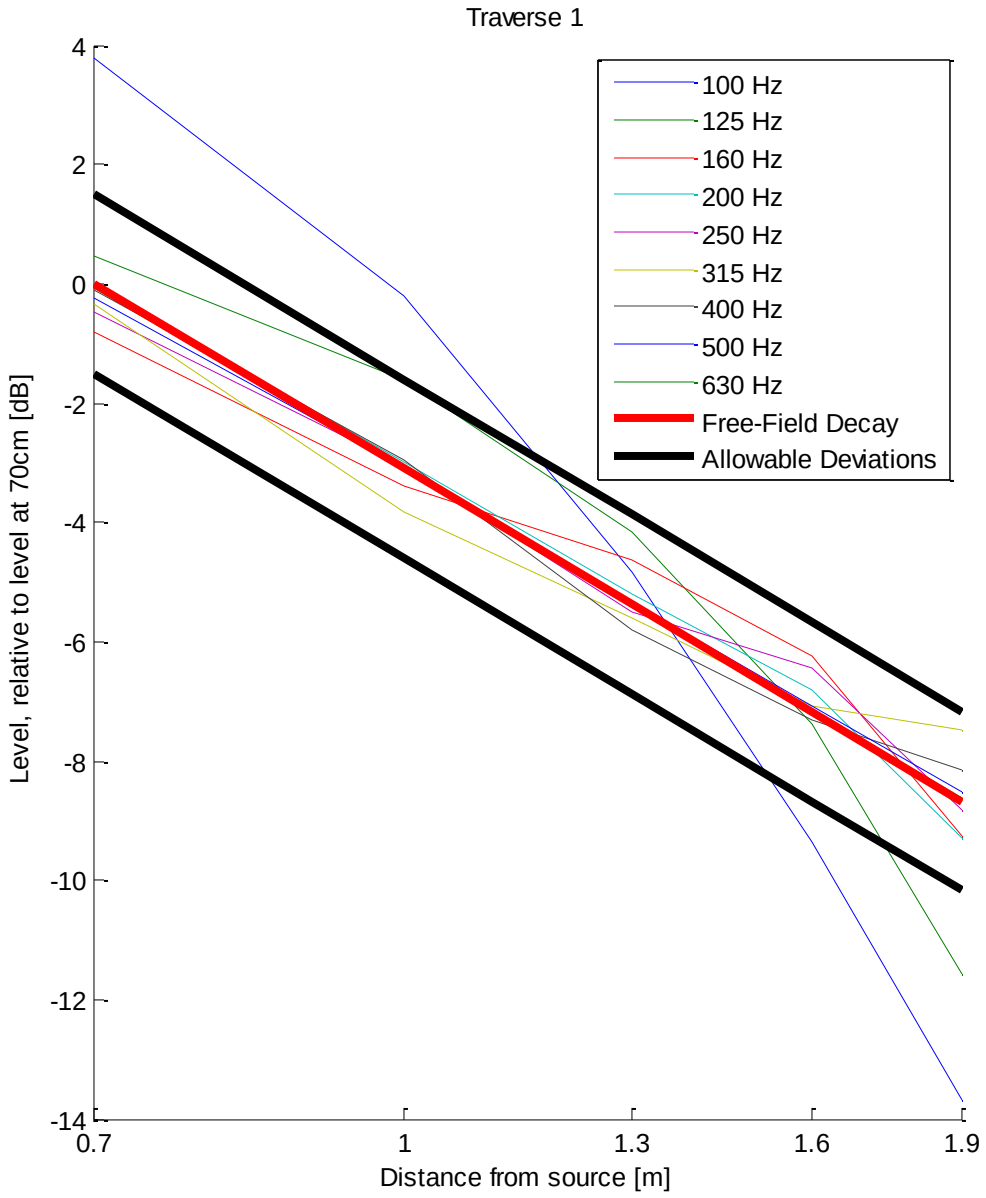
Traverse 1
100 Hz
125 Hz
160 Hz
200 Hz
250 Hz
315 Hz
400 Hz
500 Hz
630 Hz
Free-Field Decay
Allowable Deviations
Level, relative to level at 70cm [dB]
4
2
0
-2
-4
-6
-8
-10
-12
-14
0.7
1
1.3
1.6
1.9
Distance from source [m]

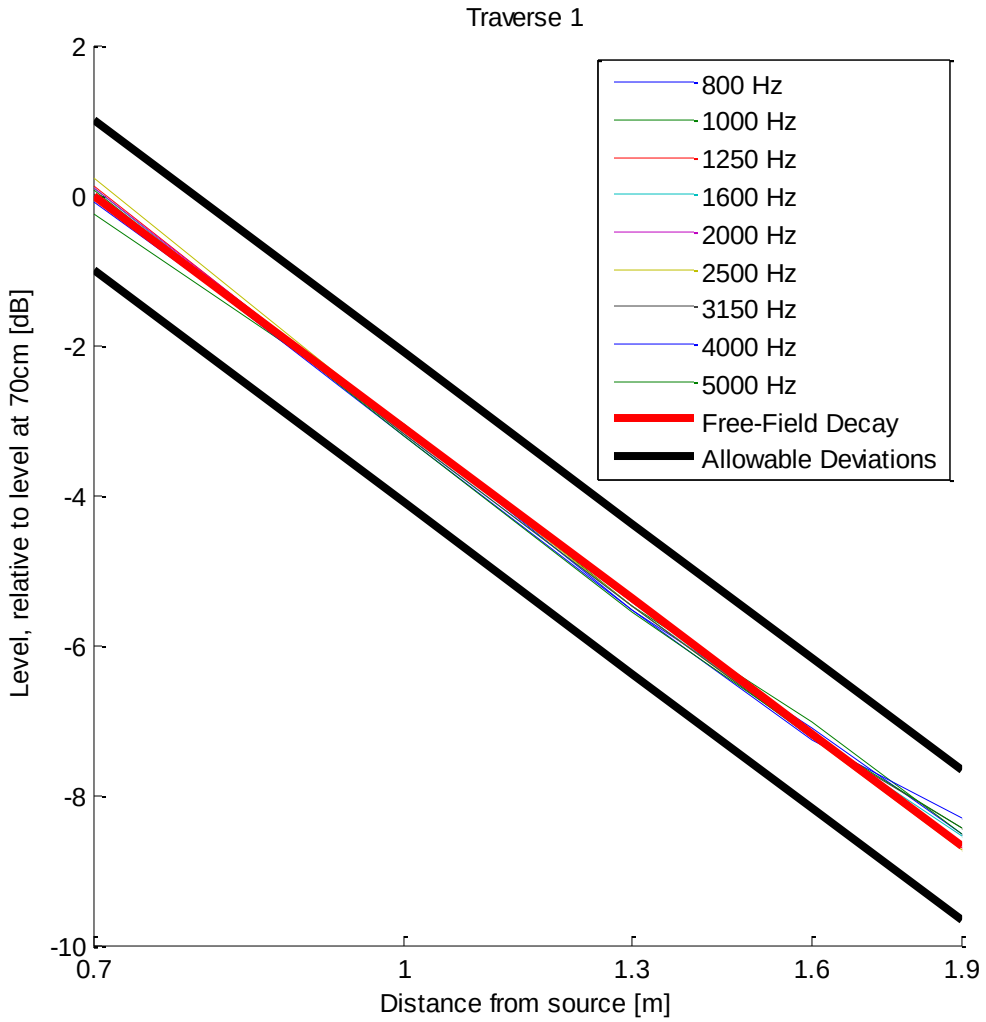
Traverse 1
800 Hz
1000 Hz
1250 Hz
1600 Hz
2000 Hz
2500 Hz
3150 Hz
4000 Hz
5000 Hz
Free-Field Decay
Allowable Deviations
Level, relative to level at 70cm [dB]
2
0
-2
-4
-6
-8
-10
0.7
1
1.3
1.6
1.9
Distance from source [m]

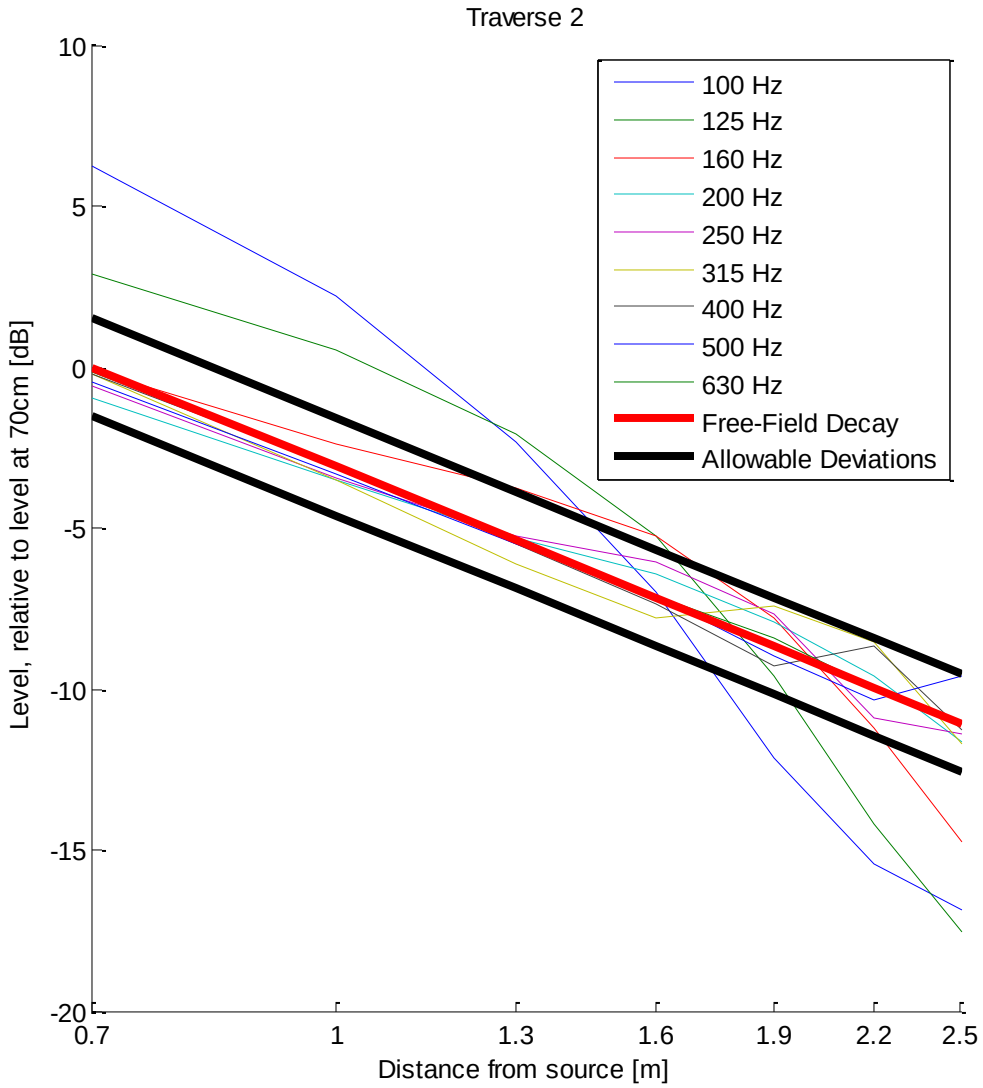
Traverse 2
100 Hz
125 Hz
160 Hz
200 Hz
250 Hz
315 Hz
400 Hz
500 Hz
630 Hz
Free-Field Decay
Allowable Deviations
Level, relative to level at 70cm [dB]
10
5
0
-5
-10
-15
-20
0.7
1
1.3
1.6
1.9
2.2
2.5
Distance from source [m]

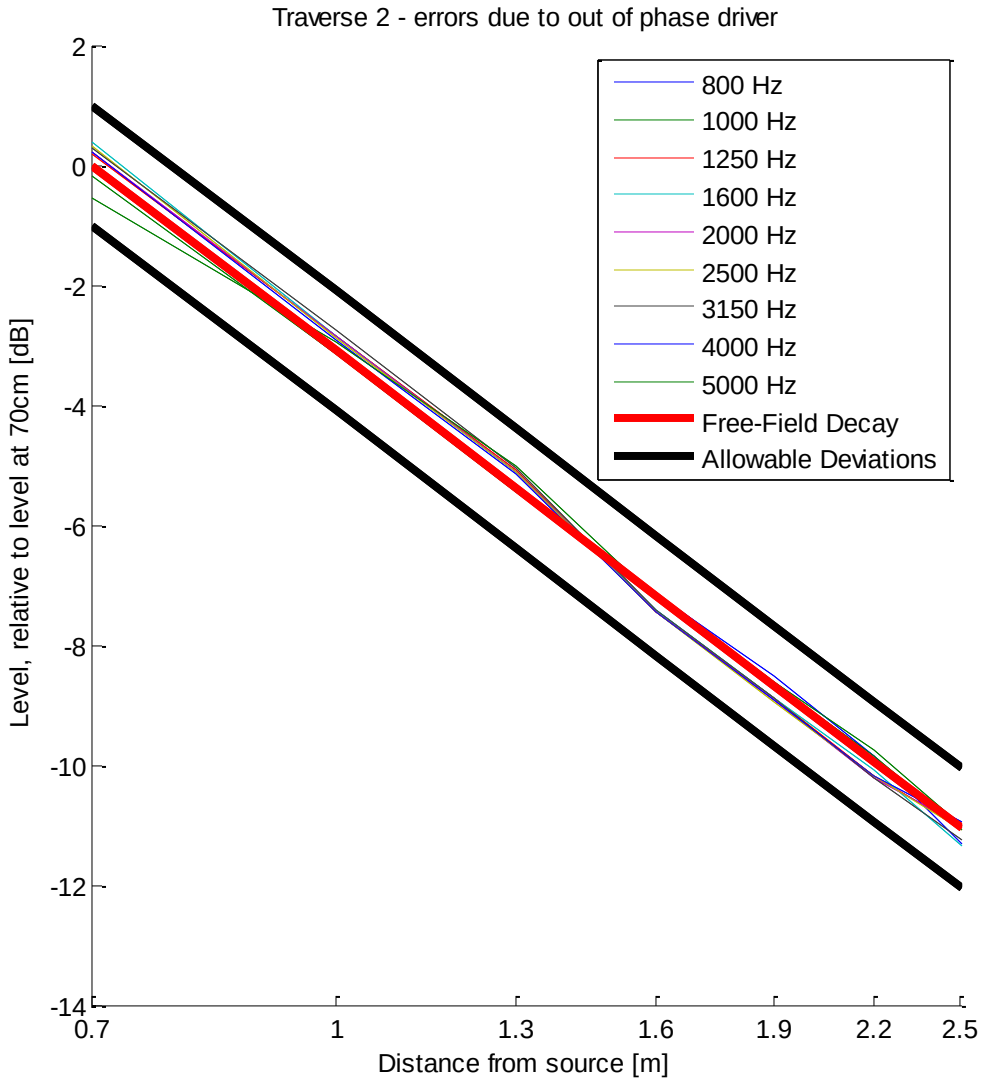
Traverse 2 - errors due to out of phase driver
Level, relative to level at 70cm [dB]
Distance from source [m]
2
0
-2
-4
-6
-8
-10
-12
-14
0.7
1
1.3
1.6
1.9
2.2
2.5
800 Hz
1000 Hz
1250 Hz
1600 Hz
2000 Hz
2500 Hz
3150 Hz
4000 Hz
5000 Hz
Free-Field Decay
Allowable Deviations

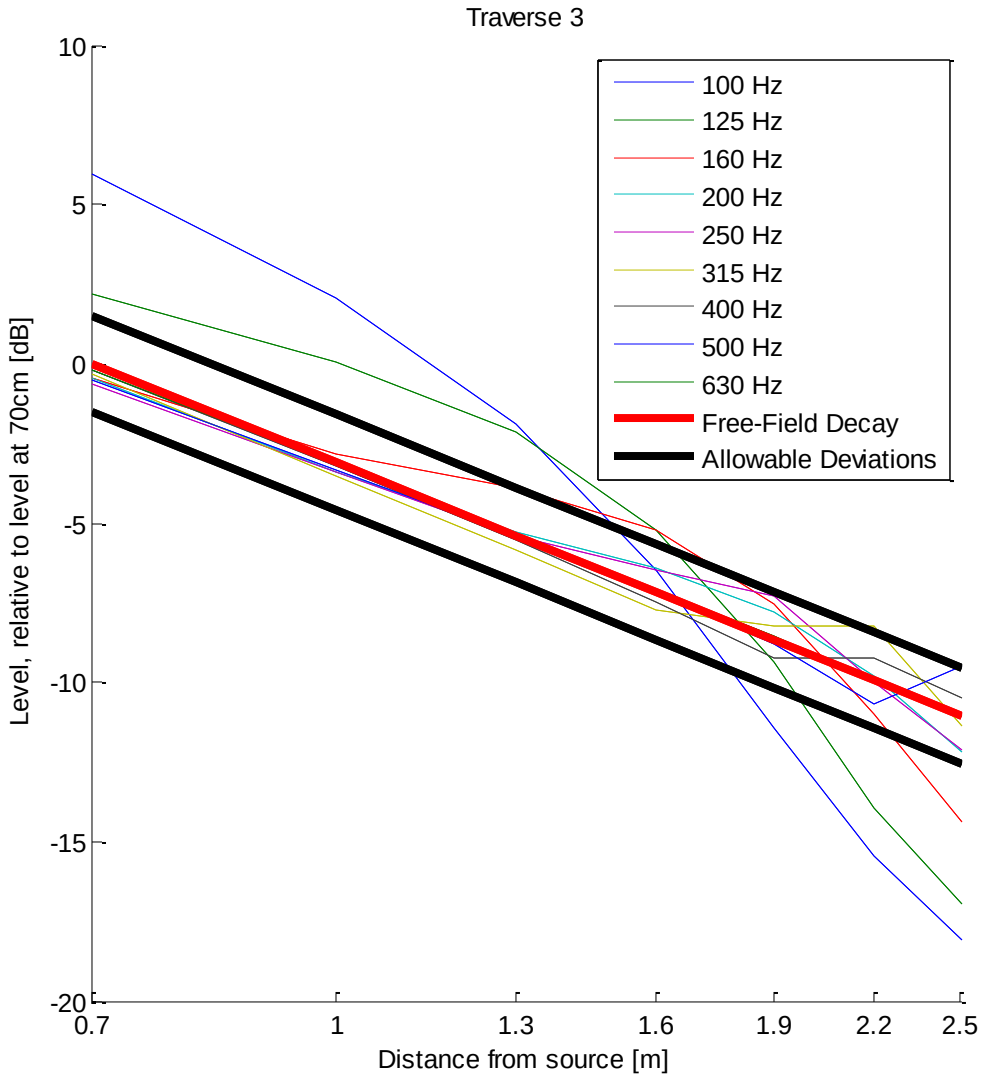
Traverse 3
100 Hz
125 Hz
160 Hz
200 Hz
250 Hz
315 Hz
400 Hz
500 Hz
630 Hz
Free-Field Decay
Allowable Deviations
Level, relative to level at 70cm [dB]
10
5
0
-5
-10
-15
-20
0.7
1
1.3
1.6
1.9
2.2
2.5
Distance from source [m]

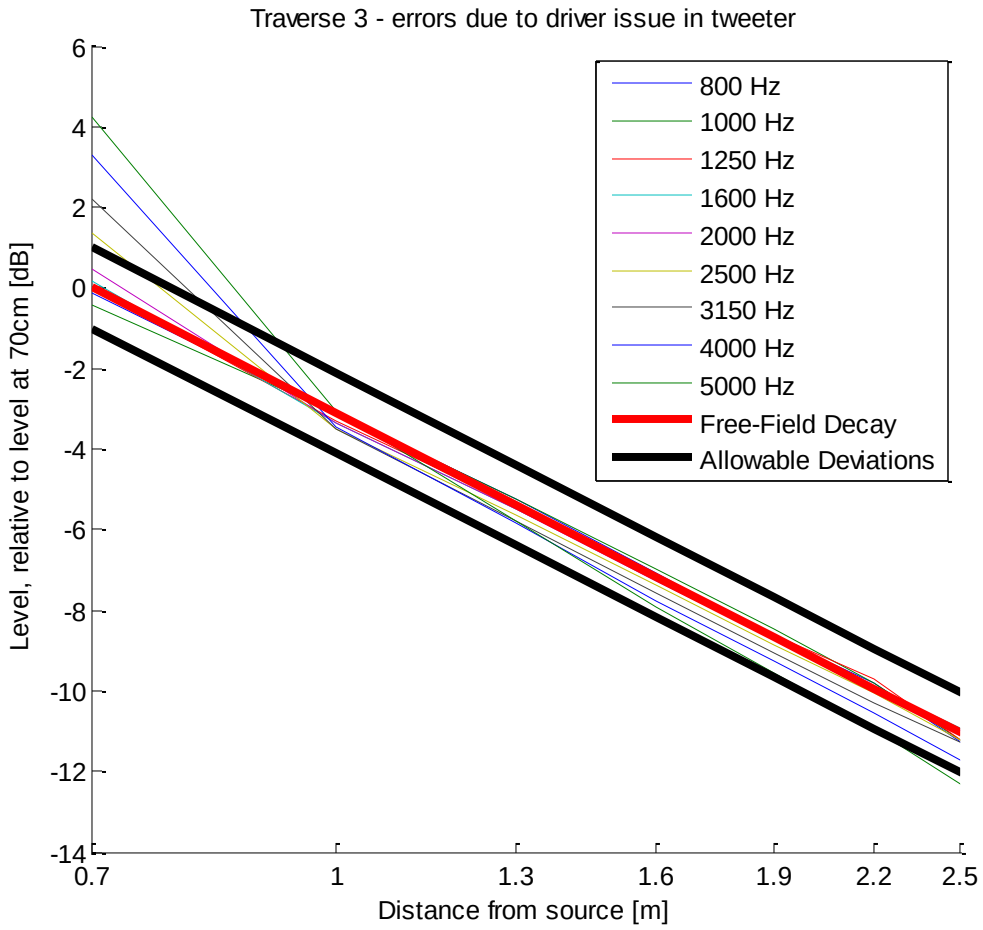
Traverse 3 - errors due to driver issue in tweeter
Level, relative to level at 70cm [dB]
Distance from source [m]
6
4
2
0
-2
-4
-6
-8
-10
-12
-14
0.7
1
1.3
1.6
1.9
2.2
2.5
800 Hz
1000 Hz
1250 Hz
1600 Hz
2000 Hz
2500 Hz
3150 Hz
4000 Hz
5000 Hz
Free-Field Decay
Allowable Deviations

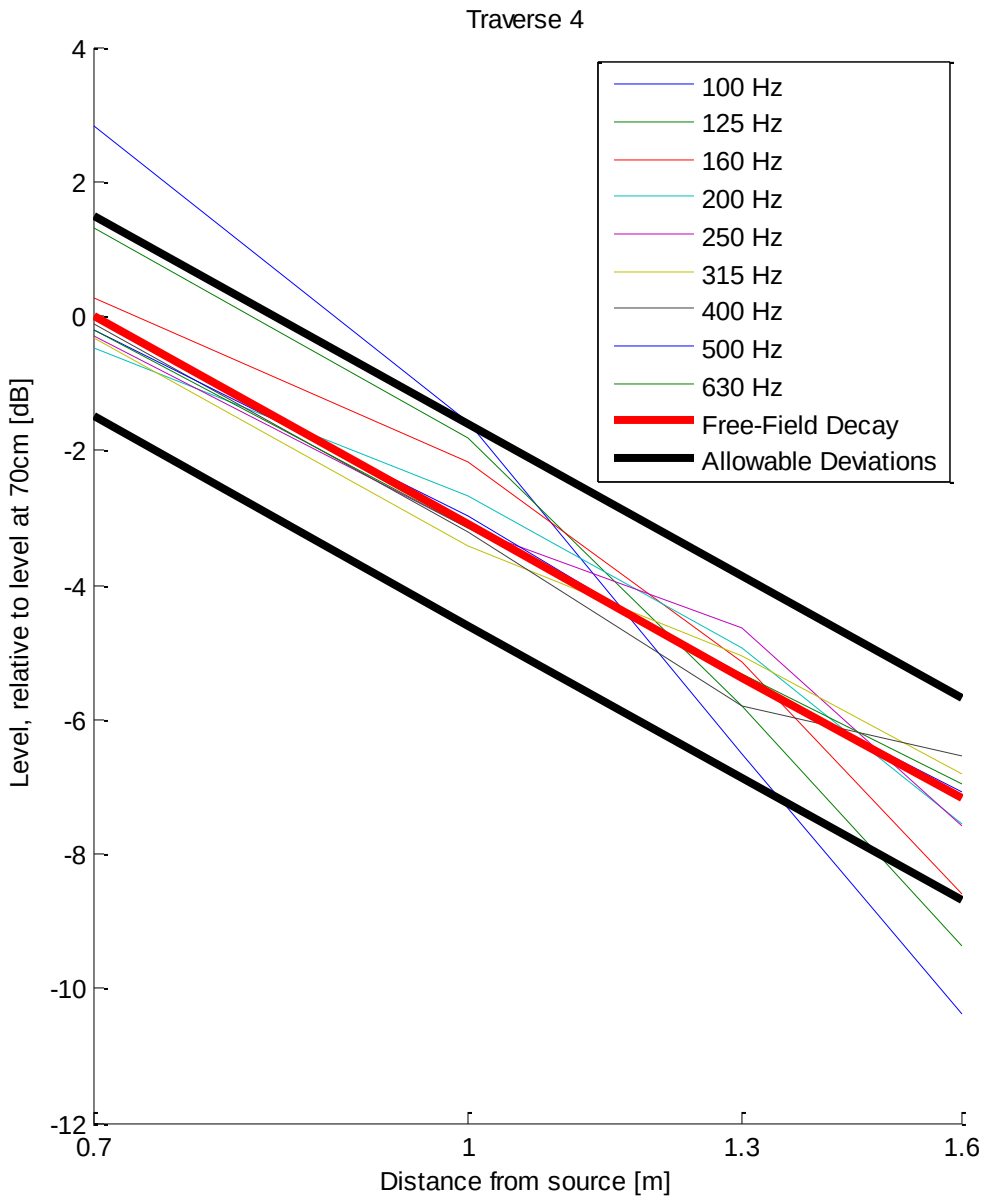
Traverse 4
100 Hz
125 Hz
160 Hz
200 Hz
250 Hz
315 Hz
400 Hz
500 Hz
630 Hz
Free-Field Decay
Allowable Deviations
Level, relative to level at 70cm [dB]
4
2
0
-2
-4
-6
-8
-10
-12
0.7
1
1.3
1.6
Distance from source [m]

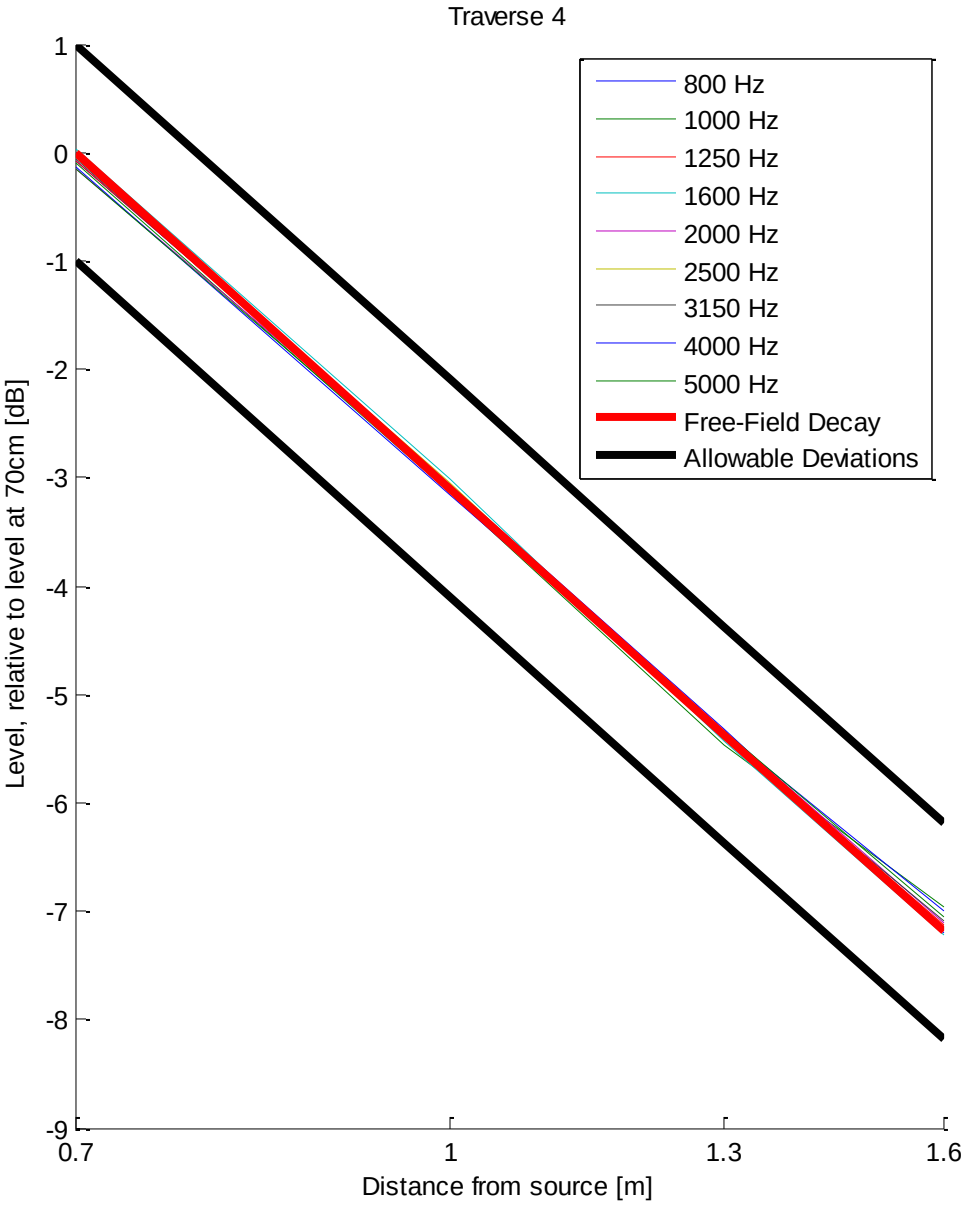
Traverse 4
800 Hz
1000 Hz
1250 Hz
1600 Hz
2000 Hz
2500 Hz
3150 Hz
4000 Hz
5000 Hz
Free-Field Decay
Allowable Deviations
Level, relative to level at 70cm [dB]
1
0
-1
-2
-3
-4
-5
-6
-7
-8
-9
0.7
1
1.3
1.6
Distance from source [m]

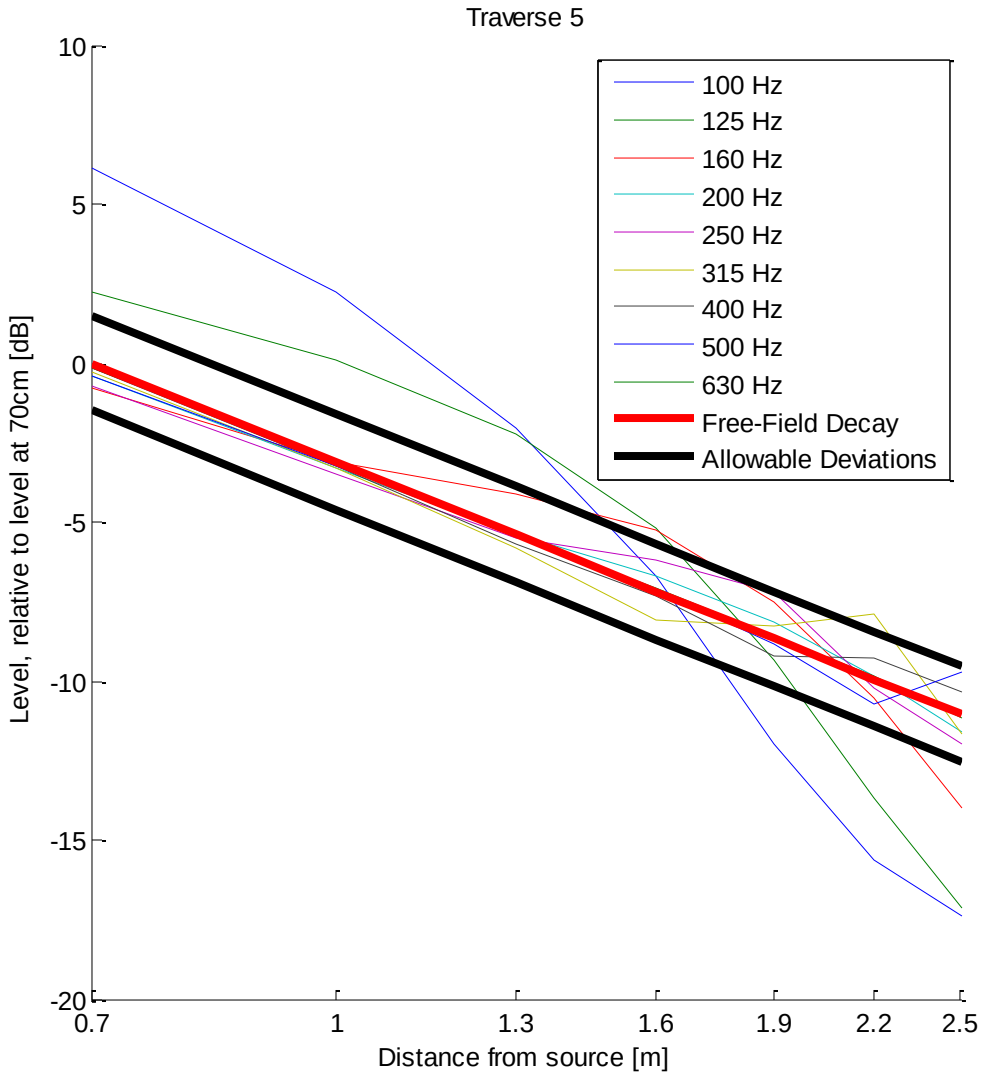
Traverse 5
100 Hz
125 Hz
160 Hz
200 Hz
250 Hz
315 Hz
400 Hz
500 Hz
630 Hz
Free-Field Decay
Allowable Deviations
Level, relative to level at 70cm [dB]
10
5
0
-5
-10
-15
-20
0.7
1
1.3
1.6
1.9
2.2
2.5
Distance from source [m]

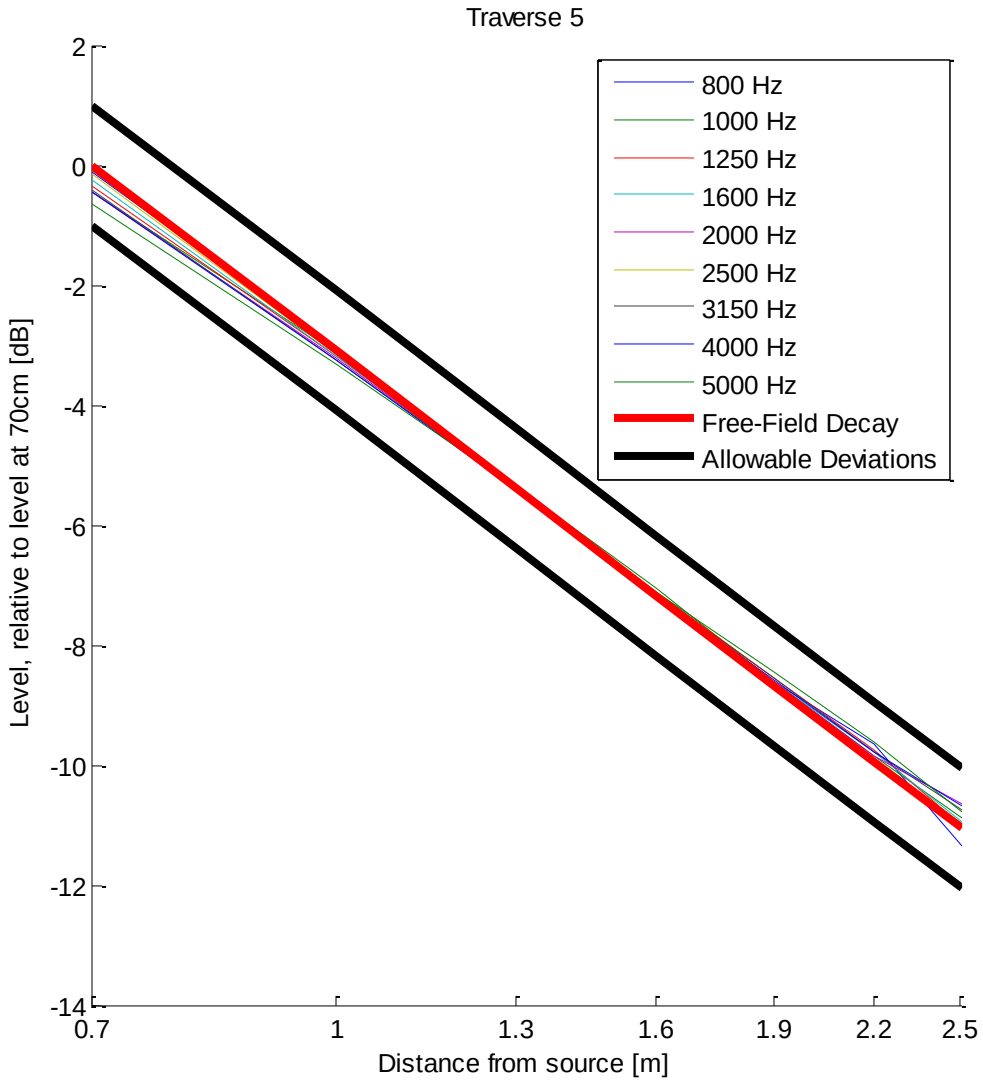
Traverse 5
800 Hz
1000 Hz
1250 Hz
1600 Hz
2000 Hz
2500 Hz
3150 Hz
4000 Hz
5000 Hz
Free-Field Decay
Allowable Deviations
Level, relative to level at 70cm [dB]
2
0
-2
-4
-6
-8
-10
-12
-14
0.7
1
1.3
1.6
1.9
2.2
2.5
Distance from source [m]

# Appendix C: Image Source Location Equations

Below are the equations for up to the third-order images sources for a rectangular room. They are labeled with the respective walls over which they have been reflected from first to third-order images. For the subscripts, $l$ is the first wall reflection, $m$ is the second wall reflection, and $n$ is the third wall reflection. A graphic of the coordinate axis and wall labels is provided in Section 4.2.1.

$$I_{l,m,n} = [x, y, z]$$

Equations:

$Image\ 1$: $I_1 = [S_x, S_y, -S_z]$

$Image\ 2$: $I_2 = [S_x, 2W - S_y, S_z]$

$Image\ 3$: $I_3 = [-S_x, S_y, S_z]$

$Image\ 4$: $I_4 = [2L - S_x, S_y, S_z]$

$Image\ 5$: $I_5 = [S_x, -S_y, S_z]$

$Image\ 6$: $I_6 = [S_x, S_y, 2H - S_z]$

$Image\ 7$: $I_{1,2} = [S_x, 2W - S_y, -S_z]$

$Image\ 8$: $I_{1,3} = [-S_x, S_y, -S_z]$

$Image\ 9$: $I_{1,4} = [2L - S_x, S_y, -S_z]$

$Image\ 10$: $I_{1,5} = [S_x, -S_y, -S_z]$

$Image\ 11$: $I_{1,6} = [S_x, S_y, 2H + S_z]$

$Image\ 12$: $I_{2,3} = [-S_x, 2W - S_y, S_z]$

$Image\ 13$: $I_{2,4} = [2L - S_x, 2W - S_y, S_z]$

$Image\ 14$: $I_{2,5} = [S_x, -2W + S_y, S_z]$

$Image\ 15\colon\ I_{2,6} = [S_x, 2W - S_y, 2H - S_z]$

$Image\ 16\colon\ I_{3,4} = [2L + S_x, S_y, S_z]$

$Image\ 17\colon\ I_{3,5} = [-S_x, -S_y, S_z]$

$Image\ 18\colon\ I_{3,6} = [-S_x, S_y, 2H - S_z]$

$Image\ 19\colon\ I_{4,3} = [-2L + S_x, S_y, S_z]$

$Image\ 20\colon\ I_{4,5} = [2L - S_x, -S_y, S_z]$

$Image\ 21\colon\ I_{4,6} = [2L - S_x, S_y, 2H - S_z]$

$Image\ 22\colon\ I_{5,2} = [S_x, 2W + S_y, S_z]$

$Image\ 23\colon\ I_{5,6} = [S_x, -S_y, 2H - S_z]$

$Image\ 24\colon\ I_{6,1} = [S_x, S_y, -2H + S_z]$

$Image\ 25\colon\ I_{1,2,3} = [-S_x, 2W - S_y, -S_z]$

$Image\ 26\colon\ I_{1,2,4} = [2L - S_x, 2W - S_y, -S_z]$

$Image\ 27\colon\ I_{1,2,6} = [S_x, 2W - S_y, 2H + S_z]$

$Image\ 28\colon\ I_{1,3,5} = [-S_x, -S_y, -S_z]$

$Image\ 29\colon\ I_{1,3,6} = [-S_x, S_y, 2H + S_z]$

$Image\ 30\colon\ I_{1,4,5} = [2L - S_x, -S_y, -S_z]$

$Image\ 31\colon\ I_{1,4,6} = [2L - S_x, S_y, 2H + S_z]$

$Image\ 32\colon\ I_{1,5,6} = [S_x, -S_y, 2H + S_z]$

$Image\ 33\colon\ I_{1,6,1} = [S_x, S_y, -2H - S_z]$

$Image\ 34\colon\ I_{2,3,5} = [-S_x, -2W + S_y, S_z]$

$Image\ 35\colon\ I_{2,3,6} = [-S_x, 2W - S_y, 2H - S_z]$

$Image\ 36\text{:}\ I_{2,4,5} = [-L - S_x, -2W + S_y, S_z]$

$Image\ 37\text{:}\ I_{2,4,6} = [2L - S_x, 2W - S_y, 2H - S_z]$

$Image\ 38\text{:}\ I_{2,5,1} = [S_x, -2W + S_y, -S_z]$

$Image\ 39\text{:}\ I_{2,5,2} = [S_x, 4W - S_y, S_z]$

$Image\ 40\text{:}\ I_{2,5,6} = [S_x, -2W + S_y, 2H - S_z]$

$Image\ 41\text{:}\ I_{3,4,1} = [2L + S_x, S_y, -S_z]$

$Image\ 42\text{:}\ I_{3,4,2} = [2L + S_x, 2W - S_y, S_z]$

$Image\ 43\text{:}\ I_{3,4,3} = [-2L - S_x, S_y, S_z]$

$Image\ 44\text{:}\ I_{3,4,5} = [2L + S_x, -S_y, S_z]$

$Image\ 45\text{:}\ I_{3,4,6} = [2L + S_x, S_y, 2H - S_z]$

$Image\ 46\text{:}\ I_{3,5,6} = [-S_x, -S_y, 2H - S_z]$

$Image\ 47\text{:}\ I_{4,3,1} = [-2L + S_x, S_y, -S_z]$

$Image\ 48\text{:}\ I_{4,3,2} = [-2L + S_x, 2W - S_y, S_z]$

$Image\ 49\text{:}\ I_{4,3,4} = [4L - S_x, S_y, S_z]$

$Image\ 50\text{:}\ I_{4,3,5} = [-2L + S_x, -S_y, S_z]$

$Image\ 51\text{:}\ I_{4,3,6} = [-2L + S_x, S_y, 2H - S_z]$

$Image\ 52\text{:}\ I_{4,5,6} = [2L - S_x, -S_y, 2H - S_z]$

$Image\ 53\text{:}\ I_{5,2,1} = [S_x, 2W + S_y, -S_z]$

$Image\ 54\text{:}\ I_{5,2,3} = [-S_x, 2W + S_y, S_z]$

$Image\ 55\text{:}\ I_{5,2,4} = [2L - S_x, 2W + S_y, S_z]$

$Image\ 56\text{:}\ I_{5,2,5} = [S_x, -2W - S_y, S_z]$

$Image\ 57\text{:}\ I_{5,2,6} = [S_x, 2W + S_y, 2H - S_z]$

$Image\ 58\text{:}\ I_{6,1,2} = [S_x, 2W - S_y, -2H + S_z]$

$Image\ 59\text{:}\ I_{6,1,3} = [-S_x, S_y, -2H + S_z]$

$Image\ 60\text{:}\ I_{6,1,4} = [2L - S_x, S_y, -2H + S_z]$

$Image\ 61\text{:}\ I_{6,1,5} = [S_x, -S_y, -2H + S_z]$

$Image\ 62\text{:}\ I_{6,1,6} = [S_x, S_y, 4H - S_z]$

# Appendix D: Equations Governing the Encoding of Ambisonic Signals

Below, equations for generating the plane-wave coefficients used in Ambisonic panning for a sound source located at azimuth $\varphi$ and elevation $\theta$ are provided. The equations were generated using the ambiX format, which utilizes a SN3D normalization scheme and the Ambisonics Channel Numbering (ACN) ordering format. As well, the Condon-Shortley phase term is omitted. Elevation is defined as the angle from the horizontal plane, and this coordinate axis is shown in Figure 2-11.

$$Y_l^m(\varphi,\theta) = N_l^{|m|} P_l^{|m|}(\sin(\theta)) \begin{cases} \sin(|m|\varphi) & \text{for } m < 0 \\ \cos(|m|\varphi) & \text{for } m \geq 0 \end{cases}$$

0: $Y_0^0(\varphi,\theta) = \sqrt{\frac{1}{4\pi}}$

1: $Y_1^{-1}(\varphi,\theta) = \sqrt{\frac{1}{4\pi}} * \cos(\theta) * \sin(\varphi)$

2: $Y_1^0(\varphi,\theta) = \sqrt{\frac{1}{4\pi}} * \sin(\theta)$

3: $Y_1^1(\varphi,\theta) = \sqrt{\frac{1}{4\pi}} * \cos(\theta) * \cos(\varphi)$

4: $Y_2^{-2}(\varphi,\theta) = \sqrt{\frac{1}{48\pi}} * 3\cos^2(\theta) * \sin(2\varphi)$

5: $Y_2^{-1}(\varphi,\theta) = \sqrt{\frac{1}{12\pi}} * 3\sin(\theta)\cos(\theta) * \sin(\varphi)$

6: $Y_2^0(\varphi,\theta) = \sqrt{\frac{1}{4\pi}} * \frac{1}{2}(3\sin^2(\theta) - 1)$

7: $Y_2^1(\varphi,\theta) = \sqrt{\frac{1}{12\pi}} * 3\sin(\theta)\cos(\theta) * \cos(\varphi)$

8: $Y_2^2(\varphi,\theta) = \sqrt{\frac{1}{48\pi}} * 3\cos^2(\theta) * \cos(2\varphi)$

9: $Y_3^{-3}(\varphi,\theta) = \sqrt{\frac{1}{1440\pi}} * 15\cos^3(\theta) * \sin(3\varphi)$

10: $Y_3^{-2}(\varphi,\theta) = \sqrt{\frac{1}{240\pi}} * 15\sin(\theta)\cos^2(\theta) * \sin(2\varphi)$

11: $Y_3^{-1}(\varphi,\theta) = \sqrt{\frac{1}{24\pi}} * \frac{3}{2}(5\sin^2(\theta) - 1)\cos(\theta) * \sin(\varphi)$

12: $Y_3^0(\varphi,\theta) = \sqrt{\frac{1}{4\pi}} * \frac{1}{2}(5\sin^3(\theta) - 3\sin(\theta))$

13: $Y_3^1(\varphi,\theta) = \sqrt{\frac{1}{24\pi}} * \frac{3}{2}(5\sin^2(\theta) - 1)\cos(\theta) * \cos(\varphi)$

14: $Y_3^2(\varphi,\theta) = \sqrt{\frac{1}{240\pi}} * 15\sin(\theta)\cos^2(\theta) * \cos(2\varphi)$

15: $Y_3^3(\varphi,\theta) = \sqrt{\frac{1}{1440\pi}} * 15\cos^3(\theta) * \cos(3\varphi)$

Additionally, for a reader's reference, the same equations are now provided using another common coordinate axis, where elevation is defined below in Figure 12-1.

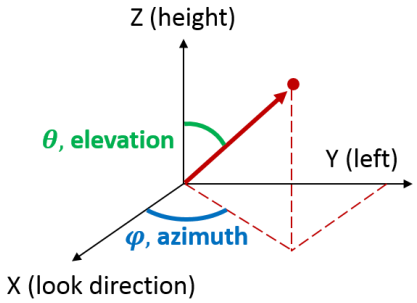


Figure 12-1: Another common way of defining the elevation angle, commonly used in many scientific disciplines. This coordinate axis is used to define the second set of Ambisonics equations for the reader's convenience.

Again, these equations were generated using the AmbiX format, which utilizes a SN3D normalization scheme and the Ambisonics Channel Numbering (ACN) ordering format, with the Condon-Shortley phase term omitted. The equations are the same as the previous equations, but the trigonometric functions associated with the elevation angle are swapped between the sine and cosine functions.

$$Y_l^m(\varphi,\theta) = N_l^{|m|} P_l^{|m|}(\cos(\theta)) \begin{cases} \sin(|m|\varphi) & \text{for } m < 0 \\ \cos(|m|\varphi) & \text{for } m \geq 0 \end{cases}$$

0: $Y_0^0(\varphi,\theta) = \sqrt{\frac{1}{4\pi}}$

1: $Y_1^{-1}(\varphi,\theta) = \sqrt{\frac{1}{4\pi}} * \sin(\theta) * \sin(\varphi)$

2: $Y_1^0(\varphi,\theta) = \sqrt{\frac{1}{4\pi}} * \cos(\theta)$

3: $Y_1^1(\varphi,\theta) = \sqrt{\frac{1}{4\pi}} * \sin(\theta) * \cos(\varphi)$

4: $Y_2^{-2}(\varphi,\theta) = \sqrt{\frac{1}{48\pi}} * 3\sin^2(\theta) * \sin(2\varphi)$

5: $Y_2^{-1}(\varphi,\theta) = \sqrt{\frac{1}{12\pi}} * 3\cos(\theta)\sin(\theta) * \sin(\varphi)$

6: $Y_2^{0}(\varphi,\theta) = \sqrt{\frac{1}{4\pi}} * \frac{1}{2}(3\cos^2(\theta) - 1)$

7: $Y_2^{1}(\varphi,\theta) = \sqrt{\frac{1}{12\pi}} * 3\cos(\theta)\sin(\theta) * \cos(\varphi)$

8: $Y_2^{2}(\varphi,\theta) = \sqrt{\frac{1}{48\pi}} * 3\sin^2(\theta) * \cos(2\varphi)$

9: $Y_3^{-3}(\varphi,\theta) = \sqrt{\frac{1}{1440\pi}} * 15\sin^3(\theta) * \sin(3\varphi)$

10: $Y_3^{-2}(\varphi,\theta) = \sqrt{\frac{1}{240\pi}} * 15\cos(\theta)\sin^2(\theta) * \sin(2\varphi)$

11: $Y_3^{-1}(\varphi,\theta) = \sqrt{\frac{1}{24\pi}} * \frac{3}{2}(5\cos^2(\theta) - 1)\sin(\theta) * \sin(\varphi)$

12: $Y_3^{0}(\varphi,\theta) = \sqrt{\frac{1}{4\pi}} * \frac{1}{2}(5\cos^3(\theta) - 3\cos(\theta))$

13: $Y_3^{1}(\varphi,\theta) = \sqrt{\frac{1}{24\pi}} * \frac{3}{2}(5\cos^2(\theta) - 1)\sin(\theta) * \cos(\varphi)$

14: $Y_3^{2}(\varphi,\theta) = \sqrt{\frac{1}{240\pi}} * 15\cos(\theta)\sin^2(\theta) * \cos(2\varphi)$

15: $Y_3^{3}(\varphi,\theta) = \sqrt{\frac{1}{1440\pi}} * 15\sin^3(\theta) * \cos(3\varphi)$

# Appendix E: Auralization Simulation Input Data

This appendix contains the input data for the simulation of the Ambisonic impulse responses of the room, which was used to create the final auralizations. Each summary table provides source-receiver information, hall dimensions, material properties, directional reverberation weights, and impulse response parameters.

## Stimuli: Set 1 Number 1 - 80% BSH 1.1 RT

| Hall Size | | | Source Location | | | Receiver Location | | | Units |
|---|---|---|---|---|---|---|---|---|---|
| Length (x) | Height (y) | Width (z) | X | Y | Z | X | Y | Z | |
| 128.0 | 60.0 | 48.8 | 108.0 | 30.0 | 8.0 | 48.0 | 26.0 | 4.0 | Feet |
| 39.0 | 18.3 | 14.9 | 32.9 | 9.1 | 2.4 | 14.6 | 7.9 | 1.2 | Meters |

| Surface | Absorption Coefficient (alpha) - Octave Bands (Hz) | | | | | | | |
|---|---|---|---|---|---|---|---|---|
| | 63 | 125 | 250 | 500 | 1000 | 2000 | 4000 | 8000 |
| Floor | 0.360 | 0.504 | 0.612 | 0.711 | 0.747 | 0.774 | 0.774 | 0.774 |
| Front Wall | 0.075 | 0.030 | 0.030 | 0.045 | 0.060 | 0.060 | 0.045 | 0.045 |
| Left Wall | 0.075 | 0.030 | 0.030 | 0.045 | 0.060 | 0.060 | 0.045 | 0.045 |
| Right Wall | 0.075 | 0.030 | 0.030 | 0.045 | 0.060 | 0.060 | 0.045 | 0.045 |
| Back Wall | 0.075 | 0.030 | 0.030 | 0.045 | 0.060 | 0.060 | 0.045 | 0.045 |
| Ceiling | 0.075 | 0.030 | 0.030 | 0.045 | 0.060 | 0.060 | 0.045 | 0.045 |

| Surface | Scattering Coefficient (alpha) - Octave Bands (Hz) | | | | | | | |
|---|---|---|---|---|---|---|---|---|
| | 63 | 125 | 250 | 500 | 1000 | 2000 | 4000 | 8000 |
| Floor | 0.02 | 0.05 | 0.30 | 0.72 | 0.88 | 0.90 | 0.92 | 0.93 |
| Front Wall | 0.01 | 0.01 | 0.03 | 0.04 | 0.10 | 0.20 | 0.25 | 0.30 |
| Left Wall | 0.01 | 0.01 | 0.03 | 0.04 | 0.10 | 0.20 | 0.25 | 0.30 |
| Right Wall | 0.01 | 0.01 | 0.03 | 0.04 | 0.10 | 0.20 | 0.25 | 0.30 |
| Back Wall | 0.01 | 0.01 | 0.03 | 0.04 | 0.10 | 0.20 | 0.25 | 0.30 |
| Ceiling | 0.01 | 0.01 | 0.03 | 0.04 | 0.10 | 0.20 | 0.25 | 0.30 |

**Directional Weights**

| Direction | Weight Value | Direction | Weight Value | Direction | Weight Value |
|---|---|---|---|---|---|
| Omni | 100 | Left | 0 | Front Bottom | 0 |
| Front | 0 | Front Left | 0 | Right Bottom | 0 |
| Front Right | 0 | Front Top | 0 | Back Bottom | 0 |
| Right | 0 | Right Top | 0 | Left Bottom | 0 |
| Back Right | 0 | Back Top | 0 | Bottom | 0 |
| Back | 0 | Left Top | 0 | | |
| Back Left | 0 | Top | 0 | | |

| **Sample Rate:** | 44100 Hz | **IR Length:** | 5 sec. | **Image Source Order:** | 3 |
|---|---|---|---|---|---|

## Stimuli: Set 1 Number 2 - 80% BSH 1.4 RT

| Hall Size | | | Source Location | | | Receiver Location | | | Units |
|---|---|---|---|---|---|---|---|---|---|
| Length (x) | Height (y) | Width (z) | X | Y | Z | X | Y | Z | |
| 128.0 | 60.0 | 48.8 | 108.0 | 30.0 | 8.0 | 48.0 | 26.0 | 4.0 | Feet |
| 39.0 | 18.3 | 14.9 | 32.9 | 9.1 | 2.4 | 14.6 | 7.9 | 1.2 | Meters |

| Surface | Absorption Coefficient (alpha) - Octave Bands (Hz) | | | | | | | |
|---|---|---|---|---|---|---|---|---|
| | 63 | 125 | 250 | 500 | 1000 | 2000 | 4000 | 8000 |
| Floor | 0.240 | 0.336 | 0.408 | 0.474 | 0.498 | 0.516 | 0.516 | 0.516 |
| Front Wall | 0.050 | 0.020 | 0.020 | 0.030 | 0.040 | 0.040 | 0.030 | 0.030 |
| Left Wall | 0.050 | 0.020 | 0.020 | 0.030 | 0.040 | 0.040 | 0.030 | 0.030 |
| Right Wall | 0.050 | 0.020 | 0.020 | 0.030 | 0.040 | 0.040 | 0.030 | 0.030 |
| Back Wall | 0.050 | 0.020 | 0.020 | 0.030 | 0.040 | 0.040 | 0.030 | 0.030 |
| Ceiling | 0.050 | 0.020 | 0.020 | 0.030 | 0.040 | 0.040 | 0.030 | 0.030 |

| Surface | Scattering Coefficient (alpha) - Octave Bands (Hz) | | | | | | | |
|---|---|---|---|---|---|---|---|---|
| | 63 | 125 | 250 | 500 | 1000 | 2000 | 4000 | 8000 |
| Floor | 0.02 | 0.05 | 0.30 | 0.72 | 0.88 | 0.90 | 0.92 | 0.93 |
| Front Wall | 0.01 | 0.01 | 0.03 | 0.04 | 0.10 | 0.20 | 0.25 | 0.30 |
| Left Wall | 0.01 | 0.01 | 0.03 | 0.04 | 0.10 | 0.20 | 0.25 | 0.30 |
| Right Wall | 0.01 | 0.01 | 0.03 | 0.04 | 0.10 | 0.20 | 0.25 | 0.30 |
| Back Wall | 0.01 | 0.01 | 0.03 | 0.04 | 0.10 | 0.20 | 0.25 | 0.30 |
| Ceiling | 0.01 | 0.01 | 0.03 | 0.04 | 0.10 | 0.20 | 0.25 | 0.30 |

**Directional Weights**

| Direction | Weight Value | Direction | Weight Value | Direction | Weight Value |
|---|---|---|---|---|---|
| Omni | 100 | Left | 0 | Front Bottom | 0 |
| Front | 0 | Front Left | 0 | Right Bottom | 0 |
| Front Right | 0 | Front Top | 0 | Back Bottom | 0 |
| Right | 0 | Right Top | 0 | Left Bottom | 0 |
| Back Right | 0 | Back Top | 0 | Bottom | 0 |
| Back | 0 | Left Top | 0 | | |
| Back Left | 0 | Top | 0 | | |

| **Sample Rate:** | 44100 Hz | **IR Length:** | 5 sec. | **Image Source Order:** | 3 |
|---|---|---|---|---|---|

## Stimuli: Set 1 Number 3 - 80% BSH 1.9 RT

| Hall Size | | | Source Location | | | Receiver Location | | | Units |
|---|---|---|---|---|---|---|---|---|---|
| Length (x) | Height (y) | Width (z) | X | Y | Z | X | Y | Z | |
| 128.0 | 60.0 | 48.8 | 108.0 | 30.0 | 8.0 | 48.0 | 26.0 | 4.0 | Feet |
| 39.0 | 18.3 | 14.9 | 32.9 | 9.1 | 2.4 | 14.6 | 7.9 | 1.2 | Meters |

| Surface | Absorption Coefficient (alpha) - Octave Bands (Hz) | | | | | | | |
|---|---|---|---|---|---|---|---|---|
| | 63 | 125 | 250 | 500 | 1000 | 2000 | 4000 | 8000 |
| Floor | 0.163 | 0.228 | 0.277 | 0.322 | 0.339 | 0.351 | 0.351 | 0.351 |
| Front Wall | 0.034 | 0.014 | 0.014 | 0.020 | 0.027 | 0.027 | 0.020 | 0.020 |
| Left Wall | 0.034 | 0.014 | 0.014 | 0.020 | 0.027 | 0.027 | 0.020 | 0.020 |
| Right Wall | 0.034 | 0.014 | 0.014 | 0.020 | 0.027 | 0.027 | 0.020 | 0.020 |
| Back Wall | 0.034 | 0.014 | 0.014 | 0.020 | 0.027 | 0.027 | 0.020 | 0.020 |
| Ceiling | 0.034 | 0.014 | 0.014 | 0.020 | 0.027 | 0.027 | 0.020 | 0.020 |

| Surface | Scattering Coefficient (alpha) - Octave Bands (Hz) | | | | | | | |
|---|---|---|---|---|---|---|---|---|
| | 63 | 125 | 250 | 500 | 1000 | 2000 | 4000 | 8000 |
| Floor | 0.02 | 0.05 | 0.30 | 0.72 | 0.88 | 0.90 | 0.92 | 0.93 |
| Front Wall | 0.01 | 0.01 | 0.03 | 0.04 | 0.10 | 0.20 | 0.25 | 0.30 |
| Left Wall | 0.01 | 0.01 | 0.03 | 0.04 | 0.10 | 0.20 | 0.25 | 0.30 |
| Right Wall | 0.01 | 0.01 | 0.03 | 0.04 | 0.10 | 0.20 | 0.25 | 0.30 |
| Back Wall | 0.01 | 0.01 | 0.03 | 0.04 | 0.10 | 0.20 | 0.25 | 0.30 |
| Ceiling | 0.01 | 0.01 | 0.03 | 0.04 | 0.10 | 0.20 | 0.25 | 0.30 |

**Directional Weights**

| Direction | Weight Value | Direction | Weight Value | Direction | Weight Value |
|---|---|---|---|---|---|
| Omni | 100 | Left | 0 | Front Bottom | 0 |
| Front | 0 | Front Left | 0 | Right Bottom | 0 |
| Front Right | 0 | Front Top | 0 | Back Bottom | 0 |
| Right | 0 | Right Top | 0 | Left Bottom | 0 |
| Back Right | 0 | Back Top | 0 | Bottom | 0 |
| Back | 0 | Left Top | 0 | | |
| Back Left | 0 | Top | 0 | | |

| **Sample Rate:** | 44100 Hz | **IR Length:** | 5 sec. | **Image Source Order:** | 3 |
|---|---|---|---|---|---|

## Stimuli: Set 1 Number 4 - 80% BSH 2.5 RT

| Hall Size | | | Source Location | | | Receiver Location | | | Units |
|---|---|---|---|---|---|---|---|---|---|
| Length (x) | Height (y) | Width (z) | X | Y | Z | X | Y | Z | |
| 128.0 | 60.0 | 48.8 | 108.0 | 30.0 | 8.0 | 48.0 | 26.0 | 4.0 | Feet |
| 39.0 | 18.3 | 14.9 | 32.9 | 9.1 | 2.4 | 14.6 | 7.9 | 1.2 | Meters |

| Surface | Absorption Coefficient (alpha) - Octave Bands (Hz) | | | | | | | |
|---|---|---|---|---|---|---|---|---|
| | 63 | 125 | 250 | 500 | 1000 | 2000 | 4000 | 8000 |
| Floor | 0.120 | 0.168 | 0.204 | 0.237 | 0.249 | 0.258 | 0.258 | 0.258 |
| Front Wall | 0.025 | 0.010 | 0.010 | 0.015 | 0.020 | 0.020 | 0.015 | 0.015 |
| Left Wall | 0.025 | 0.010 | 0.010 | 0.015 | 0.020 | 0.020 | 0.015 | 0.015 |
| Right Wall | 0.025 | 0.010 | 0.010 | 0.015 | 0.020 | 0.020 | 0.015 | 0.015 |
| Back Wall | 0.025 | 0.010 | 0.010 | 0.015 | 0.020 | 0.020 | 0.015 | 0.015 |
| Ceiling | 0.025 | 0.010 | 0.010 | 0.015 | 0.020 | 0.020 | 0.015 | 0.015 |

| Surface | Scattering Coefficient (alpha) - Octave Bands (Hz) | | | | | | | |
|---|---|---|---|---|---|---|---|---|
| | 63 | 125 | 250 | 500 | 1000 | 2000 | 4000 | 8000 |
| Floor | 0.02 | 0.05 | 0.30 | 0.72 | 0.88 | 0.90 | 0.92 | 0.93 |
| Front Wall | 0.01 | 0.01 | 0.03 | 0.04 | 0.10 | 0.20 | 0.25 | 0.30 |
| Left Wall | 0.01 | 0.01 | 0.03 | 0.04 | 0.10 | 0.20 | 0.25 | 0.30 |
| Right Wall | 0.01 | 0.01 | 0.03 | 0.04 | 0.10 | 0.20 | 0.25 | 0.30 |
| Back Wall | 0.01 | 0.01 | 0.03 | 0.04 | 0.10 | 0.20 | 0.25 | 0.30 |
| Ceiling | 0.01 | 0.01 | 0.03 | 0.04 | 0.10 | 0.20 | 0.25 | 0.30 |

**Directional Weights**

| Direction | Weight Value | Direction | Weight Value | Direction | Weight Value |
|---|---|---|---|---|---|
| Omni | 100 | Left | 0 | Front Bottom | 0 |
| Front | 0 | Front Left | 0 | Right Bottom | 0 |
| Front Right | 0 | Front Top | 0 | Back Bottom | 0 |
| Right | 0 | Right Top | 0 | Left Bottom | 0 |
| Back Right | 0 | Back Top | 0 | Bottom | 0 |
| Back | 0 | Left Top | 0 | | |
| Back Left | 0 | Top | 0 | | |

| **Sample Rate:** | 44100 Hz | **IR Length:** | 5 sec. | **Image Source Order:** | 3 |
|---|---|---|---|---|---|

## Stimuli: Set 1 Number 5 - 120% BSH 1.4 RT

| Hall Size | | | Source Location | | | Receiver Location | | | Units |
|---|---|---|---|---|---|---|---|---|---|
| Length (x) | Height (y) | Width (z) | X | Y | Z | X | Y | Z | |
| 192.0 | 90.0 | 73.2 | 172.0 | 45.0 | 8.0 | 112.0 | 41.0 | 4.0 | Feet |
| 58.5 | 27.4 | 22.3 | 52.4 | 13.7 | 2.4 | 34.1 | 12.5 | 1.2 | Meters |

| Surface | Absorption Coefficient (alpha) - Octave Bands (Hz) | | | | | | | |
|---|---|---|---|---|---|---|---|---|
| | 63 | 125 | 250 | 500 | 1000 | 2000 | 4000 | 8000 |
| Floor | 0.408 | 0.571 | 0.694 | 0.806 | 0.847 | 0.877 | 0.877 | 0.877 |
| Front Wall | 0.085 | 0.034 | 0.034 | 0.051 | 0.068 | 0.068 | 0.051 | 0.051 |
| Left Wall | 0.085 | 0.034 | 0.034 | 0.051 | 0.068 | 0.068 | 0.051 | 0.051 |
| Right Wall | 0.085 | 0.034 | 0.034 | 0.051 | 0.068 | 0.068 | 0.051 | 0.051 |
| Back Wall | 0.085 | 0.034 | 0.034 | 0.051 | 0.068 | 0.068 | 0.051 | 0.051 |
| Ceiling | 0.085 | 0.034 | 0.034 | 0.051 | 0.068 | 0.068 | 0.051 | 0.051 |

| Surface | Scattering Coefficient (alpha) - Octave Bands (Hz) | | | | | | | |
|---|---|---|---|---|---|---|---|---|
| | 63 | 125 | 250 | 500 | 1000 | 2000 | 4000 | 8000 |
| Floor | 0.02 | 0.05 | 0.30 | 0.72 | 0.88 | 0.90 | 0.92 | 0.93 |
| Front Wall | 0.01 | 0.01 | 0.03 | 0.04 | 0.10 | 0.20 | 0.25 | 0.30 |
| Left Wall | 0.01 | 0.01 | 0.03 | 0.04 | 0.10 | 0.20 | 0.25 | 0.30 |
| Right Wall | 0.01 | 0.01 | 0.03 | 0.04 | 0.10 | 0.20 | 0.25 | 0.30 |
| Back Wall | 0.01 | 0.01 | 0.03 | 0.04 | 0.10 | 0.20 | 0.25 | 0.30 |
| Ceiling | 0.01 | 0.01 | 0.03 | 0.04 | 0.10 | 0.20 | 0.25 | 0.30 |

**Directional Weights**

| Direction | Weight Value | Direction | Weight Value | Direction | Weight Value |
|---|---|---|---|---|---|
| Omni | 100 | Left | 0 | Front Bottom | 0 |
| Front | 0 | Front Left | 0 | Right Bottom | 0 |
| Front Right | 0 | Front Top | 0 | Back Bottom | 0 |
| Right | 0 | Right Top | 0 | Left Bottom | 0 |
| Back Right | 0 | Back Top | 0 | Bottom | 0 |
| Back | 0 | Left Top | 0 | | |
| Back Left | 0 | Top | 0 | | |

| **Sample Rate:** | 44100 Hz | **IR Length:** | 5 sec. | **Image Source Order:** | 3 |
|---|---|---|---|---|---|

## Stimuli: Set 1 Number 6 - 120% BSH 1.9 RT

| Hall Size | | | Source Location | | | Receiver Location | | | Units |
|---|---|---|---|---|---|---|---|---|---|
| Length (x) | Height (y) | Width (z) | X | Y | Z | X | Y | Z | |
| 192.0 | 90.0 | 73.2 | 172.0 | 45.0 | 8.0 | 112.0 | 41.0 | 4.0 | Feet |
| 58.5 | 27.4 | 22.3 | 52.4 | 13.7 | 2.4 | 34.1 | 12.5 | 1.2 | Meters |

| Surface | Absorption Coefficient (alpha) - Octave Bands (Hz) | | | | | | | |
|---|---|---|---|---|---|---|---|---|
| | 63 | 125 | 250 | 500 | 1000 | 2000 | 4000 | 8000 |
| Floor | 0.300 | 0.420 | 0.510 | 0.593 | 0.623 | 0.645 | 0.645 | 0.645 |
| Front Wall | 0.063 | 0.025 | 0.025 | 0.038 | 0.050 | 0.050 | 0.038 | 0.038 |
| Left Wall | 0.063 | 0.025 | 0.025 | 0.038 | 0.050 | 0.050 | 0.038 | 0.038 |
| Right Wall | 0.063 | 0.025 | 0.025 | 0.038 | 0.050 | 0.050 | 0.038 | 0.038 |
| Back Wall | 0.063 | 0.025 | 0.025 | 0.038 | 0.050 | 0.050 | 0.038 | 0.038 |
| Ceiling | 0.063 | 0.025 | 0.025 | 0.038 | 0.050 | 0.050 | 0.038 | 0.038 |

| Surface | Scattering Coefficient (alpha) - Octave Bands (Hz) | | | | | | | |
|---|---|---|---|---|---|---|---|---|
| | 63 | 125 | 250 | 500 | 1000 | 2000 | 4000 | 8000 |
| Floor | 0.02 | 0.05 | 0.30 | 0.72 | 0.88 | 0.90 | 0.92 | 0.93 |
| Front Wall | 0.01 | 0.01 | 0.03 | 0.04 | 0.10 | 0.20 | 0.25 | 0.30 |
| Left Wall | 0.01 | 0.01 | 0.03 | 0.04 | 0.10 | 0.20 | 0.25 | 0.30 |
| Right Wall | 0.01 | 0.01 | 0.03 | 0.04 | 0.10 | 0.20 | 0.25 | 0.30 |
| Back Wall | 0.01 | 0.01 | 0.03 | 0.04 | 0.10 | 0.20 | 0.25 | 0.30 |
| Ceiling | 0.01 | 0.01 | 0.03 | 0.04 | 0.10 | 0.20 | 0.25 | 0.30 |

**Directional Weights**

| Direction | Weight Value | Direction | Weight Value | Direction | Weight Value |
|---|---|---|---|---|---|
| Omni | 100 | Left | 0 | Front Bottom | 0 |
| Front | 0 | Front Left | 0 | Right Bottom | 0 |
| Front Right | 0 | Front Top | 0 | Back Bottom | 0 |
| Right | 0 | Right Top | 0 | Left Bottom | 0 |
| Back Right | 0 | Back Top | 0 | Bottom | 0 |
| Back | 0 | Left Top | 0 | | |
| Back Left | 0 | Top | 0 | | |

| **Sample Rate:** | 44100 Hz | **IR Length:** | 5 sec. | **Image Source Order:** | 3 |
|---|---|---|---|---|---|

## Stimuli: Set 1 Number 7 - 120% BSH 2.5 RT

| Hall Size | | | Source Location | | | Receiver Location | | | Units |
|---|---|---|---|---|---|---|---|---|---|
| Length (x) | Height (y) | Width (z) | X | Y | Z | X | Y | Z | |
| 192.0 | 90.0 | 73.2 | 172.0 | 45.0 | 8.0 | 112.0 | 41.0 | 4.0 | Feet |
| 58.5 | 27.4 | 22.3 | 52.4 | 13.7 | 2.4 | 34.1 | 12.5 | 1.2 | Meters |

| Surface | Absorption Coefficient (alpha) - Octave Bands (Hz) | | | | | | | |
|---|---|---|---|---|---|---|---|---|
| | 63 | 125 | 250 | 500 | 1000 | 2000 | 4000 | 8000 |
| Floor | 0.194 | 0.272 | 0.349 | 0.427 | 0.448 | 0.464 | 0.464 | 0.464 |
| Front Wall | 0.041 | 0.016 | 0.017 | 0.027 | 0.036 | 0.036 | 0.027 | 0.027 |
| Left Wall | 0.041 | 0.016 | 0.017 | 0.027 | 0.036 | 0.036 | 0.027 | 0.027 |
| Right Wall | 0.041 | 0.016 | 0.017 | 0.027 | 0.036 | 0.036 | 0.027 | 0.027 |
| Back Wall | 0.041 | 0.016 | 0.017 | 0.027 | 0.036 | 0.036 | 0.027 | 0.027 |
| Ceiling | 0.041 | 0.016 | 0.017 | 0.027 | 0.036 | 0.036 | 0.027 | 0.027 |

| Surface | Scattering Coefficient (alpha) - Octave Bands (Hz) | | | | | | | |
|---|---|---|---|---|---|---|---|---|
| | 63 | 125 | 250 | 500 | 1000 | 2000 | 4000 | 8000 |
| Floor | 0.02 | 0.05 | 0.30 | 0.72 | 0.88 | 0.90 | 0.92 | 0.93 |
| Front Wall | 0.01 | 0.01 | 0.03 | 0.04 | 0.10 | 0.20 | 0.25 | 0.30 |
| Left Wall | 0.01 | 0.01 | 0.03 | 0.04 | 0.10 | 0.20 | 0.25 | 0.30 |
| Right Wall | 0.01 | 0.01 | 0.03 | 0.04 | 0.10 | 0.20 | 0.25 | 0.30 |
| Back Wall | 0.01 | 0.01 | 0.03 | 0.04 | 0.10 | 0.20 | 0.25 | 0.30 |
| Ceiling | 0.01 | 0.01 | 0.03 | 0.04 | 0.10 | 0.20 | 0.25 | 0.30 |

**Directional Weights**

| Direction | Weight Value | Direction | Weight Value | Direction | Weight Value |
|---|---|---|---|---|---|
| Omni | 100 | Left | 0 | Front Bottom | 0 |
| Front | 0 | Front Left | 0 | Right Bottom | 0 |
| Front Right | 0 | Front Top | 0 | Back Bottom | 0 |
| Right | 0 | Right Top | 0 | Left Bottom | 0 |
| Back Right | 0 | Back Top | 0 | Bottom | 0 |
| Back | 0 | Left Top | 0 | | |
| Back Left | 0 | Top | 0 | | |

| **Sample Rate:** | 44100 Hz | **IR Length:** | 5 sec. | **Image Source Order:** | 3 |
|---|---|---|---|---|---|

## Stimuli: Set 1 Number 8 - 120% BSH 2.9 RT

| Hall Size | | | Source Location | | | Receiver Location | | | Units |
|---|---|---|---|---|---|---|---|---|---|
| Length (x) | Height (y) | Width (z) | X | Y | Z | X | Y | Z | |
| 192.0 | 90.0 | 73.2 | 172.0 | 45.0 | 8.0 | 112.0 | 41.0 | 4.0 | Feet |
| 58.5 | 27.4 | 22.3 | 52.4 | 13.7 | 2.4 | 34.1 | 12.5 | 1.2 | Meters |

| Surface | Absorption Coefficient (alpha) - Octave Bands (Hz) | | | | | | | |
|---|---|---|---|---|---|---|---|---|
| | 63 | 125 | 250 | 500 | 1000 | 2000 | 4000 | 8000 |
| Floor | 0.152 | 0.212 | 0.272 | 0.333 | 0.350 | 0.362 | 0.362 | 0.362 |
| Front Wall | 0.032 | 0.013 | 0.013 | 0.021 | 0.028 | 0.028 | 0.021 | 0.021 |
| Left Wall | 0.032 | 0.013 | 0.013 | 0.021 | 0.028 | 0.028 | 0.021 | 0.021 |
| Right Wall | 0.032 | 0.013 | 0.013 | 0.021 | 0.028 | 0.028 | 0.021 | 0.021 |
| Back Wall | 0.032 | 0.013 | 0.013 | 0.021 | 0.028 | 0.028 | 0.021 | 0.021 |
| Ceiling | 0.032 | 0.013 | 0.013 | 0.021 | 0.028 | 0.028 | 0.021 | 0.021 |

| Surface | Scattering Coefficient (alpha) - Octave Bands (Hz) | | | | | | | |
|---|---|---|---|---|---|---|---|---|
| | 63 | 125 | 250 | 500 | 1000 | 2000 | 4000 | 8000 |
| Floor | 0.02 | 0.05 | 0.30 | 0.72 | 0.88 | 0.90 | 0.92 | 0.93 |
| Front Wall | 0.01 | 0.01 | 0.03 | 0.04 | 0.10 | 0.20 | 0.25 | 0.30 |
| Left Wall | 0.01 | 0.01 | 0.03 | 0.04 | 0.10 | 0.20 | 0.25 | 0.30 |
| Right Wall | 0.01 | 0.01 | 0.03 | 0.04 | 0.10 | 0.20 | 0.25 | 0.30 |
| Back Wall | 0.01 | 0.01 | 0.03 | 0.04 | 0.10 | 0.20 | 0.25 | 0.30 |
| Ceiling | 0.01 | 0.01 | 0.03 | 0.04 | 0.10 | 0.20 | 0.25 | 0.30 |

**Directional Weights**

| Direction | Weight Value | Direction | Weight Value | Direction | Weight Value |
|---|---|---|---|---|---|
| Omni | 100 | Left | 0 | Front Bottom | 0 |
| Front | 0 | Front Left | 0 | Right Bottom | 0 |
| Front Right | 0 | Front Top | 0 | Back Bottom | 0 |
| Right | 0 | Right Top | 0 | Left Bottom | 0 |
| Back Right | 0 | Back Top | 0 | Bottom | 0 |
| Back | 0 | Left Top | 0 | | |
| Back Left | 0 | Top | 0 | | |

| **Sample Rate:** | 44100 Hz | **IR Length:** | 5 sec. | **Image Source Order:** | 3 |
|---|---|---|---|---|---|

## Stimuli: Set 2 Number 1 - Early / Late, R1, 0.5 Scaled Late

| Hall Size | | | Source Location | | | Receiver Location | | | Units |
|---|---|---|---|---|---|---|---|---|---|
| Length (x) | Height (y) | Width (z) | X | Y | Z | X | Y | Z | |
| 128.0 | 60.0 | 48.8 | 108.0 | 30.0 | 8.0 | 48.0 | 26.0 | 4.0 | Feet |
| 39.0 | 18.3 | 14.9 | 32.9 | 9.1 | 2.4 | 14.6 | 7.9 | 1.2 | Meters |

| Surface | Absorption Coefficient (alpha) - Octave Bands (Hz) | | | | | | | |
|---|---|---|---|---|---|---|---|---|
| | 63 | 125 | 250 | 500 | 1000 | 2000 | 4000 | 8000 |
| Floor | 0.240 | 0.336 | 0.408 | 0.474 | 0.498 | 0.516 | 0.516 | 0.516 |
| Front Wall | 0.050 | 0.020 | 0.020 | 0.030 | 0.040 | 0.040 | 0.030 | 0.030 |
| Left Wall | 0.050 | 0.020 | 0.020 | 0.030 | 0.040 | 0.040 | 0.030 | 0.030 |
| Right Wall | 0.050 | 0.020 | 0.020 | 0.030 | 0.040 | 0.040 | 0.030 | 0.030 |
| Back Wall | 0.050 | 0.020 | 0.020 | 0.030 | 0.040 | 0.040 | 0.030 | 0.030 |
| Ceiling | 0.050 | 0.020 | 0.020 | 0.030 | 0.040 | 0.040 | 0.030 | 0.030 |

| Surface | Scattering Coefficient (alpha) - Octave Bands (Hz) | | | | | | | |
|---|---|---|---|---|---|---|---|---|
| | 63 | 125 | 250 | 500 | 1000 | 2000 | 4000 | 8000 |
| Floor | 0.02 | 0.05 | 0.30 | 0.72 | 0.88 | 0.90 | 0.92 | 0.93 |
| Front Wall | 0.01 | 0.01 | 0.03 | 0.04 | 0.10 | 0.20 | 0.25 | 0.30 |
| Left Wall | 0.01 | 0.01 | 0.03 | 0.04 | 0.10 | 0.20 | 0.25 | 0.30 |
| Right Wall | 0.01 | 0.01 | 0.03 | 0.04 | 0.10 | 0.20 | 0.25 | 0.30 |
| Back Wall | 0.01 | 0.01 | 0.03 | 0.04 | 0.10 | 0.20 | 0.25 | 0.30 |
| Ceiling | 0.01 | 0.01 | 0.03 | 0.04 | 0.10 | 0.20 | 0.25 | 0.30 |

**Directional Weights**

| Direction | Weight Value | Direction | Weight Value | Direction | Weight Value |
|---|---|---|---|---|---|
| Omni | 100 | Left | 0 | Front Bottom | 0 |
| Front | 0 | Front Left | 0 | Right Bottom | 0 |
| Front Right | 0 | Front Top | 0 | Back Bottom | 0 |
| Right | 0 | Right Top | 0 | Left Bottom | 0 |
| Back Right | 0 | Back Top | 0 | Bottom | 0 |
| Back | 0 | Left Top | 0 | | |
| Back Left | 0 | Top | 0 | | |

| **Sample Rate:** | 44100 Hz | **IR Length:** | 5 sec. | **Image Source Order:** | 3 |
|---|---|---|---|---|---|

## Stimuli: Set 2 Number 2 - Early / Late, R1, 0.7 Scaled Late

| Hall Size | | | Source Location | | | Receiver Location | | | Units |
|---|---|---|---|---|---|---|---|---|---|
| Length (x) | Height (y) | Width (z) | X | Y | Z | X | Y | Z | |
| 128.0 | 60.0 | 48.8 | 108.0 | 30.0 | 8.0 | 48.0 | 26.0 | 4.0 | Feet |
| 39.0 | 18.3 | 14.9 | 32.9 | 9.1 | 2.4 | 14.6 | 7.9 | 1.2 | Meters |

| Surface | Absorption Coefficient (alpha) - Octave Bands (Hz) | | | | | | | |
|---|---|---|---|---|---|---|---|---|
| | 63 | 125 | 250 | 500 | 1000 | 2000 | 4000 | 8000 |
| Floor | 0.240 | 0.336 | 0.408 | 0.474 | 0.498 | 0.516 | 0.516 | 0.516 |
| Front Wall | 0.050 | 0.020 | 0.020 | 0.030 | 0.040 | 0.040 | 0.030 | 0.030 |
| Left Wall | 0.050 | 0.020 | 0.020 | 0.030 | 0.040 | 0.040 | 0.030 | 0.030 |
| Right Wall | 0.050 | 0.020 | 0.020 | 0.030 | 0.040 | 0.040 | 0.030 | 0.030 |
| Back Wall | 0.050 | 0.020 | 0.020 | 0.030 | 0.040 | 0.040 | 0.030 | 0.030 |
| Ceiling | 0.050 | 0.020 | 0.020 | 0.030 | 0.040 | 0.040 | 0.030 | 0.030 |

| Surface | Scattering Coefficient (alpha) - Octave Bands (Hz) | | | | | | | |
|---|---|---|---|---|---|---|---|---|
| | 63 | 125 | 250 | 500 | 1000 | 2000 | 4000 | 8000 |
| Floor | 0.02 | 0.05 | 0.30 | 0.72 | 0.88 | 0.90 | 0.92 | 0.93 |
| Front Wall | 0.01 | 0.01 | 0.03 | 0.04 | 0.10 | 0.20 | 0.25 | 0.30 |
| Left Wall | 0.01 | 0.01 | 0.03 | 0.04 | 0.10 | 0.20 | 0.25 | 0.30 |
| Right Wall | 0.01 | 0.01 | 0.03 | 0.04 | 0.10 | 0.20 | 0.25 | 0.30 |
| Back Wall | 0.01 | 0.01 | 0.03 | 0.04 | 0.10 | 0.20 | 0.25 | 0.30 |
| Ceiling | 0.01 | 0.01 | 0.03 | 0.04 | 0.10 | 0.20 | 0.25 | 0.30 |

**Directional Weights**

| Direction | Weight Value | Direction | Weight Value | Direction | Weight Value |
|---|---|---|---|---|---|
| Omni | 100 | Left | 0 | Front Bottom | 0 |
| Front | 0 | Front Left | 0 | Right Bottom | 0 |
| Front Right | 0 | Front Top | 0 | Back Bottom | 0 |
| Right | 0 | Right Top | 0 | Left Bottom | 0 |
| Back Right | 0 | Back Top | 0 | Bottom | 0 |
| Back | 0 | Left Top | 0 | | |
| Back Left | 0 | Top | 0 | | |

| **Sample Rate:** | 44100 Hz | **IR Length:** | 5 sec. | **Image Source Order:** | 3 |
|---|---|---|---|---|---|

## Stimuli: Set 2 Number 3 - Early / Late, R1, 1.0 Scaled Late

| Hall Size | | | Source Location | | | Receiver Location | | | Units |
|---|---|---|---|---|---|---|---|---|---|
| Length (x) | Height (y) | Width (z) | X | Y | Z | X | Y | Z | |
| 128.0 | 60.0 | 48.8 | 108.0 | 30.0 | 8.0 | 48.0 | 26.0 | 4.0 | Feet |
| 39.0 | 18.3 | 14.9 | 32.9 | 9.1 | 2.4 | 14.6 | 7.9 | 1.2 | Meters |

| Surface | Absorption Coefficient (alpha) - Octave Bands (Hz) | | | | | | | |
|---|---|---|---|---|---|---|---|---|
| | 63 | 125 | 250 | 500 | 1000 | 2000 | 4000 | 8000 |
| Floor | 0.240 | 0.336 | 0.408 | 0.474 | 0.498 | 0.516 | 0.516 | 0.516 |
| Front Wall | 0.050 | 0.020 | 0.020 | 0.030 | 0.040 | 0.040 | 0.030 | 0.030 |
| Left Wall | 0.050 | 0.020 | 0.020 | 0.030 | 0.040 | 0.040 | 0.030 | 0.030 |
| Right Wall | 0.050 | 0.020 | 0.020 | 0.030 | 0.040 | 0.040 | 0.030 | 0.030 |
| Back Wall | 0.050 | 0.020 | 0.020 | 0.030 | 0.040 | 0.040 | 0.030 | 0.030 |
| Ceiling | 0.050 | 0.020 | 0.020 | 0.030 | 0.040 | 0.040 | 0.030 | 0.030 |

| Surface | Scattering Coefficient (alpha) - Octave Bands (Hz) | | | | | | | |
|---|---|---|---|---|---|---|---|---|
| | 63 | 125 | 250 | 500 | 1000 | 2000 | 4000 | 8000 |
| Floor | 0.02 | 0.05 | 0.30 | 0.72 | 0.88 | 0.90 | 0.92 | 0.93 |
| Front Wall | 0.01 | 0.01 | 0.03 | 0.04 | 0.10 | 0.20 | 0.25 | 0.30 |
| Left Wall | 0.01 | 0.01 | 0.03 | 0.04 | 0.10 | 0.20 | 0.25 | 0.30 |
| Right Wall | 0.01 | 0.01 | 0.03 | 0.04 | 0.10 | 0.20 | 0.25 | 0.30 |
| Back Wall | 0.01 | 0.01 | 0.03 | 0.04 | 0.10 | 0.20 | 0.25 | 0.30 |
| Ceiling | 0.01 | 0.01 | 0.03 | 0.04 | 0.10 | 0.20 | 0.25 | 0.30 |

**Directional Weights**

| Direction | Weight Value | Direction | Weight Value | Direction | Weight Value |
|---|---|---|---|---|---|
| Omni | 100 | Left | 0 | Front Bottom | 0 |
| Front | 0 | Front Left | 0 | Right Bottom | 0 |
| Front Right | 0 | Front Top | 0 | Back Bottom | 0 |
| Right | 0 | Right Top | 0 | Left Bottom | 0 |
| Back Right | 0 | Back Top | 0 | Bottom | 0 |
| Back | 0 | Left Top | 0 | | |
| Back Left | 0 | Top | 0 | | |

| **Sample Rate:** | 44100 Hz | **IR Length:** | 5 sec. | **Image Source Order:** | 3 |
|---|---|---|---|---|---|

## Stimuli: Set 2 Number 4 - Early / Late, R1, 1.5 Scaled Late

| Hall Size | | | Source Location | | | Receiver Location | | | Units |
|---|---|---|---|---|---|---|---|---|---|
| Length (x) | Height (y) | Width (z) | X | Y | Z | X | Y | Z | |
| 128.0 | 60.0 | 48.8 | 108.0 | 30.0 | 8.0 | 48.0 | 26.0 | 4.0 | Feet |
| 39.0 | 18.3 | 14.9 | 32.9 | 9.1 | 2.4 | 14.6 | 7.9 | 1.2 | Meters |

| Surface | Absorption Coefficient (alpha) - Octave Bands (Hz) | | | | | | | |
|---|---|---|---|---|---|---|---|---|
| | 63 | 125 | 250 | 500 | 1000 | 2000 | 4000 | 8000 |
| Floor | 0.240 | 0.336 | 0.408 | 0.474 | 0.498 | 0.516 | 0.516 | 0.516 |
| Front Wall | 0.050 | 0.020 | 0.020 | 0.030 | 0.040 | 0.040 | 0.030 | 0.030 |
| Left Wall | 0.050 | 0.020 | 0.020 | 0.030 | 0.040 | 0.040 | 0.030 | 0.030 |
| Right Wall | 0.050 | 0.020 | 0.020 | 0.030 | 0.040 | 0.040 | 0.030 | 0.030 |
| Back Wall | 0.050 | 0.020 | 0.020 | 0.030 | 0.040 | 0.040 | 0.030 | 0.030 |
| Ceiling | 0.050 | 0.020 | 0.020 | 0.030 | 0.040 | 0.040 | 0.030 | 0.030 |

| Surface | Scattering Coefficient (alpha) - Octave Bands (Hz) | | | | | | | |
|---|---|---|---|---|---|---|---|---|
| | 63 | 125 | 250 | 500 | 1000 | 2000 | 4000 | 8000 |
| Floor | 0.02 | 0.05 | 0.30 | 0.72 | 0.88 | 0.90 | 0.92 | 0.93 |
| Front Wall | 0.01 | 0.01 | 0.03 | 0.04 | 0.10 | 0.20 | 0.25 | 0.30 |
| Left Wall | 0.01 | 0.01 | 0.03 | 0.04 | 0.10 | 0.20 | 0.25 | 0.30 |
| Right Wall | 0.01 | 0.01 | 0.03 | 0.04 | 0.10 | 0.20 | 0.25 | 0.30 |
| Back Wall | 0.01 | 0.01 | 0.03 | 0.04 | 0.10 | 0.20 | 0.25 | 0.30 |
| Ceiling | 0.01 | 0.01 | 0.03 | 0.04 | 0.10 | 0.20 | 0.25 | 0.30 |

**Directional Weights**

| Direction | Weight Value | Direction | Weight Value | Direction | Weight Value |
|---|---|---|---|---|---|
| Omni | 100 | Left | 0 | Front Bottom | 0 |
| Front | 0 | Front Left | 0 | Right Bottom | 0 |
| Front Right | 0 | Front Top | 0 | Back Bottom | 0 |
| Right | 0 | Right Top | 0 | Left Bottom | 0 |
| Back Right | 0 | Back Top | 0 | Bottom | 0 |
| Back | 0 | Left Top | 0 | | |
| Back Left | 0 | Top | 0 | | |

| **Sample Rate:** | 44100 Hz | **IR Length:** | 5 sec. | **Image Source Order:** | 3 |
|---|---|---|---|---|---|

## Stimuli: Set 2 Number 5 - Early / Late, R2, 0.5 Scaled Late

| Hall Size | | | Source Location | | | Receiver Location | | | Units |
|---|---|---|---|---|---|---|---|---|---|
| Length (x) | Height (y) | Width (z) | X | Y | Z | X | Y | Z | |
| 128.0 | 60.0 | 48.8 | 108.0 | 30.0 | 8.0 | 18.0 | 10.0 | 4.0 | Feet |
| 39.0 | 18.3 | 14.9 | 32.9 | 9.1 | 2.4 | 5.5 | 3.0 | 1.2 | Meters |

| Surface | Absorption Coefficient (alpha) - Octave Bands (Hz) | | | | | | | |
|---|---|---|---|---|---|---|---|---|
| | 63 | 125 | 250 | 500 | 1000 | 2000 | 4000 | 8000 |
| Floor | 0.240 | 0.336 | 0.408 | 0.474 | 0.498 | 0.516 | 0.516 | 0.516 |
| Front Wall | 0.050 | 0.020 | 0.020 | 0.030 | 0.040 | 0.040 | 0.030 | 0.030 |
| Left Wall | 0.050 | 0.020 | 0.020 | 0.030 | 0.040 | 0.040 | 0.030 | 0.030 |
| Right Wall | 0.050 | 0.020 | 0.020 | 0.030 | 0.040 | 0.040 | 0.030 | 0.030 |
| Back Wall | 0.050 | 0.020 | 0.020 | 0.030 | 0.040 | 0.040 | 0.030 | 0.030 |
| Ceiling | 0.050 | 0.020 | 0.020 | 0.030 | 0.040 | 0.040 | 0.030 | 0.030 |

| Surface | Scattering Coefficient (alpha) - Octave Bands (Hz) | | | | | | | |
|---|---|---|---|---|---|---|---|---|
| | 63 | 125 | 250 | 500 | 1000 | 2000 | 4000 | 8000 |
| Floor | 0.02 | 0.05 | 0.30 | 0.72 | 0.88 | 0.90 | 0.92 | 0.93 |
| Front Wall | 0.01 | 0.01 | 0.03 | 0.04 | 0.10 | 0.20 | 0.25 | 0.30 |
| Left Wall | 0.01 | 0.01 | 0.03 | 0.04 | 0.10 | 0.20 | 0.25 | 0.30 |
| Right Wall | 0.01 | 0.01 | 0.03 | 0.04 | 0.10 | 0.20 | 0.25 | 0.30 |
| Back Wall | 0.01 | 0.01 | 0.03 | 0.04 | 0.10 | 0.20 | 0.25 | 0.30 |
| Ceiling | 0.01 | 0.01 | 0.03 | 0.04 | 0.10 | 0.20 | 0.25 | 0.30 |

**Directional Weights**

| Direction | Weight Value | Direction | Weight Value | Direction | Weight Value |
|---|---|---|---|---|---|
| Omni | 100 | Left | 0 | Front Bottom | 0 |
| Front | 0 | Front Left | 0 | Right Bottom | 0 |
| Front Right | 0 | Front Top | 0 | Back Bottom | 0 |
| Right | 0 | Right Top | 0 | Left Bottom | 0 |
| Back Right | 0 | Back Top | 0 | Bottom | 0 |
| Back | 0 | Left Top | 0 | | |
| Back Left | 0 | Top | 0 | | |

| **Sample Rate:** | 44100 Hz | **IR Length:** | 5 sec. | **Image Source Order:** | 3 |
|---|---|---|---|---|---|

## Stimuli: Set 2 Number 6 - Early / Late, R2, 0.7 Scaled Late

| Hall Size | | | Source Location | | | Receiver Location | | | Units |
|---|---|---|---|---|---|---|---|---|---|
| Length (x) | Height (y) | Width (z) | X | Y | Z | X | Y | Z | |
| 128.0 | 60.0 | 48.8 | 108.0 | 30.0 | 8.0 | 18.0 | 10.0 | 4.0 | Feet |
| 39.0 | 18.3 | 14.9 | 32.9 | 9.1 | 2.4 | 5.5 | 3.0 | 1.2 | Meters |

| Surface | Absorption Coefficient (alpha) - Octave Bands (Hz) | | | | | | | |
|---|---|---|---|---|---|---|---|---|
| | 63 | 125 | 250 | 500 | 1000 | 2000 | 4000 | 8000 |
| Floor | 0.240 | 0.336 | 0.408 | 0.474 | 0.498 | 0.516 | 0.516 | 0.516 |
| Front Wall | 0.050 | 0.020 | 0.020 | 0.030 | 0.040 | 0.040 | 0.030 | 0.030 |
| Left Wall | 0.050 | 0.020 | 0.020 | 0.030 | 0.040 | 0.040 | 0.030 | 0.030 |
| Right Wall | 0.050 | 0.020 | 0.020 | 0.030 | 0.040 | 0.040 | 0.030 | 0.030 |
| Back Wall | 0.050 | 0.020 | 0.020 | 0.030 | 0.040 | 0.040 | 0.030 | 0.030 |
| Ceiling | 0.050 | 0.020 | 0.020 | 0.030 | 0.040 | 0.040 | 0.030 | 0.030 |

| Surface | Scattering Coefficient (alpha) - Octave Bands (Hz) | | | | | | | |
|---|---|---|---|---|---|---|---|---|
| | 63 | 125 | 250 | 500 | 1000 | 2000 | 4000 | 8000 |
| Floor | 0.02 | 0.05 | 0.30 | 0.72 | 0.88 | 0.90 | 0.92 | 0.93 |
| Front Wall | 0.01 | 0.01 | 0.03 | 0.04 | 0.10 | 0.20 | 0.25 | 0.30 |
| Left Wall | 0.01 | 0.01 | 0.03 | 0.04 | 0.10 | 0.20 | 0.25 | 0.30 |
| Right Wall | 0.01 | 0.01 | 0.03 | 0.04 | 0.10 | 0.20 | 0.25 | 0.30 |
| Back Wall | 0.01 | 0.01 | 0.03 | 0.04 | 0.10 | 0.20 | 0.25 | 0.30 |
| Ceiling | 0.01 | 0.01 | 0.03 | 0.04 | 0.10 | 0.20 | 0.25 | 0.30 |

**Directional Weights**

| Direction | Weight Value | Direction | Weight Value | Direction | Weight Value |
|---|---|---|---|---|---|
| Omni | 100 | Left | 0 | Front Bottom | 0 |
| Front | 0 | Front Left | 0 | Right Bottom | 0 |
| Front Right | 0 | Front Top | 0 | Back Bottom | 0 |
| Right | 0 | Right Top | 0 | Left Bottom | 0 |
| Back Right | 0 | Back Top | 0 | Bottom | 0 |
| Back | 0 | Left Top | 0 | | |
| Back Left | 0 | Top | 0 | | |

| **Sample Rate:** | 44100 Hz | **IR Length:** | 5 sec. | **Image Source Order:** | 3 |
|---|---|---|---|---|---|

## Stimuli: Set 2 Number 7 - Early / Late, R2, 1.0 Scaled Late

| Hall Size | | | Source Location | | | Receiver Location | | | Units |
|---|---|---|---|---|---|---|---|---|---|
| Length (x) | Height (y) | Width (z) | X | Y | Z | X | Y | Z | |
| 128.0 | 60.0 | 48.8 | 108.0 | 30.0 | 8.0 | 18.0 | 10.0 | 4.0 | Feet |
| 39.0 | 18.3 | 14.9 | 32.9 | 9.1 | 2.4 | 5.5 | 3.0 | 1.2 | Meters |

| Surface | Absorption Coefficient (alpha) - Octave Bands (Hz) | | | | | | | |
|---|---|---|---|---|---|---|---|---|
| | 63 | 125 | 250 | 500 | 1000 | 2000 | 4000 | 8000 |
| Floor | 0.240 | 0.336 | 0.408 | 0.474 | 0.498 | 0.516 | 0.516 | 0.516 |
| Front Wall | 0.050 | 0.020 | 0.020 | 0.030 | 0.040 | 0.040 | 0.030 | 0.030 |
| Left Wall | 0.050 | 0.020 | 0.020 | 0.030 | 0.040 | 0.040 | 0.030 | 0.030 |
| Right Wall | 0.050 | 0.020 | 0.020 | 0.030 | 0.040 | 0.040 | 0.030 | 0.030 |
| Back Wall | 0.050 | 0.020 | 0.020 | 0.030 | 0.040 | 0.040 | 0.030 | 0.030 |
| Ceiling | 0.050 | 0.020 | 0.020 | 0.030 | 0.040 | 0.040 | 0.030 | 0.030 |

| Surface | Scattering Coefficient (alpha) - Octave Bands (Hz) | | | | | | | |
|---|---|---|---|---|---|---|---|---|
| | 63 | 125 | 250 | 500 | 1000 | 2000 | 4000 | 8000 |
| Floor | 0.02 | 0.05 | 0.30 | 0.72 | 0.88 | 0.90 | 0.92 | 0.93 |
| Front Wall | 0.01 | 0.01 | 0.03 | 0.04 | 0.10 | 0.20 | 0.25 | 0.30 |
| Left Wall | 0.01 | 0.01 | 0.03 | 0.04 | 0.10 | 0.20 | 0.25 | 0.30 |
| Right Wall | 0.01 | 0.01 | 0.03 | 0.04 | 0.10 | 0.20 | 0.25 | 0.30 |
| Back Wall | 0.01 | 0.01 | 0.03 | 0.04 | 0.10 | 0.20 | 0.25 | 0.30 |
| Ceiling | 0.01 | 0.01 | 0.03 | 0.04 | 0.10 | 0.20 | 0.25 | 0.30 |

**Directional Weights**

| Direction | Weight Value | Direction | Weight Value | Direction | Weight Value |
|---|---|---|---|---|---|
| Omni | 100 | Left | 0 | Front Bottom | 0 |
| Front | 0 | Front Left | 0 | Right Bottom | 0 |
| Front Right | 0 | Front Top | 0 | Back Bottom | 0 |
| Right | 0 | Right Top | 0 | Left Bottom | 0 |
| Back Right | 0 | Back Top | 0 | Bottom | 0 |
| Back | 0 | Left Top | 0 | | |
| Back Left | 0 | Top | 0 | | |

| **Sample Rate:** | 44100 Hz | **IR Length:** | 5 sec. | **Image Source Order:** | 3 |
|---|---|---|---|---|---|

## Stimuli: Set 2 Number 8 - Early / Late, R2, 1.5 Scaled Late

| Hall Size | | | Source Location | | | Receiver Location | | | Units |
|---|---|---|---|---|---|---|---|---|---|
| Length (x) | Height (y) | Width (z) | X | Y | Z | X | Y | Z | |
| 128.0 | 60.0 | 48.8 | 108.0 | 30.0 | 8.0 | 18.0 | 10.0 | 4.0 | Feet |
| 39.0 | 18.3 | 14.9 | 32.9 | 9.1 | 2.4 | 5.5 | 3.0 | 1.2 | Meters |

| Surface | Absorption Coefficient (alpha) - Octave Bands (Hz) | | | | | | | |
|---|---|---|---|---|---|---|---|---|
| | 63 | 125 | 250 | 500 | 1000 | 2000 | 4000 | 8000 |
| Floor | 0.240 | 0.336 | 0.408 | 0.474 | 0.498 | 0.516 | 0.516 | 0.516 |
| Front Wall | 0.050 | 0.020 | 0.020 | 0.030 | 0.040 | 0.040 | 0.030 | 0.030 |
| Left Wall | 0.050 | 0.020 | 0.020 | 0.030 | 0.040 | 0.040 | 0.030 | 0.030 |
| Right Wall | 0.050 | 0.020 | 0.020 | 0.030 | 0.040 | 0.040 | 0.030 | 0.030 |
| Back Wall | 0.050 | 0.020 | 0.020 | 0.030 | 0.040 | 0.040 | 0.030 | 0.030 |
| Ceiling | 0.050 | 0.020 | 0.020 | 0.030 | 0.040 | 0.040 | 0.030 | 0.030 |

| Surface | Scattering Coefficient (alpha) - Octave Bands (Hz) | | | | | | | |
|---|---|---|---|---|---|---|---|---|
| | 63 | 125 | 250 | 500 | 1000 | 2000 | 4000 | 8000 |
| Floor | 0.02 | 0.05 | 0.30 | 0.72 | 0.88 | 0.90 | 0.92 | 0.93 |
| Front Wall | 0.01 | 0.01 | 0.03 | 0.04 | 0.10 | 0.20 | 0.25 | 0.30 |
| Left Wall | 0.01 | 0.01 | 0.03 | 0.04 | 0.10 | 0.20 | 0.25 | 0.30 |
| Right Wall | 0.01 | 0.01 | 0.03 | 0.04 | 0.10 | 0.20 | 0.25 | 0.30 |
| Back Wall | 0.01 | 0.01 | 0.03 | 0.04 | 0.10 | 0.20 | 0.25 | 0.30 |
| Ceiling | 0.01 | 0.01 | 0.03 | 0.04 | 0.10 | 0.20 | 0.25 | 0.30 |

**Directional Weights**

| Direction | Weight Value | Direction | Weight Value | Direction | Weight Value |
|---|---|---|---|---|---|
| Omni | 100 | Left | 0 | Front Bottom | 0 |
| Front | 0 | Front Left | 0 | Right Bottom | 0 |
| Front Right | 0 | Front Top | 0 | Back Bottom | 0 |
| Right | 0 | Right Top | 0 | Left Bottom | 0 |
| Back Right | 0 | Back Top | 0 | Bottom | 0 |
| Back | 0 | Left Top | 0 | | |
| Back Left | 0 | Top | 0 | | |

| **Sample Rate:** | 44100 Hz | **IR Length:** | 5 sec. | **Image Source Order:** | 3 |
|---|---|---|---|---|---|

## Stimuli: Set 3 & 4 Number 1 - 80% BSH 1.4 RT (Level EQ & No Level EQ)

| Hall Size | | | Source Location | | | Receiver Location | | | Units |
|---|---|---|---|---|---|---|---|---|---|
| Length (x) | Height (y) | Width (z) | X | Y | Z | X | Y | Z | |
| 128.0 | 60.0 | 48.8 | 108.0 | 30.0 | 8.0 | 48.0 | 26.0 | 4.0 | Feet |
| 39.0 | 18.3 | 14.9 | 32.9 | 9.1 | 2.4 | 14.6 | 7.9 | 1.2 | Meters |

| Surface | Absorption Coefficient (alpha) - Octave Bands (Hz) | | | | | | | |
|---|---|---|---|---|---|---|---|---|
| | 63 | 125 | 250 | 500 | 1000 | 2000 | 4000 | 8000 |
| Floor | 0.240 | 0.336 | 0.408 | 0.474 | 0.498 | 0.516 | 0.516 | 0.516 |
| Front Wall | 0.050 | 0.020 | 0.020 | 0.030 | 0.040 | 0.040 | 0.030 | 0.030 |
| Left Wall | 0.050 | 0.020 | 0.020 | 0.030 | 0.040 | 0.040 | 0.030 | 0.030 |
| Right Wall | 0.050 | 0.020 | 0.020 | 0.030 | 0.040 | 0.040 | 0.030 | 0.030 |
| Back Wall | 0.050 | 0.020 | 0.020 | 0.030 | 0.040 | 0.040 | 0.030 | 0.030 |
| Ceiling | 0.050 | 0.020 | 0.020 | 0.030 | 0.040 | 0.040 | 0.030 | 0.030 |

| Surface | Scattering Coefficient (alpha) - Octave Bands (Hz) | | | | | | | |
|---|---|---|---|---|---|---|---|---|
| | 63 | 125 | 250 | 500 | 1000 | 2000 | 4000 | 8000 |
| Floor | 0.02 | 0.05 | 0.30 | 0.72 | 0.88 | 0.90 | 0.92 | 0.93 |
| Front Wall | 0.01 | 0.01 | 0.03 | 0.04 | 0.10 | 0.20 | 0.25 | 0.30 |
| Left Wall | 0.01 | 0.01 | 0.03 | 0.04 | 0.10 | 0.20 | 0.25 | 0.30 |
| Right Wall | 0.01 | 0.01 | 0.03 | 0.04 | 0.10 | 0.20 | 0.25 | 0.30 |
| Back Wall | 0.01 | 0.01 | 0.03 | 0.04 | 0.10 | 0.20 | 0.25 | 0.30 |
| Ceiling | 0.01 | 0.01 | 0.03 | 0.04 | 0.10 | 0.20 | 0.25 | 0.30 |

**Directional Weights**

| Direction | Weight Value | Direction | Weight Value | Direction | Weight Value |
|---|---|---|---|---|---|
| Omni | 100 | Left | 0 | Front Bottom | 0 |
| Front | 0 | Front Left | 0 | Right Bottom | 0 |
| Front Right | 0 | Front Top | 0 | Back Bottom | 0 |
| Right | 0 | Right Top | 0 | Left Bottom | 0 |
| Back Right | 0 | Back Top | 0 | Bottom | 0 |
| Back | 0 | Left Top | 0 | | |
| Back Left | 0 | Top | 0 | | |

| **Sample Rate:** | 44100 Hz | **IR Length:** | 5 sec. | **Image Source Order:** | 3 |
|---|---|---|---|---|---|

## Stimuli: Set 3 & 4 Number 2 - 80% BSH 2.2 RT (Level EQ & No Level EQ)

| Hall Size | | | Source Location | | | Receiver Location | | | Units |
|---|---|---|---|---|---|---|---|---|---|
| Length (x) | Height (y) | Width (z) | X | Y | Z | X | Y | Z | |
| 128.0 | 60.0 | 48.8 | 108.0 | 30.0 | 8.0 | 48.0 | 26.0 | 4.0 | Feet |
| 39.0 | 18.3 | 14.9 | 32.9 | 9.1 | 2.4 | 14.6 | 7.9 | 1.2 | Meters |

| Surface | Absorption Coefficient (alpha) - Octave Bands (Hz) | | | | | | | |
|---|---|---|---|---|---|---|---|---|
| | 63 | 125 | 250 | 500 | 1000 | 2000 | 4000 | 8000 |
| Floor | 0.139 | 0.195 | 0.237 | 0.275 | 0.289 | 0.299 | 0.299 | 0.299 |
| Front Wall | 0.029 | 0.012 | 0.012 | 0.017 | 0.023 | 0.023 | 0.017 | 0.017 |
| Left Wall | 0.029 | 0.012 | 0.012 | 0.017 | 0.023 | 0.023 | 0.017 | 0.017 |
| Right Wall | 0.029 | 0.012 | 0.012 | 0.017 | 0.023 | 0.023 | 0.017 | 0.017 |
| Back Wall | 0.029 | 0.012 | 0.012 | 0.017 | 0.023 | 0.023 | 0.017 | 0.017 |
| Ceiling | 0.029 | 0.012 | 0.012 | 0.017 | 0.023 | 0.023 | 0.017 | 0.017 |

| Surface | Scattering Coefficient (alpha) - Octave Bands (Hz) | | | | | | | |
|---|---|---|---|---|---|---|---|---|
| | 63 | 125 | 250 | 500 | 1000 | 2000 | 4000 | 8000 |
| Floor | 0.02 | 0.05 | 0.30 | 0.72 | 0.88 | 0.90 | 0.92 | 0.93 |
| Front Wall | 0.01 | 0.01 | 0.03 | 0.04 | 0.10 | 0.20 | 0.25 | 0.30 |
| Left Wall | 0.01 | 0.01 | 0.03 | 0.04 | 0.10 | 0.20 | 0.25 | 0.30 |
| Right Wall | 0.01 | 0.01 | 0.03 | 0.04 | 0.10 | 0.20 | 0.25 | 0.30 |
| Back Wall | 0.01 | 0.01 | 0.03 | 0.04 | 0.10 | 0.20 | 0.25 | 0.30 |
| Ceiling | 0.01 | 0.01 | 0.03 | 0.04 | 0.10 | 0.20 | 0.25 | 0.30 |

**Directional Weights**

| Direction | Weight Value | Direction | Weight Value | Direction | Weight Value |
|---|---|---|---|---|---|
| Omni | 100 | Left | 0 | Front Bottom | 0 |
| Front | 0 | Front Left | 0 | Right Bottom | 0 |
| Front Right | 0 | Front Top | 0 | Back Bottom | 0 |
| Right | 0 | Right Top | 0 | Left Bottom | 0 |
| Back Right | 0 | Back Top | 0 | Bottom | 0 |
| Back | 0 | Left Top | 0 | | |
| Back Left | 0 | Top | 0 | | |

| **Sample Rate:** | 44100 Hz | **IR Length:** | 5 sec. | **Image Source Order:** | 3 |
|---|---|---|---|---|---|

## Stimuli: Set 3 & 4 Number 3 - 100% BSH 1.4 RT (Level EQ & No Level EQ)

| Hall Size | | | Source Location | | | Receiver Location | | | Units |
|---|---|---|---|---|---|---|---|---|---|
| Length (x) | Height (y) | Width (z) | X | Y | Z | X | Y | Z | |
| 160.0 | 75.0 | 61.0 | 140.0 | 37.5 | 8.0 | 80.0 | 33.5 | 4.0 | Feet |
| 48.8 | 22.9 | 18.6 | 42.7 | 11.4 | 2.4 | 24.4 | 10.2 | 1.2 | Meters |

| Surface | Absorption Coefficient (alpha) - Octave Bands (Hz) | | | | | | | |
|---|---|---|---|---|---|---|---|---|
| | 63 | 125 | 250 | 500 | 1000 | 2000 | 4000 | 8000 |
| Floor | 0.324 | 0.454 | 0.551 | 0.640 | 0.672 | 0.697 | 0.697 | 0.697 |
| Front Wall | 0.068 | 0.027 | 0.027 | 0.041 | 0.054 | 0.054 | 0.041 | 0.041 |
| Left Wall | 0.068 | 0.027 | 0.027 | 0.041 | 0.054 | 0.054 | 0.041 | 0.041 |
| Right Wall | 0.068 | 0.027 | 0.027 | 0.041 | 0.054 | 0.054 | 0.041 | 0.041 |
| Back Wall | 0.068 | 0.027 | 0.027 | 0.041 | 0.054 | 0.054 | 0.041 | 0.041 |
| Ceiling | 0.068 | 0.027 | 0.027 | 0.041 | 0.054 | 0.054 | 0.041 | 0.041 |

| Surface | Scattering Coefficient (alpha) - Octave Bands (Hz) | | | | | | | |
|---|---|---|---|---|---|---|---|---|
| | 63 | 125 | 250 | 500 | 1000 | 2000 | 4000 | 8000 |
| Floor | 0.02 | 0.05 | 0.30 | 0.72 | 0.88 | 0.90 | 0.92 | 0.93 |
| Front Wall | 0.01 | 0.01 | 0.03 | 0.04 | 0.10 | 0.20 | 0.25 | 0.30 |
| Left Wall | 0.01 | 0.01 | 0.03 | 0.04 | 0.10 | 0.20 | 0.25 | 0.30 |
| Right Wall | 0.01 | 0.01 | 0.03 | 0.04 | 0.10 | 0.20 | 0.25 | 0.30 |
| Back Wall | 0.01 | 0.01 | 0.03 | 0.04 | 0.10 | 0.20 | 0.25 | 0.30 |
| Ceiling | 0.01 | 0.01 | 0.03 | 0.04 | 0.10 | 0.20 | 0.25 | 0.30 |

**Directional Weights**

| Direction | Weight Value | Direction | Weight Value | Direction | Weight Value |
|---|---|---|---|---|---|
| Omni | 100 | Left | 0 | Front Bottom | 0 |
| Front | 0 | Front Left | 0 | Right Bottom | 0 |
| Front Right | 0 | Front Top | 0 | Back Bottom | 0 |
| Right | 0 | Right Top | 0 | Left Bottom | 0 |
| Back Right | 0 | Back Top | 0 | Bottom | 0 |
| Back | 0 | Left Top | 0 | | |
| Back Left | 0 | Top | 0 | | |

| **Sample Rate:** | 44100 Hz | **IR Length:** | 5 sec. | **Image Source Order:** | 3 |
|---|---|---|---|---|---|

## Stimuli: Set 3 & 4 Number 4 - 100% BSH 2.2 RT (Level EQ & No Level EQ)

| Hall Size | | | Source Location | | | Receiver Location | | | Units |
|---|---|---|---|---|---|---|---|---|---|
| Length (x) | Height (y) | Width (z) | X | Y | Z | X | Y | Z | |
| 160.0 | 75.0 | 61.0 | 140.0 | 37.5 | 8.0 | 80.0 | 33.5 | 4.0 | Feet |
| 48.8 | 22.9 | 18.6 | 42.7 | 11.4 | 2.4 | 24.4 | 10.2 | 1.2 | Meters |

| Surface | Absorption Coefficient (alpha) - Octave Bands (Hz) | | | | | | | |
|---|---|---|---|---|---|---|---|---|
| | 63 | 125 | 250 | 500 | 1000 | 2000 | 4000 | 8000 |
| Floor | 0.192 | 0.269 | 0.326 | 0.379 | 0.398 | 0.413 | 0.413 | 0.413 |
| Front Wall | 0.040 | 0.016 | 0.016 | 0.024 | 0.032 | 0.032 | 0.024 | 0.024 |
| Left Wall | 0.040 | 0.016 | 0.016 | 0.024 | 0.032 | 0.032 | 0.024 | 0.024 |
| Right Wall | 0.040 | 0.016 | 0.016 | 0.024 | 0.032 | 0.032 | 0.024 | 0.024 |
| Back Wall | 0.040 | 0.016 | 0.016 | 0.024 | 0.032 | 0.032 | 0.024 | 0.024 |
| Ceiling | 0.040 | 0.016 | 0.016 | 0.024 | 0.032 | 0.032 | 0.024 | 0.024 |

| Surface | Scattering Coefficient (alpha) - Octave Bands (Hz) | | | | | | | |
|---|---|---|---|---|---|---|---|---|
| | 63 | 125 | 250 | 500 | 1000 | 2000 | 4000 | 8000 |
| Floor | 0.02 | 0.05 | 0.30 | 0.72 | 0.88 | 0.90 | 0.92 | 0.93 |
| Front Wall | 0.01 | 0.01 | 0.03 | 0.04 | 0.10 | 0.20 | 0.25 | 0.30 |
| Left Wall | 0.01 | 0.01 | 0.03 | 0.04 | 0.10 | 0.20 | 0.25 | 0.30 |
| Right Wall | 0.01 | 0.01 | 0.03 | 0.04 | 0.10 | 0.20 | 0.25 | 0.30 |
| Back Wall | 0.01 | 0.01 | 0.03 | 0.04 | 0.10 | 0.20 | 0.25 | 0.30 |
| Ceiling | 0.01 | 0.01 | 0.03 | 0.04 | 0.10 | 0.20 | 0.25 | 0.30 |

**Directional Weights**

| Direction | Weight Value | Direction | Weight Value | Direction | Weight Value |
|---|---|---|---|---|---|
| Omni | 100 | Left | 0 | Front Bottom | 0 |
| Front | 0 | Front Left | 0 | Right Bottom | 0 |
| Front Right | 0 | Front Top | 0 | Back Bottom | 0 |
| Right | 0 | Right Top | 0 | Left Bottom | 0 |
| Back Right | 0 | Back Top | 0 | Bottom | 0 |
| Back | 0 | Left Top | 0 | | |
| Back Left | 0 | Top | 0 | | |

| **Sample Rate:** | 44100 Hz | **IR Length:** | 5 sec. | **Image Source Order:** | 3 |
|---|---|---|---|---|---|

## Stimuli: Set 3 & 4 Number 5 - 110% BSH 1.4 RT (Level EQ & No Level EQ)

| Hall Size | | | Source Location | | | Receiver Location | | | Units |
|---|---|---|---|---|---|---|---|---|---|
| Length (x) | Height (y) | Width (z) | X | Y | Z | X | Y | Z | |
| 176.0 | 82.5 | 67.1 | 156.0 | 41.3 | 8.0 | 96.0 | 37.3 | 4.0 | Feet |
| 53.7 | 25.2 | 20.5 | 47.6 | 12.6 | 2.4 | 29.3 | 11.4 | 1.2 | Meters |

| Surface | Absorption Coefficient (alpha) - Octave Bands (Hz) | | | | | | | |
|---|---|---|---|---|---|---|---|---|
| | 63 | 125 | 250 | 500 | 1000 | 2000 | 4000 | 8000 |
| Floor | 0.367 | 0.514 | 0.624 | 0.725 | 0.762 | 0.789 | 0.789 | 0.789 |
| Front Wall | 0.077 | 0.031 | 0.031 | 0.046 | 0.061 | 0.061 | 0.046 | 0.046 |
| Left Wall | 0.077 | 0.031 | 0.031 | 0.046 | 0.061 | 0.061 | 0.046 | 0.046 |
| Right Wall | 0.077 | 0.031 | 0.031 | 0.046 | 0.061 | 0.061 | 0.046 | 0.046 |
| Back Wall | 0.077 | 0.031 | 0.031 | 0.046 | 0.061 | 0.061 | 0.046 | 0.046 |
| Ceiling | 0.077 | 0.031 | 0.031 | 0.046 | 0.061 | 0.061 | 0.046 | 0.046 |

| Surface | Scattering Coefficient (alpha) - Octave Bands (Hz) | | | | | | | |
|---|---|---|---|---|---|---|---|---|
| | 63 | 125 | 250 | 500 | 1000 | 2000 | 4000 | 8000 |
| Floor | 0.02 | 0.05 | 0.30 | 0.72 | 0.88 | 0.90 | 0.92 | 0.93 |
| Front Wall | 0.01 | 0.01 | 0.03 | 0.04 | 0.10 | 0.20 | 0.25 | 0.30 |
| Left Wall | 0.01 | 0.01 | 0.03 | 0.04 | 0.10 | 0.20 | 0.25 | 0.30 |
| Right Wall | 0.01 | 0.01 | 0.03 | 0.04 | 0.10 | 0.20 | 0.25 | 0.30 |
| Back Wall | 0.01 | 0.01 | 0.03 | 0.04 | 0.10 | 0.20 | 0.25 | 0.30 |
| Ceiling | 0.01 | 0.01 | 0.03 | 0.04 | 0.10 | 0.20 | 0.25 | 0.30 |

**Directional Weights**

| Direction | Weight Value | Direction | Weight Value | Direction | Weight Value |
|---|---|---|---|---|---|
| Omni | 100 | Left | 0 | Front Bottom | 0 |
| Front | 0 | Front Left | 0 | Right Bottom | 0 |
| Front Right | 0 | Front Top | 0 | Back Bottom | 0 |
| Right | 0 | Right Top | 0 | Left Bottom | 0 |
| Back Right | 0 | Back Top | 0 | Bottom | 0 |
| Back | 0 | Left Top | 0 | | |
| Back Left | 0 | Top | 0 | | |

| **Sample Rate:** | 44100 Hz | **IR Length:** | 5 sec. | **Image Source Order:** | 3 |
|---|---|---|---|---|---|

## Stimuli: Set 3 & 4 Number 6 - 110% BSH 2.2 RT (Level EQ & No Level EQ)

| Hall Size | | | Source Location | | | Receiver Location | | | Units |
|---|---|---|---|---|---|---|---|---|---|
| Length (x) | Height (y) | Width (z) | X | Y | Z | X | Y | Z | |
| 176.0 | 82.5 | 67.1 | 156.0 | 41.3 | 8.0 | 96.0 | 37.3 | 4.0 | Feet |
| 53.7 | 25.2 | 20.5 | 47.6 | 12.6 | 2.4 | 29.3 | 11.4 | 1.2 | Meters |

| Surface | Absorption Coefficient (alpha) - Octave Bands (Hz) | | | | | | | |
|---|---|---|---|---|---|---|---|---|
| | 63 | 125 | 250 | 500 | 1000 | 2000 | 4000 | 8000 |
| Floor | 0.238 | 0.333 | 0.386 | 0.405 | 0.448 | 0.464 | 0.464 | 0.464 |
| Front Wall | 0.050 | 0.020 | 0.019 | 0.026 | 0.036 | 0.036 | 0.027 | 0.027 |
| Left Wall | 0.050 | 0.020 | 0.019 | 0.026 | 0.036 | 0.036 | 0.027 | 0.027 |
| Right Wall | 0.050 | 0.020 | 0.019 | 0.026 | 0.036 | 0.036 | 0.027 | 0.027 |
| Back Wall | 0.050 | 0.020 | 0.019 | 0.026 | 0.036 | 0.036 | 0.027 | 0.027 |
| Ceiling | 0.050 | 0.020 | 0.019 | 0.026 | 0.036 | 0.036 | 0.027 | 0.027 |

| Surface | Scattering Coefficient (alpha) - Octave Bands (Hz) | | | | | | | |
|---|---|---|---|---|---|---|---|---|
| | 63 | 125 | 250 | 500 | 1000 | 2000 | 4000 | 8000 |
| Floor | 0.02 | 0.05 | 0.30 | 0.72 | 0.88 | 0.90 | 0.92 | 0.93 |
| Front Wall | 0.01 | 0.01 | 0.03 | 0.04 | 0.10 | 0.20 | 0.25 | 0.30 |
| Left Wall | 0.01 | 0.01 | 0.03 | 0.04 | 0.10 | 0.20 | 0.25 | 0.30 |
| Right Wall | 0.01 | 0.01 | 0.03 | 0.04 | 0.10 | 0.20 | 0.25 | 0.30 |
| Back Wall | 0.01 | 0.01 | 0.03 | 0.04 | 0.10 | 0.20 | 0.25 | 0.30 |
| Ceiling | 0.01 | 0.01 | 0.03 | 0.04 | 0.10 | 0.20 | 0.25 | 0.30 |

**Directional Weights**

| Direction | Weight Value | Direction | Weight Value | Direction | Weight Value |
|---|---|---|---|---|---|
| Omni | 100 | Left | 0 | Front Bottom | 0 |
| Front | 0 | Front Left | 0 | Right Bottom | 0 |
| Front Right | 0 | Front Top | 0 | Back Bottom | 0 |
| Right | 0 | Right Top | 0 | Left Bottom | 0 |
| Back Right | 0 | Back Top | 0 | Bottom | 0 |
| Back | 0 | Left Top | 0 | | |
| Back Left | 0 | Top | 0 | | |

| **Sample Rate:** | 44100 Hz | **IR Length:** | 5 sec. | **Image Source Order:** | 3 |
|---|---|---|---|---|---|

## Stimuli: Set 3 & 4 Number 7 - 120% BSH 1.4 RT (Level EQ & No Level EQ)

| Hall Size | | | Source Location | | | Receiver Location | | | Units |
|---|---|---|---|---|---|---|---|---|---|
| Length (x) | Height (y) | Width (z) | X | Y | Z | X | Y | Z | |
| 192.0 | 90.0 | 73.2 | 172.0 | 45.0 | 8.0 | 112.0 | 41.0 | 4.0 | Feet |
| 58.5 | 27.4 | 22.3 | 52.4 | 13.7 | 2.4 | 34.1 | 12.5 | 1.2 | Meters |

| Surface | Absorption Coefficient (alpha) - Octave Bands (Hz) | | | | | | | |
|---|---|---|---|---|---|---|---|---|
| | 63 | 125 | 250 | 500 | 1000 | 2000 | 4000 | 8000 |
| Floor | 0.449 | 0.628 | 0.728 | 0.766 | 0.847 | 0.877 | 0.877 | 0.877 |
| Front Wall | 0.094 | 0.037 | 0.036 | 0.048 | 0.068 | 0.068 | 0.051 | 0.051 |
| Left Wall | 0.094 | 0.037 | 0.036 | 0.048 | 0.068 | 0.068 | 0.051 | 0.051 |
| Right Wall | 0.094 | 0.037 | 0.036 | 0.048 | 0.068 | 0.068 | 0.051 | 0.051 |
| Back Wall | 0.094 | 0.037 | 0.036 | 0.048 | 0.068 | 0.068 | 0.051 | 0.051 |
| Ceiling | 0.094 | 0.037 | 0.036 | 0.048 | 0.068 | 0.068 | 0.051 | 0.051 |

| Surface | Scattering Coefficient (alpha) - Octave Bands (Hz) | | | | | | | |
|---|---|---|---|---|---|---|---|---|
| | 63 | 125 | 250 | 500 | 1000 | 2000 | 4000 | 8000 |
| Floor | 0.02 | 0.05 | 0.30 | 0.72 | 0.88 | 0.90 | 0.92 | 0.93 |
| Front Wall | 0.01 | 0.01 | 0.03 | 0.04 | 0.10 | 0.20 | 0.25 | 0.30 |
| Left Wall | 0.01 | 0.01 | 0.03 | 0.04 | 0.10 | 0.20 | 0.25 | 0.30 |
| Right Wall | 0.01 | 0.01 | 0.03 | 0.04 | 0.10 | 0.20 | 0.25 | 0.30 |
| Back Wall | 0.01 | 0.01 | 0.03 | 0.04 | 0.10 | 0.20 | 0.25 | 0.30 |
| Ceiling | 0.01 | 0.01 | 0.03 | 0.04 | 0.10 | 0.20 | 0.25 | 0.30 |

**Directional Weights**

| Direction | Weight Value | Direction | Weight Value | Direction | Weight Value |
|---|---|---|---|---|---|
| Omni | 100 | Left | 0 | Front Bottom | 0 |
| Front | 0 | Front Left | 0 | Right Bottom | 0 |
| Front Right | 0 | Front Top | 0 | Back Bottom | 0 |
| Right | 0 | Right Top | 0 | Left Bottom | 0 |
| Back Right | 0 | Back Top | 0 | Bottom | 0 |
| Back | 0 | Left Top | 0 | | |
| Back Left | 0 | Top | 0 | | |

| **Sample Rate:** | 44100 Hz | **IR Length:** | 5 sec. | **Image Source Order:** | 3 |
|---|---|---|---|---|---|

## Stimuli: Set 3 & 4 Number 8 - 120% BSH 2.2 RT (Level EQ & No Level EQ)

| Hall Size | | | Source Location | | | Receiver Location | | | Units |
|---|---|---|---|---|---|---|---|---|---|
| Length (x) | Height (y) | Width (z) | X | Y | Z | X | Y | Z | |
| 192.0 | 90.0 | 73.2 | 172.0 | 45.0 | 8.0 | 112.0 | 41.0 | 4.0 | Feet |
| 58.5 | 27.4 | 22.3 | 52.4 | 13.7 | 2.4 | 34.1 | 12.5 | 1.2 | Meters |

| Surface | Absorption Coefficient (alpha) - Octave Bands (Hz) | | | | | | | |
|---|---|---|---|---|---|---|---|---|
| | 63 | 125 | 250 | 500 | 1000 | 2000 | 4000 | 8000 |
| Floor | 0.264 | 0.370 | 0.428 | 0.450 | 0.498 | 0.516 | 0.516 | 0.516 |
| Front Wall | 0.055 | 0.022 | 0.021 | 0.029 | 0.040 | 0.040 | 0.030 | 0.030 |
| Left Wall | 0.055 | 0.022 | 0.021 | 0.029 | 0.040 | 0.040 | 0.030 | 0.030 |
| Right Wall | 0.055 | 0.022 | 0.021 | 0.029 | 0.040 | 0.040 | 0.030 | 0.030 |
| Back Wall | 0.055 | 0.022 | 0.021 | 0.029 | 0.040 | 0.040 | 0.030 | 0.030 |
| Ceiling | 0.055 | 0.022 | 0.021 | 0.029 | 0.040 | 0.040 | 0.030 | 0.030 |

| Surface | Scattering Coefficient (alpha) - Octave Bands (Hz) | | | | | | | |
|---|---|---|---|---|---|---|---|---|
| | 63 | 125 | 250 | 500 | 1000 | 2000 | 4000 | 8000 |
| Floor | 0.02 | 0.05 | 0.30 | 0.72 | 0.88 | 0.90 | 0.92 | 0.93 |
| Front Wall | 0.01 | 0.01 | 0.03 | 0.04 | 0.10 | 0.20 | 0.25 | 0.30 |
| Left Wall | 0.01 | 0.01 | 0.03 | 0.04 | 0.10 | 0.20 | 0.25 | 0.30 |
| Right Wall | 0.01 | 0.01 | 0.03 | 0.04 | 0.10 | 0.20 | 0.25 | 0.30 |
| Back Wall | 0.01 | 0.01 | 0.03 | 0.04 | 0.10 | 0.20 | 0.25 | 0.30 |
| Ceiling | 0.01 | 0.01 | 0.03 | 0.04 | 0.10 | 0.20 | 0.25 | 0.30 |

**Directional Weights**

| Direction | Weight Value | Direction | Weight Value | Direction | Weight Value |
|---|---|---|---|---|---|
| Omni | 100 | Left | 0 | Front Bottom | 0 |
| Front | 0 | Front Left | 0 | Right Bottom | 0 |
| Front Right | 0 | Front Top | 0 | Back Bottom | 0 |
| Right | 0 | Right Top | 0 | Left Bottom | 0 |
| Back Right | 0 | Back Top | 0 | Bottom | 0 |
| Back | 0 | Left Top | 0 | | |
| Back Left | 0 | Top | 0 | | |

| **Sample Rate:** | 44100 Hz | **IR Length:** | 5 sec. | **Image Source Order:** | 3 |
|---|---|---|---|---|---|

# Appendix F: Loudspeaker Equalization Plots

This appendix shows plots comparing the frequency response of the loudspeakers with and without equalization applied. The measurements were made for each loudspeaker placed within the Hammond, room 30, anechoic chamber, with all 30 loudspeakers in place. The equalization was based upon individual loudspeaker responses measured in the Garfield Thomas Water Tunnel building anechoic chamber which has a lower free field cutoff frequency (3' (0.91 m) fiberglass wedges). The equalization was performed to achieve a flat response down to 60 Hz. The frequency responses have been centered around 0 dB to allow comparison between both cases.

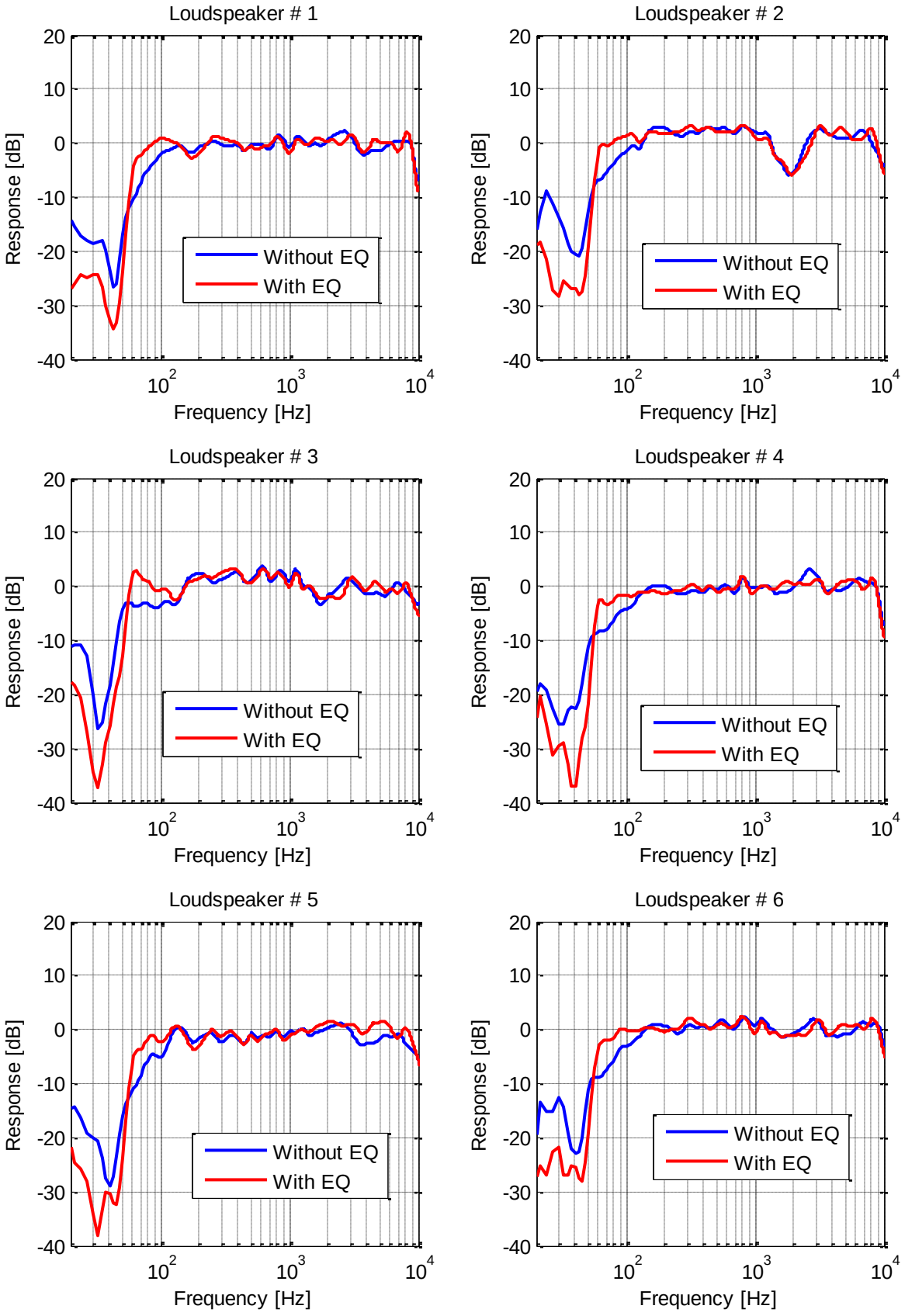
Loudspeaker # 1
Loudspeaker # 2
Loudspeaker # 3
Loudspeaker # 4
Loudspeaker # 5
Loudspeaker # 6
Response [dB]
Frequency [Hz]
Without EQ
With EQ
20
10
0
-10
-20
-30
-40
$10^2$
$10^3$
$10^4$

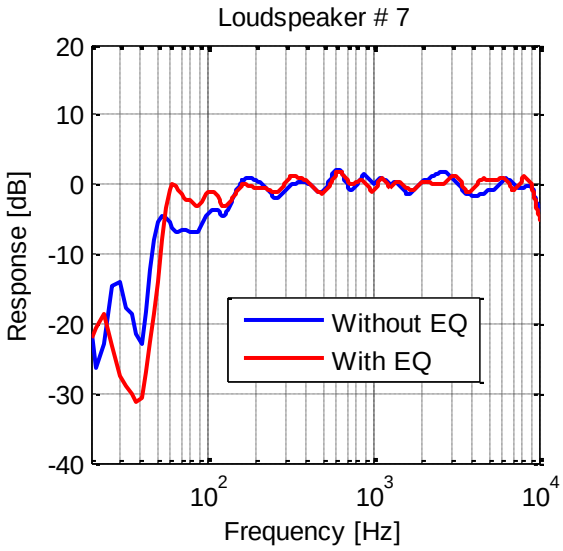
Loudspeaker # 7
Response [dB]
Frequency [Hz]
Without EQ
With EQ

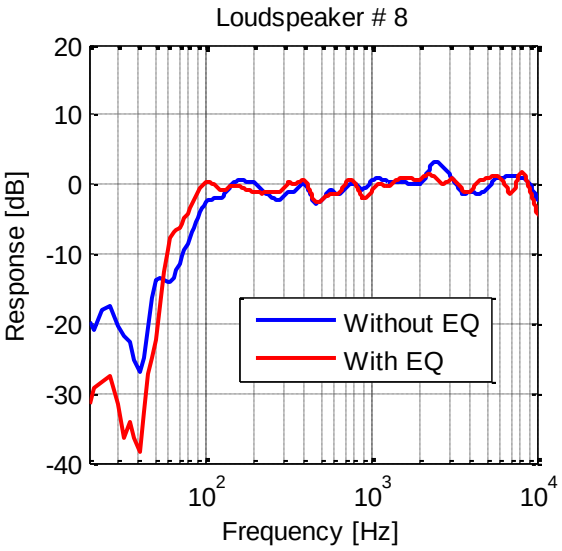
Loudspeaker # 8
Response [dB]
Frequency [Hz]
Without EQ
With EQ

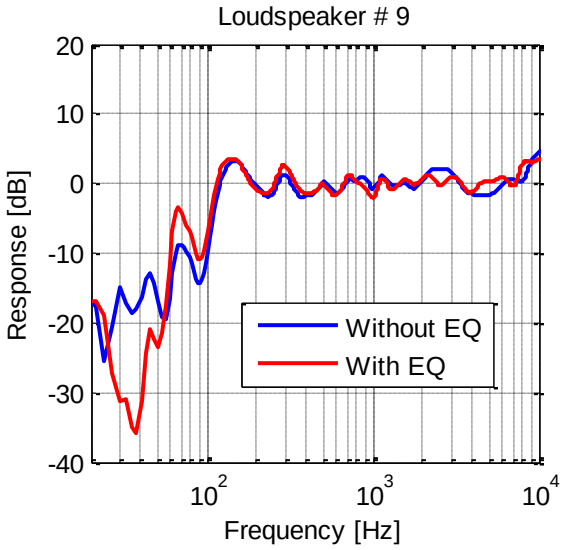
Loudspeaker # 9
Response [dB]
Frequency [Hz]
Without EQ
With EQ

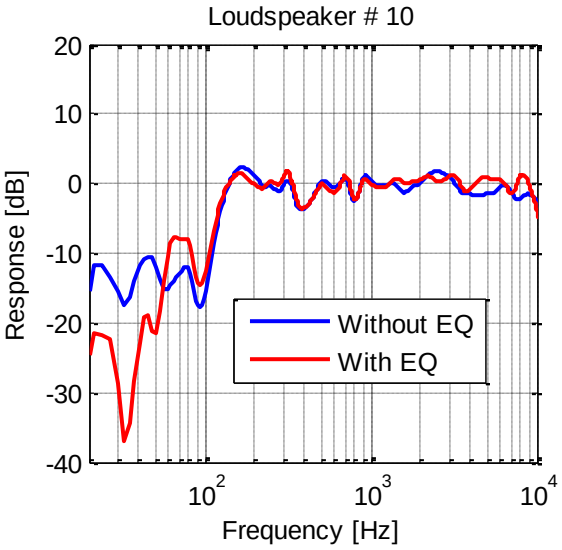
Loudspeaker # 10
Response [dB]
Frequency [Hz]
Without EQ
With EQ

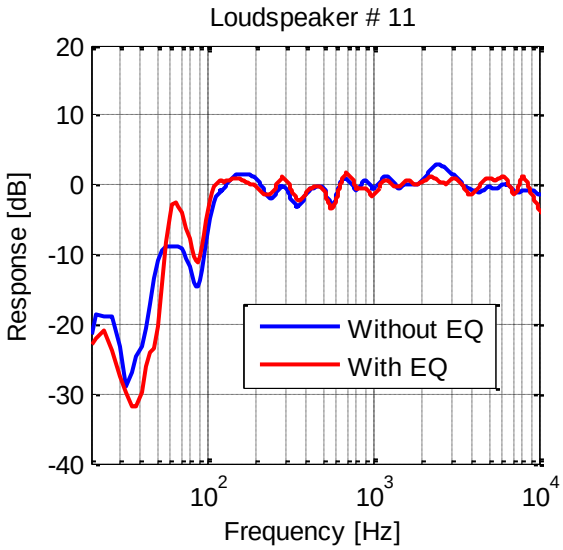
Loudspeaker # 11
Response [dB]
Frequency [Hz]
Without EQ
With EQ

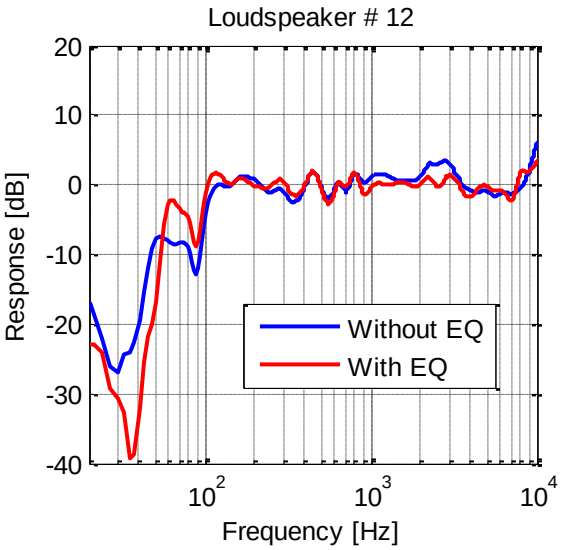
Loudspeaker # 12
Response [dB]
Frequency [Hz]
Without EQ
With EQ

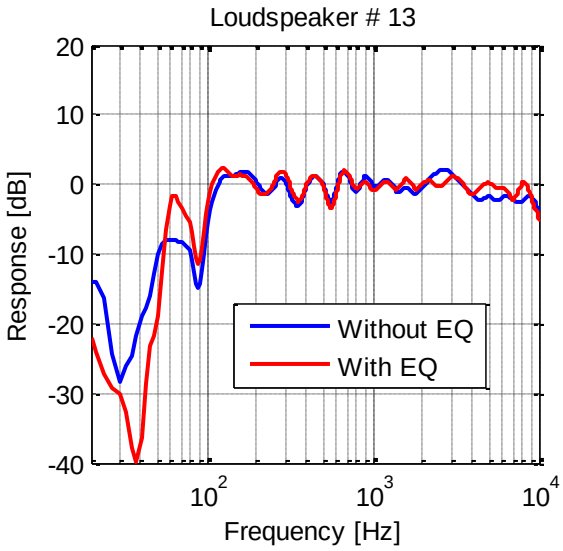
Loudspeaker # 13
Response [dB]
Frequency [Hz]
Without EQ
With EQ

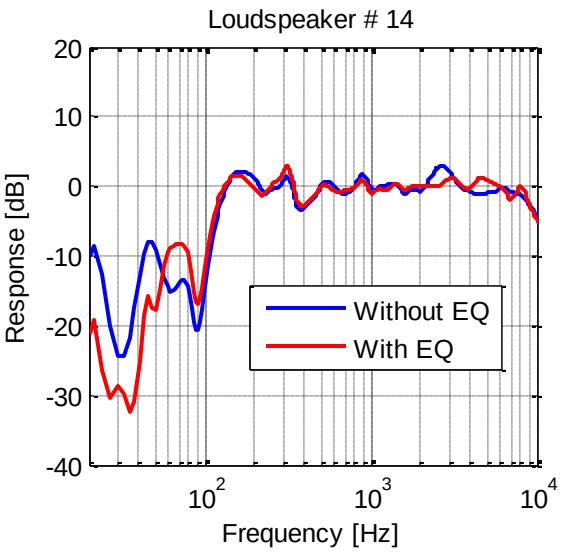
Loudspeaker # 14
Response [dB]
Frequency [Hz]
Without EQ
With EQ

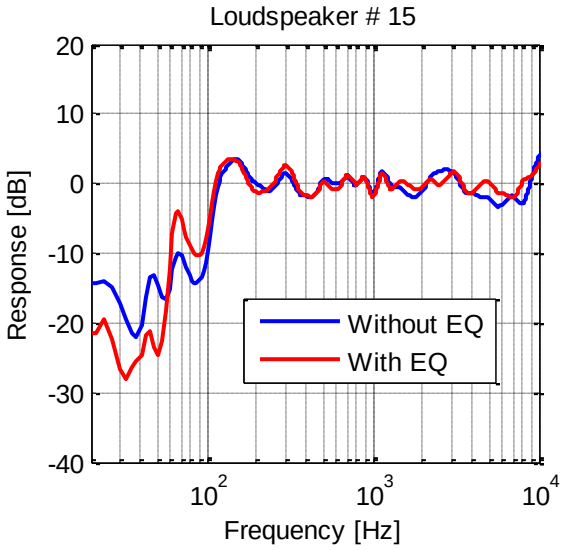
Loudspeaker # 15
Response [dB]
Frequency [Hz]
Without EQ
With EQ

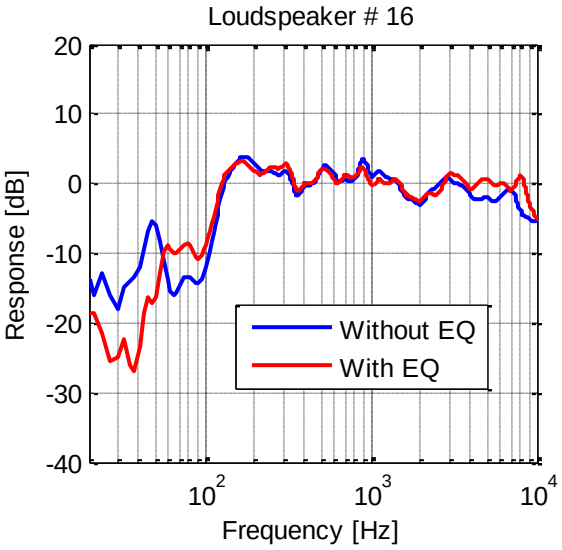
Loudspeaker # 16
Response [dB]
Frequency [Hz]
Without EQ
With EQ

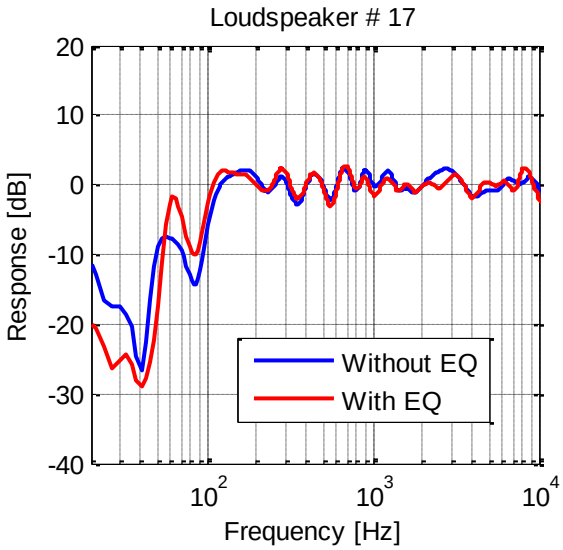
Loudspeaker # 17
Response [dB]
Frequency [Hz]
Without EQ
With EQ

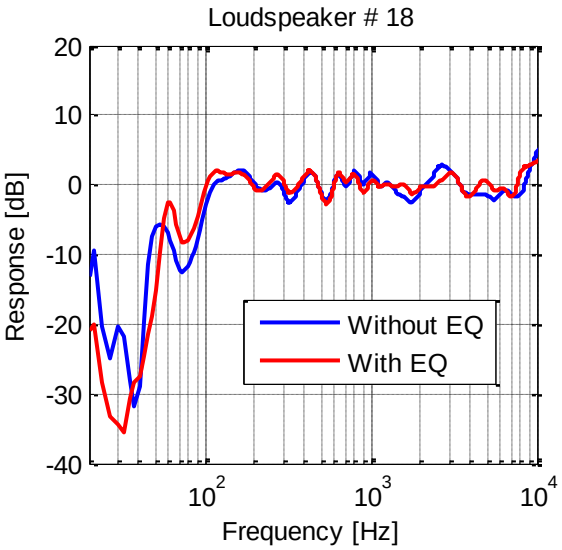
Loudspeaker # 18
Response [dB]
Frequency [Hz]
Without EQ
With EQ

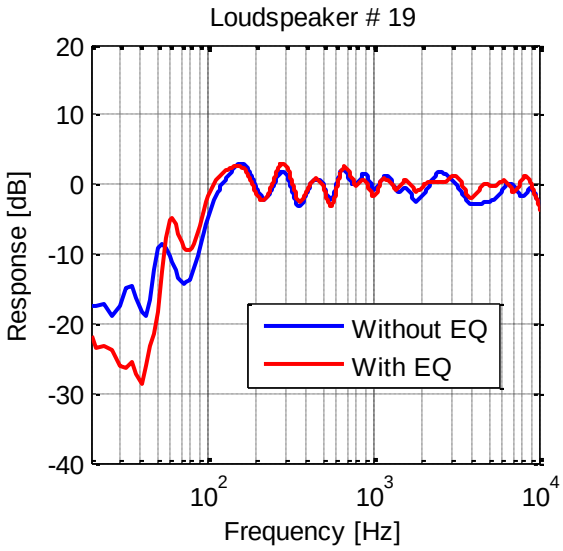
Loudspeaker # 19
Response [dB]
Frequency [Hz]
Without EQ
With EQ

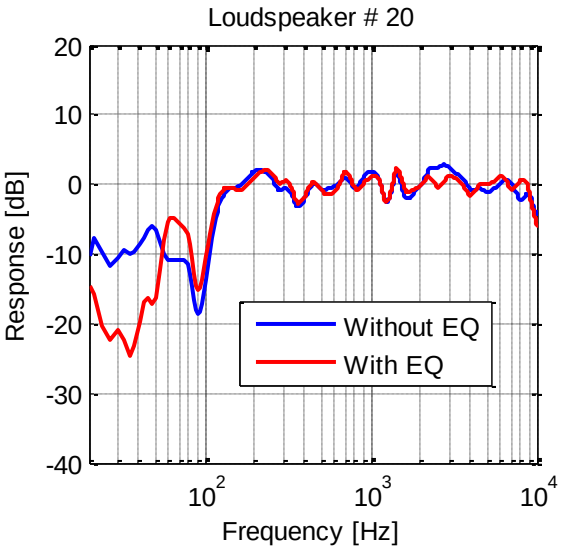
Loudspeaker # 20
Response [dB]
Frequency [Hz]
Without EQ
With EQ

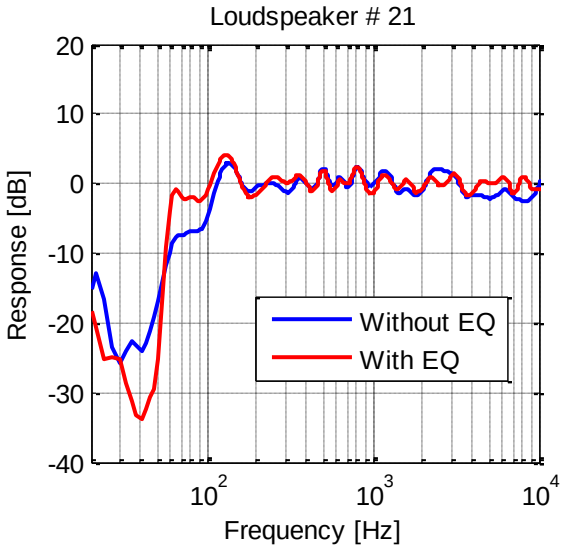
Loudspeaker # 21
Response [dB]
Frequency [Hz]
Without EQ
With EQ

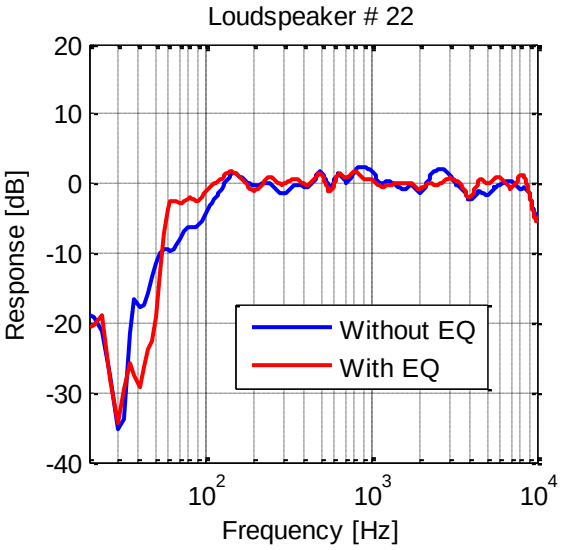
Loudspeaker # 22
Response [dB]
Frequency [Hz]
Without EQ
With EQ

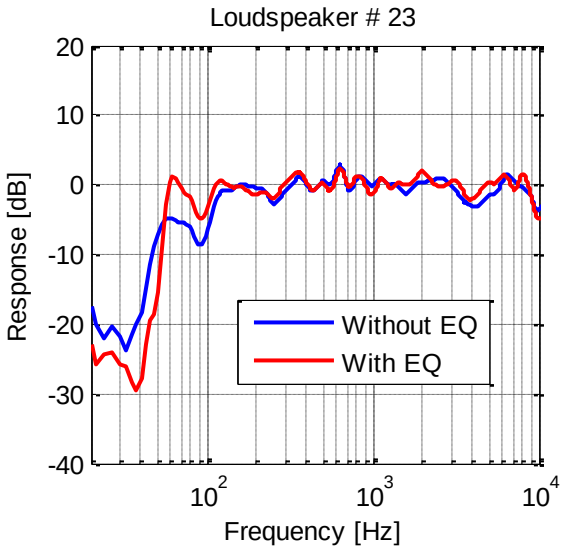
Loudspeaker # 23
Response [dB]
Frequency [Hz]
Without EQ
With EQ

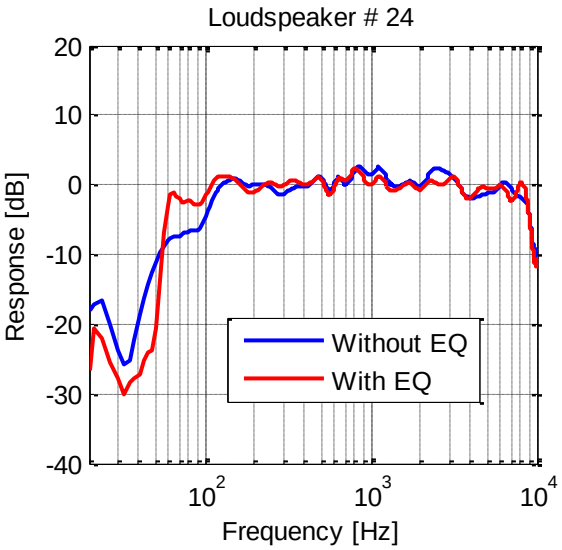
Loudspeaker # 24
Response [dB]
Frequency [Hz]
Without EQ
With EQ

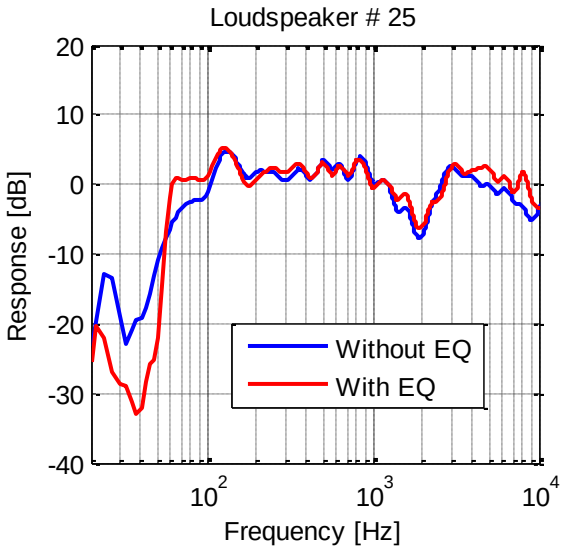
Loudspeaker # 25
Response [dB]
Frequency [Hz]
Without EQ
With EQ

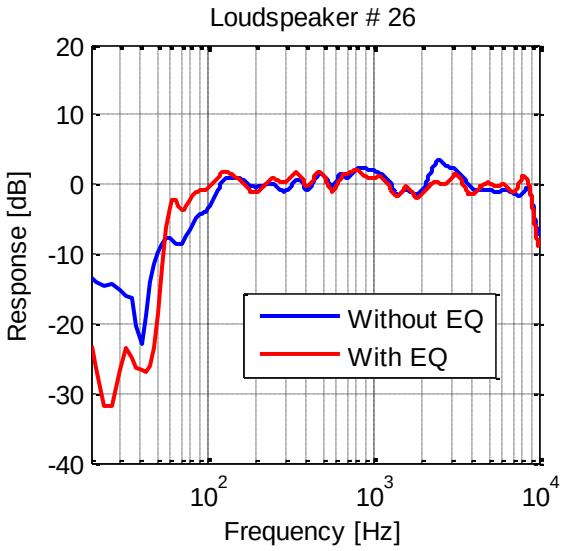
Loudspeaker # 26
Response [dB]
Frequency [Hz]
Without EQ
With EQ

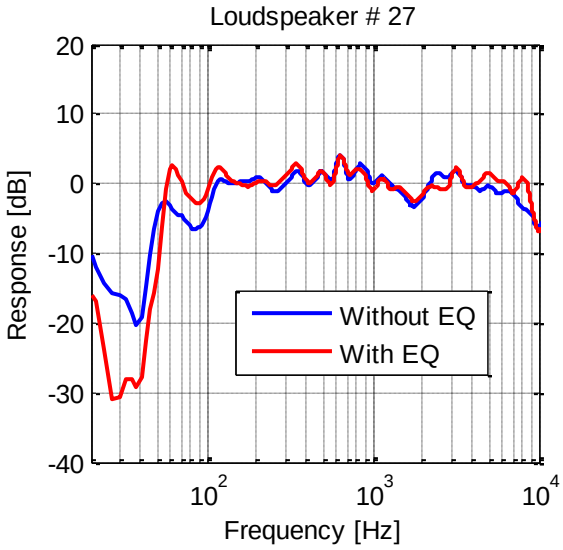
Loudspeaker # 27
Response [dB]
Frequency [Hz]
Without EQ
With EQ

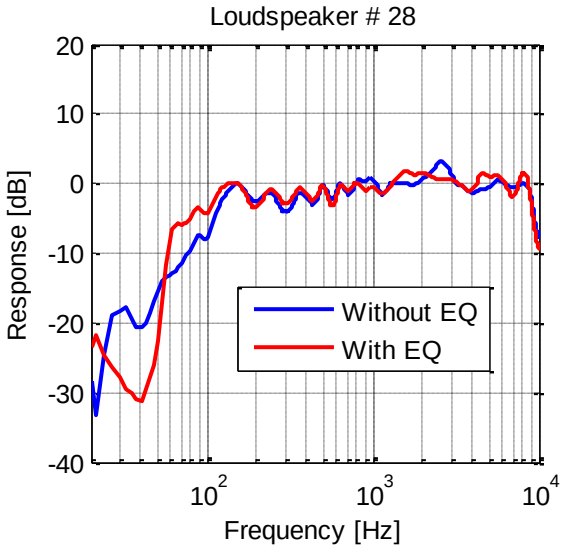
Loudspeaker # 28
Response [dB]
Frequency [Hz]
Without EQ
With EQ

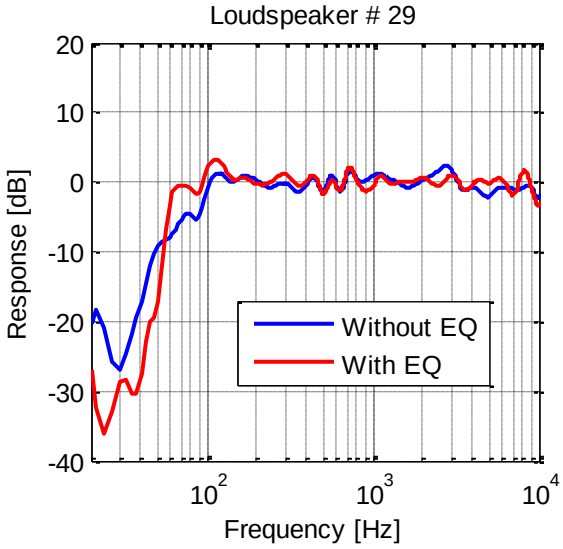
Loudspeaker # 29
Response [dB]
Frequency [Hz]
Without EQ
With EQ

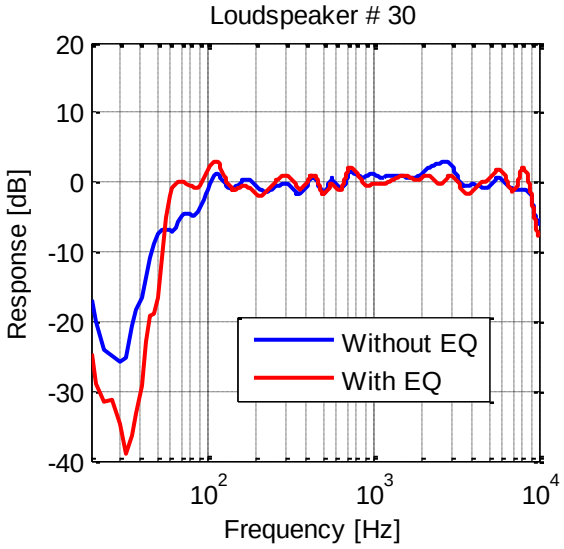
Loudspeaker # 30
Response [dB]
Frequency [Hz]
Without EQ
With EQ

# Appendix G: Directivity of Small Dodecahedron

Three dimensional and two dimensional plots of the small dodecahedron loudspeaker made by the Sound Perception and Room Acoustics Laboratory (SPRAL) were made in an anechoic chamber. Initially, 3D plots of the directivity are shown, all plotted using a 40 dB scale on the radial axis, with the maximum shown relative to 30 dB. The 2D plots are provided after, to show plots in which deviations can be seen as azimuth or orientation of the sound source is changed.

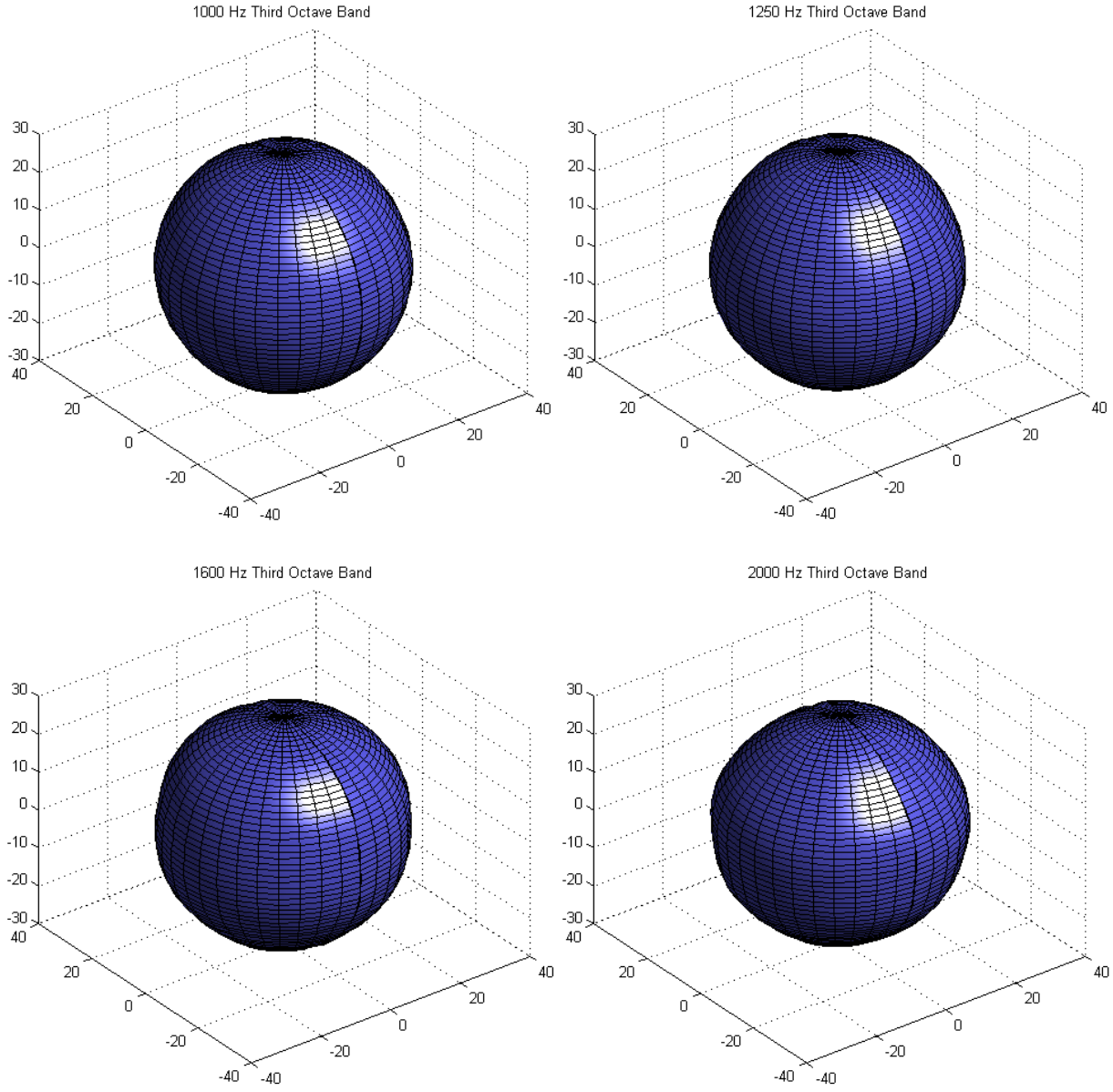

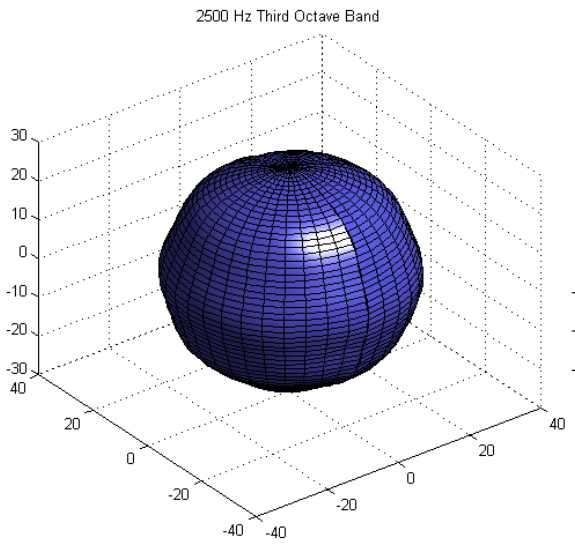
2500 Hz Third Octave Band
30
20
10
0
-10
-20
-30
40
20
0
-20
-40
-40
-20
0
20
40

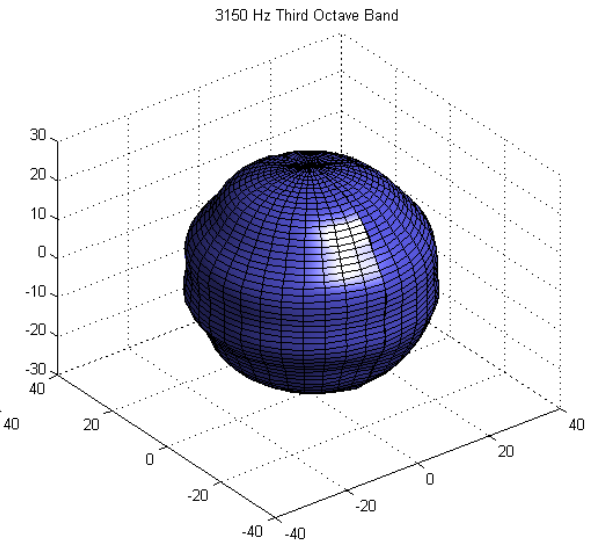
3150 Hz Third Octave Band
30
20
10
0
-10
-20
-30
40
20
0
-20
-40
-40
-20
0
20
40

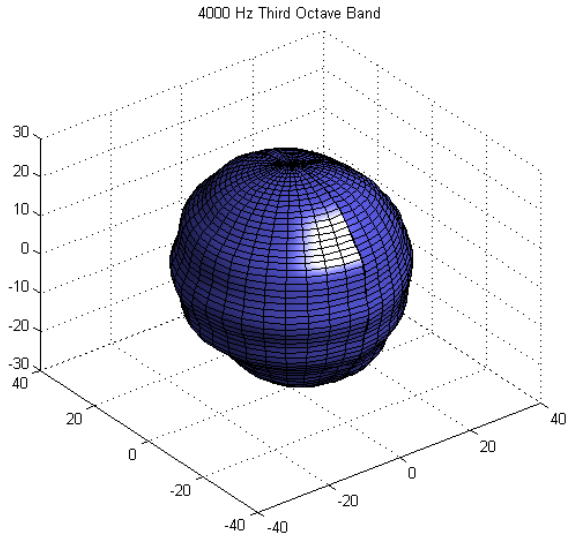
4000 Hz Third Octave Band
30
20
10
0
-10
-20
-30
40
20
0
-20
-40
-40
-20
0
20
40

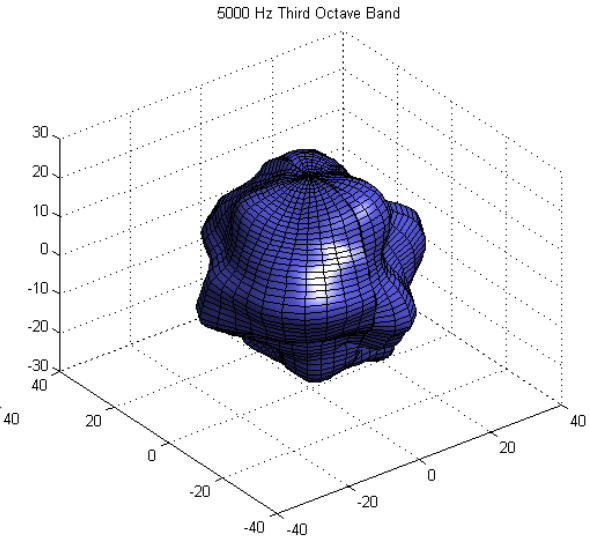
5000 Hz Third Octave Band
30
20
10
0
-10
-20
-30
40
20
0
-20
-40
-40
-20
0
20
40

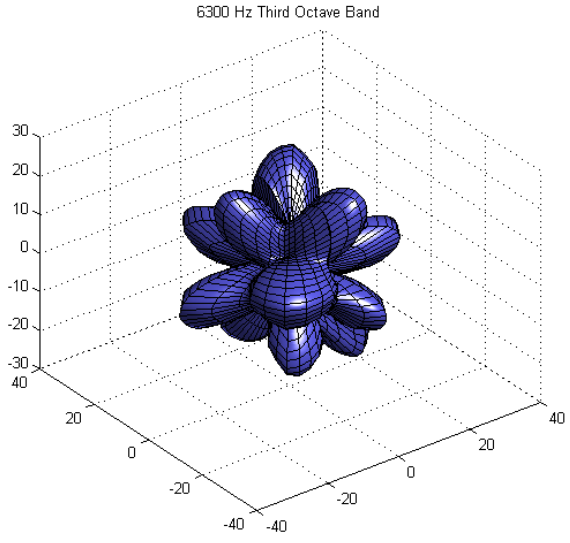
6300 Hz Third Octave Band
30
20
10
0
-10
-20
-30
40
20
0
-20
-40
-40
-20
0
20
40

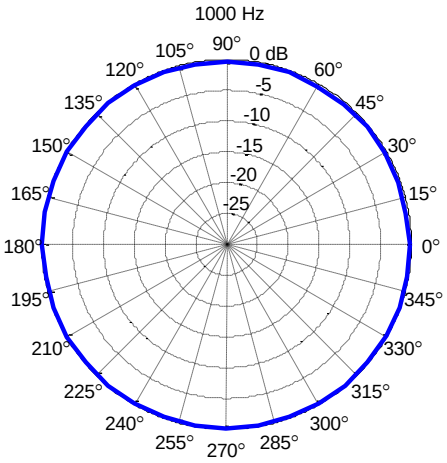
1000 Hz
90°
105°
120°
135°
150°
165°
180°
195°
210°
225°
240°
255°
270°
285°
300°
315°
330°
345°
0°
15°
30°
45°
60°
0 dB
-5
-10
-15
-20
-25

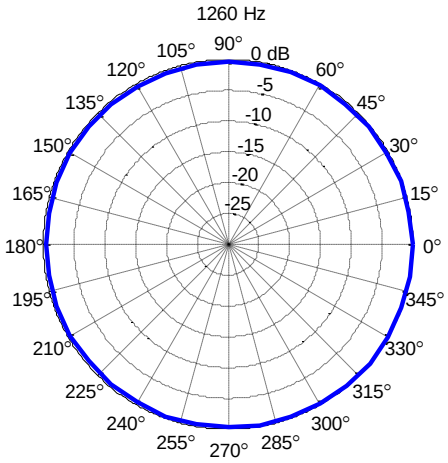
1260 Hz
90°
105°
120°
135°
150°
165°
180°
195°
210°
225°
240°
255°
270°
285°
300°
315°
330°
345°
0°
15°
30°
45°
60°
0 dB
-5
-10
-15
-20
-25

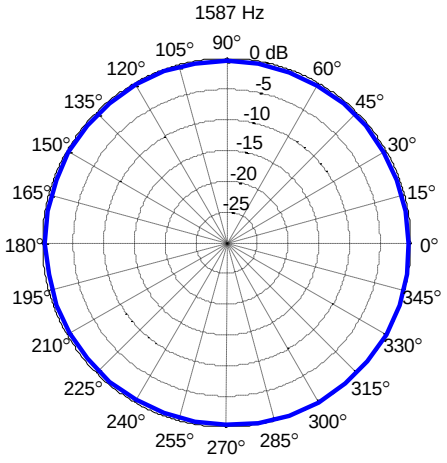
1587 Hz
90°
105°
120°
135°
150°
165°
180°
195°
210°
225°
240°
255°
270°
285°
300°
315°
330°
345°
0°
15°
30°
45°
60°
0 dB
-5
-10
-15
-20
-25

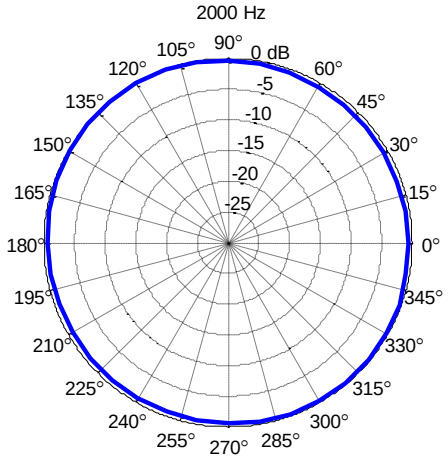
2000 Hz
90°
105°
120°
135°
150°
165°
180°
195°
210°
225°
240°
255°
270°
285°
300°
315°
330°
345°
0°
15°
30°
45°
60°
0 dB
-5
-10
-15
-20
-25

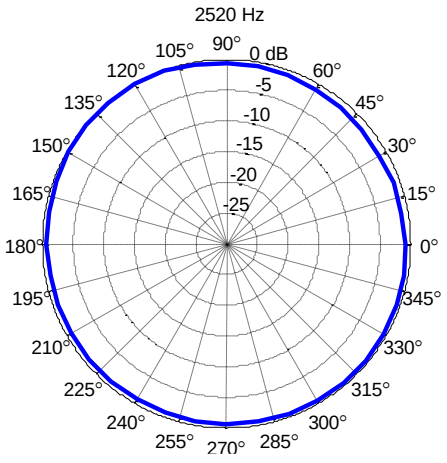
2520 Hz
90°
105°
120°
135°
150°
165°
180°
195°
210°
225°
240°
255°
270°
285°
300°
315°
330°
345°
0°
15°
30°
45°
60°
0 dB
-5
-10
-15
-20
-25

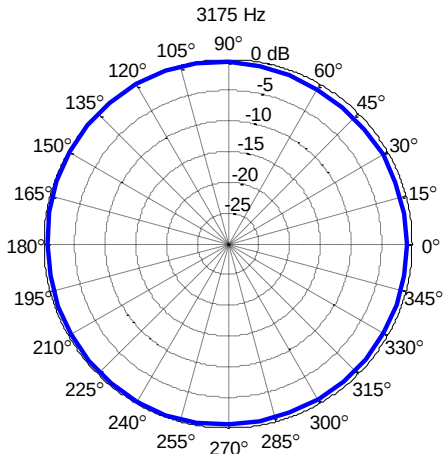
3175 Hz
90°
105°
120°
135°
150°
165°
180°
195°
210°
225°
240°
255°
270°
285°
300°
315°
330°
345°
0°
15°
30°
45°
60°
0 dB
-5
-10
-15
-20
-25

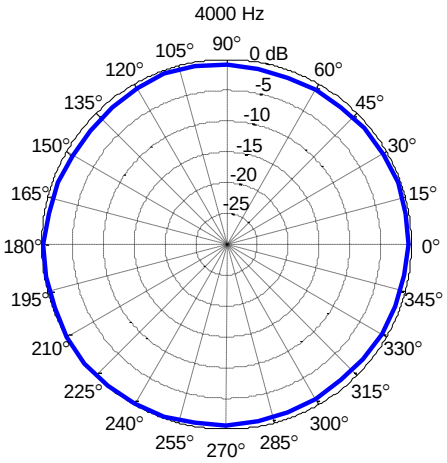
4000 Hz
90°
105°
120°
135°
150°
165°
180°
195°
210°
225°
240°
255°
270°
285°
300°
315°
330°
345°
0°
15°
30°
45°
60°
0 dB
-5
-10
-15
-20
-25

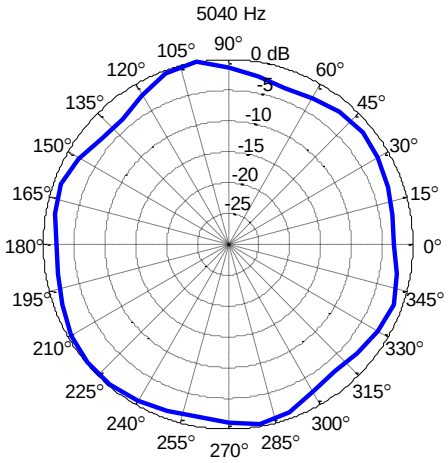
5040 Hz
90°
105°
120°
135°
150°
165°
180°
195°
210°
225°
240°
255°
270°
285°
300°
315°
330°
345°
0°
15°
30°
45°
60°
0 dB
-5
-10
-15
-20
-25

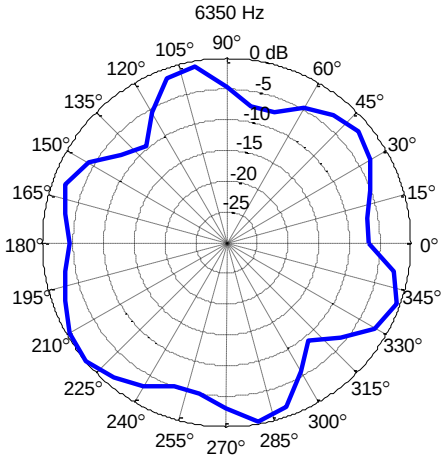
6350 Hz
90°
105°
120°
135°
150°
165°
180°
195°
210°
225°
240°
255°
270°
285°
300°
315°
330°
345°
0°
15°
30°
45°
60°
0 dB
-5
-10
-15
-20
-25

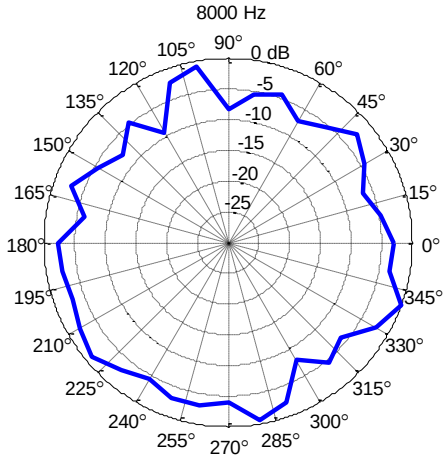
8000 Hz
90°
105°
120°
135°
150°
165°
180°
195°
210°
225°
240°
255°
270°
285°
300°
315°
330°
345°
0°
15°
30°
45°
60°
0 dB
-5
-10
-15
-20
-25

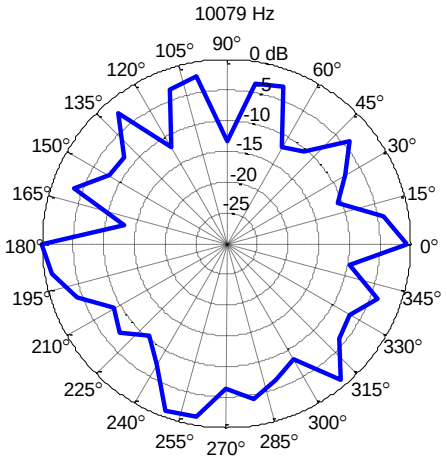
10079 Hz
90°
105°
120°
135°
150°
165°
180°
195°
210°
225°
240°
255°
270°
285°
300°
315°
330°
345°
0°
15°
30°
45°
60°
0 dB
-5
-10
-15
-20
-25

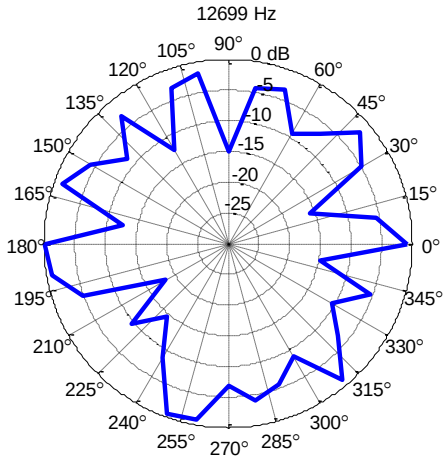
12699 Hz
90°
105°
120°
135°
150°
165°
180°
195°
210°
225°
240°
255°
270°
285°
300°
315°
330°
345°
0°
15°
30°
45°
60°
0 dB
-5
-10
-15
-20
-25

# Appendix H: Measured Stimuli Metric Values

For each set of stimuli, calculations were made of various room acoustics metrics using measurements of the Ambisonics reproductions. This was done for all four stimuli sets, and results are presented in this appendix. The parameters provided are Early Decay Time (EDT), Reverberation Time (T20 & T30), Late Lateral Energy Level ($L_J$), Lateral Fraction ($J_{LF}$), Clarity Index for Music (C80), and Strength (G).

**Measured Parameter Values: Auralization from Set 1 Number 1**

| Parameter | Measured Octave Band Parameter Values | | | | | | | |
|---|---|---|---|---|---|---|---|---|
| | 125 Hz | 250 Hz | 500 Hz | 1000 Hz | 2000 Hz | 4000 Hz | 500 - 1000 Avg. | 250 - 1000 Avg. |
| EDT (s) | 1.86 | 1.01 | 1.07 | 0.93 | 0.98 | 1.03 | 1.00 | 1.00 |
| T20 (s) | 1.37 | 1.28 | 1.10 | 1.01 | 0.97 | 0.92 | 1.06 | 1.09 |
| T30 (s) | 1.45 | 1.23 | 1.04 | 0.95 | 0.92 | 0.87 | 0.99 | 1.03 |
| $L_J$ (dB) | -0.24 | -3.77 | -4.53 | -5.00 | -6.46 | -5.47 | -4.76 | -1.82 |
| $J_{LF}$ (dB) | 0.13 | 0.13 | 0.16 | 0.12 | 0.10 | 0.08 | 0.14 | 0.13 |
| C80 (dB) | -1.76 | 1.08 | 0.40 | 1.19 | 2.24 | 3.02 | 0.82 | 1.28 |
| G (dB) | 7.95 | 7.12 | 5.77 | 6.40 | 6.86 | 8.81 | 6.10 | 9.58 |

**Measured Parameter Values: Auralization from Set 1 Number 2**

| Parameter | Measured Octave Band Parameter Values | | | | | | | |
|---|---|---|---|---|---|---|---|---|
| | 125 Hz | 250 Hz | 500 Hz | 1000 Hz | 2000 Hz | 4000 Hz | 500 - 1000 Avg. | 250 - 1000 Avg. |
| EDT (s) | 1.96 | 1.71 | 1.62 | 1.50 | 1.54 | 1.41 | 1.56 | 1.59 |
| T20 (s) | 1.90 | 1.86 | 1.41 | 1.32 | 1.25 | 1.16 | 1.37 | 1.46 |
| T30 (s) | 1.93 | 1.72 | 1.40 | 1.29 | 1.19 | 1.09 | 1.34 | 1.40 |
| $L_J$ (dB) | 0.32 | -2.75 | -3.94 | -3.92 | -4.25 | -3.25 | -3.93 | -0.67 |
| $J_{LF}$ (dB) | 0.16 | 0.14 | 0.17 | 0.12 | 0.10 | 0.08 | 0.14 | 0.13 |
| C80 (dB) | -4.14 | 0.38 | -3.06 | -1.72 | -1.66 | -1.09 | -2.34 | -1.34 |
| G (dB) | 8.44 | 6.30 | 5.92 | 6.13 | 6.88 | 8.74 | 6.03 | 9.33 |

## Measured Parameter Values: Auralization from Set 1 Number 3

| Parameter | Measured Octave Band Parameter Values | | | | | | | |
|---|---|---|---|---|---|---|---|---|
| | 125 Hz | 250 Hz | 500 Hz | 1000 Hz | 2000 Hz | 4000 Hz | 500 - 1000 Avg. | 250 - 1000 Avg. |
| EDT (s) | 2.61 | 2.35 | 2.13 | 2.08 | 2.04 | 1.79 | 2.10 | 2.15 |
| T20 (s) | 2.69 | 2.13 | 1.86 | 1.63 | 1.58 | 1.35 | 1.75 | 1.80 |
| T30 (s) | 2.67 | 2.27 | 1.92 | 1.73 | 1.62 | 1.39 | 1.82 | 1.88 |
| $L_J$ (dB) | 0.16 | -2.41 | -2.33 | -2.39 | -2.33 | -1.87 | -2.36 | 0.65 |
| $J_{LF}$ (dB) | 0.14 | 0.15 | 0.16 | 0.11 | 0.10 | 0.08 | 0.14 | 0.13 |
| C80 (dB) | -5.04 | -3.04 | -5.75 | -4.44 | -4.18 | -3.45 | -5.05 | -4.25 |
| G (dB) | 8.00 | 6.79 | 6.26 | 6.28 | 6.95 | 8.58 | 6.27 | 9.59 |

## Measured Parameter Values: Auralization from Set 1 Number 4

| Parameter | Measured Octave Band Parameter Values | | | | | | | |
|---|---|---|---|---|---|---|---|---|
| | 125 Hz | 250 Hz | 500 Hz | 1000 Hz | 2000 Hz | 4000 Hz | 500 - 1000 Avg. | 250 - 1000 Avg. |
| EDT (s) | 3.19 | 2.81 | 2.48 | 2.53 | 2.38 | 2.13 | 2.50 | 2.55 |
| T20 (s) | 3.01 | 2.79 | 2.36 | 2.07 | 1.91 | 1.58 | 2.22 | 2.28 |
| T30 (s) | 3.57 | 3.09 | 2.54 | 2.23 | 2.01 | 1.64 | 2.38 | 2.47 |
| $L_J$ (dB) | 0.98 | -1.96 | -1.68 | -1.76 | -1.92 | -1.68 | -1.72 | 1.18 |
| $J_{LF}$ (dB) | 0.17 | 0.17 | 0.19 | 0.11 | 0.11 | 0.08 | 0.15 | 0.15 |
| C80 (dB) | -6.25 | -3.92 | -6.97 | -5.16 | -5.46 | -4.30 | -5.97 | -5.24 |
| G (dB) | 7.97 | 6.34 | 5.90 | 6.13 | 7.05 | 8.34 | 6.02 | 9.39 |

## Measured Parameter Values: Auralization from Set 1 Number 5

| Parameter | Measured Octave Band Parameter Values | | | | | | | |
|---|---|---|---|---|---|---|---|---|
| | 125 Hz | 250 Hz | 500 Hz | 1000 Hz | 2000 Hz | 4000 Hz | 500 - 1000 Avg. | 250 - 1000 Avg. |
| EDT (s) | 2.06 | 1.74 | 1.69 | 1.52 | 1.57 | 1.38 | 1.61 | 1.63 |
| T20 (s) | 2.19 | 1.77 | 1.42 | 1.32 | 1.24 | 1.19 | 1.37 | 1.44 |
| T30 (s) | 2.06 | 1.79 | 1.44 | 1.31 | 1.23 | 1.18 | 1.38 | 1.44 |
| $L_J$ (dB) | -0.98 | -3.34 | -4.04 | -4.99 | -6.07 | -6.05 | -4.49 | -1.48 |
| $J_{LF}$ (dB) | 0.12 | 0.14 | 0.13 | 0.11 | 0.07 | 0.05 | 0.12 | 0.11 |
| C80 (dB) | -0.54 | 1.54 | 1.53 | 2.84 | 4.28 | 6.00 | 2.23 | 2.70 |
| G (dB) | 7.89 | 6.42 | 6.22 | 6.47 | 7.48 | 9.39 | 6.34 | 9.68 |

## Measured Parameter Values: Auralization from Set 1 Number 6

| Parameter | Measured Octave Band Parameter Values | | | | | | | |
|---|---|---|---|---|---|---|---|---|
| | 125 Hz | 250 Hz | 500 Hz | 1000 Hz | 2000 Hz | 4000 Hz | 500 - 1000 Avg. | 250 - 1000 Avg. |
| EDT (s) | 2.57 | 2.52 | 2.08 | 2.05 | 2.11 | 2.08 | 2.06 | 2.19 |
| T20 (s) | 2.91 | 2.24 | 1.94 | 1.78 | 1.68 | 1.50 | 1.86 | 1.91 |
| T30 (s) | 2.79 | 2.18 | 1.88 | 1.72 | 1.63 | 1.49 | 1.80 | 1.85 |
| $L_J$ (dB) | -0.26 | -3.06 | -3.26 | -4.09 | -5.04 | -4.96 | -3.65 | -0.78 |
| $J_{LF}$ (dB) | 0.12 | 0.15 | 0.14 | 0.11 | 0.07 | 0.05 | 0.12 | 0.12 |
| C80 (dB) | -1.14 | 0.22 | -0.64 | 0.71 | 2.04 | 3.57 | 0.09 | 0.69 |
| G (dB) | 7.67 | 6.33 | 5.94 | 6.07 | 6.99 | 8.77 | 6.01 | 9.36 |

## Measured Parameter Values: Auralization from Set 1 Number 7

| Parameter | Measured Octave Band Parameter Values | | | | | | | |
|---|---|---|---|---|---|---|---|---|
| | 125 Hz | 250 Hz | 500 Hz | 1000 Hz | 2000 Hz | 4000 Hz | 500 - 1000 Avg. | 250 - 1000 Avg. |
| EDT (s) | 4.12 | 3.61 | 2.79 | 2.73 | 2.62 | 2.31 | 2.76 | 2.94 |
| T20 (s) | 3.70 | 2.94 | 2.50 | 2.31 | 2.15 | 1.85 | 2.41 | 2.47 |
| T30 (s) | 3.61 | 2.92 | 2.45 | 2.21 | 2.03 | 1.78 | 2.33 | 2.40 |
| $L_J$ (dB) | 0.20 | -2.63 | -2.94 | -3.43 | -4.09 | -4.26 | -3.18 | -0.23 |
| $J_{LF}$ (dB) | 0.13 | 0.16 | 0.15 | 0.11 | 0.07 | 0.05 | 0.13 | 0.12 |
| C80 (dB) | -3.27 | -1.53 | -2.67 | -1.57 | -0.78 | 0.83 | -2.09 | -1.59 |
| G (dB) | 8.09 | 6.21 | 5.57 | 5.72 | 6.76 | 8.24 | 5.64 | 9.10 |

## Measured Parameter Values: Auralization from Set 1 Number 8

| Parameter | Measured Octave Band Parameter Values | | | | | | | |
|---|---|---|---|---|---|---|---|---|
| | 125 Hz | 250 Hz | 500 Hz | 1000 Hz | 2000 Hz | 4000 Hz | 500 - 1000 Avg. | 250 - 1000 Avg. |
| EDT (s) | 5.26 | 4.57 | 3.66 | 3.42 | 3.25 | 2.64 | 3.54 | 3.72 |
| T20 (s) | 4.08 | 3.35 | 2.77 | 2.69 | 2.47 | 2.15 | 2.73 | 2.82 |
| T30 (s) | 4.32 | 3.55 | 2.95 | 2.65 | 2.35 | 2.03 | 2.80 | 2.88 |
| $L_J$ (dB) | 0.73 | -2.55 | -2.58 | -2.86 | -3.42 | -3.56 | -2.72 | 0.17 |
| $J_{LF}$ (dB) | 0.13 | 0.16 | 0.15 | 0.11 | 0.07 | 0.05 | 0.13 | 0.12 |
| C80 (dB) | -4.16 | -2.07 | -3.81 | -2.81 | -1.99 | -0.26 | -3.29 | -2.61 |
| G (dB) | 8.17 | 5.95 | 5.50 | 5.66 | 6.64 | 7.94 | 5.58 | 8.97 |

## Measured Parameter Values: Auralization from Set 2 Number 1

| Parameter | Measured Octave Band Parameter Values | | | | | | | |
|---|---|---|---|---|---|---|---|---|
| | 125 Hz | 250 Hz | 500 Hz | 1000 Hz | 2000 Hz | 4000 Hz | 500 - 1000 Avg. | 250 - 1000 Avg. |
| EDT (s) | 3.27 | 2.82 | 2.52 | 2.70 | 2.57 | 2.24 | 2.61 | 2.65 |
| T20 (s) | 3.23 | 2.74 | 2.39 | 2.01 | 1.87 | 1.53 | 2.20 | 2.25 |
| T30 (s) | 3.57 | 2.89 | 2.50 | 2.25 | 1.97 | 1.64 | 2.38 | 2.40 |
| $L_J$ (dB) | 0.82 | -1.47 | -1.76 | -2.10 | -2.33 | -1.67 | -1.93 | 1.11 |
| $J_{LF}$ (dB) | 0.13 | 0.14 | 0.16 | 0.13 | 0.11 | 0.08 | 0.15 | 0.14 |
| C80 (dB) | -5.38 | -4.19 | -6.28 | -5.39 | -5.03 | -3.86 | -5.81 | -5.16 |
| G (dB) | 7.48 | 6.60 | 6.14 | 6.53 | 7.27 | 8.64 | 6.34 | 9.67 |

## Measured Parameter Values: Auralization from Set 2 Number 2

| Parameter | Measured Octave Band Parameter Values | | | | | | | |
|---|---|---|---|---|---|---|---|---|
| | 125 Hz | 250 Hz | 500 Hz | 1000 Hz | 2000 Hz | 4000 Hz | 500 - 1000 Avg. | 250 - 1000 Avg. |
| EDT (s) | 2.55 | 2.48 | 2.22 | 2.17 | 2.09 | 1.82 | 2.20 | 2.24 |
| T20 (s) | 2.50 | 2.01 | 1.79 | 1.62 | 1.54 | 1.37 | 1.70 | 1.74 |
| T30 (s) | 2.53 | 2.18 | 1.87 | 1.69 | 1.57 | 1.35 | 1.78 | 1.83 |
| $L_J$ (dB) | 1.00 | -1.64 | -2.11 | -2.82 | -2.62 | -1.87 | -2.45 | 0.74 |
| $J_{LF}$ (dB) | 0.14 | 0.14 | 0.16 | 0.13 | 0.10 | 0.08 | 0.14 | 0.13 |
| C80 (dB) | -5.36 | -2.71 | -4.51 | -3.68 | -3.49 | -2.57 | -4.08 | -3.55 |
| G (dB) | 7.91 | 6.73 | 5.62 | 6.32 | 7.25 | 8.73 | 5.99 | 9.53 |

## Measured Parameter Values: Auralization from Set 2 Number 3

| Parameter | Measured Octave Band Parameter Values | | | | | | | |
|---|---|---|---|---|---|---|---|---|
| | 125 Hz | 250 Hz | 500 Hz | 1000 Hz | 2000 Hz | 4000 Hz | 500 - 1000 Avg. | 250 - 1000 Avg. |
| EDT (s) | 2.29 | 1.33 | 1.71 | 1.64 | 1.58 | 1.38 | 1.68 | 1.57 |
| T20 (s) | 1.85 | 1.78 | 1.47 | 1.36 | 1.27 | 1.18 | 1.41 | 1.47 |
| T30 (s) | 1.85 | 1.73 | 1.45 | 1.30 | 1.19 | 1.12 | 1.37 | 1.41 |
| $L_J$ (dB) | -0.74 | -4.34 | -3.39 | -4.36 | -4.55 | -3.76 | -3.84 | -1.12 |
| $J_{LF}$ (dB) | 0.13 | 0.15 | 0.18 | 0.13 | 0.11 | 0.08 | 0.16 | 0.14 |
| C80 (dB) | -2.07 | -0.77 | -1.88 | -1.56 | -1.71 | -0.53 | -1.72 | -1.46 |
| G (dB) | 7.71 | 7.06 | 5.23 | 5.86 | 6.88 | 8.55 | 5.56 | 9.33 |

## Measured Parameter Values: Auralization from Set 2 Number 4

| Parameter | Measured Octave Band Parameter Values | | | | | | | |
|---|---|---|---|---|---|---|---|---|
| | 125 Hz | 250 Hz | 500 Hz | 1000 Hz | 2000 Hz | 4000 Hz | 500 - 1000 Avg. | 250 - 1000 Avg. |
| EDT (s) | 1.79 | 1.01 | 1.02 | 0.95 | 0.99 | 1.00 | 0.98 | 0.99 |
| T20 (s) | 1.43 | 1.26 | 1.08 | 0.99 | 0.96 | 0.88 | 1.04 | 1.07 |
| T30 (s) | 1.38 | 1.15 | 1.02 | 0.95 | 0.90 | 0.85 | 0.98 | 1.00 |
| $L_J$ (dB) | -0.76 | -4.67 | -4.76 | -5.59 | -6.70 | -5.79 | -5.16 | -2.34 |
| $J_{LF}$ (dB) | 0.13 | 0.14 | 0.17 | 0.12 | 0.10 | 0.08 | 0.15 | 0.13 |
| C80 (dB) | 0.42 | 1.86 | -0.05 | 1.59 | 1.97 | 2.37 | 0.85 | 1.42 |
| G (dB) | 7.58 | 7.12 | 5.33 | 5.87 | 6.54 | 8.60 | 5.61 | 9.28 |

## Measured Parameter Values: Auralization from Set 2 Number 5

| Parameter | Measured Octave Band Parameter Values | | | | | | | |
|---|---|---|---|---|---|---|---|---|
| | 125 Hz | 250 Hz | 500 Hz | 1000 Hz | 2000 Hz | 4000 Hz | 500 - 1000 Avg. | 250 - 1000 Avg. |
| EDT (s) | 2.80 | 2.55 | 2.62 | 2.45 | 2.32 | 2.03 | 2.53 | 2.48 |
| T20 (s) | 3.27 | 2.84 | 2.36 | 2.16 | 1.90 | 1.58 | 2.26 | 2.32 |
| T30 (s) | 3.45 | 3.11 | 2.53 | 2.28 | 2.02 | 1.66 | 2.40 | 2.48 |
| $L_J$ (dB) | 0.61 | -1.28 | -1.97 | -1.61 | -1.92 | -1.54 | -1.79 | 1.32 |
| $J_{LF}$ (dB) | 0.17 | 0.12 | 0.17 | 0.14 | 0.09 | 0.09 | 0.15 | 0.13 |
| C80 (dB) | -7.73 | -3.61 | -4.54 | -4.98 | -4.73 | -3.80 | -4.75 | -4.43 |
| G (dB) | 8.37 | 6.53 | 6.19 | 6.45 | 7.85 | 8.88 | 6.32 | 9.82 |

## Measured Parameter Values: Auralization from Set 2 Number 6

| Parameter | Measured Octave Band Parameter Values | | | | | | | |
|---|---|---|---|---|---|---|---|---|
| | 125 Hz | 250 Hz | 500 Hz | 1000 Hz | 2000 Hz | 4000 Hz | 500 - 1000 Avg. | 250 - 1000 Avg. |
| EDT (s) | 2.87 | 2.48 | 2.04 | 2.05 | 2.04 | 1.75 | 2.05 | 2.15 |
| T20 (s) | 2.39 | 2.09 | 1.88 | 1.57 | 1.51 | 1.33 | 1.73 | 1.76 |
| T30 (s) | 2.46 | 2.27 | 1.97 | 1.71 | 1.57 | 1.36 | 1.84 | 1.88 |
| $L_J$ (dB) | 1.69 | -2.26 | -2.83 | -2.43 | -2.65 | -2.46 | -2.62 | 0.48 |
| $J_{LF}$ (dB) | 0.21 | 0.12 | 0.13 | 0.14 | 0.11 | 0.09 | 0.14 | 0.13 |
| C80 (dB) | -5.11 | -1.32 | -3.75 | -2.82 | -3.45 | -2.11 | -3.26 | -2.73 |
| G (dB) | 8.29 | 6.46 | 6.04 | 6.22 | 7.09 | 8.39 | 6.13 | 9.48 |

## Measured Parameter Values: Auralization from Set 2 Number 7

| Parameter | Measured Octave Band Parameter Values | | | | | | | |
|---|---|---|---|---|---|---|---|---|
| | 125 Hz | 250 Hz | 500 Hz | 1000 Hz | 2000 Hz | 4000 Hz | 500 - 1000 Avg. | 250 - 1000 Avg. |
| EDT (s) | 2.34 | 1.60 | 1.59 | 1.43 | 1.50 | 1.37 | 1.51 | 1.53 |
| T20 (s) | 1.72 | 1.60 | 1.41 | 1.34 | 1.24 | 1.15 | 1.38 | 1.40 |
| T30 (s) | 1.95 | 1.65 | 1.39 | 1.31 | 1.22 | 1.11 | 1.35 | 1.39 |
| $L_J$ (dB) | 0.77 | -2.82 | -3.08 | -4.22 | -3.79 | -3.12 | -3.61 | -0.43 |
| $J_{LF}$ (dB) | 0.15 | 0.12 | 0.11 | 0.12 | 0.10 | 0.08 | 0.12 | 0.11 |
| C80 (dB) | -3.40 | 0.41 | -0.21 | 0.16 | -0.82 | -0.48 | -0.02 | -0.09 |
| G (dB) | 8.49 | 7.44 | 6.42 | 6.15 | 6.98 | 8.62 | 6.28 | 9.79 |

## Measured Parameter Values: Auralization from Set 2 Number 8

| Parameter | Measured Octave Band Parameter Values | | | | | | | |
|---|---|---|---|---|---|---|---|---|
| | 125 Hz | 250 Hz | 500 Hz | 1000 Hz | 2000 Hz | 4000 Hz | 500 - 1000 Avg. | 250 - 1000 Avg. |
| EDT (s) | 1.55 | 0.84 | 1.07 | 0.93 | 0.90 | 0.92 | 1.00 | 0.93 |
| T20 (s) | 1.32 | 1.29 | 1.02 | 0.91 | 0.94 | 0.87 | 0.97 | 1.04 |
| T30 (s) | 1.34 | 1.22 | 1.02 | 0.91 | 0.89 | 0.84 | 0.96 | 1.01 |
| $L_J$ (dB) | -1.39 | -6.06 | -4.76 | -6.54 | -6.82 | -5.86 | -5.56 | -2.96 |
| $J_{LF}$ (dB) | 0.19 | 0.10 | 0.13 | 0.13 | 0.09 | 0.08 | 0.13 | 0.11 |
| C80 (dB) | -0.89 | 5.55 | 3.27 | 2.93 | 3.25 | 3.76 | 3.10 | 3.89 |
| G (dB) | 8.38 | 7.53 | 6.07 | 6.09 | 6.62 | 8.29 | 6.08 | 9.63 |

## Measured Parameter Values: Auralization from Set 3 Number 1

| Parameter | Measured Octave Band Parameter Values | | | | | | | |
|---|---|---|---|---|---|---|---|---|
| | 125 Hz | 250 Hz | 500 Hz | 1000 Hz | 2000 Hz | 4000 Hz | 500 - 1000 Avg. | 250 - 1000 Avg. |
| EDT (s) | 2.46 | 1.71 | 1.75 | 1.49 | 1.52 | 1.40 | 1.62 | 1.62 |
| T20 (s) | 1.99 | 1.54 | 1.38 | 1.34 | 1.24 | 1.15 | 1.36 | 1.38 |
| T30 (s) | 1.86 | 1.58 | 1.37 | 1.28 | 1.21 | 1.10 | 1.33 | 1.36 |
| $L_J$ (dB) | 0.43 | -3.31 | -3.93 | -3.45 | -4.11 | -3.40 | -3.68 | -0.68 |
| $J_{LF}$ (dB) | 0.14 | 0.14 | 0.16 | 0.11 | 0.10 | 0.08 | 0.14 | 0.13 |
| C80 (dB) | -3.16 | -1.27 | -2.25 | -1.54 | -1.70 | -0.80 | -1.88 | -1.68 |
| G (dB) | 7.52 | 6.90 | 5.22 | 5.92 | 6.72 | 8.51 | 5.58 | 9.25 |

## Measured Parameter Values: Auralization from Set 3 Number 2

| Parameter | Measured Octave Band Parameter Values | | | | | | | |
|---|---|---|---|---|---|---|---|---|
| | 125 Hz | 250 Hz | 500 Hz | 1000 Hz | 2000 Hz | 4000 Hz | 500 - 1000 Avg. | 250 - 1000 Avg. |
| EDT (s) | 3.17 | 2.74 | 2.42 | 2.40 | 2.26 | 1.93 | 2.41 | 2.45 |
| T20 (s) | 2.96 | 2.31 | 2.11 | 1.84 | 1.72 | 1.48 | 1.97 | 2.00 |
| T30 (s) | 2.89 | 2.58 | 2.23 | 1.92 | 1.80 | 1.53 | 2.08 | 2.13 |
| $L_J$ (dB) | 1.04 | -2.71 | -2.87 | -2.61 | -2.63 | -2.19 | -2.74 | 0.30 |
| $J_{LF}$ (dB) | 0.16 | 0.15 | 0.17 | 0.13 | 0.11 | 0.08 | 0.15 | 0.14 |
| C80 (dB) | -5.94 | -3.49 | -5.65 | -5.44 | -5.00 | -3.78 | -5.54 | -4.81 |
| G (dB) | 8.07 | 6.69 | 5.68 | 6.44 | 7.08 | 8.51 | 6.08 | 9.51 |

## Measured Parameter Values: Auralization from Set 3 Number 3

| Parameter | Measured Octave Band Parameter Values | | | | | | | |
|---|---|---|---|---|---|---|---|---|
| | 125 Hz | 250 Hz | 500 Hz | 1000 Hz | 2000 Hz | 4000 Hz | 500 - 1000 Avg. | 250 - 1000 Avg. |
| EDT (s) | 2.18 | 1.73 | 1.64 | 1.48 | 1.50 | 1.52 | 1.56 | 1.59 |
| T20 (s) | 2.05 | 1.83 | 1.58 | 1.46 | 1.37 | 1.21 | 1.52 | 1.56 |
| T30 (s) | 1.87 | 1.68 | 1.46 | 1.32 | 1.26 | 1.17 | 1.39 | 1.43 |
| $L_J$ (dB) | -0.25 | -2.91 | -3.10 | -3.70 | -5.06 | -4.45 | -3.39 | -0.60 |
| $J_{LF}$ (dB) | 0.10 | 0.13 | 0.16 | 0.11 | 0.08 | 0.06 | 0.13 | 0.12 |
| C80 (dB) | 0.32 | -0.14 | -1.16 | 0.84 | 1.72 | 2.52 | -0.04 | 0.45 |
| G (dB) | 8.34 | 6.21 | 5.29 | 6.03 | 7.00 | 8.79 | 5.67 | 9.18 |

## Measured Parameter Values: Auralization from Set 3 Number 4

| Parameter | Measured Octave Band Parameter Values | | | | | | | |
|---|---|---|---|---|---|---|---|---|
| | 125 Hz | 250 Hz | 500 Hz | 1000 Hz | 2000 Hz | 4000 Hz | 500 - 1000 Avg. | 250 - 1000 Avg. |
| EDT (s) | 3.59 | 2.97 | 2.64 | 2.49 | 2.36 | 2.04 | 2.57 | 2.62 |
| T20 (s) | 2.80 | 2.38 | 2.17 | 1.99 | 1.80 | 1.70 | 2.08 | 2.09 |
| T30 (s) | 2.77 | 2.50 | 2.17 | 1.96 | 1.77 | 1.59 | 2.06 | 2.10 |
| $L_J$ (dB) | 0.63 | -2.66 | -3.17 | -2.87 | -3.79 | -3.20 | -3.02 | -0.09 |
| $J_{LF}$ (dB) | 0.10 | 0.13 | 0.16 | 0.11 | 0.08 | 0.07 | 0.13 | 0.12 |
| C80 (dB) | -2.94 | -2.70 | -4.45 | -2.71 | -2.51 | -1.05 | -3.49 | -3.02 |
| G (dB) | 8.97 | 6.30 | 5.31 | 5.94 | 7.15 | 8.34 | 5.64 | 9.24 |

## Measured Parameter Values: Auralization from Set 3 Number 5

| Parameter | Measured Octave Band Parameter Values | | | | | | | |
|---|---|---|---|---|---|---|---|---|
| | 125 Hz | 250 Hz | 500 Hz | 1000 Hz | 2000 Hz | 4000 Hz | 500 - 1000 Avg. | 250 - 1000 Avg. |
| EDT (s) | 2.03 | 1.73 | 1.63 | 1.58 | 1.53 | 1.55 | 1.60 | 1.62 |
| T20 (s) | 1.93 | 1.83 | 1.34 | 1.27 | 1.22 | 1.17 | 1.30 | 1.41 |
| T30 (s) | 1.83 | 1.72 | 1.43 | 1.30 | 1.23 | 1.17 | 1.36 | 1.42 |
| $L_J$ (dB) | -0.29 | -3.09 | -3.69 | -4.73 | -5.30 | -4.65 | -4.17 | -1.10 |
| $J_{LF}$ (dB) | 0.12 | 0.18 | 0.14 | 0.11 | 0.07 | 0.06 | 0.12 | 0.12 |
| C80 (dB) | -1.17 | -0.25 | 0.08 | 1.52 | 2.57 | 3.92 | 0.86 | 1.13 |
| G (dB) | 8.64 | 6.12 | 5.59 | 6.12 | 7.10 | 8.98 | 5.86 | 9.28 |

## Measured Parameter Values: Auralization from Set 3 Number 6

| Parameter | Measured Octave Band Parameter Values | | | | | | | |
|---|---|---|---|---|---|---|---|---|
| | 125 Hz | 250 Hz | 500 Hz | 1000 Hz | 2000 Hz | 4000 Hz | 500 - 1000 Avg. | 250 - 1000 Avg. |
| EDT (s) | 3.11 | 3.24 | 2.85 | 2.49 | 2.35 | 2.16 | 2.67 | 2.73 |
| T20 (s) | 2.53 | 2.36 | 2.32 | 2.05 | 2.01 | 1.71 | 2.18 | 2.18 |
| T30 (s) | 2.66 | 2.44 | 2.25 | 2.02 | 1.89 | 1.64 | 2.13 | 2.15 |
| $L_J$ (dB) | 0.31 | -2.24 | -2.66 | -3.12 | -3.51 | -3.44 | -2.88 | 0.15 |
| $J_{LF}$ (dB) | 0.12 | 0.19 | 0.15 | 0.11 | 0.07 | 0.06 | 0.13 | 0.13 |
| C80 (dB) | -3.44 | -2.67 | -3.10 | -2.09 | -1.08 | 0.32 | -2.56 | -2.17 |
| G (dB) | 8.77 | 6.09 | 5.22 | 5.88 | 6.72 | 8.28 | 5.56 | 9.02 |

## Measured Parameter Values: Auralization from Set 3 Number 7

| Parameter | Measured Octave Band Parameter Values | | | | | | | |
|---|---|---|---|---|---|---|---|---|
| | 125 Hz | 250 Hz | 500 Hz | 1000 Hz | 2000 Hz | 4000 Hz | 500 - 1000 Avg. | 250 - 1000 Avg. |
| EDT (s) | 2.02 | 1.71 | 1.62 | 1.59 | 1.48 | 1.38 | 1.60 | 1.60 |
| T20 (s) | 1.86 | 1.68 | 1.53 | 1.31 | 1.27 | 1.17 | 1.42 | 1.45 |
| T30 (s) | 1.85 | 1.63 | 1.49 | 1.33 | 1.27 | 1.17 | 1.41 | 1.43 |
| $L_J$ (dB) | -1.18 | -4.51 | -4.18 | -4.86 | -5.26 | -5.42 | -4.50 | -1.67 |
| $J_{LF}$ (dB) | 0.12 | 0.14 | 0.13 | 0.11 | 0.07 | 0.05 | 0.12 | 0.11 |
| C80 (dB) | -0.61 | 1.61 | 1.57 | 2.84 | 4.63 | 5.82 | 2.25 | 2.85 |
| G (dB) | 7.91 | 6.52 | 6.46 | 6.76 | 7.68 | 9.73 | 6.61 | 9.89 |

## Measured Parameter Values: Auralization from Set 3 Number 8

| Parameter | Measured Octave Band Parameter Values | | | | | | | |
|---|---|---|---|---|---|---|---|---|
| | 125 Hz | 250 Hz | 500 Hz | 1000 Hz | 2000 Hz | 4000 Hz | 500 - 1000 Avg. | 250 - 1000 Avg. |
| EDT (s) | 3.59 | 2.78 | 2.85 | 2.49 | 2.45 | 2.28 | 2.67 | 2.64 |
| T20 (s) | 2.79 | 2.75 | 2.36 | 2.15 | 2.04 | 1.70 | 2.26 | 2.33 |
| T30 (s) | 2.82 | 2.56 | 2.30 | 2.06 | 1.94 | 1.68 | 2.18 | 2.21 |
| $L_J$ (dB) | -0.84 | -3.37 | -2.41 | -2.76 | -3.54 | -3.67 | -2.58 | 0.01 |
| $J_{LF}$ (dB) | 0.12 | 0.16 | 0.14 | 0.11 | 0.07 | 0.05 | 0.13 | 0.12 |
| C80 (dB) | -2.22 | -0.82 | -1.84 | -0.91 | 0.33 | 1.79 | -1.35 | -0.74 |
| G (dB) | 7.88 | 6.44 | 5.94 | 6.26 | 7.12 | 8.77 | 6.11 | 9.47 |

## Measured Parameter Values: Auralization from Set 4 Number 1

| Parameter | Measured Octave Band Parameter Values | | | | | | | |
|---|---|---|---|---|---|---|---|---|
| | 125 Hz | 250 Hz | 500 Hz | 1000 Hz | 2000 Hz | 4000 Hz | 500 - 1000 Avg. | 250 - 1000 Avg. |
| EDT (s) | 2.47 | 1.71 | 1.75 | 1.50 | 1.52 | 1.40 | 1.62 | 1.62 |
| T20 (s) | 1.98 | 1.54 | 1.38 | 1.34 | 1.24 | 1.15 | 1.36 | 1.38 |
| T30 (s) | 1.85 | 1.58 | 1.37 | 1.28 | 1.21 | 1.11 | 1.33 | 1.36 |
| $L_J$ (dB) | -1.54 | -5.31 | -5.94 | -5.46 | -6.13 | -5.45 | -5.70 | -2.69 |
| $J_{LF}$ (dB) | 0.14 | 0.14 | 0.16 | 0.11 | 0.10 | 0.08 | 0.14 | 0.13 |
| C80 (dB) | -3.15 | -1.27 | -2.25 | -1.54 | -1.70 | -0.79 | -1.88 | -1.67 |
| G (dB) | 5.51 | 4.89 | 3.21 | 3.91 | 4.71 | 6.49 | 3.57 | 7.24 |

## Measured Parameter Values: Auralization from Set 4 Number 2

| Parameter | Measured Octave Band Parameter Values | | | | | | | |
|---|---|---|---|---|---|---|---|---|
| | 125 Hz | 250 Hz | 500 Hz | 1000 Hz | 2000 Hz | 4000 Hz | 500 - 1000 Avg. | 250 - 1000 Avg. |
| EDT (s) | 3.17 | 2.74 | 2.42 | 2.40 | 2.26 | 1.93 | 2.41 | 2.45 |
| T20 (s) | 2.94 | 2.31 | 2.11 | 1.84 | 1.73 | 1.48 | 1.97 | 2.00 |
| T30 (s) | 2.79 | 2.58 | 2.23 | 1.92 | 1.80 | 1.53 | 2.08 | 2.13 |
| $L_J$ (dB) | 1.08 | -2.70 | -2.87 | -2.61 | -2.63 | -2.20 | -2.74 | 0.31 |
| $J_{LF}$ (dB) | 0.16 | 0.15 | 0.17 | 0.13 | 0.11 | 0.08 | 0.15 | 0.14 |
| C80 (dB) | -5.93 | -3.48 | -5.64 | -5.44 | -5.00 | -3.77 | -5.54 | -4.80 |
| G (dB) | 8.05 | 6.68 | 5.67 | 6.44 | 7.08 | 8.51 | 6.07 | 9.51 |

## Measured Parameter Values: Auralization from Set 4 Number 3

| Parameter | Measured Octave Band Parameter Values | | | | | | | |
|---|---|---|---|---|---|---|---|---|
| | 125 Hz | 250 Hz | 500 Hz | 1000 Hz | 2000 Hz | 4000 Hz | 500 - 1000 Avg. | 250 - 1000 Avg. |
| EDT (s) | 2.19 | 1.73 | 1.64 | 1.47 | 1.50 | 1.52 | 1.56 | 1.59 |
| T20 (s) | 2.07 | 1.82 | 1.58 | 1.46 | 1.37 | 1.21 | 1.52 | 1.56 |
| T30 (s) | 1.90 | 1.68 | 1.46 | 1.32 | 1.26 | 1.17 | 1.39 | 1.43 |
| $L_J$ (dB) | -5.14 | -7.86 | -8.09 | -8.70 | -10.06 | -9.48 | -8.38 | -5.58 |
| $J_{LF}$ (dB) | 0.10 | 0.13 | 0.16 | 0.11 | 0.08 | 0.06 | 0.13 | 0.12 |
| C80 (dB) | 0.35 | -0.12 | -1.15 | 0.85 | 1.73 | 2.52 | -0.04 | 0.46 |
| G (dB) | 3.39 | 1.25 | 0.30 | 1.03 | 2.01 | 3.78 | 0.68 | 4.20 |

## Measured Parameter Values: Auralization from Set 4 Number 4

| Parameter | Measured Octave Band Parameter Values | | | | | | | |
|---|---|---|---|---|---|---|---|---|
| | 125 Hz | 250 Hz | 500 Hz | 1000 Hz | 2000 Hz | 4000 Hz | 500 - 1000 Avg. | 250 - 1000 Avg. |
| EDT (s) | 3.58 | 2.97 | 2.64 | 2.49 | 2.36 | 2.04 | 2.57 | 2.62 |
| T20 (s) | 2.81 | 2.38 | 2.17 | 1.99 | 1.80 | 1.70 | 2.08 | 2.09 |
| T30 (s) | 2.79 | 2.50 | 2.17 | 1.96 | 1.77 | 1.59 | 2.06 | 2.10 |
| $L_J$ (dB) | -2.14 | -5.47 | -6.00 | -5.70 | -6.62 | -6.06 | -5.85 | -2.92 |
| $J_{LF}$ (dB) | 0.10 | 0.13 | 0.16 | 0.11 | 0.08 | 0.07 | 0.13 | 0.12 |
| C80 (dB) | -2.96 | -2.68 | -4.44 | -2.70 | -2.50 | -1.04 | -3.49 | -3.01 |
| G (dB) | 6.17 | 3.49 | 2.48 | 3.11 | 4.32 | 5.50 | 2.81 | 6.41 |

## Measured Parameter Values: Auralization from Set 4 Number 5

| Parameter | Measured Octave Band Parameter Values | | | | | | | |
|---|---|---|---|---|---|---|---|---|
| | 125 Hz | 250 Hz | 500 Hz | 1000 Hz | 2000 Hz | 4000 Hz | 500 - 1000 Avg. | 250 - 1000 Avg. |
| EDT (s) | 2.02 | 1.73 | 1.63 | 1.58 | 1.53 | 1.55 | 1.60 | 1.62 |
| T20 (s) | 1.91 | 1.83 | 1.34 | 1.27 | 1.22 | 1.17 | 1.30 | 1.41 |
| T30 (s) | 1.84 | 1.72 | 1.43 | 1.30 | 1.23 | 1.17 | 1.36 | 1.42 |
| $L_J$ (dB) | -6.20 | -9.05 | -9.67 | -10.72 | -11.29 | -10.67 | -10.16 | -7.09 |
| $J_{LF}$ (dB) | 0.12 | 0.18 | 0.14 | 0.11 | 0.07 | 0.06 | 0.12 | 0.12 |
| C80 (dB) | -1.18 | -0.22 | 0.09 | 1.53 | 2.58 | 3.92 | 0.87 | 4.15 |
| G (dB) | 2.72 | 0.17 | -0.40 | 0.12 | 1.10 | 2.98 | -0.13 | 3.29 |

## Measured Parameter Values: Auralization from Set 4 Number 6

| Parameter | Measured Octave Band Parameter Values | | | | | | | |
|---|---|---|---|---|---|---|---|---|
| | 125 Hz | 250 Hz | 500 Hz | 1000 Hz | 2000 Hz | 4000 Hz | 500 - 1000 Avg. | 250 - 1000 Avg. |
| EDT (s) | 3.11 | 3.24 | 2.85 | 2.50 | 2.35 | 2.16 | 2.67 | 2.73 |
| T20 (s) | 2.54 | 2.35 | 2.32 | 2.05 | 2.01 | 1.71 | 2.18 | 2.18 |
| T30 (s) | 2.67 | 2.43 | 2.25 | 2.02 | 1.89 | 1.64 | 2.13 | 2.15 |
| $L_J$ (dB) | -3.48 | -6.05 | -6.49 | -6.95 | -7.35 | -7.32 | -6.71 | -3.67 |
| $J_{LF}$ (dB) | 0.12 | 0.19 | 0.15 | 0.11 | 0.07 | 0.06 | 0.13 | 0.13 |
| C80 (dB) | -3.45 | -2.65 | -3.09 | -2.08 | -1.07 | 0.33 | -2.56 | 0.86 |
| G (dB) | 4.99 | 2.28 | 1.38 | 2.04 | 2.87 | 4.43 | 1.72 | 5.19 |

## Measured Parameter Values: Auralization from Set 4 Number 7

| Parameter | Measured Octave Band Parameter Values | | | | | | | |
|---|---|---|---|---|---|---|---|---|
| | 125 Hz | 250 Hz | 500 Hz | 1000 Hz | 2000 Hz | 4000 Hz | 500 - 1000 Avg. | 250 - 1000 Avg. |
| EDT (s) | 2.00 | 1.71 | 1.63 | 1.61 | 1.53 | 1.45 | 1.62 | 1.62 |
| T20 (s) | 1.86 | 1.68 | 1.52 | 1.31 | 1.27 | 1.17 | 1.42 | 1.45 |
| T30 (s) | 1.89 | 1.64 | 1.49 | 1.33 | 1.27 | 1.17 | 1.41 | 1.43 |
| $L_J$ (dB) | -8.45 | -11.79 | -11.50 | -12.18 | -12.59 | -12.76 | -11.83 | -8.98 |
| $J_{LF}$ (dB) | 0.12 | 0.14 | 0.13 | 0.11 | 0.07 | 0.05 | 0.12 | 0.11 |
| C80 (dB) | -0.57 | 1.63 | 1.58 | 2.85 | 4.64 | 5.82 | 2.26 | 2.86 |
| G (dB) | 0.66 | -0.75 | -0.86 | -0.57 | 0.35 | 2.39 | -0.71 | 2.58 |

## Measured Parameter Values: Auralization from Set 4 Number 8

| Parameter | Measured Octave Band Parameter Values | | | | | | | |
|---|---|---|---|---|---|---|---|---|
| | 125 Hz | 250 Hz | 500 Hz | 1000 Hz | 2000 Hz | 4000 Hz | 500 - 1000 Avg. | 250 - 1000 Avg. |
| EDT (s) | 3.59 | 2.78 | 2.85 | 2.49 | 2.46 | 2.28 | 2.67 | 2.64 |
| T20 (s) | 2.75 | 2.75 | 2.36 | 2.15 | 2.04 | 1.70 | 2.26 | 2.33 |
| T30 (s) | 2.78 | 2.56 | 2.30 | 2.06 | 1.94 | 1.68 | 2.18 | 2.21 |
| $L_J$ (dB) | -5.88 | -8.42 | -7.49 | -7.84 | -8.63 | -8.81 | -7.66 | -5.06 |
| $J_{LF}$ (dB) | 0.12 | 0.15 | 0.14 | 0.11 | 0.07 | 0.05 | 0.13 | 0.12 |
| C80 (dB) | -2.18 | -0.79 | -1.83 | -0.90 | 0.34 | 1.78 | -1.34 | -0.73 |
| G (dB) | 2.84 | 1.39 | 0.86 | 1.17 | 2.02 | 3.67 | 1.02 | 4.39 |

# Appendix I: MATLAB Simulation Code

Contained in this appendix is the MATLAB code used to simulate Ambisonic RIRs, as was described in Chapter 4. The main script is entitled RoomSynthesis.m, and a folder of supporting functions is provided along with it. This script and the supporting functions are included as code below.

```
% This script compiles all of the functions and input parameters into a
% single spot to perform simple room simulate for a rectangular geometry.
% This code was developed by Matthew Neal for his MS Thesis (2015) and
% creates third-order Ambisonic IRs. The first section simulates the room
% and the Ambisonic IR for the room. The second section creates an
% Ambisonic auralization. The third section plots the room, source, receiver,
% and image source locations. The fourth section plots the impulse response
and
% the octave-filtered impulse response, both omnidirectional. The fifth
% section plots the early and late part of the IR separately, separated by
% the image source simulation and the statistical reverberation simulation.
% The sixth section plots a polar reflection diagram in azimuth for
% direct sound and image source early reflections. The final section,
% section seven, plots a two dimensional energy histogram, showing the
% directional distribution of reflections after a desired cut-on time in
% the impulse response. This is helpful for assessing the directional
% performance of the weighted late reverberation.

% Start timer to time simulation
tic;

% add path to the functions from this script
addpath 'Room Simulation Functions';

% clear current variables and workspace
clear;
clc;
close all;

% define room size [length,width,height], source and receiver locations
% [x,y,z] where x is measured from the back wall, y is measured from the
% right sidewall, and z is measured from the floor.
room = 1.2*[160,75,61];
source = [room(1)-20,room(2)/2,8];
receiver = [room(1)-80,room(2)/2-4,4];

% specify the units in which the room dimensions and source-receiver
% locations are given. either 'feet' or 'meters'.
units = 'feet';

% specify absorption coefficients of the wall materials. You can also add
% multipliers out front of individual materials to scale / change their
% absorption coefficients.
floor = [0.4 0.56 0.68 0.79 0.83 0.86 0.86 0.86];
```

```
ceiling = [0.05 0.02 0.02 0.03 0.04 0.04 0.03 0.03];
leftsidewall = [0.05 0.02 0.02 0.03 0.04 0.04 0.03 0.03];
rightsidewall = [0.05 0.02 0.02 0.03 0.04 0.04 0.03 0.03];
backwall = [0.05 0.02 0.02 0.03 0.04 0.04 0.03 0.03];
frontwall = [0.05 0.02 0.02 0.03 0.04 0.04 0.03 0.03];

% this adjustment allows you to equally scale all of the absorption
% coefficients for the room over all materials and all octave bands.
adj = 1;

% the room adjustment allows you to scale all materials, but do so
% separately for each octave band. This helps if you are trying to 'tune'
% the performance of T30 for one hall setting to another over octave bands.
room_abs_adjust = adj*[1,1,1,1,1,1,1,1];
floor = floor.*room_abs_adjust;
ceiling = ceiling.*room_abs_adjust;
leftsidewall = leftsidewall.*room_abs_adjust;
rightsidewall = rightsidewall.*room_abs_adjust;
backwall = backwall.*room_abs_adjust;
frontwall = frontwall.*room_abs_adjust;

% Assign scattering coefficients to the wall materials. These coefficients
% will attenuate the early reflections, making them less strong if higher
% scattering coefficients are used. They do not impact the statistical
% reverberation simulation.

% NOTE: Scattering coefficients are frequency dependent (lower at lower
% frequencies) so be sure to take this into account. For sample values of
% scattering coefficients, please see the Odeon manual, v.11, page 6.75.
floor_scat = [0.02 0.05 0.3 0.72 0.88 0.9 0.92 0.93];
ceiling_scat = [0.01 0.01 0.03 0.04 0.1 0.2 0.25 0.3];
leftsidewall_scat = [0.01 0.01 0.03 0.04 0.1 0.2 0.25 0.3];
rightsidewall_scat = [0.01 0.01 0.03 0.04 0.1 0.2 0.25 0.3];
backwall_scat = [0.01 0.01 0.03 0.04 0.1 0.2 0.25 0.3];
frontwall_scat = [0.01 0.01 0.03 0.04 0.1 0.2 0.25 0.3];

% Weighted Directional Reverb: these adjustments begin to focus the
% reverberant energy into particular directions, while still randomizing
% the overall directions of the energy. The directional processing is
% contained in the ReverbDirections function.

% NOTE: The realism of highly directional reverb could be questions, so
% keep this under consideration when creating auralizations that are
% directionally weighted. The default is to assume a diffuse late
% reverberant energy, where all factors are zero except the omni factor.
Dweights = zeros(18,1);
Dweights(1) = 100; %Omni (all uniformly)
Dweights(2) = 0; %Front (from
Dweights(3) = 0; %Front Right
Dweights(4) = 0; %Right
Dweights(5) = 0; %Back Right
Dweights(6) = 0; %Back
Dweights(7) = 0; %Back Left
Dweights(8) = 0; %Left
Dweights(9) = 0; %Front Left
Dweights(10) = 0; %Front Top
```

```
Dweights(11) = 0; %Right Top
Dweights(12) = 0; %Back Top
Dweights(13) = 0; %Left Top
Dweights(14) = 0; %Top
Dweights(15) = 0; %Front Bottom
Dweights(16) = 0; %Right Bottom
Dweights(17) = 0; %Back Bottom
Dweights(18) = 0; %Left Bottom
Dweights(19) = 0; %Bottom

% A reverberant energy scale factor can be applied, which will simply scale
% the reverberant energy, increased or decreased, to manipulate the late
% part of the IR, without changing the early part.
Reverb_Scale = 1.0;

% Specify impulse response parameters. Ensure that the impulse response is
% long enough for the room being simulated.
fs = 44100;      %Sampling Rate
N = 3;           %Image Source order (1, 2, or 3)
IRLength = 5;    %Impulse response length in seconds
EQ = 'off';
SaveData = 'off';
SaveDataName = 'Auralization1';

mixing_point = 0.08;       % Center point in time (seconds) at which the
impulse response will switch from the image source to the reverberant
simulated energy
mixing_time = 0.005;     % length of time, in seconds, over which the
simulation will transition between image source and reverberant simulation.
short is quick and long is gradual.

% Parameters defined for the start and end of the time windows for each
% simulation type
IS_mix_end = mixing_point + mixing_time;
REV_mix_start = mixing_point - mixing_time;

% This function calculates the levels, time delays, azimuths, and
% elevations up to the specified image order for the simulated room.
[IS_levels,IS_timedelays,IS_azimuths,IS_elevations] =
ISLevels(room,source,receiver,units,N,floor,ceiling,leftsidewall,rightsidewal
l,backwall,frontwall,floor_scat,ceiling_scat,leftsidewall_scat,rightsidewall_
scat,backwall_scat,frontwall_scat,IRLength,fs,IS_mix_end,mixing_point);
currenttime=toc;
fprintf('Image source method complete. (time = %3.2f s)\nOrder =
%1.0f\n',currenttime,N);
tic;

% This functions simulated the levels, time delays, azimuths, and
% elevations for the reverberant reflections. It also outputs a time vector
% for the simulated impulse response.
[Rev_levels,Rev_azimuths,Rev_elevations,Rev_timedelays] =
ReverbSim(IRLength,room,units,floor,ceiling,leftsidewall,rightsidewall,backwa
ll,frontwall,fs,source,receiver,mixing_point,REV_mix_start,Dweights,Reverb_Sc
ale);
currenttime=toc;
```

```
fprintf('Reverberant energy simulation complete. (time = %3.2f
s)\n',currenttime);
tic;

% This function takes the level, time-delay, and directional information,
% and creates third-order Ambisonic impulse responses of the room.
[SpHarmIRs,OctspharmIRs,OctISspharmIRs,OctREVspahrmIRs] =
SphericalHarmonics(IRLength,fs,IS_levels,Rev_levels,IS_timedelays,Rev_timedel
ays,IS_elevations,Rev_elevations,IS_azimuths,Rev_azimuths,N);
currenttime=toc;
fprintf('Ambisonic & spherical harmonics processing complete. (time = %3.2f
s)\n',currenttime);
toc;

% Perform optional level equalization, where level will be set to the
% target dB level set. The target dB level is arbitrary, as long as all
% levels are equal. Note that level equalization will change parameters
% such as strength (G) and Late Lateral Energy Level (Lj). The result is a
% scaled version of each Ambisonic impulse response.
if strcmp(EQ,'on') == 1
    target_level = -40;
    [SpHarmIRs_withEQ,Actual_Lp,Scaling_Factor] =
Level_Adjusted(SpHarmIRs,target_level);
    fprintf('Level equalization complete.\n');
elseif strcmp(EQ,'off') == 1
    Scaling_Factor = 1;
else
    error('Please specity either ''on'' or ''off'' for level
equalization.\n');
end

fprintf('Impulse response simulaiton done.\n');

% calculate EDT, T20, T30, and C80 for the impulse response, and store the
% values in the variable parameters.
[RT] = calc_RT(SpHarmIRs(:,1),fs);
[C80] = calc_C80(SpHarmIRs(:,1),fs);
Parameters = [RT;C80];

% plot the early decay time, T20, and T30 for the calculated impulse
% response
figure();
bar(RT');
legend('EDT','T20','T30');
xlabel('Octave Bands: 125-4000 [Hz]');
ylabel('Value [s]');

% plot the clarity index for the impulse response
figure();
bar(C80');
xlabel('Octave Bands: 125-4000 [Hz]');
ylabel('Clarity Index [dB]');
fprintf('Parameter calculations complete.\n');

% If data saving is turned on, it will save all relevant parameter values
```

```
% as a .mat file containing all simulation variables needed to recreate or
% save the current simulation.
if strcmp(SaveData,'on') == 1
    if strcmp(EQ,'on') == 1

save(SaveDataName,'room','source','receiver','Dweights','units','floor','ceil
ing','leftsidewall','rightsidewall','backwall','frontwall','floor_scat','ceil
ing_scat','leftsidewall_scat','rightsidewall_scat','backwall_scat','frontwall
_scat','fs','N','IRLength','EQ','mixing_point','mixing_time','IS_levels','IS_
timedelays','IS_azimuths','IS_elevations','Rev_levels','Rev_azimuths','Rev_el
evations','Rev_timedelays','t','reverbalpha','SpHarmIRs','OctspharmIRs','OctI
SspharmIRs','OctREVspahrmIRs','Scaling_Factor','SpHarmIRs_withEQ');
    elseif strcmp(EQ,'off') == 1

save(SaveDataName,'room','source','receiver','Dweights','units','floor','ceil
ing','leftsidewall','rightsidewall','backwall','frontwall','floor_scat','ceil
ing_scat','leftsidewall_scat','rightsidewall_scat','backwall_scat','frontwall
_scat','fs','N','IRLength','EQ','mixing_point','mixing_time','IS_levels','IS_
timedelays','IS_azimuths','IS_elevations','Rev_levels','Rev_azimuths','Rev_el
evations','Rev_timedelays','t','reverbalpha','SpHarmIRs','OctspharmIRs','OctI
SspharmIRs','OctREVspahrmIRs','Scaling_Factor');
    end
elseif strcmp(SaveData,'off') == 1
    fprintf('Data not saved.\n');
else
    error('Please specify the SaveData variable as either ''on'' or
''off''.');
end

fprintf('\nDone.\n');

totaltime = toc;
fprintf('\nTotal simulation time was %5.2f seconds.\n',totaltime);
%%

% read in the anechoic file used to create the final auralization. Replace
% the text below with the desired anechoic file;
anechoic = audioread('Track5.wav');
fprintf('Anechoic file loaded.\n');

% Set a file name for the final auralization to be saved as.
audiofilename = 'Set1number1.wav';

% Choose whether to use the equalized or unequalized version of the .wav
% file for the Ambisonic fftfilt.
if strcmp(EQ,'on') == 1
    AmbisonicIR = SpHarmIRs_withEQ;
elseif strcmp(EQ,'off') == 1
    AmbisonicIR = SpHarmIRs;
end

% filter the anechoic music with the IR for each separate Ambisonic signal,
% and create a final 16 channel auralization of all 16 Ambisonic
% components.
AmbisonicSignals = Ambisonic_fftfilt(anechoic,AmbisonicIR);
fprintf('Anechoic filtering with Ambisonic IRs complete.\n');
```

```
% Report final level of auralization.
Final_Level = 20*log10(sqrt(mean(mean(AmbisonicSignals.^2))));
fprintf('The final relative level of the auralization is %4.2f
dB.\n\nDone.\n',Final_Level);

% write final audio file
audiowrite(audiofilename,AmbisonicSignals,fs,'BitsPerSample',32);

%%

% This section will plot the simulated room with the source, receiver, and
% image source locations
figure();
ImageSourcePlot(room,source,receiver,N);
xlim([-3*room(1) 4*room(1)]);
ylim([-3*room(2) 4*room(2)]);
zlim([-3*room(3) 4*room(3)]);
view(3);

%%

% Calculate the time-vector for the impulse response.
Points = round(IRLength*fs);
dt = 1/fs;
t = (0:1:(Points-1))*dt;

% Plot the omnidirectional impulse response for the room.
figure();
plot(t,SpHarmIRs(:,1));
title('Full Frequency IR');

% Plot the different octave bands of the impulse response, overlaid upon
% one another.
figure();
plot(t,OctspharmIRs(:,1,8),'k');
hold on;
plot(t,OctspharmIRs(:,1,7),'r');
plot(t,OctspharmIRs(:,1,6),'b');
plot(t,OctspharmIRs(:,1,5),'y');
plot(t,OctspharmIRs(:,1,4),'c');
plot(t,OctspharmIRs(:,1,3),'g');
plot(t,OctspharmIRs(:,1,2),'m');
plot(t,OctspharmIRs(:,1,1),'k');
legend('8000 Hz','4000 Hz','2000 Hz','1000 Hz','500 Hz','250 Hz','125 Hz','63
Hz');
title('Octave Band Filtered IR');

%%

% Plot both the early and late part of the impulse response overlaid with
% each other, found from the image source and statistical reverberation
% respectively.
figure();
plot(t,sum(OctISspharmIRs(:,1,:),3),'k');
```

```
hold on;
plot(t,sum(OctREVspahrmIRs(:,1,:),3),'r');
plot(t,sum(OctISspharmIRs(:,1,:),3),'k');

%%

% Plot a polar azimuthal diagram of the direct sound and early reflections
from the
% image source method, showing a top view of the receiver, looking down
ISPolarReflection(IS_azimuths,IS_levels,N);

%%

% This section will create plot showing the directional distribution of
% the late energy in a histogram type data format. The impulse response is
% analyzed at a particular starting time, and reflections occurring after
% that time are grouped into directional bins. This shows the azimuthal and
% elevation based directional dependence of the impulse response after a
% specified cut-on time.

% specify resolution of azimuth and elevation histogram (center number in
% array population code
azsteps =-180:5:180;
elsteps = -90:5:90;
[elgrid,azgrid] = meshgrid(elsteps,azsteps);

% create matrix to populate reflections into
reflections = zeros(size(azgrid));

% combine image source and reverberant simulation methods together
Total_levels = sum([IS_levels Rev_levels],3);
Total_timedelays = [IS_timedelays;Rev_timedelays];
Total_Az = [IS_azimuths;Rev_azimuths];
Total_El = [IS_elevations;Rev_elevations];

% specify a start time to begin analyzing the 'late' energy
T_cuton = 0.07;

% Populate individual reflections into their corresponding azimuth &
% elevation bin, only if they occur after the specified time in the impulse
% response.
for zz=1:length(Total_levels)
    if Total_timedelays(zz) >= (T_cuton + IS_timedelays(1))
        for pp=1:(length(azsteps)-1)
            for qq=1:(length(elsteps)-1)
                if Total_Az(zz) >= azsteps(pp) && Total_Az(zz) <
azsteps(pp+1)
                    if Total_El(zz) >= elsteps(qq) && Total_El(zz) <
elsteps(qq+1)
                        reflections(pp,qq) = reflections(pp,qq) +
Total_levels(zz);
                    end
                end
            end
        end
```

```
    end
end
reflections = reflections/max(reflections(:));

% produce a plot showing the directional histogram of the energy and
% reflections occurring after the specified cut-on time.
figure(100);
surf(azgrid,elgrid,db(abs(reflections)));
view([0 90]);
axis equal;
colorbar;
caxis([-50 0]);
```

```
function [OctaveLevels,TimeDelays,Azimuths,Elevations] =
ISLevels(dimensions,source,receiver,units,ImageOrder,floor,ceiling,leftsidewa
ll,rightsidewall,backwall,frontwall,floor_scat,ceiling_scat,leftsidewall_scat
,rightsidewall_scat,backwall_scat,frontwall_scat,IRLength,fs,mix_time,mix_sta
rt)
%This function calculates the image source locations for a specific source
%in a rectangular room of a certain size. Image source locations are
%calculated for either first, second, or third order, and then, the
%locations are adjusted so that they are given in distances from the
%receiver location, and azimuth and elevation values when the receiver is
%pointed at the source. Finally, time delays are calculated based upon the
%speed of sound (in feet or meters), and the levels are attenuated for
%spherical spreading, air absorption, wall absorption, and wall scattering.

% First input room parameters and source/receiver locations
length_o = dimensions(1);
width = dimensions(2);
height = dimensions(3);
N = ImageOrder;

% check to see if maximum possible image order is exceeded.
if N>3
    error('Exceeded Max Image Source Order for this model!!!');
else

% define speed of sound based upon units
if strcmp(units,'meters') == 1
    c = 343;
elseif strcmp(units,'feet') == 1
    c = 343*100/2.54/12;
else
    disp('Improper Units specified. Please enter either ''meters'' or
''feet''.');
end

% define vector to contain x,y,z location of images, relative to coordinate
% axes
if N==1
    Numimages = 7;
elseif N==2
    Numimages = 25;
elseif N==3
    Numimages = 63;
end
locations = zeros(Numimages,3);
% Compute image source locations, all defined by the coordinate axes and
% equations defined in Matthew Neal's thesis.
if N >= 1
    locations(1,1:3) = [source(1),source(2),source(3)];
    locations(2,1:3) = [source(1),source(2),-source(3)];
    locations(3,1:3) = [source(1),2*width-source(2),source(3)];
    locations(4,1:3) = [-source(1),source(2),source(3)];
    locations(5,1:3) = [2*length_o-source(1),source(2),source(3)];
    locations(6,1:3) = [source(1),-source(2),source(3)];
    locations(7,1:3) = [source(1),source(2),2*height-source(3)];
end
```

```
if N >= 2
    locations(8,1:3) = [source(1),2*width-source(2),-source(3)];
    locations(9,1:3) = [-source(1),source(2),-source(3)];
    locations(10,1:3) = [2*length_o-source(1),source(2),-source(3)];
    locations(11,1:3) = [source(1),-source(2),-source(3)];
    locations(12,1:3) = [source(1),source(2),2*height+source(3)];
    locations(13,1:3) = [-source(1),2*width-source(2),source(3)];
    locations(14,1:3) = [2*length_o-source(1),2*width-source(2),source(3)];
    locations(15,1:3) = [source(1),-2*width+source(2),source(3)];
    locations(16,1:3) = [source(1),2*width-source(2),2*height-source(3)];
    locations(17,1:3) = [2*length_o+source(1),source(2),source(3)];
    locations(18,1:3) = [-source(1),-source(2),source(3)];
    locations(19,1:3) = [-source(1),source(2),2*height-source(3)];
    locations(20,1:3) = [-2*length_o+source(1),source(2),source(3)];
    locations(21,1:3) = [2*length_o-source(1),-source(2),source(3)];
    locations(22,1:3) = [2*length_o-source(1),source(2),2*height-source(3)];
    locations(23,1:3) = [source(1),2*width+source(2),source(3)];
    locations(24,1:3) = [source(1),-source(2),2*height-source(3)];
    locations(25,1:3) = [source(1),source(2),-2*height+source(3)];
end
if N >= 3
    locations(26,1:3) = [-source(1),2*width-source(2),-source(3)];
    locations(27,1:3) = [2*length_o-source(1),2*width-source(2),-source(3)];
    locations(28,1:3) = [source(1),2*width-source(2),2*height+source(3)];
    locations(29,1:3) = [-source(1),-source(2),-source(3)];
    locations(30,1:3) = [-source(1),source(2),2*height+source(3)];
    locations(31,1:3) = [2*length_o-source(1),-source(2),-source(3)];
    locations(32,1:3) = [2*length_o-source(1),source(2),2*height+source(3)];
    locations(33,1:3) = [source(1),-source(2),2*height+source(3)];
    locations(34,1:3) = [source(1),source(2),-2*height-source(3)];
    locations(35,1:3) = [-source(1),-2*width+source(2),source(3)];
    locations(36,1:3) = [-source(1),2*width-source(2),2*height-source(3)];
    locations(37,1:3) = [2*length_o-source(1),-2*width+source(2),source(3)];
    locations(38,1:3) = [2*length_o-source(1),2*width-source(2),2*height-
source(3)];
    locations(39,1:3) = [source(1),-2*width+source(2),-source(3)];
    locations(40,1:3) = [source(1),4*width-source(2),source(3)];
    locations(41,1:3) = [source(1),-2*width+source(2),2*height-source(3)];
    locations(42,1:3) = [2*length_o+source(1),source(2),-source(3)];
    locations(43,1:3) = [2*length_o+source(1),2*width-source(2),source(3)];
    locations(44,1:3) = [-2*length_o-source(1),source(2),source(3)];
    locations(45,1:3) = [2*length_o+source(1),-source(2),source(3)];
    locations(46,1:3) = [2*length_o+source(1),source(2),2*height-source(3)];
    locations(47,1:3) = [-source(1),-source(2),2*height-source(3)];
    locations(48,1:3) = [-2*length_o+source(1),source(2),-source(3)];
    locations(49,1:3) = [-2*length_o+source(1),2*width-source(2),source(3)];
    locations(50,1:3) = [4*length_o-source(1),source(2),source(3)];
    locations(51,1:3) = [-2*length_o+source(1),-source(2),source(3)];
    locations(52,1:3) = [-2*length_o+source(1),source(2),2*height-source(3)];
    locations(53,1:3) = [2*length_o-source(1),-source(2),2*height-source(3)];
    locations(54,1:3) = [source(1),2*width+source(2),-source(3)];
    locations(55,1:3) = [-source(1),2*width+source(2),source(3)];
    locations(56,1:3) = [2*length_o-source(1),2*width+source(2),source(3)];
    locations(57,1:3) = [source(1),-2*width-source(2),source(3)];
    locations(58,1:3) = [source(1),2*width+source(2),2*height-source(3)];
    locations(59,1:3) = [source(1),2*width-source(2),-2*height+source(3)];
```

```
    locations(60,1:3) = [-source(1),source(2),-2*height+source(3)];
    locations(61,1:3) = [2*length_o-source(1),source(2),-2*height+source(3)];
    locations(62,1:3) = [source(1),-source(2),-2*height+source(3)];
    locations(63,1:3) = [source(1),source(2),4*height-source(3)];
end
% determine IS locations and source location relative to receiver locations
location_rel_receiver = locations - [ones(Numimages,1)*receiver(1)
ones(Numimages,1)*receiver(2) ones(Numimages,1)*receiver(3)];
source_rel_receiver = source - receiver;

% compute azimuth and elevation of the source relative to the x axis
% extending from the receiver (the length dimension of the room). compute
% the distance from the source to the receiver
source_az = atan2(source_rel_receiver(2),source_rel_receiver(1))*(180/pi);
source_elev = 90 - acosd(source_rel_receiver(3)/sqrt(source_rel_receiver(1)^2
+ source_rel_receiver(2)^2 + source_rel_receiver(3)^2));
SRdistance = sqrt(source_rel_receiver(1)^2 + source_rel_receiver(2)^2 +
source_rel_receiver(3)^2);

% compute the distance, azimuth, and elevation from the receiver to each
% image source, and rotate the coordinate axes so that the receiver is
% facing the source, by subtracting off the source azimuth and elevation
% of the source. Also, make distances all relative to the Source-Receiver
% distance by subtracting the source-receiver distance from each IS
% distance.
distances = sqrt(location_rel_receiver(:,1).^2 +
location_rel_receiver(:,3).^2 + location_rel_receiver(:,2).^2);
Azimuths = (-
atan2(location_rel_receiver(:,2),location_rel_receiver(:,1)))*(180/pi) -
source_az*ones(Numimages,1);
Elevations = 90*ones(Numimages,1) -
acosd(location_rel_receiver(:,3)./distances) - source_elev*ones(Numimages,1);

% Computer time delays, all relative to a time of zero, when sound is
% emitted from the source. This means that the direct sound will be
% delayed by the propagation time from source to receiver.
TimeDelays = distances/c;

% Compute air attenuation on a dB per 100 m basis. Performed according to
% ISO standard.
bandnumber = 18:3:39;
centers = 1000*2.^((bandnumber-30)/3);
AirAbs = zeros(length(centers),1);

for nn=1:length(centers)
    AirAbs(nn,1) = AirAbsorption(centers(nn),293.15,50,101325);
end

% Convert air attenuation as an alpha attenuation per foot basis. See
% thesis for details of derivation.
if strcmp(units,'meters') == 1
    AirAbs = (AirAbs./100);
elseif strcmp(units,'feet') == 1
    AirAbs = (AirAbs./100)*(1/100)*(2.54/1)*(12/1);
end
```

```
% Create a time window with indices corresponding to the given time, to
% multiply and apply a transition time for the image source reflections.
% This is based upon the location of the direct sound, then a mixing start
% time, which is a certain amount of time after the direct sound in which the
% time window begins, and a mixing length, which is the length in seconds of
% the window until it is equal to zero.
direct_delay = round(fs*sqrt((source(1)-receiver(1))^2 + (source(2)-
receiver(2))^2 + (source(3)-receiver(3))^2)/c);
window = zeros(1,round(IRLength*fs));
temp = hann(round(2*fs*(mix_time-mix_start)))';
transition = temp(1,round(length(temp)/2):end);
window(1,(round(fs*mix_time)-
length(transition)+1+direct_delay):round(fs*mix_time)+direct_delay) =
transition;
window(1,1:(round(fs*mix_start)+direct_delay)) =
ones(1,round(fs*mix_start)+direct_delay);


OctaveLevels = ones(8,Numimages);

% Apply attenuation due to spherical spreading, wall absorption, and air
% absorption, for each image source in each octave band. Do it for certain
% images sources depending upon the specified image source order.
% Additionally, the weightings from the time window are also applied here,
% corresponding to the time delay in which they are input into the impulse
% response.

% if first, second, or third order image source methods is selected.
if N>=1
    for n = 1:length(centers)
        OctaveLevels(n,1) = (1/distances(1))*10.^(-
AirAbs(n,1)*distances(1)/20)*window(round(fs*TimeDelays(1)))/8;
        OctaveLevels(n,2) = (1/distances(2))*(1-floor(n))*(1-
floor_scat(n))*10.^(-
AirAbs(n,1)*distances(2)/20)*window(round(fs*TimeDelays(2)))/8;
        OctaveLevels(n,3) = (1/distances(3))*(1-leftsidewall(n))*(1-
leftsidewall_scat(n))*10.^(-
AirAbs(n,1)*distances(3)/20)*window(round(fs*TimeDelays(3)))/8;
        OctaveLevels(n,4) = (1/distances(4))*(1-backwall(n))*(1-
backwall_scat(n))*10.^(-
AirAbs(n,1)*distances(4)/20)*window(round(fs*TimeDelays(4)))/8;
        OctaveLevels(n,5) = (1/distances(5))*(1-frontwall(n))*(1-
frontwall_scat(n))*10.^(-
AirAbs(n,1)*distances(5)/20)*window(round(fs*TimeDelays(5)))/8;
        OctaveLevels(n,6) = (1/distances(6))*(1-rightsidewall(n))*(1-
rightsidewall_scat(n))*10.^(-
AirAbs(n,1)*distances(6)/20)*window(round(fs*TimeDelays(6)))/8;
        OctaveLevels(n,7) = (1/distances(7))*(1-ceiling(n))*(1-
ceiling_scat(n))*10.^(-
AirAbs(n,1)*distances(7)/20)*window(round(fs*TimeDelays(7)))/8;
    end

end
```

```
% if second or third order image source methods are selected.
if N >= 2
    for n = 1:length(centers)
        OctaveLevels(n,8) = (1/distances(8))*(1-floor(n))*(1-
leftsidewall(n))*(1-floor_scat(n))*(1-leftsidewall_scat(n))*10.^(-
AirAbs(n,1)*distances(8)/20)*window(round(fs*TimeDelays(8)))/8;
        OctaveLevels(n,9) = (1/distances(9))*(1-floor(n))*(1-backwall(n))*(1-
floor_scat(n))*(1-backwall_scat(n))*10.^(-
AirAbs(n,1)*distances(9)/20)*window(round(fs*TimeDelays(9)))/8;
        OctaveLevels(n,10) = (1/distances(10))*(1-floor(n))*(1-
frontwall(n))*(1-floor_scat(n))*(1-frontwall_scat(n))*10.^(-
AirAbs(n,1)*distances(10)/20)*window(round(fs*TimeDelays(10)))/8;
        OctaveLevels(n,11) = (1/distances(11))*(1-floor(n))*(1-
rightsidewall(n))*(1-floor_scat(n))*(1-rightsidewall_scat(n))*10.^(-
AirAbs(n,1)*distances(11)/20)*window(round(fs*TimeDelays(11)))/8;
        OctaveLevels(n,12) = (1/distances(12))*(1-floor(n))*(1-
ceiling(n))*(1-floor_scat(n))*(1-ceiling_scat(n))*10.^(-
AirAbs(n,1)*distances(12)/20)*window(round(fs*TimeDelays(12)))/8;
        OctaveLevels(n,13) = (1/distances(13))*(1-leftsidewall(n))*(1-
backwall(n))*(1-leftsidewall_scat(n))*(1-backwall_scat(n))*10.^(-
AirAbs(n,1)*distances(13)/20)*window(round(fs*TimeDelays(13)))/8;
        OctaveLevels(n,14) = (1/distances(14))*(1-leftsidewall(n))*(1-
frontwall(n))*(1-leftsidewall_scat(n))*(1-frontwall_scat(n))*10.^(-
AirAbs(n,1)*distances(14)/20)*window(round(fs*TimeDelays(14)))/8;
        OctaveLevels(n,15) = (1/distances(15))*(1-leftsidewall(n))*(1-
rightsidewall(n))*(1-leftsidewall_scat(n))*(1-rightsidewall_scat(n))*10.^(-
AirAbs(n,1)*distances(15)/20)*window(round(fs*TimeDelays(15)))/8;
        OctaveLevels(n,16) = (1/distances(16))*(1-leftsidewall(n))*(1-
ceiling(n))*(1-leftsidewall_scat(n))*(1-ceiling_scat(n))*10.^(-
AirAbs(n,1)*distances(16)/20)*window(round(fs*TimeDelays(16)))/8;
        OctaveLevels(n,17) = (1/distances(17))*(1-backwall(n))*(1-
frontwall(n))*(1-backwall_scat(n))*(1-frontwall_scat(n))*10.^(-
AirAbs(n,1)*distances(17)/20)*window(round(fs*TimeDelays(17)))/8;
        OctaveLevels(n,18) = (1/distances(18))*(1-backwall(n))*(1-
rightsidewall(n))*(1-backwall_scat(n))*(1-rightsidewall_scat(n))*10.^(-
AirAbs(n,1)*distances(18)/20)*window(round(fs*TimeDelays(18)))/8;
        OctaveLevels(n,19) = (1/distances(19))*(1-backwall(n))*(1-
ceiling(n))*(1-backwall_scat(n))*(1-ceiling_scat(n))*10.^(-
AirAbs(n,1)*distances(19)/20)*window(round(fs*TimeDelays(19)))/8;
        OctaveLevels(n,20) = (1/distances(20))*(1-frontwall(n))*(1-
backwall(n))*(1-frontwall_scat(n))*(1-backwall_scat(n))*10.^(-
AirAbs(n,1)*distances(20)/20)*window(round(fs*TimeDelays(20)))/8;
        OctaveLevels(n,21) = (1/distances(21))*(1-frontwall(n))*(1-
rightsidewall(n))*(1-frontwall_scat(n))*(1-rightsidewall_scat(n))*10.^(-
AirAbs(n,1)*distances(21)/20)*window(round(fs*TimeDelays(21)))/8;
        OctaveLevels(n,22) = (1/distances(22))*(1-frontwall(n))*(1-
ceiling(n))*(1-frontwall_scat(n))*(1-ceiling_scat(n))*10.^(-
AirAbs(n,1)*distances(22)/20)*window(round(fs*TimeDelays(22)))/8;
        OctaveLevels(n,23) = (1/distances(23))*(1-rightsidewall(n))*(1-
leftsidewall(n))*(1-rightsidewall_scat(n))*(1-leftsidewall_scat(n))*10.^(-
AirAbs(n,1)*distances(23)/20)*window(round(fs*TimeDelays(23)))/8;
        OctaveLevels(n,24) = (1/distances(24))*(1-rightsidewall(n))*(1-
ceiling(n))*(1-rightsidewall_scat(n))*(1-ceiling_scat(n))*10.^(-
AirAbs(n,1)*distances(24)/20)*window(round(fs*TimeDelays(24)))/8;
        OctaveLevels(n,25) = (1/distances(25))*(1-ceiling(n))*(1-
floor(n))*(1-ceiling_scat(n))*(1-floor_scat(n))*10.^(-
AirAbs(n,1)*distances(25)/20)*window(round(fs*TimeDelays(25)))/8;
```

```
    end
end

% if the third order image source method is selected.
if N >= 3
    for n=1:length(centers)
        OctaveLevels(n,26) = (1/distances(26))*(1-floor(n))*(1-
leftsidewall(n))*(1-backwall(n))*(1-floor_scat(n))*(1-
leftsidewall_scat(n))*(1-backwall_scat(n))*10.^(-
AirAbs(n,1)*distances(26)/20)*window(round(fs*TimeDelays(26)))/8;
        OctaveLevels(n,27) = (1/distances(27))*(1-floor(n))*(1-
leftsidewall(n))*(1-frontwall(n))*(1-floor_scat(n))*(1-
leftsidewall_scat(n))*(1-frontwall_scat(n))*10.^(-
AirAbs(n,1)*distances(27)/20)*window(round(fs*TimeDelays(27)))/8;
        OctaveLevels(n,28) = (1/distances(28))*(1-floor(n))*(1-
leftsidewall(n))*(1-ceiling(n))*(1-floor_scat(n))*(1-
leftsidewall_scat(n))*(1-ceiling_scat(n))*10.^(-
AirAbs(n,1)*distances(28)/20)*window(round(fs*TimeDelays(28)))/8;
        OctaveLevels(n,29) = (1/distances(29))*(1-floor(n))*(1-
backwall(n))*(1-rightsidewall(n))*(1-floor_scat(n))*(1-backwall_scat(n))*(1-
rightsidewall_scat(n))*10.^(-
AirAbs(n,1)*distances(29)/20)*window(round(fs*TimeDelays(29)))/8;
        OctaveLevels(n,30) = (1/distances(30))*(1-floor(n))*(1-
backwall(n))*(1-ceiling(n))*(1-floor_scat(n))*(1-backwall_scat(n))*(1-
ceiling_scat(n))*10.^(-
AirAbs(n,1)*distances(30)/20)*window(round(fs*TimeDelays(30)))/8;
        OctaveLevels(n,31) = (1/distances(31))*(1-floor(n))*(1-
frontwall(n))*(1-rightsidewall(n))*(1-floor_scat(n))*(1-
frontwall_scat(n))*(1-rightsidewall_scat(n))*10.^(-
AirAbs(n,1)*distances(31)/20)*window(round(fs*TimeDelays(31)))/8;
        OctaveLevels(n,32) = (1/distances(32))*(1-floor(n))*(1-
frontwall(n))*(1-ceiling(n))*(1-floor_scat(n))*(1-frontwall_scat(n))*(1-
ceiling_scat(n))*10.^(-
AirAbs(n,1)*distances(32)/20)*window(round(fs*TimeDelays(32)))/8;
        OctaveLevels(n,33) = (1/distances(33))*(1-floor(n))*(1-
rightsidewall(n))*(1-ceiling(n))*(1-floor_scat(n))*(1-
rightsidewall_scat(n))*(1-ceiling_scat(n))*10.^(-
AirAbs(n,1)*distances(33)/20)*window(round(fs*TimeDelays(33)))/8;
        OctaveLevels(n,34) = (1/distances(34))*(1-floor(n))*(1-
ceiling(n))*(1-floor(n))*(1-floor_scat(n))*(1-ceiling_scat(n))*(1-
floor_scat(n))*10.^(-
AirAbs(n,1)*distances(34)/20)*window(round(fs*TimeDelays(34)))/8;
        OctaveLevels(n,35) = (1/distances(35))*(1-leftsidewall(n))*(1-
backwall(n))*(1-rightsidewall(n))*(1-leftsidewall_scat(n))*(1-
backwall_scat(n))*(1-rightsidewall_scat(n))*10.^(-
AirAbs(n,1)*distances(35)/20)*window(round(fs*TimeDelays(35)))/8;
        OctaveLevels(n,36) = (1/distances(36))*(1-leftsidewall(n))*(1-
backwall(n))*(1-ceiling(n))*(1-leftsidewall_scat(n))*(1-backwall_scat(n))*(1-
ceiling_scat(n))*10.^(-
AirAbs(n,1)*distances(36)/20)*window(round(fs*TimeDelays(36)))/8;
        OctaveLevels(n,37) = (1/distances(37))*(1-leftsidewall(n))*(1-
frontwall(n))*(1-rightsidewall(n))*(1-leftsidewall_scat(n))*(1-
frontwall_scat(n))*(1-rightsidewall_scat(n))*10.^(-
AirAbs(n,1)*distances(37)/20)*window(round(fs*TimeDelays(37)))/8;
        OctaveLevels(n,38) = (1/distances(38))*(1-leftsidewall(n))*(1-
frontwall(n))*(1-ceiling(n))*(1-leftsidewall_scat(n))*(1-
```

```
frontwall_scat(n))*(1-ceiling_scat(n))*10.^(-
AirAbs(n,1)*distances(38)/20)*window(round(fs*TimeDelays(38)))/8;
        OctaveLevels(n,39) = (1/distances(39))*(1-leftsidewall(n))*(1-
rightsidewall(n))*(1-floor(n))*(1-leftsidewall_scat(n))*(1-
rightsidewall_scat(n))*(1-floor_scat(n))*10.^(-
AirAbs(n,1)*distances(39)/20)*window(round(fs*TimeDelays(39)))/8;
        OctaveLevels(n,40) = (1/distances(40))*(1-leftsidewall(n))*(1-
rightsidewall(n))*(1-leftsidewall(n))*(1-leftsidewall_scat(n))*(1-
rightsidewall_scat(n))*(1-leftsidewall_scat(n))*10.^(-
AirAbs(n,1)*distances(40)/20)*window(round(fs*TimeDelays(40)))/8;
        OctaveLevels(n,41) = (1/distances(41))*(1-leftsidewall(n))*(1-
rightsidewall(n))*(1-ceiling(n))*(1-leftsidewall_scat(n))*(1-
rightsidewall_scat(n))*(1-ceiling_scat(n))*10.^(-
AirAbs(n,1)*distances(41)/20)*window(round(fs*TimeDelays(41)))/8;
        OctaveLevels(n,42) = (1/distances(42))*(1-backwall(n))*(1-
frontwall(n))*(1-floor(n))*(1-backwall_scat(n))*(1-frontwall_scat(n))*(1-
floor_scat(n))*10.^(-
AirAbs(n,1)*distances(42)/20)*window(round(fs*TimeDelays(42)))/8;
        OctaveLevels(n,43) = (1/distances(43))*(1-backwall(n))*(1-
frontwall(n))*(1-leftsidewall(n))*(1-backwall_scat(n))*(1-
frontwall_scat(n))*(1-leftsidewall_scat(n))*10.^(-
AirAbs(n,1)*distances(43)/20)*window(round(fs*TimeDelays(43)))/8;
        OctaveLevels(n,44) = (1/distances(44))*(1-backwall(n))*(1-
frontwall(n))*(1-backwall(n))*(1-backwall_scat(n))*(1-frontwall_scat(n))*(1-
backwall_scat(n))*10.^(-
AirAbs(n,1)*distances(44)/20)*window(round(fs*TimeDelays(44)))/8;
        OctaveLevels(n,45) = (1/distances(45))*(1-backwall(n))*(1-
frontwall(n))*(1-rightsidewall(n))*(1-backwall_scat(n))*(1-
frontwall_scat(n))*(1-rightsidewall_scat(n))*10.^(-
AirAbs(n,1)*distances(45)/20)*window(round(fs*TimeDelays(45)))/8;
        OctaveLevels(n,46) = (1/distances(46))*(1-backwall(n))*(1-
frontwall(n))*(1-ceiling(n))*(1-backwall_scat(n))*(1-frontwall_scat(n))*(1-
ceiling_scat(n))*10.^(-
AirAbs(n,1)*distances(46)/20)*window(round(fs*TimeDelays(46)))/8;
        OctaveLevels(n,47) = (1/distances(47))*(1-backwall(n))*(1-
rightsidewall(n))*(1-ceiling(n))*(1-backwall_scat(n))*(1-
rightsidewall_scat(n))*(1-ceiling_scat(n))*10.^(-
AirAbs(n,1)*distances(47)/20)*window(round(fs*TimeDelays(47)))/8;
        OctaveLevels(n,48) = (1/distances(48))*(1-frontwall(n))*(1-
backwall(n))*(1-floor(n))*(1-frontwall_scat(n))*(1-backwall_scat(n))*(1-
floor_scat(n))*10.^(-
AirAbs(n,1)*distances(48)/20)*window(round(fs*TimeDelays(48)))/8;
        OctaveLevels(n,49) = (1/distances(49))*(1-frontwall(n))*(1-
backwall(n))*(1-leftsidewall(n))*(1-frontwall_scat(n))*(1-
backwall_scat(n))*(1-leftsidewall_scat(n))*10.^(-
AirAbs(n,1)*distances(49)/20)*window(round(fs*TimeDelays(49)))/8;
        OctaveLevels(n,50) = (1/distances(50))*(1-frontwall(n))*(1-
backwall(n))*(1-frontwall(n))*(1-frontwall_scat(n))*(1-backwall_scat(n))*(1-
frontwall_scat(n))*10.^(-
AirAbs(n,1)*distances(50)/20)*window(round(fs*TimeDelays(50)))/8;
        OctaveLevels(n,51) = (1/distances(51))*(1-frontwall(n))*(1-
backwall(n))*(1-rightsidewall(n))*(1-frontwall_scat(n))*(1-
backwall_scat(n))*(1-rightsidewall_scat(n))*10.^(-
AirAbs(n,1)*distances(51)/20)*window(round(fs*TimeDelays(51)))/8;
        OctaveLevels(n,52) = (1/distances(52))*(1-frontwall(n))*(1-
backwall(n))*(1-ceiling(n))*(1-frontwall_scat(n))*(1-backwall_scat(n))*(1-
```

```
ceiling_scat(n))*10.^(-
AirAbs(n,1)*distances(52)/20)*window(round(fs*TimeDelays(52)))/8;
        OctaveLevels(n,53) = (1/distances(53))*(1-frontwall(n))*(1-
rightsidewall(n))*(1-ceiling(n))*(1-frontwall_scat(n))*(1-
rightsidewall_scat(n))*(1-ceiling_scat(n))*10.^(-
AirAbs(n,1)*distances(53)/20)*window(round(fs*TimeDelays(53)))/8;
        OctaveLevels(n,54) = (1/distances(54))*(1-rightsidewall(n))*(1-
leftsidewall(n))*(1-floor(n))*(1-rightsidewall_scat(n))*(1-
leftsidewall_scat(n))*(1-floor_scat(n))*10.^(-
AirAbs(n,1)*distances(54)/20)*window(round(fs*TimeDelays(54)))/8;
        OctaveLevels(n,55) = (1/distances(55))*(1-rightsidewall(n))*(1-
leftsidewall(n))*(1-backwall(n))*(1-rightsidewall_scat(n))*(1-
leftsidewall_scat(n))*(1-backwall_scat(n))*10.^(-
AirAbs(n,1)*distances(55)/20)*window(round(fs*TimeDelays(55)))/8;
        OctaveLevels(n,56) = (1/distances(56))*(1-rightsidewall(n))*(1-
leftsidewall(n))*(1-frontwall(n))*(1-rightsidewall_scat(n))*(1-
leftsidewall_scat(n))*(1-frontwall_scat(n))*10.^(-
AirAbs(n,1)*distances(56)/20)*window(round(fs*TimeDelays(56)))/8;
        OctaveLevels(n,57) = (1/distances(57))*(1-rightsidewall(n))*(1-
leftsidewall(n))*(1-rightsidewall(n))*(1-rightsidewall_scat(n))*(1-
leftsidewall_scat(n))*(1-rightsidewall_scat(n))*10.^(-
AirAbs(n,1)*distances(57)/20)*window(round(fs*TimeDelays(57)))/8;
        OctaveLevels(n,58) = (1/distances(58))*(1-rightsidewall(n))*(1-
leftsidewall(n))*(1-ceiling(n))*(1-rightsidewall_scat(n))*(1-
leftsidewall_scat(n))*(1-ceiling_scat(n))*10.^(-
AirAbs(n,1)*distances(58)/20)*window(round(fs*TimeDelays(58)))/8;
        OctaveLevels(n,59) = (1/distances(59))*(1-ceiling(n))*(1-
floor(n))*(1-leftsidewall(n))*(1-ceiling_scat(n))*(1-floor_scat(n))*(1-
leftsidewall_scat(n))*10.^(-
AirAbs(n,1)*distances(59)/20)*window(round(fs*TimeDelays(59)))/8;
        OctaveLevels(n,60) = (1/distances(60))*(1-ceiling(n))*(1-
floor(n))*(1-backwall(n))*(1-ceiling_scat(n))*(1-floor_scat(n))*(1-
backwall_scat(n))*10.^(-
AirAbs(n,1)*distances(60)/20)*window(round(fs*TimeDelays(60)))/8;
        OctaveLevels(n,61) = (1/distances(61))*(1-ceiling(n))*(1-
floor(n))*(1-frontwall(n))*(1-ceiling_scat(n))*(1-floor_scat(n))*(1-
frontwall_scat(n))*10.^(-
AirAbs(n,1)*distances(61)/20)*window(round(fs*TimeDelays(61)))/8;
        OctaveLevels(n,62) = (1/distances(62))*(1-ceiling(n))*(1-
floor(n))*(1-rightsidewall(n))*(1-ceiling_scat(n))*(1-floor_scat(n))*(1-
rightsidewall_scat(n))*10.^(-
AirAbs(n,1)*distances(62)/20)*window(round(fs*TimeDelays(62)))/8;
        OctaveLevels(n,63) = (1/distances(63))*(1-ceiling(n))*(1-
floor(n))*(1-ceiling(n))*(1-ceiling_scat(n))*(1-floor_scat(n))*(1-
ceiling_scat(n))*10.^(-
AirAbs(n,1)*distances(63)/20)*window(round(fs*TimeDelays(63)))/8;
    end
end

OctaveLevels = OctaveLevels';

end
```

```
function [Reverb_Levels,azimuths,elevations,timedelays] =
ReverbSim(IRLength,dimensions,units,floor,ceiling,leftsidewall,rightsidewall,
backwall,frontwall,fs,source,receiver,mix_time,mix_start,Dweights,reverb_scal
e)
%This function simulates random reflections for the late reverberation in
%an impulse response. Reflections are artificially created in the time
%domain using a random Poisson noise process. Then, the levels of these
%reflections (which are initially Dirac-delta functions) are attenuated for
%spherical spreading, air absorption, and wall absorption. As well, time
%delays are calculated for each reflection based upon the speed of sound.
%The direction of each reflection is randomly assigned, but certain
%directions are given more chance of selection based upon the directional
%weighted input into the ReverbDirections function.

% Define volume of room and the source-receiver distance from the room
% dimensions and source receiver positions.
V = dimensions(1)*dimensions(2)*dimensions(3);

% Compute the speed of sound, assumed to be at room temperature and room
% atmospheric pressure. This is done for either a m/s or ft/s basis,
% depending upon the input dimensions of the room/source/receiver inputs.
if strcmp(units,'meters') == 1
    c = 343;
elseif strcmp(units,'feet') == 1
    c = 343*100/2.54/12;
else
    disp('Improper Units specified. Please enter either ''meters'' or
''feet''.');
end

% Use function Air Absorption to calculate the air absorption in the room
% for each octave band. All energy content in a given band is assumed to
% decay by the value calculated for the band center frequency. The
% function AirAbsorption uses the ISO standard to calculate these values on
% a dB/100m basis, given the frequency, temperature, relative humidity, and
% pressure. Also calculate band centers from third octave filtering
% standard, to use as references for octave bands
bandnumber = 18:3:39;
centers = 1000*2.^((bandnumber-30)/3);
AirAbs = zeros(length(centers),1);

for nn=1:length(centers)
    AirAbs(nn,1) = AirAbsorption(centers(nn),293.15,50,101325);
end

% Convert the air absorption values for each octave band to either a dB/m
% basis, or a dB/ft basis, depending upon the desired units
if strcmp(units,'meters') == 1
    AirAbs = (AirAbs./100);
elseif strcmp(units,'feet') == 1
    AirAbs = (AirAbs./100)*(1/100)*(2.54/1)*(12/1);
end

% Determine average absorption alpha coefficients, based upon a surface
% area weighted average of absorption coefficients for the room
% First define surface areas
```

```
SA_lr = dimensions(1)*dimensions(3);
SA_cf = dimensions(1)*dimensions(2);
SA_fb = dimensions(2)*dimensions(3);
SA_tot = 2*SA_lr + 2*SA_cf + 2*SA_fb;

% Now, average alphas with a weighted surface area for each octave band
reverbalpha = zeros(length(centers),1);
for nn=1:length(centers)
    reverbalpha(nn) = (SA_cf*floor(nn) + SA_cf*ceiling(nn) +
SA_lr*leftsidewall(nn) + SA_lr*rightsidewall(nn) + SA_fb*frontwall(nn) +
SA_fb*backwall(nn))/SA_tot;
end
reverbalpha = reverbalpha*reverb_scale;
% Define IR parameters for simulate impulse response
Points = round(fs*IRLength);

% Define a zero vector to populate the IRs a starting time, t_o,
% calculated based upon the value mu, being the mean event occurrence for
% the Poisson distributed process. For reverberation, this is equated to
% the reflection density, or the number of reflections occurring in each
% second.
Poisson = [];

% Define a starting time, t_o, calculated based upon the value mu,
% which is the mean event occurrence for the Poisson distributed process.
% For reverberation, this is equated to the reflection density, or the
% number of reflections occurring in each second.

% while still within a time interval less than the maximum of the IR
% length, populate the IRs initially with a sequence of dirac delta
% functions following a Poisson process. This should naturally create
% reverberant reflections which are increasing with reflection density,
% according to the reflection density derived for a simple rectangular
% geometry

% More details and the specifics of this process can be found in Chapter 4
% of Matthew Neal's MS thesis.

t_o =(2*V*log(2)/(4*pi*c^3))^(1/3); % Set staring time for Poisson
distribution process
timedelays = [];    %define a vector to record the time delays for the late
reflections;

while (1+round(t_o*fs)) < IRLength*fs
    mu = 4*pi*c^3*t_o^2/V;          % update reflection density for each new
time

    if mu > 10000
        mu = 10000;  % Set a maximum limit on reflection density, to avoid an
rattling artifacts (Dirk Schroeder)
    end

    if (round(t_o*fs)-t_o*fs) < 0  % Randomly assign either a positive or
negative sign to dirac deltas, based upon rounding
        Poisson = [Poisson 1/8];
```

```
    elseif (round(t_o*fs)-t_o*fs) > 0
        Poisson = [Poisson -1/8];
    end
    timedelays = [timedelays;t_o];
    delta_t = (1/mu).*log(1/rand);   % Compute time interval between
successive reflections from mu and a random number
    t_o = t_o + delta_t;            % calculate new time for next run of loop
end

% Generate directional distribution of reflections
[azimuths,elevations] = ReverbDirections(length(Poisson),Dweights);

% Assuming a diffuse field in a simple rectangular geometry, we can
% estimate the average number of times a particular ray has hit a wall, per
% second as the following (from Kuttruff). Note, the directional weighting
% of the reverberation does deviate from this assumption, so be aware that
% the most 'correct' method should be in assuming 00% omnidirectional
% reverberant energy.
n_refl = c*SA_tot/(4*V);

% Create a time window with indices corresponding to the given time, to
% multiply and apply a transition time for the reverberant energy. The
% time window will begin at the specified mixing start time (specified by
% the start time minus the mixing length time), and will gradually increase
% to one, spanning the length of time specified by the mixing length.
direct_delay = round(fs*sqrt((source(1)-receiver(1))^2 + (source(2)-
receiver(2))^2 + (source(3)-receiver(3))^2)/c);
window = zeros(1,Points);
temp = hann(round(2*fs*(mix_time-mix_start)))';
transition = temp(1,1:round(length(temp)/2));
window(1,(round(fs*mix_time)-
length(transition)+1+direct_delay):round(fs*mix_time)+direct_delay) =
transition;
window(1,round(fs*mix_time)+direct_delay:Points) = ones(1,Points-
(round(fs*mix_time)+direct_delay)+1);

% Now, we can apply air absorption, wall reflection attenuation, and
% spherical spreading to each Poisson process, for each octave
% band. Frist create a new vector this this called OctaveIRs
Reverb_Levels = zeros(length(centers),length(Poisson));

% apply the spherical spreading, air attenuation, and wall absorption to
% the diffuse reverberant energy, for every octave band, and to each of
% individual reflections in the Poisson process. Additionally, the time
% window is also applied, based upon the time delay of each individual
% reflection.
for qq=1:length(Poisson)
    for nn=1:length(centers)
        Reverb_Levels(nn,qq) = Poisson(1,qq)./(c*timedelays(qq,1)).*10.^(-
AirAbs(nn,1)*c*timedelays(qq,1)/20).*(1-
reverbalpha(nn)).^(n_refl*timedelays(qq,1))*window(round(1+timedelays(qq,1)*f
s));
    end
end
Reverb_Levels = Reverb_Levels';
end
```

```
function [azimuths,elevations] = ReverbDirections(num_rfl,directionweights)
%This function takes a list of reflections, populated from the Poisson
%noise process, specified by the number of reflections, num_rfl. Then,
%using the directional weights, each reflections is randomly assigned a
%direction, which bias given to the directions with a higher specified
%weight.

% First, convert all of the direction weights into decimal percentage
% values, by dividing by the sum of all the directional weights.
D_percent = directionweights/sum(directionweights);

% specify a uniform random variable, between 0 and 1, uniquely for each
% reflection given by num_rfl.
random = rand(num_rfl,1);

% create two matrices, corresponding to both azimuth and elevation, in
% which the randomly assigned azimuth and elevations will be matched to
% each reflection.
azimuths = zeros(1,num_rfl);
elevations = zeros(1,num_rfl);

% Now the range of numbers from 0 to 1 is segmented into ranges for each
% given direction specified by the directional weighting factors. By
% assigning a range of the numbers between 0 and 1 for each direction, with
% a width corresponding to the decimal percentage calculated from each
% direction's weight, reflections are randomly assigned azimuths and
% elevations. Using the variable random, whichever directional range that
% the random variable corresponds to, a random azimuth and elevation is
% assigned to it, but limited to values within that given direction.
% The random directions are randomly created using a Gaussian distribution,
% so that the energy is focused in one direction, and it provides a smooth
% transition from the focused direction to the omnidirectional, diffuse
% reverberant energy. This prevents the energy from sounding like
% reverberant energy being played out of one loudspeaker, which is not
% natural at all.

% Omni          -180<=az<=+180          -90<=elev<=+90
% Front         -22.5<=az<=+22.5        -22.5<=elev<=+22.5
% Front Right   -67.5<=az<=-22.5        -22.5<=elev<=+22.5
% Right         -112.5<=az<=-67.5       -22.5<=elev<=+22.5
% Back Right    -157.5<=az<=-112.5      -22.5<=elev<=+22.5
% Back          -157.5>=az & az<=+157.5 -22.5<=elev<=+22.5
% Back Left     +112.5<=az<=+157.5      -22.5<=elev<=+22.5
% Left          +67.5<=az<=+112.5      -22.5<=elev<=+22.5
% Front Left    +22.5<=az<=+67.5        -22.5<=elev<=+22.5
% Front Top     -45<=az<=+45            +22.5<=elev<=+67.5
% Right Top     -135<=az<=-45           +22.5<=elev<=+67.5
% Back Top      +135<=az & az<=-135     +22.5<=elev<=+67.5
% Left Top      +45<=az<=+135           +22.5<=elev<=+67.5
% Top           -180<=az<=+180          +67.5<=elev<=+90
% Front Bottom  -45<=az<=+45            -22.5<=elev<=-67.5
% Right Bottom  -135<=az<=-45           -22.5<=elev<=-67.5
% Back Bottom   +135<=az & az<=-135     -22.5<=elev<=-67.5
% Left Bottom   +45<=az<=+135           -22.5<=elev<=-67.5
% Bottom        -180<=az<=+180          -67.5<=elev<=-90
```

```
% The random number for each reflection is selected, and the loop is
% performed for each number. It is then distributed in the direction, based
% upon where the random number falls between zero and one. Then it is
% assigned a direction randomly, but based upon either a uniform random
% number for an omnidirectional reflection (diffuse) or a Gaussian random
% number for a specific direction (directionally weighted). This ensures
% that the overall energy in the reverberant simulation is unchanged, but
% it provides for adjusting directional characteristics of the IR without
% changing energy.
for zz=1:length(random)
    if random(zz)<D_percent(1)  % Omni
        azimuths(zz) = 180*2*(rand()-0.5);
        elevations(zz) = 90*2*(rand()-0.5);
    elseif D_percent(1)<= random(zz) && random(zz) <sum(D_percent(1:2)) %
Front
        azimuths(zz) = 22.5*randn()/2;
        elevations(zz) = 22.5*randn()/2;
    elseif sum(D_percent(1:2)) <= random(zz) && random(zz) <
sum(D_percent(1:3)) %Front Right
        azimuths(zz) = -45 + 22.5*randn()/2;
        elevations(zz) = 22.5*randn()/2;
    elseif sum(D_percent(1:3)) <= random(zz) && random(zz) <
sum(D_percent(1:4)) %Right
        azimuths(zz) = -90 + 22.5*randn()/2;
        elevations(zz) = 22.5*randn()/2;
    elseif sum(D_percent(1:4)) <= random(zz) && random(zz) <
sum(D_percent(1:5)) %Back Right
        azimuths(zz) = -135 + 22.5*randn()/2;
        elevations(zz) = 22.5*randn()/2;
    elseif sum(D_percent(1:5)) <= random(zz) && random(zz) <
sum(D_percent(1:6)) %Back
        azimuths(zz) = 180 + 22.5*randn()/2;
        if azimuths(zz) > 180
            azimuths(zz) = azimuths(zz)-360;
        end
        elevations(zz) = 22.5*randn()/2;
    elseif sum(D_percent(1:6)) <= random(zz) && random(zz) <
sum(D_percent(1:7)) %Back Left
        azimuths(zz) = 135 + 22.5*randn()/2;
        elevations(zz) = 22.5*randn()/2;
    elseif sum(D_percent(1:7)) <= random(zz) && random(zz) <
sum(D_percent(1:8)) %Left
        azimuths(zz) = 90 + 22.5*randn()/2;
        elevations(zz) = 22.5*randn()/2;
    elseif sum(D_percent(1:8)) <= random(zz) && random(zz) <
sum(D_percent(1:9)) %Front Left
        azimuths(zz) = 45 + 22.5*randn()/2;
        elevations(zz) = 22.5*randn()/2;
    elseif sum(D_percent(1:9)) <= random(zz) && random(zz) <
sum(D_percent(1:10)) %Front Top
        azimuths(zz) = 45*randn()/2;
        elevations(zz) = 45 + 22.5*randn()/2;
    elseif sum(D_percent(1:10)) <= random(zz) && random(zz) <
sum(D_percent(1:11)) %Right Top
        azimuths(zz) = -90 + 45*randn()/2;
        elevations(zz) = 45 + 22.5*randn()/2;
```

```
    elseif sum(D_percent(1:11)) <= random(zz) && random(zz) <
sum(D_percent(1:12)) %Back Top
        azimuths(zz) = 180 + 45*randn()/2;
        if azimuths(zz) > 180
            azimuths(zz) = azimuths(zz)-360;
        end
        elevations(zz) = 45 + 22.5*randn()/2;
    elseif sum(D_percent(1:12)) <= random(zz) && random(zz) <
sum(D_percent(1:13)) %Left Top
        azimuths(zz) = 90 + 45*randn()/2;
        elevations(zz) = 45 + 22.5*randn()/2;
    elseif sum(D_percent(1:13)) <= random(zz) && random(zz) <
sum(D_percent(1:14)) %Top
        azimuths(zz) = 180*2*(rand()-0.5);
        elevations(zz) = 90 - abs(22.5*randn()/2);
    elseif sum(D_percent(1:14)) <= random(zz) && random(zz) <
sum(D_percent(1:15)) %Front Bottom
        azimuths(zz) = 45*randn()/2;
        elevations(zz) = -45 + 22.5*randn()/2;
    elseif sum(D_percent(1:15)) <= random(zz) && random(zz) <
sum(D_percent(1:16)) %Right Bottom
        azimuths(zz) = -90 + 45*randn()/2;
        elevations(zz) = -45 + 22.5*randn()/2;
    elseif sum(D_percent(1:16)) <= random(zz) && random(zz) <
sum(D_percent(1:17)) %Back Bottom
        azimuths(zz) = 180 + 45*randn()/2;
        if azimuths(zz) > 180
            azimuths(zz) = azimuths(zz)-360;
        end
        elevations(zz) = -45 + 22.5*randn()/2;
    elseif sum(D_percent(1:17)) <= random(zz) && random(zz) <
sum(D_percent(1:18)) %Left Bottom
        azimuths(zz) = 90 + 45*randn()/2;
        elevations(zz) = -45 + 22.5*randn()/2;
    elseif sum(D_percent(1:18)) <= random(zz) && random(zz) <
sum(D_percent(1:19)) %Bottom
        azimuths(zz) = 180*2*(rand()-0.5);
        elevations(zz) = -90 + abs(22.5*randn()/2);
    end
end

% transpose the azimuth and elevation vectors for formatting
azimuths = azimuths.';
elevations = elevations.';
end
```

```
function [spharmIRs,octspharmIRs,octISspharmIRs,octREVspharmIRs] =
SphericalHarmonics(IRlength,fs,IS_levels,Rev_levels,IS_timedelays,Rev_timedel
ays,IS_elevations,Rev_elevations,IS_azimuths,Rev_azimuths,N)
%This function takes the time delay, level, and direction information for
%both the image source and reverberant simulations, and populates this
%information into third order Ambisonic impulse responses, for each
%different octave band.

% find the total number of points in the impulse responses being simulated,
% and the total number of reverberant reflections from the reverberation
% simulation method.
L = round(IRlength*fs);
n_Rev = length(Rev_levels);

% specify p, which is the total number of sources to be encoded into
% spherical harmonic components. This includes direct sound (the original
% source), early reflections (image source), and late energy (reverberant
% simulation). This is now based upon the chose image source order.
if N==1
    zz = 7;
    p = zz + n_Rev;
elseif N==2
    zz = 25;
    p = zz + n_Rev;
elseif N==3
    zz = 63;
    p = zz + n_Rev;
end

% combine level, time delay, elevation, and azimuth information from
% separate simulation techniques into the same vectors.
octavelevels = [IS_levels;Rev_levels];
timedelays = [IS_timedelays;Rev_timedelays];
elevations = [IS_elevations;Rev_elevations];
azimuths = [IS_azimuths;Rev_azimuths];

% predefine variables for impulse responses which will be populated by in
% the loops below, looping through every octave band and every image
% soruce.
octISspharmIRs=zeros(16,L,8);
octREVspharmIRs=zeros(16,L,8);

% populate impulse responses for the image source method of simulation.
% Loop through each octave band (nn) and loop through each image source
% from the previous simulation (ii). Each of the 16 lines of code
% correspond to the 16 different Ambisonic impulse responses, ordered in
% ACN format. The individual levels are populated into the correct sample
% of the IR based upon the time delay, and the amplitudes of the
% reflections are multiplied by the spherical harmonics equation for each
% component. These equations can be found in appendix D in Matthew Neal's
% thesis. They use the ambiX format, using SN3D normalization and, as
% previously stated ACN ordering.
for nn=1:8
    for ii=1:zz
```

```
        octISspharmIRs(1,1+round(timedelays(ii)*fs),nn)=
octISspharmIRs(1,1+round(timedelays(ii)*fs),nn) +
octavelevels(ii,nn)*sqrt(1/(4*pi));
        octISspharmIRs(2,1+round(timedelays(ii)*fs),nn)=
octISspharmIRs(2,1+round(timedelays(ii)*fs),nn) +
octavelevels(ii,nn)*sqrt(1/(4*pi))*cosd(elevations(ii)).*sind(azimuths(ii));
        octISspharmIRs(3,1+round(timedelays(ii)*fs),nn)=
octISspharmIRs(3,1+round(timedelays(ii)*fs),nn) +
octavelevels(ii,nn)*sqrt(1/(4*pi))*sind(elevations(ii));
        octISspharmIRs(4,1+round(timedelays(ii)*fs),nn)=
octISspharmIRs(4,1+round(timedelays(ii)*fs),nn) +
octavelevels(ii,nn)*sqrt(1/(4*pi))*cosd(elevations(ii)).*cosd(azimuths(ii));
        octISspharmIRs(5,1+round(timedelays(ii)*fs),nn)=
octISspharmIRs(5,1+round(timedelays(ii)*fs),nn) +
octavelevels(ii,nn)*sqrt(1/(48*pi))*3*(cosd(elevations(ii))).^2.*sind(2*azimu
ths(ii));
        octISspharmIRs(6,1+round(timedelays(ii)*fs),nn)=
octISspharmIRs(6,1+round(timedelays(ii)*fs),nn) +
octavelevels(ii,nn)*sqrt(1/(12*pi))*3*sind(elevations(ii)).*cosd(elevations(i
i)).*sind(azimuths(ii));
        octISspharmIRs(7,1+round(timedelays(ii)*fs),nn)=
octISspharmIRs(7,1+round(timedelays(ii)*fs),nn) +
octavelevels(ii,nn)*sqrt(1/(4*pi))*(1/2)*(3*(sind(elevations(ii))).^2-1);
        octISspharmIRs(8,1+round(timedelays(ii)*fs),nn)=
octISspharmIRs(8,1+round(timedelays(ii)*fs),nn) +
octavelevels(ii,nn)*sqrt(1/(12*pi))*3*sind(elevations(ii)).*cosd(elevations(i
i)).*cosd(azimuths(ii));
        octISspharmIRs(9,1+round(timedelays(ii)*fs),nn)=
octISspharmIRs(9,1+round(timedelays(ii)*fs),nn) +
octavelevels(ii,nn)*sqrt(1/(48*pi))*3*(cosd(elevations(ii))).^2.*cosd(2*azimu
ths(ii));
        octISspharmIRs(10,1+round(timedelays(ii)*fs),nn)=
octISspharmIRs(10,1+round(timedelays(ii)*fs),nn) +
octavelevels(ii,nn)*sqrt(1/(1440*pi))*15*(cosd(elevations(ii))).^3.*sind(3*az
imuths(ii));
        octISspharmIRs(11,1+round(timedelays(ii)*fs),nn)=
octISspharmIRs(11,1+round(timedelays(ii)*fs),nn) +
octavelevels(ii,nn)*sqrt(1/(240*pi))*15*sind(elevations(ii)).*(cosd(elevation
s(ii))).^2.*sind(2*azimuths(ii));
        octISspharmIRs(12,1+round(timedelays(ii)*fs),nn)=
octISspharmIRs(12,1+round(timedelays(ii)*fs),nn) +
octavelevels(ii,nn)*sqrt(1/(24*pi))*(3/2)*(5*(sind(elevations(ii))).^2-
1).*cosd(elevations(ii)).*sind(azimuths(ii));
        octISspharmIRs(13,1+round(timedelays(ii)*fs),nn)=
octISspharmIRs(13,1+round(timedelays(ii)*fs),nn) +
octavelevels(ii,nn)*sqrt(1/(4*pi))*(1/2)*(5*(sind(elevations(ii))).^3-
3*sind(elevations(ii)));
        octISspharmIRs(14,1+round(timedelays(ii)*fs),nn)=
octISspharmIRs(14,1+round(timedelays(ii)*fs),nn) +
octavelevels(ii,nn)*sqrt(1/(24*pi))*(3/2)*(5*(sind(elevations(ii))).^2-
1).*cosd(elevations(ii)).*cosd(azimuths(ii));
        octISspharmIRs(15,1+round(timedelays(ii)*fs),nn)=
octISspharmIRs(15,1+round(timedelays(ii)*fs),nn) +
octavelevels(ii,nn)*sqrt(1/(240*pi))*15*sind(elevations(ii)).*(cosd(elevation
s(ii))).^2.*cosd(2*azimuths(ii));
        octISspharmIRs(16,1+round(timedelays(ii)*fs),nn)=
octISspharmIRs(16,1+round(timedelays(ii)*fs),nn) +
```

```
octavelevels(ii,nn)*sqrt(1/(1440*pi))*15*(cosd(elevations(ii))).^3.*cosd(3*az
imuths(ii));
    end
end

% repeat the same process as used in the image source spherical harmonic
% IRs. Now, the processing is done separately so that the different
% contributions of the reverberation simulation and the image source
% simulation can be extracted later.
for nn=1:8
    for ii=zz+1:p
        octREVspharmIRs(1,1+round(timedelays(ii)*fs),nn)=
octREVspharmIRs(1,1+round(timedelays(ii)*fs),nn) +
octavelevels(ii,nn)*sqrt(1/(4*pi));
        octREVspharmIRs(2,1+round(timedelays(ii)*fs),nn)=
octREVspharmIRs(2,1+round(timedelays(ii)*fs),nn) +
octavelevels(ii,nn)*sqrt(1/(4*pi))*cosd(elevations(ii)).*sind(azimuths(ii));
        octREVspharmIRs(3,1+round(timedelays(ii)*fs),nn)=
octREVspharmIRs(3,1+round(timedelays(ii)*fs),nn) +
octavelevels(ii,nn)*sqrt(1/(4*pi))*sind(elevations(ii));
        octREVspharmIRs(4,1+round(timedelays(ii)*fs),nn)=
octREVspharmIRs(4,1+round(timedelays(ii)*fs),nn) +
octavelevels(ii,nn)*sqrt(1/(4*pi))*cosd(elevations(ii)).*cosd(azimuths(ii));
        octREVspharmIRs(5,1+round(timedelays(ii)*fs),nn)=
octREVspharmIRs(5,1+round(timedelays(ii)*fs),nn) +
octavelevels(ii,nn)*sqrt(1/(48*pi))*3*(cosd(elevations(ii))).^2.*sind(2*azimu
ths(ii));
        octREVspharmIRs(6,1+round(timedelays(ii)*fs),nn)=
octREVspharmIRs(6,1+round(timedelays(ii)*fs),nn) +
octavelevels(ii,nn)*sqrt(1/(12*pi))*3*sind(elevations(ii)).*cosd(elevations(i
i)).*sind(azimuths(ii));
        octREVspharmIRs(7,1+round(timedelays(ii)*fs),nn)=
octREVspharmIRs(7,1+round(timedelays(ii)*fs),nn) +
octavelevels(ii,nn)*sqrt(1/(4*pi))*(1/2)*(3*(sind(elevations(ii))).^2-1);
        octREVspharmIRs(8,1+round(timedelays(ii)*fs),nn)=
octREVspharmIRs(8,1+round(timedelays(ii)*fs),nn) +
octavelevels(ii,nn)*sqrt(1/(12*pi))*3*sind(elevations(ii)).*cosd(elevations(i
i)).*cosd(azimuths(ii));
        octREVspharmIRs(9,1+round(timedelays(ii)*fs),nn)=
octREVspharmIRs(9,1+round(timedelays(ii)*fs),nn) +
octavelevels(ii,nn)*sqrt(1/(48*pi))*3*(cosd(elevations(ii))).^2.*cosd(2*azimu
ths(ii));
        octREVspharmIRs(10,1+round(timedelays(ii)*fs),nn)=
octREVspharmIRs(10,1+round(timedelays(ii)*fs),nn) +
octavelevels(ii,nn)*sqrt(1/(1440*pi))*15*(cosd(elevations(ii))).^3.*sind(3*az
imuths(ii));
        octREVspharmIRs(11,1+round(timedelays(ii)*fs),nn)=
octREVspharmIRs(11,1+round(timedelays(ii)*fs),nn) +
octavelevels(ii,nn)*sqrt(1/(240*pi))*15*sind(elevations(ii)).*(cosd(elevation
s(ii))).^2.*sind(2*azimuths(ii));
        octREVspharmIRs(12,1+round(timedelays(ii)*fs),nn)=
octREVspharmIRs(12,1+round(timedelays(ii)*fs),nn) +
octavelevels(ii,nn)*sqrt(1/(24*pi))*(3/2)*(5*(sind(elevations(ii))).^2-
1).*cosd(elevations(ii)).*sind(azimuths(ii));
        octREVspharmIRs(13,1+round(timedelays(ii)*fs),nn)=
octREVspharmIRs(13,1+round(timedelays(ii)*fs),nn) +
```

```
octavelevels(ii,nn)*sqrt(1/(4*pi))*(1/2)*(5*(sind(elevations(ii))).^3-
3*sind(elevations(ii)));
        octREVspharmIRs(14,1+round(timedelays(ii)*fs),nn)=
octREVspharmIRs(14,1+round(timedelays(ii)*fs),nn) +
octavelevels(ii,nn)*sqrt(1/(24*pi))*(3/2)*(5*(sind(elevations(ii))).^2-
1).*cosd(elevations(ii)).*cosd(azimuths(ii));
        octREVspharmIRs(15,1+round(timedelays(ii)*fs),nn)=
octREVspharmIRs(15,1+round(timedelays(ii)*fs),nn) +
octavelevels(ii,nn)*sqrt(1/(240*pi))*15*sind(elevations(ii)).*(cosd(elevation
s(ii))).^2.*cosd(2*azimuths(ii));
        octREVspharmIRs(16,1+round(timedelays(ii)*fs),nn)=
octREVspharmIRs(16,1+round(timedelays(ii)*fs),nn) +
octavelevels(ii,nn)*sqrt(1/(1440*pi))*15*(cosd(elevations(ii))).^3.*cosd(3*az
imuths(ii));
    end
end

% Perform octave band filtering for the reverberant and image source
% simulated IRs, for each respective octave band. This will cause only the
% energy in that octave band to remain for the impulse response which was
% simulated.
bandnumber = 18:3:39;
centers = 1000*2.^((bandnumber-30)/3);
for nn=1:length(centers)
    [b,a] = Octave_Filter(centers(nn),fs);
    for qq=1:16
        octISspharmIRs(qq,:,nn) = filter(b,a,octISspharmIRs(qq,:,nn));
        octREVspharmIRs(qq,:,nn) = filter(b,a,octREVspharmIRs(qq,:,nn));
    end
end

% rearrange the matrices so that each channel is contained in a row
% vector, over 16 columns for each channel. This allows for the
% proper format later to using the auidowrite command.
octISspharmIRs = permute(octISspharmIRs,[2,1,3]);
octREVspharmIRs = permute(octREVspharmIRs,[2,1,3]);

% Add together the two simulation methods to produce the final IRs in each
% octave band.
octspharmIRs = octISspharmIRs + octREVspharmIRs;

% Sum together the octave band IRs to produce final, broadband IRs for each
% Ambisonic signal for 3rd order reproduction.
spharmIRs = sum(octspharmIRs,3);

end
```

```
function [newsignal,Adjusted_Lp,Adjustment] =
Level_Adjusted(signal,Target_Lp)
%This function performs level equalization on an Ambisonic signal. The
%total RMS level of all Ambisonic channels is calculated, and the input
%signals is scales so that the total RMS level across all channels will be
%the target level, set by Target_Lp

% calculate current level of ambisonic signal
Total_Lp = 20*log10(sqrt(mean(mean(signal.^2))));

% calculate adjustment, as a simple multiplier, which is needed to scale
% the original signal so that it is the target level specified.
Adjustment = 10^((Target_Lp-Total_Lp)/20);

% scale new signals and calculate new level, which is equal to the target
% level specified as Target_Lp
newsignal = signal*Adjustment;
Adjusted_Lp = 20*log10(sqrt(mean(mean(newsignal.^2))));

end
```

```
function [AmbisonicSignals] = Ambisonic_fftfilt(anechoic,spharmIRs)
%This function filters an anechoic file with a third order Ambisonic
%impulse response
  %filename

% If the anechoic file is not given as a row vector, it will be transposed
% into a row vector
[row,col] = size(anechoic);
if row > col
    anechoic = anechoic';
end

% The anechoic motif is filtered with each of the 16 Ambisonic impulse
% responses. This will create the final, unequaled Ambisonic signals
% which can be reproduced or rendered over the loudspeaker array using
% REAPER. First, predefine size of AmbisonicSignals since it is a looped
% variable.
AmbisonicSignals = zeros(size(length(anechoic),16));
for qq=1:16
    AmbisonicSignals(qq,:) = fftfilt(spharmIRs(:,qq),anechoic(1,:));
end

end
```

```
function [] = ImageSourcePlot(dimensions,source,receiver,ImageOrder)
%This function will plot the dimensions of a specified room size, plot a
%source and a receiver location, and plot the image source locations based
%upon the desired image source order.

% import specified room dimensions and image source order, N
length = dimensions(1);
width = dimensions(2);
height = dimensions(3);
N = ImageOrder;

% Check for max order possible for algorithm (3)
if N>3
    error('Exceeded Max Image Source Order for this model!!!');
else

% Plot Room Boundaries on figure
x =
[0,0,length,length,0,0,0,0,0,length,length,length,length,length,length,0];
y = [0,width, width,0,0,0,width,width,width,width,width,width,0,0,0,0];
z =
[0,0,0,0,0,height,height,0,height,height,0,height,height,0,height,height];
plot3(x,y,z,'k','Linelength',2);
hold on;
axis equal;
axis([-N*length (N+1)*length -N*width (N+1)*width -N*height (N+1)*height]);

% Plot the source location
plot3(source(1),source(2),source(3),'-or','MarkerFaceColor','r');

% Plot the receiver
plot3(receiver(1),receiver(2),receiver(3),'-ok','MarkerFaceColor','k');

% Find first order IS's
% 1 is the floor, 2 is the front wall, 3 is the right side wall, 4 is the
% left side wall, 5 is the back wall, and 6 is the ceiling
if N>=1
    I1 = [source(1),source(2),-source(3)];
    I2 = [source(1),2*width-source(2),source(3)];
    I3 = [-source(1),source(2),source(3)];
    I4 = [2*length-source(1),source(2),source(3)];
    I5 = [source(1),-source(2),source(3)];
    I6 = [source(1),source(2),2*height-source(3)];

    % Plot first order images
    plot3(I1(1),I1(2),I1(3),'-ob');
    plot3(I2(1),I2(2),I2(3),'-ob');
    plot3(I3(1),I3(2),I3(3),'-ob');
    plot3(I4(1),I4(2),I4(3),'-ob');
    plot3(I5(1),I5(2),I5(3),'-ob');
    plot3(I6(1),I6(2),I6(3),'-ob');
end

% Find second order IS's for a rectangular room. The numbers following the
% image source correspond to the walls in which the original source was
```

```
% reflected across to produce the image source. Order matters.

% 1 is the floor, 2 is the front wall, 3 is the right side wall, 4 is the
% left side wall, 5 is the back wall, and 6 is the ceiling
if N>=2
    I1_2 = [source(1),2*width-source(2),-source(3)];
    I1_3 = [-source(1),source(2),-source(3)];
    I1_4 = [2*length-source(1),source(2),-source(3)];
    I1_5 = [source(1),-source(2),-source(3)];
    I1_6 = [source(1),source(2),2*height+source(3)];
    I2_3 = [-source(1),2*width-source(2),source(3)];
    I2_4 = [2*length-source(1),2*width-source(2),source(3)];
    I2_5 = [source(1),-2*width+source(2),source(3)];
    I2_6 = [source(1),2*width-source(2),2*height-source(3)];
    I3_4 = [2*length+source(1),source(2),source(3)];
    I3_5 = [-source(1),-source(2),source(3)];
    I3_6 = [-source(1),source(2),2*height-source(3)];
    I4_3 = [-2*length+source(1),source(2),source(3)];
    I4_5 = [2*length-source(1),-source(2),source(3)];
    I4_6 = [2*length-source(1),source(2),2*height-source(3)];
    I5_2 = [source(1),2*width+source(2),source(3)];
    I5_6 = [source(1),-source(2),2*height-source(3)];
    I6_1 = [source(1),source(2),-2*height+source(3)];

    % Plot second order images
    plot3(I1_2(1),I1_2(2),I1_2(3),'-og');
    plot3(I1_3(1),I1_3(2),I1_3(3),'-og');
    plot3(I1_4(1),I1_4(2),I1_4(3),'-og');
    plot3(I1_5(1),I1_5(2),I1_5(3),'-og');
    plot3(I1_6(1),I1_6(2),I1_6(3),'-og');
    plot3(I2_3(1),I2_3(2),I2_3(3),'-og');
    plot3(I2_4(1),I2_4(2),I2_4(3),'-og');
    plot3(I2_5(1),I2_5(2),I2_5(3),'-og');
    plot3(I2_6(1),I2_6(2),I2_6(3),'-og');
    plot3(I3_4(1),I3_4(2),I3_4(3),'-og');
    plot3(I3_5(1),I3_5(2),I3_5(3),'-og');
    plot3(I3_6(1),I3_6(2),I3_6(3),'-og');
    plot3(I4_3(1),I4_3(2),I4_3(3),'-og');
    plot3(I4_5(1),I4_5(2),I4_5(3),'-og');
    plot3(I4_6(1),I4_6(2),I4_6(3),'-og');
    plot3(I5_2(1),I5_2(2),I5_2(3),'-og');
    plot3(I5_6(1),I5_6(2),I5_6(3),'-og');
    plot3(I6_1(1),I6_1(2),I6_1(3),'-og');
end

% Find second order IS's for a rectangular room. The numbers following the
% image source correspond to the walls in which the original source was
% reflected across to produce the image source. Order matters.

% 1 is the floor, 2 is the front wall, 3 is the right side wall, 4 is the
% left side wall, 5 is the back wall, and 6 is the ceiling
if N==3
    I1_2_3 = [-source(1),2*width-source(2),-source(3)];
    I1_2_4 = [2*length-source(1),2*width-source(2),-source(3)];
    I1_2_6 = [source(1),2*width-source(2),2*height+source(3)];
    I1_3_5 = [-source(1),-source(2),-source(3)];
```

```
I1_3_6 = [-source(1),source(2),2*height+source(3)];
I1_4_5 = [2*length-source(1),-source(2),-source(3)];
I1_4_6 = [2*length-source(1),source(2),2*height+source(3)];
I1_5_6 = [source(1),-source(2),2*height+source(3)];
I1_6_1 = [source(1),source(2),-2*height-source(3)];
I2_3_5 = [-source(1),-2*width+source(2),source(3)];
I2_3_6 = [-source(1),2*width-source(2),2*height-source(3)];
I2_4_5 = [2*length-source(1),-2*width+source(2),source(3)];
I2_4_6 = [2*length-source(1),2*width-source(2),2*height-source(3)];
I2_5_1 = [source(1),-2*width+source(2),-source(3)];
I2_5_2 = [source(1),4*width-source(2),source(3)];
I2_5_6 = [source(1),-2*width+source(2),2*height-source(3)];
I3_4_1 = [2*length+source(1),source(2),-source(3)];
I3_4_2 = [2*length+source(1),2*width-source(2),source(3)];
I3_4_3 = [-2*length-source(1),source(2),source(3)];
I3_4_5 = [2*length+source(1),-source(2),source(3)];
I3_4_6 = [2*length+source(1),source(2),2*height-source(3)];
I3_5_6 = [-source(1),-source(2),2*height-source(3)];
I4_3_1 = [-2*length+source(1),source(2),-source(3)];
I4_3_2 = [-2*length+source(1),2*width-source(2),source(3)];
I4_3_4 = [4*length-source(1),source(2),source(3)];
I4_3_5 = [-2*length+source(1),-source(2),source(3)];
I4_3_6 = [-2*length+source(1),source(2),2*height-source(3)];
I4_5_6 = [2*length-source(1),-source(2),2*height-source(3)];
I5_2_1 = [source(1),2*width+source(2),-source(3)];
I5_2_3 = [-source(1),2*width+source(2),source(3)];
I5_2_4 = [2*length-source(1),2*width+source(2),source(3)];
I5_2_5 = [source(1),-2*width-source(2),source(3)];
I5_2_6 = [source(1),2*width+source(2),2*height-source(3)];
I6_1_2 = [source(1),2*width-source(2),-2*height+source(3)];
I6_1_3 = [-source(1),source(2),-2*height+source(3)];
I6_1_4 = [2*length-source(1),source(2),-2*height+source(3)];
I6_1_5 = [source(1),-source(2),-2*height+source(3)];
I6_1_6 = [source(1),source(2),4*height-source(3)];

% Plot third order IS's
plot3(I1_2_3(1),I1_2_3(2),I1_2_3(3),'-om');
plot3(I1_2_4(1),I1_2_4(2),I1_2_4(3),'-om');
plot3(I1_2_6(1),I1_2_6(2),I1_2_6(3),'-om');
plot3(I1_3_5(1),I1_3_5(2),I1_3_5(3),'-om');
plot3(I1_3_6(1),I1_3_6(2),I1_3_6(3),'-om');
plot3(I1_4_5(1),I1_4_5(2),I1_4_5(3),'-om');
plot3(I1_4_6(1),I1_4_6(2),I1_4_6(3),'-om');
plot3(I1_5_6(1),I1_5_6(2),I1_5_6(3),'-om');
plot3(I1_6_1(1),I1_6_1(2),I1_6_1(3),'-om');
plot3(I2_3_5(1),I2_3_5(2),I2_3_5(3),'-om');
plot3(I2_3_6(1),I2_3_6(2),I2_3_6(3),'-om');
plot3(I2_4_5(1),I2_4_5(2),I2_4_5(3),'-om');
plot3(I2_4_6(1),I2_4_6(2),I2_4_6(3),'-om');
plot3(I2_5_1(1),I2_5_1(2),I2_5_1(3),'-om');
plot3(I2_5_2(1),I2_5_2(2),I2_5_2(3),'-om');
plot3(I2_5_6(1),I2_5_6(2),I2_5_6(3),'-om');
plot3(I3_4_1(1),I3_4_1(2),I3_4_1(3),'-om');
plot3(I3_4_2(1),I3_4_2(2),I3_4_2(3),'-om');
plot3(I3_4_3(1),I3_4_3(2),I3_4_3(3),'-om');
plot3(I3_4_5(1),I3_4_5(2),I3_4_5(3),'-om');
plot3(I3_4_6(1),I3_4_6(2),I3_4_6(3),'-om');
```

```
    plot3(I3_5_6(1),I3_5_6(2),I3_5_6(3),'-om');
    plot3(I4_3_1(1),I4_3_1(2),I4_3_1(3),'-om');
    plot3(I4_3_2(1),I4_3_2(2),I4_3_2(3),'-om');
    plot3(I4_3_4(1),I4_3_4(2),I4_3_4(3),'-om');
    plot3(I4_3_5(1),I4_3_5(2),I4_3_5(3),'-om');
    plot3(I4_3_6(1),I4_3_6(2),I4_3_6(3),'-om');
    plot3(I4_5_6(1),I4_5_6(2),I4_5_6(3),'-om');
    plot3(I5_2_1(1),I5_2_1(2),I5_2_1(3),'-om');
    plot3(I5_2_3(1),I5_2_3(2),I5_2_3(3),'-om');
    plot3(I5_2_4(1),I5_2_4(2),I5_2_4(3),'-om');
    plot3(I5_2_5(1),I5_2_5(2),I5_2_5(3),'-om');
    plot3(I5_2_6(1),I5_2_6(2),I5_2_6(3),'-om');
    plot3(I6_1_2(1),I6_1_2(2),I6_1_2(3),'-om');
    plot3(I6_1_3(1),I6_1_3(2),I6_1_3(3),'-om');
    plot3(I6_1_4(1),I6_1_4(2),I6_1_4(3),'-om');
    plot3(I6_1_5(1),I6_1_5(2),I6_1_5(3),'-om');
    plot3(I6_1_6(1),I6_1_6(2),I6_1_6(3),'-om');
end

end

end
```

```
function [] = ISPolarReflection(IS_azimuths,IS_levels,ImageOrder)
%This function produces a 2D polar diagram of the reflections in the final
%IR from the image source method. Directional and level information is
%input from the image source location calculations, and it is combined into
%a 2D polar plot

% format and input level and azimuth information
levels = sum(IS_levels,1);
azimuths = IS_azimuths;

% create a polar plot, and initially plot the direct sound in red. The
% direct sound is contained in the first 'image source'
figure();
polar((pi/180)*[0,0],[0,levels(1)],'r');
hold on;

% if using third order image source method, loop through and plot all of
% the third order images in magenta.
if ImageOrder == 3
    for n = 26:63
        polar((pi/180)*[0,azimuths(n)],[0,levels(n)],'m');
    end
end
% if using second or third order image source method, loop through and
% plot all of the second order images in green.
if ImageOrder >= 2
    for n = 8:25
        polar((pi/180)*[0,azimuths(n)],[0,levels(n)],'g');
    end
end

% if using first, second, or third order image source method, loop through
% and plot all of the first order images in blue.
if ImageOrder >= 1
    for n = 2:7
        polar((pi/180)*[0,azimuths(n)],[0,levels(n)],'b');
    end
end

end
```

```
function [bb aa] = Octave_Filter(f_c,fs)
%Octave_Filter This function provides a Butterworth bandpass filter
%than can be used for octave band filtering.
%   This function, based upon the sampling rate and center frequency of the
%   desired band, will create a third or fourth order low and high pass
%   filter, making a bandpass filter that can be implemented for an
%   octave band filtering program.

if f_c/fs > 0.3200;
    error('Center frequqnecy of third-octave filter too high');
end;

if f_c/fs < 0.0013;
    error('Center frequency of third-octave filter too low');
end;

N = 3;
if f_c/fs > 0.15;
    N = 4;
end;

f1 = f_c/2^(1/2);
f2 = f_c*2^(1/2);

[bb aa] = butter(N,[f1/(fs/2) f2/(fs/2)],'bandpass');

end
```

```
function [alpha] = AirAbsorption(f,Temp,RelH,Pressure)
%This function calculates values for the air attenuation factor in air, on a
%dB per 100 meter basis. It is defined using the ISO standard
%ISO 9613-1: 1993

% by just inputting the frequency, temperature in Kelvin, relative humidity,
% and pressure, the air attenuation factor can be calculated.

% Define the triple point temperature of water
T_triplepoint = 273.16;

% Calculate the relative humidity of the air using the triple-point of
% water, the temperature of the air, and the pressure of the atmosphere.
C_sat = -6.8346*(T_triplepoint/Temp)^1.261 + 4.6151;
rho_sat = 10^C_sat;
h = RelH*rho_sat/(Pressure/101325);

% Calculate the relaxation frequencies of both oxygen and nitrogen
F_rO = (Pressure/101325)*(24 + 4.04*10^4*h*(0.02 + h)/(0.391 + h));
F_rN = (Pressure/101325)*(Temp/293.15)^(-1/2)*(9 + 280*h*exp(-
4.17*((Temp/293.15)^(-1/3)-1)));

% Calculate the final air attenuation factor for a given frequency, using
% the temperature of the air, the relative humidity of the air, the
% relaxation frequencies of oxygen and nitrogen, the pressure of the
% atmosphere. This is all done according to the equation given below, from
% ISO 9613-1: 1993
alpha = 868.6*f^2*(1.84*10^-11*(Temp/293.15)^(1/2)*(Pressure/101325)^-1 +
(Temp/293.15)^(-5/2)*(0.01275*exp(-2239.1/Temp)/(F_rO + (f^2/F_rO)) +
0.1068*exp(-3352/Temp)/(F_rN + (f^2/F_rN))));

end
```